



# **The control of starch degradation in *Arabidopsis thaliana* leaves at night**

**Doreen Feike**

A thesis submitted to the University of East Anglia for the degree  
of Doctor of Philosophy

John Innes Centre  
Norwich  
September 2013

© This copy of the thesis has been supplied on condition that anyone who consults it is understood to recognise that its copyright rests with the author and that no quotation from the thesis, nor any information derived there from, may be published without the author's prior written consent.

## Abstract

The aim of this work was to understand how *Arabidopsis thaliana* plants control starch degradation at night. Starch is the major energy reserve in *Arabidopsis*. It is broken down at night to maintain growth and metabolism of the plant, when photosynthesis is not possible. The rate of starch degradation follows a linear pattern and is matched to the length of the night period such that almost all starch is exhausted by dawn. The mechanisms and the proteins involved in controlling starch degradation rates are largely unknown.

With my work I wanted to identify components involved in the control of starch degradation rates. Using a forward genetic screen, I discovered several mutants with new starch degradation phenotypes. One of them was affected in the circadian clock component EARLY FLOWERING 3 (ELF3). It degraded its starch slower than wild-type plants and in a non-linear way. Two mutants degraded their starch at a much faster rate than wild-type plants and exhausted their reserves before dawn. One of them lacks a novel protein, which was named EXCESS STARCH TURNOVER 1 (EST1). This protein is required for normal starch degradation rates, but its function is still unknown. The second mutant is affected in *BETA-AMYLASE 1* (*BAM1*) and produces aberrant BAM1 protein containing a serine to asparagine amino acid substitution in position 132. Faster starch degradation rates in this mutant depend on the presence of another protein of the pathway, LIKE SEX FOUR 1 (LSF1). The data indicate that modulation of BAM1 activity can strongly affect the rates of starch degradation, although starch is degraded normally in absence of BAM1. In a second approach, I analysed which known components of the starch degradation pathway are necessary for the adjustment of starch degradation rates. I found that PHOSPHOGLUCAN WATER DIKINASE (PWD) and BAM3 might play a role in adjusting starch degradation rates in response to an unexpectedly early night.

In summary, in this thesis I introduce a novel protein necessary for normal starch degradation rates in *Arabidopsis* leaves and provide insights into proteins and mechanisms which might control starch degradation rates in response to an early night.

## Acknowledgements

First of all I would like to thank my supervisor Professor Alison Smith for her guidance and invaluable advice, for her enthusiasm and her help in developing my scientific skills. Also, I would like to thank the members of my supervisory committee, Professor Robert Sablowski and Professor Ray Dixon, for their constructive advice on the project.

Many thanks to the Gatsby Charitable Foundation for funding my project and to the Gatsby advisors for supporting me and for the numerous training and networking opportunities they offered.

Thanks also to our collaborators, especially Professor Sam Zeeman, Dr. Anthony Hall and David Seung, for giving me the opportunity to work in Zürich and Liverpool and for their help with the project. I also want to thank Dr. Martin Trick for the analysis of my sequencing data and for identifying the underlying mutation in *est1-1*.

My special thanks goes to all past and current members of the Smith lab, who were always nice and friendly people to work with. Especially, I want to thank Dr. Marilyn Pike for her scientific advice over the last four years. Also, I want to thank Dr. Alexander Graf, who developed the mutant screen and taught me most techniques during my first months in the lab. Many thanks also to Dr. Alastair Skeffington for many interesting discussions in the office and to Dr. Christian Ruzanski for his friendship and his support during my first few months in the UK.

I would like to thank my friends in Norwich, especially Philippa Borrill, Athena Chu and Ruth Bryant for making my time here so much fun and for being such lovely house mates.

Finally, I would like to thank my family, especially my parents Eckhard and Petra, my sister Katharina and my grandparents Gisela and Reinhard. They have supported me during all the ups and downs in the last ten years of studying and gave me the best home to go back to during my time in the UK.

## Table of Contents

<b>Abstract</b> .....	i
<b>Acknowledgements</b> .....	ii
<b>List of Figures</b> .....	ix
<b>List of Tables</b> .....	xii
<b>Abbreviations</b> .....	xiii
<b>1 Introduction</b> .....	1
1.1 Aim.....	1
1.2 Structure, composition and appearance of starch granules.....	2
1.3 The importance of transitory starch.....	3
1.4 Synthesis of transitory starch.....	4
1.5 Degradation of transitory starch in <i>Arabidopsis</i> leaves.....	7
1.5.1 Reversible phosphorylation of the starch granule.....	7
1.5.2 Hydrolysis of the granule.....	9
1.5.3 Further metabolism of maltose and glucose in the cytosol.....	11
1.6 The regulation of starch turnover in response to changes in day length.....	14
1.7 Circadian clock regulation of starch degradation.....	15
1.7.1 The <i>Arabidopsis</i> circadian clock.....	16
1.7.2 Evidence for the regulation of starch degradation by the circadian clock.....	18
1.8 Measurement of the starch content.....	21
1.9 Arithmetic division for the adjustment of starch degradation rates.....	22
1.10 Regulation of the starch degradation pathway.....	24
1.10.1 Evidence for post-translational control.....	25
1.10.2 Reversible glucan phosphorylation could control flux through the pathway.....	25
1.10.3 Redox-regulation of enzymes of the pathway.....	26
1.10.4 Protein complex formation between enzymes of the pathway.....	27
1.10.5 Feedback inhibition.....	27
1.10.6 Protein phosphorylation of enzymes of the pathway.....	28
1.11 Experimental approach.....	29
<b>2 Material and Methods</b> .....	30
2.1 Plant material.....	30
2.2 Plant growth conditions.....	30
2.2.1 Growth on plates.....	30

2.2.2	Growth on soil.....	30
2.3	Homogenisation of plant material .....	31
2.4	Bacterial strains .....	31
2.5	Media and Antibiotics .....	33
2.6	Plasmids.....	34
2.7	Oligonucleotides.....	34
2.8	Molecular Methods.....	40
2.8.1	Nuclei extraction from <i>Arabidopsis</i> leaves .....	40
2.8.2	DNA isolation from plants .....	41
2.8.3	DNA extraction from bacteria.....	42
2.8.4	Polymerase chain reaction (PCR) .....	42
2.8.5	Map-based cloning .....	42
2.8.6	Genotyping of mutants .....	44
2.8.7	Restriction digestion .....	44
2.8.8	Agarose gel electrophoresis .....	45
2.8.9	RNA extraction .....	45
2.8.10	DNase treatment and cDNA synthesis.....	45
2.8.11	Cloning of PCR fragments into pCR8/GW/TOPO TA.....	46
2.8.12	LR reaction.....	46
2.8.13	Site-directed mutagenesis.....	46
2.8.14	DNA sequencing .....	47
2.8.15	<i>Arabidopsis</i> re-sequencing and data analysis.....	47
2.9	Transformation of organisms .....	48
2.9.1	Transformation of <i>Escherichia coli</i> .....	48
2.9.2	Transformation of <i>Agrobacterium</i> .....	48
2.9.3	Stable transformation of <i>Arabidopsis</i> .....	49
2.10	Cross-pollination of <i>Arabidopsis</i> plants .....	49
2.11	Iodine stain of leaf starch .....	50
2.12	Measurement of luciferase (LUC) activity.....	50
2.13	Determination of starch and phtyoglycogen contents .....	50
2.13.1	Starch extraction from <i>Arabidopsis</i> leaves .....	50
2.13.2	Phytoglycogen extraction from <i>Arabidopsis</i> leaves.....	51
2.13.3	Enzymatic digestion of starch and phytoglycogen digestion.....	51
2.13.4	Glucose assay .....	52

2.14	Analysis of starch structure and composition.....	52
2.14.1	Purification of starch granules from <i>Arabidopsis</i> .....	52
2.14.2	Measurement of the amylose to amylopectin ratio .....	53
2.14.3	Determination of starch chain length profile .....	53
2.14.4	Transmission electron microscopy (TEM) .....	54
2.14.5	Scanning electron microscopy (SEM) .....	54
2.15	Native PAGE and SDS PAGE for mutant characterisation .....	55
2.15.1	Gels and running conditions .....	55
2.15.2	Preparation of extracts.....	55
2.15.3	Assay activity of starch metabolising enzymes after native PAGE.....	56
2.15.4	MDH activity assay after native PAGE .....	56
2.15.5	Immunoblotting.....	57
2.16	Analysis of the circadian clock period .....	57
2.16.1	Delayed fluorescence measurements .....	58
2.16.2	Leaf movement measurements.....	59
2.17	Statistical analysis of significance.....	59
<b>3</b>	<b>The Mutant Screen: Mutants with an early starvation phenotype.....</b>	<b>61</b>
3.1	Introduction .....	61
3.1.2	The <i>Arabidopsis</i> starvation reporter line .....	62
3.1.3	Rationale and set up of the screen .....	63
3.1.4	Results of the initial screen.....	65
3.1.6	Aim .....	66
3.2	Results .....	67
3.2.1	Re-screen of M <sub>3</sub> mutant lines.....	67
3.2.2	Characterisation of “ <i>isa</i> -like” mutants.....	68
3.2.3	Putative circadian clock mutants .....	73
3.2.4	Analysis of starch degradation in other early starvation mutants.....	77
3.2.5	Characterisation of mutants with faster starch turnover .....	81
3.2.6	Summary and conclusions .....	84
3.3	Discussion .....	85
3.3.1	Aim of the screen and outcomes.....	85
3.3.2	Why did some mutants not have a reproducible starvation phenotype in the M <sub>3</sub> generation?.....	86
3.3.3	Why did some mutants with an early starvation phenotype not exhaust their starch before dawn? .....	87

3.3.4	Why were so many <i>isa</i> mutants identified in the screen?.....	88
3.3.5	Why did “ <i>isa</i> -like” mutants not display starvation symptoms after 12 hours of the early night?.....	88
3.3.6	Is starch degradation adjusted according to the length of the night in mutants lacking isoamylase activity? .....	90
3.3.7	Circadian clock mutants.....	91
3.3.8	The circadian clock period in 357-1 .....	91
3.3.9	Starch degradation in 357-1 .....	92
3.3.10	Clock period and starch degradation in 395-1 .....	93
3.3.11	Conclusion and outlook .....	94
<b>4</b>	<b>Identification of causal mutations in mutants A and B .....</b>	<b>95</b>
4.1	Introduction .....	95
4.1.1	Aim .....	95
4.1.2	EMS induced point mutations in mutant A and mutant B.....	95
4.1.3	Characterisation of the mutation.....	96
4.1.4	Identification of the mutation by map-based cloning .....	96
4.1.5	Identification of the mutation by mapping-by-sequencing.....	98
4.1.6	Confirmation of candidate genes .....	98
4.2	Results .....	99
4.2.1	Characterisation of mutations: Segregation analysis .....	99
4.2.2	Identification of EMS-induced point mutations in mutant A .....	101
4.2.3	T-DNA insertion lines of At1g42430 and complementation of mutant A ...	106
4.2.4	New nomenclature for At1g42430: EXCESS STARCH TURNOVER 1....	112
4.2.5	<i>In silico</i> analysis of EST1 .....	112
4.2.6	Preliminary experimental data on EST1 and EST2.....	118
4.2.7	Identification of an EMS-induced point mutation in mutant B .....	118
4.2.8	<i>In silico</i> analysis of point mutation in <i>bam1-2</i> .....	121
4.2.9	Confirmation of BAM1 as gene causing the phenotype of <i>bam1-2</i> .....	124
4.2.10	Back-crossing of <i>est1-1</i> and <i>bam1-2</i> .....	124
4.3	Discussion .....	125
4.3.1	The mutation in At1g42430 causes the phenotype of <i>est1-1</i> .....	125
4.3.2	Back-crosses .....	126
4.3.3	Preliminary speculations about EST1 and EST2 function.....	126
4.3.4	Does the point mutation in BAM1 cause the phenotype of <i>bam1-2</i> ?.....	127
4.3.5	Preliminary speculations about the effect of the mutation in BAM1 .....	128

<b>5</b>	<b>Characterisation of <i>est1</i> mutants</b> .....	129
5.1	Introduction .....	129
5.1.1	Aim .....	129
5.1.2	Hypotheses for faster starch degradation in <i>est1</i> mutants.....	129
5.2	Results .....	130
5.2.1	Phenotype of <i>est1-1</i> .....	130
5.2.2	Characterisation of double mutants .....	142
5.3	Discussion .....	149
5.3.1	Interpretation of the phenotype.....	149
5.3.2	Interpretation of starch contents in double mutants.....	154
5.3.3	Conclusion and outlook .....	155
<b>6</b>	<b>Characterisation of <i>bam1-2</i></b> .....	157
6.1	Introduction and rationale .....	157
6.1.1	BAM1 and its role in starch breakdown .....	157
6.1.2	Putative BAM1 interaction partners .....	159
6.1.3	Regulation of BAM1 activity .....	159
6.1.4	BAM1 (S132N) in the pathway of starch degradation .....	160
6.2	Results .....	160
6.2.1	Growth and appearance of <i>bam1-2</i> .....	160
6.2.2	Starch degradation phenotype of <i>bam1-2</i> .....	161
6.2.3	Composition of starch in <i>bam1-2</i> .....	164
6.2.4	BAM1 activity in <i>bam1-2</i> .....	165
6.2.5	BAM1 protein levels in <i>bam1-2</i> .....	167
6.2.6	Analysis of native amylopectin and MDH activity gels for <i>bam1-2</i> .....	170
6.2.7	Starch degradation in <i>bam1-1</i> .....	171
6.2.8	BAM1 activity and redox-regulation in <i>bam1-2</i> .....	173
6.2.9	Crosses of <i>bam1-2</i> to mutants of the starch degradation pathway .....	175
6.3	Discussion .....	181
6.3.1	Hypotheses for faster starch degradation in <i>bam1-2</i> .....	181
6.3.3	Conclusion and Outlook .....	186
<b>7</b>	<b>Starch degradation rates in <i>sex</i> mutants</b> .....	188
7.1	Aim.....	188
7.1.1	Rationale and candidate genes .....	188
7.2	Results .....	189

7.3	Discussion .....	194
7.3.1	Starch contents and degradation rates in <i>sex</i> mutants .....	194
7.3.2	PWD-catalysed phosphorylation could be important to regulate starch degradation rates .....	195
7.3.3	Is BAM3 important for controlling starch degradation rates in response to an early night? .....	196
7.3.4	Conclusions and Outlook.....	197
<b>8</b>	<b>General discussion</b> .....	<b>198</b>
8.1	Summary .....	198
8.2	Is EST1 a novel regulator of starch degradation rates?.....	198
8.3	Is regulation of BAM1 activity a means of controlling transitory starch degradation? .....	201
8.4	Is C3 phosphorylation the mechanism by which starch degradation rates are adjusted according to night length and starch content?.....	202
8.5	Further evidence for an involvement of the circadian clock in adjusting starch degradation rates.....	203
8.6	The formation of starch granules is important for the adjustment of starch degradation rates according to night length.....	204
8.7	Model of the control of starch degradation rates based on the presented data...	204
8.8	Outlook.....	206
	<b>Appendix</b> .....	<b>208</b>
	<b>Bibliography</b> .....	<b>218</b>

## List of Figures

1.1	Structural organisation and appearance of starch granules	3
1.2	The pathway of starch synthesis in <i>Arabidopsis</i> chloroplasts	6
1.3	The pathway of starch degradation in <i>Arabidopsis</i> chloroplasts	13
1.4	Starch degradation rates in <i>Arabidopsis</i> adjust to an early night	15
1.5	A model of the circadian clock in <i>Arabidopsis</i> plants	17
1.6	Depletion of starch matches the time of dawn anticipated by the circadian clock	20
1.7	Starch degradation rates in <i>Arabidopsis</i> adjust to variations in starch content	21
1.8	The chemical kinetic model that explains arithmetic division during starch degradation	24
2.1	Principle of colorimetric assay for MDH activity	57
3.1	Identification of early starvation mutants in a forward genetic screen	65
3.2	Native activity gel for starch metabolising enzymes: “ <i>isa</i> -like” mutants isolated from the mutant screen	70
3.3	Phytoglycogen contents in <i>isa1</i> and control plants during normal and early nights	72
3.4	Clock period estimates of two early starvation mutants as determined by delayed fluorescence analysis	74
3.5	Starch degradation in mutant 357-1 and 395-1 in normal and early night	77
3.6	Starch contents in normal and early nights determined in mutants with strong early starvation phenotypes	79
3.7	Native activity gel to visualise activities of starch metabolising enzymes: Mutants with faster starch degradation	82
3.8	Clock period estimates as determined by leaf movement analysis or delayed fluorescence analysis	83
3.9	Summary of the results of the forward genetic screen	85
4.1	Map-based cloning approach: Schematic representation of Recombination events on <i>Arabidopsis</i> chromosomes in the out-cross of Col-0 to <i>Ler</i>	97
4.2	Segregation analysis for mutant A	100
4.3	Segregation analysis for mutant B	100

4.4	Summary of rough mapping of mutant A	102
4.5	Map-based cloning result of mutant A	103
4.6	RT-PCR for mutant A and wild-type	106
4.7	Schematic gene structure of At1g42430 and position of EMS-induced mutation and T-DNA insertions	107
4.8	Iodine stain of leaf starch of three T-DNA insertion mutants and mutant A plants transformed with At1g42430 cDNA	108
4.9	End of day and end of night starch contents of two T-DNA insertion lines of At1g42430, mutant A and mutant A transformed with cDNA of At1g42430	110
4.10	Immunoblot analysis for mutant A, T-DNA lines for At1g42430 and mutant A plants transformed with At1g42430 cDNA	111
4.11	Predicted amino acid sequence of EST1	113
4.12	Alignment of EST1 and EST2 protein sequences	115
4.13	Summary of rough mapping of mutant B	120
4.14	Map-based cloning result of mutant B	121
4.15	Protein sequence of <i>Arabidopsis</i> beta-amylase 1	122
4.16	Alignment of partial protein sequences of soybean and <i>Arabidopsis</i> beta-amylases	123
4.17	Three dimensional structure of soybean beta-amylase	123
4.18	Alignment of partial protein sequences of nine <i>Arabidopsis</i> beta-amylases	124
5.1	Growth phenotype of <i>est1</i>	131
5.2	Luciferase induced bioluminescence of <i>est1-1</i> and wild-type during normal and early night	132
5.3	Starch degradation pattern in early and normal night for wild-type and <i>est1</i>	133
5.4	Comparison of starch degradation rates for wild-type, <i>est1-1</i> and <i>est1-2</i>	135
5.5	Iodine stain of Col-0 and <i>est1-1</i>	136
5.6	Transmission electron micrographs of leaves	137
5.7	Scanning electron micrographs of starch granules <i>est1-1</i> and wild-type	138
5.8	Amylose content of leaf starch in wild-type, <i>est1-1</i> and <i>est1-2</i>	139
5.9	Chain length distribution of amylopectin before and after beta -amylolysis of external chains	140

5.10	Native activity gel showing the activity of starch modifying enzymes in wild-type and <i>est1-1</i>	142
5.11	Visualisation of leaf starch in wild-type, <i>est1-1</i> , <i>sex1-3</i> and <i>est1-1 sex1-3</i>	144
5.12	Starch contents in the <i>sex1 est1</i> double mutant	145
5.13	Visualisation of leaf starch in double mutants	148
6.1	Growth phenotype of <i>bam1-2</i>	161
6.2	Starch degradation pattern in early and normal night for wild-type (WT) and <i>bam1-2</i>	162
6.3	Comparison of starch degradation rates for <i>bam1-2</i> and wild-type	163
6.4	Amylose content of leaf starch in wild-type and <i>bam1-2</i>	165
6.5	Native gel visualising the activity of starch metabolising enzymes	167
6.6	Immunoblot of wild-type and mutant samples on a native gel and a SDS gel probed with antiserum specific for BAM1	169
6.7	Native activity gel visualising malate dehydrogenase activity	170
6.8	Starch contents of <i>bam1-1</i> and wild-type in normal and early night	172
6.9	Native activity gels of starch metabolising enzymes under oxidising and reducing conditions	174
6.10	Analysis of starch contents in wild-type, <i>bam1-2</i> , <i>lsf1</i> and <i>bam1-2 lsf</i> double mutants	176
6.11	Analysis of starch contents in wild-type, <i>bam1-2</i> , <i>bam3</i> and <i>bam1-2 bam3</i> double mutants	178
6.12	Qualitative analysis of leaf starch in double mutants	179
7. 1	Starch contents of starch excess mutants during normal and early night	190
7.2	Analysis of starch degradation rates in starch excess mutants using linear fits	193
8.1	A model illustrating the interplay between proteins shown to be involved in controlling starch degradation rates	205
A1	Re-screen of M <sub>3</sub> lines by bioluminescence analysis	208
A2	Re-screen of 11 “ <i>isa</i> -like mutants”	215
A3	Starch contents of four mutants with weak early starvation phenotype	216
A4	Alignment of soybean beta-amylase and <i>Arabidopsis</i> BAM1 protein Sequences	216

## List of Tables

2.1	Bacterial strains	32
2.2	Media used for growth of plants and bacteria	33
2.3	Antibiotic concentrations and usage	33
2.4	Cloning vectors	34
2.5	List of primers used for cloning and site-directed mutagenesis (SDM)	34
2.6	List of primers used for genotyping	35
2.7	List of primers used for sequencing	36
2.8	List of primers used for rough mapping	38
2.9	List of oligonucleotides used for fine-mapping	39
3.1	Re-screen of M3 mutant lines: List of candidates with an early starvation phenotype	68
3.2	Bioluminescence expression of “ <i>isa</i> -like” mutants	69
3.2	EMS-type point mutations found in eight mutants isolated in the screen	71
4.1	Description of EMS-induced point mutations found in the mapping interval	105
4.2	List of EST1 orthologs	116
4.3	List of EST2 orthologs	117
5.1	Estimated time of darkness when starch contents would reach zero for wild-type and <i>est1-1</i> and <i>est1-2</i>	136
6.1	Estimation of time when starch contents would reach zero in wild-type and <i>bam1-2</i>	164

## Abbreviations

ADP	Adenosine diphosphate
AGPase	ADP-glucose pyrophosphorylase
AMY	Alpha-amylase
At	<i>Arabidopsis thaliana</i>
ATP	Adenosine triphosphate
BAM	Beta-amylase
BE	Branching enzyme
bp	Base pairs
CCD	Charge-coupled device
CCA1	Circadian clock-associate 1
cDNA	Complementary DNA
CER	Controlled environment room
Col-0	Columbia-0
cps	Counts per second
cTP	Chloroplast transit peptide
DNA	Deoxyribonucleic acid
DF	Delayed fluorescence
d.p.	Degree of polymerisation
DPE	Disproportionating enzyme
DSP	Dual specificity phosphatase
DTT	Dithiothreitol
EC	Evening complex
EDTA	Ethylenediaminetetraacetic acid
ELF	Early flowering
EMS	Ethyl methanesulfonate
EOD	End of day
EON	End of night
EST	Excess starch turnover
F <sub>1</sub>	First filial generation
F6P	Fructose-6-phosphate
FW	Fresh weight
G1P	Glucose-1-phosphate
G6P	Glucose-6-phosphate
GBSS	Granule-bound starch synthase
gDNA	Genomic DNA
GI	Gigantea
Gm	<i>Glycine max</i>
GWD	Alpha-glucan, water dikinase
HEPES	4-(2-hydroxyethyl)-1-piperazineethanesulfonic acid
HPAEC-PAD	High performance anion exchange chromatography with pulsed amperometric detection
ISA	Isoamylase
JMJD	Jumonji domain containing
LB	Luria-Bertani
LDA	Limit dextrinase
Ler	Landsberg <i>erecta</i>
LHY1	Late elongated hypocotyl
LSF	Like starch excess four
LUC	Luciferase

M <sub>1</sub>	First mutant generation
M1-16	Marker
MA1-14	Marker mutant A
MB1-9	Marker mutant B
MES	2-(N-morpholino)ethanesulfonic acid
MEX	Maltose excess
MOPS	3-(N-morpholino)propanesulfonic acid
MS	Murashige and Skoog
NAD <sup>+</sup>	Nicotinamide adenine dinucleotide (oxidised)
NADH	Nicotinamide adenine dinucleotide (reduced)
NADP <sup>+</sup>	Nicotinamide adenine dinucleotide phosphate (oxidised)
NADPH	Nicotinamide adenine dinucleotide phosphate (reduced)
NADP-MDH	NADP-dependent malate dehydrogenase
NBT	Nitroblue tetrazolium
NIB	Nuclei isolation buffer
NTP	Nucleotide triphosphate
OD	Optical density
PAGE	Polyacrylamide gel electrophoresis
PCR	Polymerase chain reaction
PE	Paired-end
PGI	Phosphoglucoisomerase
pGlcT	Plastidic glucose translocator
PGM	Phosphoglucomutase
PHS	Alpha-glucan phosphorylase
PIF	Phytochrome interacting factor
PMS	Phenazine methosulfate
PRR	Pseudo response regulator
PVDF	Polyvinylidene fluoride
PWD	Phosphoglucan water dikinase
RAE	Relative amplitude error
S132N	Serine to asparagine substitution, codon 132
SBD	Starch binding domain
SBE	Starch branching enzyme
SDM	Site-directed mutagenesis
SDS	Sodium dodecyl sulphate
SEM	Scanning electron microscopy
SHG	Soluble heteroglycan
SNP	Single nucleotide polymorphism
SS	Starch synthase
SEX	Starch excess
SOC	Super optimal broth
SS	Starch synthase
T6P	Trehalose-6-phosphate
TAE	Tris base, acetic acid, EDTA buffer
TAP	Tandem affinity purification
TEM	Transmission electron microscopy
TOC1	Timing of cab expression 1
TP	Triose phosphate
TP1-4	Time point
v/v	Volume/volume
w/v	Weight/volume
WT	Wild-type

# 1 Introduction

## 1.1 Aim

This thesis considers the control of starch degradation in leaves of the model plant *Arabidopsis thaliana*.

Transitory starch is the major energy reserve in *Arabidopsis*. During the day, about half of the photoassimilate is converted to starch, which is broken down at night to provide carbon for growth and metabolism in the dark. Starch accumulates at a near-linear rate. Degradation also follows a linear pattern, so that almost all starch is exhausted by dawn. This pattern is robust to fluctuations in light environmental conditions, indicating complex mechanisms of regulation. Productivity and normal growth of *Arabidopsis* plants are largely dependent on normal starch metabolism. This is demonstrated by the phenotype of mutants affected in either starch synthesis or degradation, as these mutants show reduced growth rates and display symptoms of carbon starvation. Although many enzymes of the starch synthesis and degradation pathway have been identified, little is known about the regulation of starch metabolism in response to changes in environmental conditions. Recently, research in this field was advanced by the discovery of a link between the circadian clock and the adjustment of starch degradation rates.

With my work, I want to explore which proteins are involved in the control of starch degradation rates in *Arabidopsis* leaves. The main focus of my work is the identification of new genes involved in the regulation of starch degradation rates. However, I will also investigate which known enzymes of the starch degradation pathway are targets of the mechanism that adjusts starch degradation rates in response to an unexpected shortening of the light period.

In this chapter, I will summarize the current knowledge about transitory starch metabolism in *Arabidopsis* and focus on the enzymatic pathway of starch degradation. I will describe the flexibility of the adjustment of starch degradation rates in response to altered day lengths and explain the involvement of the circadian clock in this mechanism. Finally, I will summarise our current knowledge about regulation of the enzymes in the pathway.

## 1.2 Structure, composition and appearance of starch granules

Starch is a glucose polymer produced by plants. It forms insoluble granules in plastids of photosynthetic and non-photosynthetic cells.

Starch is made up by two glucose polymers, amylose and amylopectin. The amylose molecule is mainly linear and composed of long chains of  $\alpha$ -1,4-linked glucose residues (500-10,000 glucose residues). Amylopectin consists of many short  $\alpha$ -1,4-linked-glucose chains (6 to >100 glucose residues), that are connected by  $\alpha$ -1,6-bonds (Buléon et al., 1998). *Arabidopsis* leaf starch contains almost exclusively amylopectin, which makes up about 95% of the starch granule (Zeeman et al., 2002).

Amylopectin is responsible for the semi-crystalline structure of the starch granule (**Figure 1.1, a-e**). Branch points in amylopectin are distributed at regular intervals, therefore linear glucan chains cluster along the axis of the molecule forming a tree like structure. Adjacent chains within these clusters form double helices that pack together in organised arrays, making up crystalline lamellae in the granule matrix. These alternate with amorphous lamellae which contain the branch points of the amylopectin molecule. Crystalline and amorphous layers alternate with a periodicity of about 9 nm. The next level of organisation of the starch granule occurs in the form of growth rings, which are 120-400 nm wide. Each growth ring is made up by stacks of crystalline and amorphous layers associated with the 9 nm periodicity (Buléon et al., 1998). The material between the growth rings is of amorphous structure. Amylose is believed to be embedded within the amorphous layers of the granule (Zeeman et al., 2010). Visualisation of growth rings is possible by scanning electron microscopy after mechanical damage and subsequent partial digestion with alpha-amylase. The enzyme preferentially digests amorphous regions (Pilling and Smith, 2003).

Chloroplasts in mature *Arabidopsis* leaves contain on average five to six starch granules (Crumpton-Taylor et al., 2012). These are flat and discoid, about 1-2  $\mu\text{m}$  in diameter and about 0.2-0.5  $\mu\text{m}$  thick (**Figure 1.1, f-g**). Growth rings were not observed in fractured wild-type granules but were seen in granules of a starch degradation mutant. The mutant lacks the protein STARCH EXCESS FOUR (SEX 4) and accumulates excess amounts of starch, due to retardation of starch breakdown (Niittylä et al., 2006). Granules of the mutant are thicker and more spherical than those of wild-type plants.

The observed growth rings had a periodicity of about 0.2-0.3  $\mu\text{m}$ , thus were similar in size to wild-type starch granules (Zeeman et al., 2002).

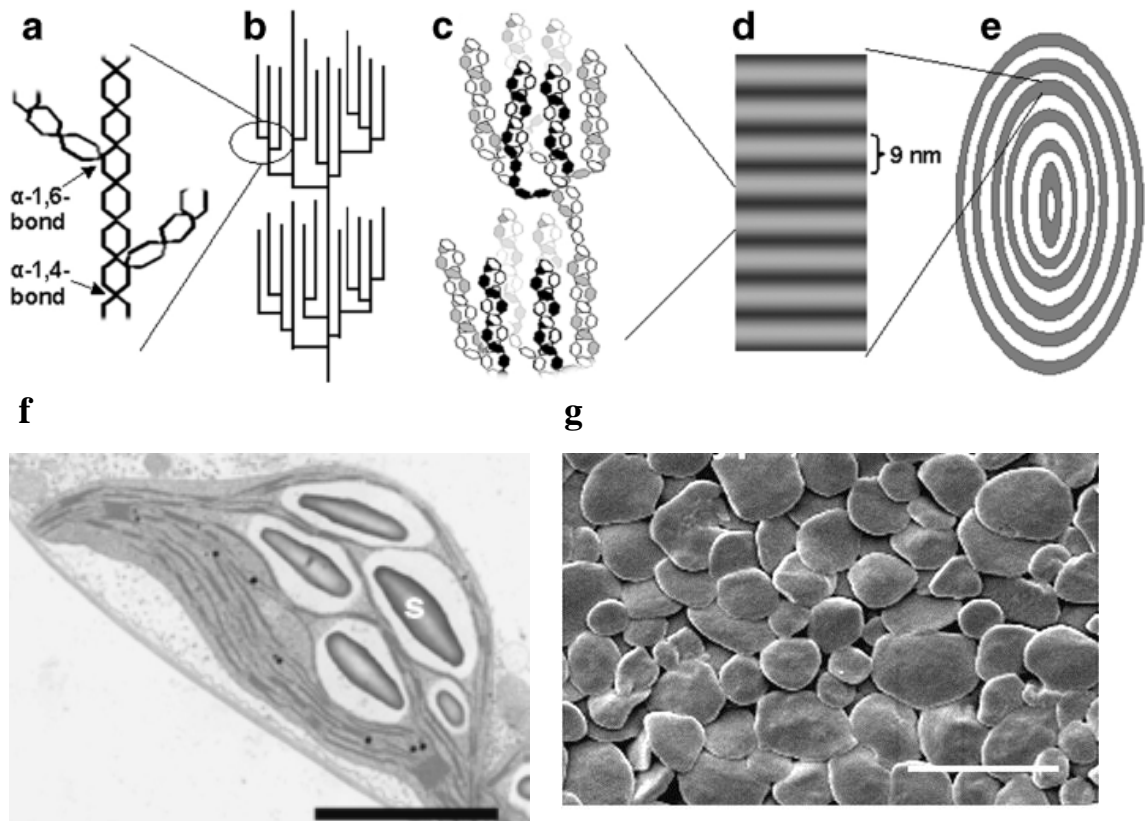


**Figure 1.1: Structural organisation and appearance of starch granules.** From Zeeman et al. (2004a). (a)  $\alpha$ -1,4- and  $\alpha$ -1,6 linked glucosyl residues of an amylopectin chain. (b) Schematic representation of clusters of amylopectin chains. (c) Drawing of double helices formed by amylopectin chains. (d) Representation of semi-crystalline and amorphous layers alternating with 9 nm periodicity. (e) Growth rings of the starch granule. (f) Transmission electron micrograph of an *Arabidopsis* mesophyll chloroplast at the end of the light period showing starch granules (S), bar 2  $\mu\text{m}$ . (g) Scanning electron micrograph of starch granules isolated from wild-type *Arabidopsis* plants at the end of a 12 hour light period, bar 2  $\mu\text{m}$  (Zeeman et al., 2002).

### 1.3 The importance of transitory starch

In starch research, “storage starch” is distinguished from “transitory starch”. The former is produced in amyloplasts of heterotrophic storage organs as roots, stems, tubers or

seeds. There, it is stored for long-term and remobilised later in development to support phases of re-growth or germination after periods of dormancy (Smith, 2012). Transitory starch is formed in chloroplasts of photosynthetically active tissue e.g. in leaves. It is built up during the day and broken down at night to provide carbon for plant growth and metabolism in the dark. Most of the starch in *Arabidopsis* is produced in photosynthetic leaf tissue and is turned over in a diurnal manner to provide carbon during the night. However, small amounts of starch are also produced in heterotrophic tissue of the plant, e.g. in root caps, or seeds (Tsai et al., 2009; Andriotis et al., 2010). It is not clear if starch metabolism in non-photosynthetic tissue differs from that in photosynthetic leaf tissue. However, it was shown that pathways of starch metabolism in seeds are similar to those in leaves (Andriotis et al., 2010). Andriotis et al (2010) showed that several mutants lacking enzymes of the leaf starch degradation pathway contained abnormally high amounts of starch in mature seeds. Thus, starch degradation in developing seeds involves enzymes necessary for normal starch degradation in leaves.

In *Arabidopsis*, starch has been identified as a major integrator in the regulation of plant growth to cope with changes in carbon availability (Sulpice et al., 2009). The importance of transitory starch is reflected in the phenotype of mutants that cannot synthesise or degrade starch. These mutants grow poorly unless subjected to continuous light or long days (Caspar et al., 1985; Yu et al., 2001; Gibon et al., 2004). Growth rates drop abruptly in wild-type plants if the night is extended beyond normal dawn so that leaf starch is exhausted (Yazdanbakhsh et al., 2011). Reduction of growth rates in starch metabolism mutants and wild-type plants in the extended night is accompanied by rapid and massive changes in gene expression and metabolism which are indicative of carbon starvation (Gibon et al., 2004; Smith and Stitt, 2007; Usadel et al., 2008). Thus, supply of sugars from starch is essential for normal growth of *Arabidopsis* plants at night.

In the following sections, I will describe the pathways of transitory starch synthesis and degradation in *Arabidopsis*.

#### **1.4 Synthesis of transitory starch**

The enzymatic pathway of starch synthesis was reviewed by Zeeman et al. (2010) and is only briefly described here.

Transitory starch in *Arabidopsis* is made in chloroplasts (**Figure 1.2**). The Calvin-Benson cycle intermediate fructose-6-phosphate (F6P) is converted into glucose-6-phosphate (G6P), by the enzyme phosphoglucose isomerase (PGI). G6P is used as a substrate of phosphoglucomutase (PGM) and converted to glucose-1-phosphate (G1P). ADP-glucose pyrophosphorylase (AGPase) produces ADP-glucose (ADPG) from G1P and ATP. ADPG is the substrate for starch synthases (SS). Based on homology studies, five classes of starch synthases are distinguished. The enzyme granule-bound starch synthase (GBSS) is involved in amylose synthesis and soluble starch synthases (SSI-SSIV) synthesise amylopectin. SSIV is required for granule formation during leaf expansion. Mutants lacking the protein have reduced numbers of starch granules with altered morphology (Roldán et al., 2007; Crumpton-Taylor et al., 2013). SSI-SSIII elongate the glucose chains via  $\alpha$ -1,4 linkages. Starch branching enzymes (SBE) introduce the  $\alpha$ -1-6-branch-points of the amylopectin molecule. In *Arabidopsis* three isoforms of SBE are known, only two of them (BE2 and BE3) are required for synthesis of normal starch (Dumez et al., 2006)

Two debranching enzymes (DBE), which are capable of hydrolysing  $\alpha$ -1,6-linked branch points of the amylopectin molecule, are important to obtain the semi-crystalline structure of the granule. Loss of either isoamylase 1 (ISA1) or isoamylase 2 (ISA2) results in the accumulation of water-soluble phytoglycogen instead of starch granules in most parts of the plant (Zeeman et al., 1998a; Delatte et al., 2005). Phytoglycogen which accumulates in the leaves of *isa1*, *isa2* or *isa1 isa2* mutants contains more  $\alpha$ -1,6-branch points than wild-type amylopectin. It was proposed that isoamylase activity accelerates crystallisation of starch by removing misplaced branch points from nascent amylopectin. Presence of misplaced branches could delay crystallisation and allow interference of starch metabolising enzymes such as alpha- and beta-amylases during starch biosynthesis. This would generate short glucan chains that prevent crystallisation (Streb et al., 2008).

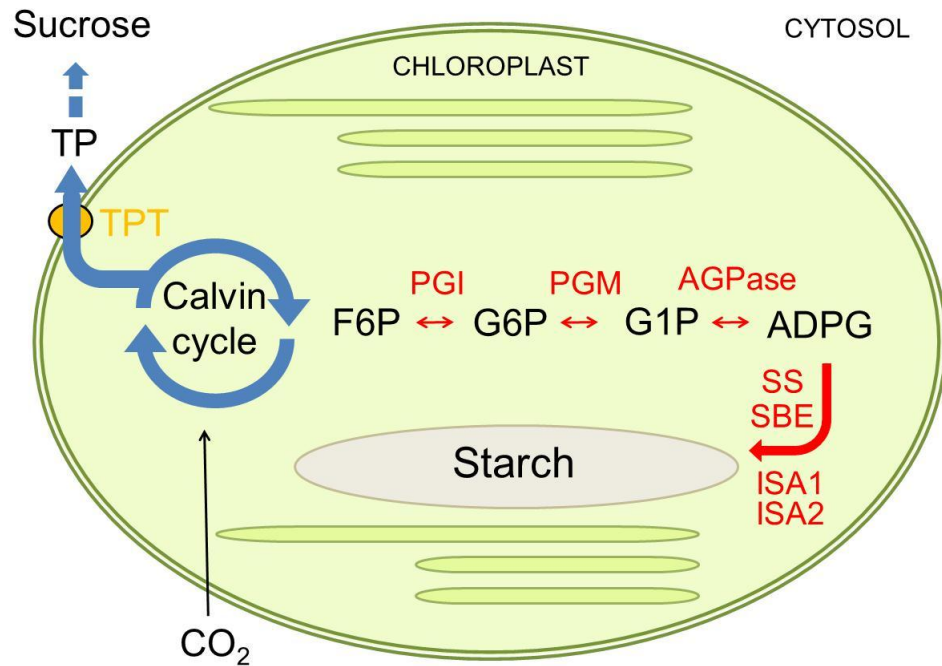


**Figure 1.2: The pathway of starch synthesis in *Arabidopsis* chloroplasts.** Carbon is assimilated via the Calvin cycle and partitioned for sucrose and starch biosynthesis. Triose phosphate (TP) intermediates are exported from the chloroplast via a triose phosphate transporter (TPT) for sucrose synthesis in the cytosol. Fructose-6-phosphate (F6P) is retained in the chloroplast and used as a precursor for starch biosynthesis. G6P: glucose-6-phosphate, G1P: glucose-1-phosphate, ADPG: ADP-glucose, PGI: phosphoglucose isomerase, PGM: phosphoglucomutase, AGPase: ADP-glucose pyrophosphorylase, SS: starch synthase, SBE: starch branching enzyme, ISA: isoamylase.

## 1.5 Degradation of transitory starch in *Arabidopsis* leaves

Degradation of transitory starch in leaves is primarily the result of hydrolysis of the constituent glucans to maltose and glucose, which are exported from the chloroplast and metabolised in the cytosol. Reversible phosphorylation of glucans at the surface of the starch granule serves to solubilize the granule surface to allow access for hydrolases to the glucan chains (Zeeman et al., 2010) (**Figure 1.3**).

The enzymes that are involved in the pathway of starch degradation were identified using forward and reverse genetic approaches. Loss-of-function mutants that lack enzymes involved in starch degradation accumulate amounts of starch that are much greater than in wild-type plants. This phenotype is called the starch-excess (*sex*) phenotype and is caused by retardation of starch breakdown.

Starch degradation in *Arabidopsis* leaves is not a linear pathway. It can rather be seen as a network of reactions. Some of the enzymes involved in starch degradation have redundant functions and the role of some proteins necessary for normal starch degradation is still not understood.

### 1.5.1 Reversible phosphorylation of the starch granule

Glucan-water dikinase (GWD) is responsible for the initial phosphorylation of amylopectin on the starch granule and is considered to be the first enzyme of the pathway. Loss of GWD function results in a severe *sex* phenotype (Yu et al., 2001) and *gwd* mutants (also called *sex1* mutants) contain about 40-100 times more starch than wild-type at the end of the night (Niittylä et al., 2006; Kötting et al., 2005). GWD transfers the  $\beta$ -phosphate group of ATP to a small proportion of glucosyl residues on the granule surface. A second kinase named phosphoglucan water dikinase (PWD) is responsible for further phosphorylation of the starch granule (Kötting et al., 2005). The enzyme adds phosphate to the C3 position of glucose molecules only after pre-phosphorylation on C6 by GWD (Baunsgaard et al., 2005; Kötting et al., 2005; Hejazi et al., 2009). Therefore, starch of *gwd* mutants is phosphate free, whereas *pwd* starch is phosphorylated only at the C6 position (Ritte et al., 2006). Loss of PWD also results in a *sex* phenotype, which is less pronounced than that of *gwd* plants (Baunsgaard et al., 2005; Kötting et al., 2005; Hejazi et al., 2009). At the end of the day, about 1 in 2,000

glycosyl residues on the starch granule is phosphorylated and the ratio of C3- to C6-bound phosphate in wild-type starch is about 1:5 (Yu et al., 2001; Ritte et al., 2006; Haebel et al., 2008; Santelia et al., 2011).

Starch phosphorylation is a prerequisite for degradation. It was proposed that phosphorylation disrupts the highly ordered structure of amylopectin, thereby facilitating the access for starch hydrolysing enzymes to their substrate (Edner et al., 2007; Hejazi et al., 2008). Using nuclear magnetic resonance (NMR) spectroscopy and simulations of molecular dynamics, it was shown that phosphorylation, especially at C3-residues, destabilises the regular helix structure of amylopectin resulting in a growing amorphous phase (Hansen et al., 2008; Blennow and Engelsen, 2010). Also, starch degradation was shown to be accelerated by simultaneous phosphorylation *in vitro* (Edner et al., 2007).

Removal of the phosphate groups is as important for normal starch degradation as phosphorylation, because beta-amylases attacking the granule cannot degrade past a phosphate group (Takeda and Hizukuri, 1981; Fulton et al., 2008). Dephosphorylation of starch is catalysed by two enzymes, SEX4 and LIKE SEX FOUR 2 (LSF2). The phosphoglucan phosphatase SEX4 is capable of dephosphorylating the starch granule at either the C6 or C3 position. The *sex4* mutant has a starch excess and accumulates phosphorylated intermediates of starch breakdown (Niittylä et al., 2006; Kötting et al., 2009; Hejazi et al., 2010). LSF2 dephosphorylates glucose residues exclusively at the C3 position. The *lsf2* mutant has no starch excess phenotype and does not accumulate phospho-oligosaccharides, but has elevated levels of C3 phosphate. The *sex4 lsf2* double mutant has a severe starch excess, which is higher than that of *sex4* single mutants (Santelia et al., 2011).

Another putative chloroplastic phosphatase called LIKE SEX FOUR 1 (LSF1) was found to be required for starch degradation, as the *lsf1* mutant has a *sex* phenotype (Comparot-Moss et al., 2010). LSF1 is closely related in sequence and structure to SEX4. The protein is located at the surface of starch granules and LSF1 contains a putative dual specificity phosphatase domain (DSP), which is similar to the DSP of SEX4. However, LSF1 does not catalyse the same reaction as SEX4, because *lsf1* starch

contains wild-type levels of C3 and C6 phosphate. Therefore, LSF1 might have a regulatory role in the pathway.

### ***1.5.2 Hydrolysis of the granule***

Starch granules of *Arabidopsis* are mainly degraded by amylolytic attack (Smith, 2012).

In *Arabidopsis* leaves, no essential role for  $\alpha$ -amylases (AMYs) in starch degradation could be demonstrated as mutants lacking the chloroplastic isoform AMY3 display normal starch metabolism (Yu et al., 2005). This is a major difference between starch degradation in *Arabidopsis* leaves and e.g. cereal endosperm, where starch degradation is predominantly the result of  $\alpha$ -amylolysis. However, there is evidence that AMY3 plays a role in leaf starch degradation in the absence of certain enzymes of the starch degradation pathway. AMY3 might be responsible for liberation of soluble, branched glucans in the absence of the DBEs isoamylase 3 (ISA3) and limit dextrinase (LDA) (Delatte et al., 2006). This is in consistence with the finding that loss of AMY3 in the *isa3 lda* background further slows down starch degradation of the double mutant (Streb et al., 2012). The starch excess of the *sex4* mutant is also increased in absence of AMY3, showing that AMY3 contributes to starch breakdown in the absence of SEX4 (Kötting et al., 2009).

Hydrolysis of linear  $\alpha$ -1,4-linked glucan chains is primarily catalysed by beta-amylases (BAMs). They liberate maltose from the non-reducing end of glucans by exo-amylolysis. The *Arabidopsis* genome contains nine beta-amylase genes (*BAM1-9*) (Fulton et al., 2008). Only four of these isoforms (BAM1 - 4) were shown to be located inside the chloroplast (Lao et al., 1999; Sparla et al., 2006; Fulton et al., 2008). Mutations in either *BAM3* or *BAM4* result in the *sex* phenotype. The *bam2* mutant has no phenotype in any genetic background tested (Fulton et al., 2008). Loss of BAM1 does not affect starch degradation rates, but increases the *sex* phenotype of the *bam3* mutant (Fulton et al., 2008). This indicates that BAM1 is only important for transitory starch degradation in the absence of BAM3 and that BAM3 plays the major role in degrading the granule. BAM4 lacks key catalytic residues present in other BAMs, and lacks beta-amylase activity *in vitro*. Loss of BAM4 results in a starch excess and lack of BAM4 in the *bam3* or *bam1 bam3* mutant background increases the starch excess of

both mutants. These experiments indicate a regulatory or structural role of BAM4 in the pathway of starch degradation (Fulton et al., 2008).

BAMs are not capable of cleaving  $\alpha$ -1,6-linked glucose at the branch points of the amylopectin molecule. Branch points are hydrolysed by DBEs, releasing linear glucans, which are further processed by beta-amylases. *Arabidopsis* contains four proteins with debranching activity: ISA1, ISA2, ISA3 and limit dextrinase (LDA, also known as pullulanase). LDA and ISA3 were shown to be involved in leaf starch degradation (Delatte et al., 2006; Wattlebled et al., 2008; Streb et al., 2008; Streb et al., 2012), while ISA1 and ISA2 have a role in starch synthesis as explained above (Delatte et al., 2005; Wattlebled et al., 2005). The *isa3* mutant has a *sex* phenotype (Wattlebled et al., 2005; Delatte et al., 2006). The *lda* mutant degrades starch normally, but LDA contributes to starch degradation in absence of ISA3. Thus, ISA3 appears to be the major DBE involved in starch degradation at night. The surface of starch of the *isa3* mutant is enriched in short chains (Delatte et al., 2006). This indicates that the main role of ISA3 is to cleave alpha-1,6 linked glucose at the base of chains degraded by beta-amylases.

The action of beta-amylase will finally result in the accumulation of maltose and minor amounts of maltotriose. The latter is too short to serve as a substrate for further processing by beta-amylases. Therefore, maltotriose is metabolised by a glucanotransferase called disproportionating enzyme 1 (DPE1) (Critchley et al., 2001). Loss of DPE1 results in retardation of starch breakdown and the accumulation of maltotriose. DPE1 catalyses the conversion of two maltotriose units to glucose and maltopentaose. The latter is then again used as a substrate for BAMs, while glucose is exported from the chloroplast via the plastidic glucose translocator (pGlcT) (Cho et al., 2011).

The importance of starch phosphorylation for beta-amylase activity was demonstrated *in vitro*. Edner et al. (2007) showed that beta-amylolytic attack on starch is stimulated by addition of GWD and ATP. However, incorporation of phosphates by GWD was also stimulated by BAM3 activity, indicating positive feedback mechanisms between beta-amylolysis and starch phosphorylation. Beta-amylases cannot degrade past a phosphate group (Takeda and Hizuri, 1981). In the absence of SEX4, the phosphorylated granule is mainly attacked by ISA3 and AMY3 (Köting et al., 2009).

Linear oligosaccharides which are liberated from the granule can also be a substrate for  $\alpha$ -glucan phosphorylase (PHS1). The enzyme releases G1P from the non-reducing end of glucan chains of at least five residues. However, the significance of phosphorolytic starch breakdown for transitory starch degradation is not clear, since mutants lacking the enzyme show normal starch metabolism. It was suggested that the enzyme supplies substrates for the plastidial oxidative pentose phosphate pathway during stress responses (Zeeman et al., 2004b).

### ***1.5.3 Further metabolism of maltose and glucose in the cytosol***

The major products of starch degradation are maltose and glucose. These are exported from the plastid by the maltose transporter MALTOSE EXCESS 1 (MEX1) and pGlcT, respectively (Niittylä et al., 2004; Cho et al., 2011). The *mex1* mutant grows slower than wild-type plants and has reduced chlorophyll contents. It has greatly elevated maltose levels and a *sex* phenotype due to retardation of starch breakdown (Niittylä et al., 2004). The *pglct* mutant grows normally and shows similar rates of starch turnover to wild-type. However, lack of pGlcT in the *mex1* background results in more severe growth retardation than observed in *mex1* single mutants. Rates of starch synthesis and degradation in the *pglct mex1* double mutant were much lower than in wild type and in both parents (Cho et al., 2011). The strong phenotype of the *mex1* single mutant demonstrates that maltose is the main product of starch degradation exported at night (Niittylä et al., 2004).

In the cytosol, maltose and glucose are converted to hexose phosphates which are used for sucrose synthesis. Maltose metabolism in the cytosol is not fully understood.

The first enzyme that acts on maltose is the cytosolic glucoamylase DPE2. The *dpe2* mutant has elevated maltose levels, a starch excess phenotype and is retarded in growth (Chia et al, 2004; Lu and Sharkey, 2004). This phenotype resembles that of the *mex1* mutant and demonstrates the importance of the DPE2-mediated glucosyl transfer reaction for cytosolic maltose metabolism. DPE2 hydrolyses the alpha-1,4 linkage of maltose, thereby releasing one glucose molecule and transferring the second glucose molecule to an acceptor. It was shown *in vitro* that DPE2 uses soluble polysaccharides e.g. glycogen as glucosyl acceptor molecules (Chia et al., 2004; Lu and Sharkey, 2004; Lu et al., 2006). However, glycogen has not been identified as constituent of plant cells.

The *in vivo* substrate of DPE2 might be a soluble heteroglycan (SHG), a complex arabinogalactan-like polysaccharide which was purified from plants including *Arabidopsis* (Fettke et al., 2004; Fettke et al., 2005). DPE2 used plant-derived SHG as acceptor molecule *in vitro* (Fettke et al., 2006; Lu et al., 2006; Fettke et al., 2009).

The glucose residues which were added to SHG are possibly removed by the cytosolic alpha-glucan phosphorylase PHS2 which converts them to G1P (Lu et al., 2006; Fettke et al., 2009). PHS2 was shown to use plant derived SHG as a substrate *in vitro* (Fettke et al., 2004; Fettke et al., 2005). The phenotype of the *phs2* mutant is less severe than that of the *dpe2* mutant. The mutant has no growth retardation and normal rates of starch turnover. Maltose levels are elevated only at night and to a much lesser extent than in *dpe2*. This suggests that an alternative pathway to remove glucose residues from SHG exists (Lu et al., 2006). It has not yet been discovered if the above described pathway involving DPE2, PHS2 and SHG operates *in vivo*. The structure and biosynthesis pathways of SHG also remain to be discovered.

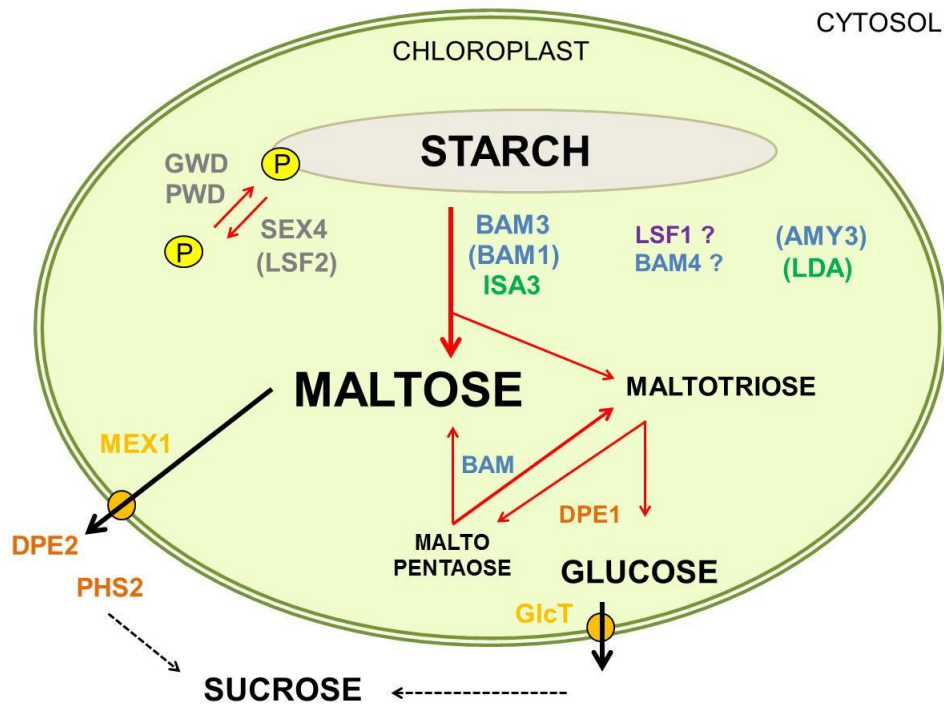


**Figure 1.3: The pathway of starch degradation in *Arabidopsis* chloroplasts.** Reversible starch phosphorylation is catalysed by glucan water dikinase (GWD), phosphoglucan water dikinase (PWD), STARCH EXCESS 4 (SEX4) and LIKE SEX FOUR 2 (LSF2) allows hydrolytic degradation of the granule by beta-amylases (BAMs) and the debranching enzyme isoamylase 3 (ISA3). Maltose, and to a lesser extent maltotriose, are the main products of BAM and ISA3 activity. Maltotriose can be metabolised by dispoportionating enzyme 1 (DPE1), releasing glucose. LSF1 and BAM4 are required for normal starch degradation, but their functions have not been established yet. It was suggested that they have a regulatory role in the pathway. Enzymes shown in brackets (alpha-amylase 3 (AMY3), limit-dextrinase (LDA), beta-amylase 1 (BAM1) and LSF2) contribute to starch degradation in certain mutant backgrounds, but lack of each of these enzymes alone does not result in retardation of starch breakdown. The main products of starch degradation are maltose and glucose which are released from the chloroplast via the transporter MALTOSE EXCESS 1 (MEX1) and plastidic glucose translocator (pGlcT), respectively. In the cytosol, maltose is further metabolised by the glucanotransferase DPE2 and reactions that putatively involve a soluble heteroglycan (SHG) as glucosyl acceptor and glucan phosphorylase 2 (PHS2). Hexose phosphates produced from maltose and glucose are further used for sucrose synthesis.

## 1.6 The regulation of starch turnover in response to changes in day length

In *Arabidopsis*, rates of starch synthesis and degradation are near-linear, when plants are grown under controlled conditions. This pattern is retained across a wide range of different day lengths. This means *Arabidopsis* plants show a remarkable flexibility in adjusting the rates of synthesis and degradation to maintain a balance between carbon assimilation, storage and growth (Smith and Stitt, 2007). The underlying regulatory mechanisms are complex and vital for plant growth and productivity.

The main product of photosynthesis is sucrose, which is used for immediate growth during the day, but in *Arabidopsis* about 30-50% of the photoassimilate is converted to starch. The proportion of fixed carbon that is partitioned into starch was found to be dependent on the length of the day. If plants are grown in short days, they partition a higher proportion of their photoassimilate into starch compared to growth in long days. In other words, the rate of starch biosynthesis increases the shorter the day and the longer the night (Gibon et al., 2004; Gibon et al, 2009; Lu and Sharkey, 2005). If plants are grown in 4 hour light – 20 hour dark cycles, the rate of starch synthesis is about two times faster compared to growth in 12 hour light – 12 hour dark cycles (Gibon et al., 2009).

The rate of starch degradation is similarly adjusted to the length of the night. Starch degradation follows a linear pattern, such that about 95% is used up by dawn (Graf et al., 2010). This pattern is retained in photoperiods of different lengths by an adjustment of the starch degradation rate. Plants grown in short days degrade starch more slowly than plants grown in long days (Gibon et al., 2009). Even more remarkably, the rate of starch degradation can immediately adjust to an unexpected shortening or extension of the light period (Lu et al., 2005; Graf et al., 2010; Scialdone et al., 2013). Plants were grown for three weeks in 12 hour light – 12 hour dark cycles and then transferred to darkness after only eight hours of light. Starch degradation in these plants was still linear, but slowed down, such that reserves lasted for the whole 16 hour night (Graf et al., 2010) (**Figure 1.4**). Conversely, plants that were grown in 12 hour light – 12 hour dark cycles for three weeks and then subjected to a late night after 16 hours of light, increased their starch degradation rates in the subsequent (shorter) night (Scialdone et al., 2013).

The observations described above show that starch degradation rates in *Arabidopsis* adjust to differences in starch contents and time remaining until dawn. Plants that experienced a shortening or extension of the light period have different amounts of starch at the beginning of the night. Also, the length of the night varies if the length of the light period is shortened or extended. This implies the existence of mechanisms that integrate information about starch content and time remaining until dawn to set the appropriate starch degradation rate. These mechanisms would ensure a constant supply of sugars from starch during the whole night. Our knowledge about these mechanisms is discussed in the following (**Chapter 1.9**).

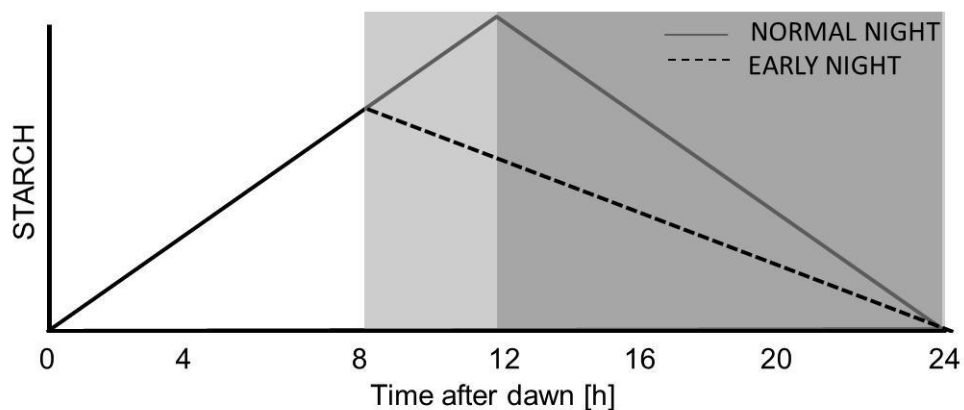


**Figure 1.4: Starch degradation rates in *Arabidopsis* adjust to an unexpectedly early night.** *Arabidopsis* plants grown in 12 hour light – 12 hour dark cycles, accumulate and degrade starch in a linear way (solid line) so that reserves are almost precisely used up by dawn. If the darkness is imposed several hours earlier than normal (light grey bar), starch degradation rates remain linear, but slow down so that enough carbon is available for the whole night (dashed line). Based on Graf et al. (2010).

### 1.7 Circadian clock regulation of starch degradation

Adjustment of the appropriate starch degradation rate according to the length of the night requires a mechanism that measures the time remaining until dawn. Recently, it was demonstrated that the circadian clock is the timer that underlies starch degradation in *Arabidopsis* leaves (Graf et al., 2010).

### 1.7.1 *The Arabidopsis circadian clock*

Circadian clocks are endogenous 24-hour timers that are present in most eukaryotes and photosynthetic bacteria. They allow the anticipation and synchronisation of biological processes with light environmental oscillations. The circadian clock is a self-sustaining mechanism which can buffer changes in environmental conditions and persist in the absence of environmental cues (Bell-Pedersen et al., 2005).

The clock is composed of a small transcriptional network that contains multiple interconnected feedback loops. Data from mutant studies and mathematical modelling were combined to establish a model of the circadian clock in *Arabidopsis*. However, this model is undergoing constant revision. A recent, simplified model of the circadian clock transcriptional network is presented in **Figure 1.5**.

In the original model, the core of the oscillator was formed by transcriptional regulatory feedback loops between the two MYB domain containing transcription factors CIRCADIAN CLOCK ASSOCIATED 1 (CCA1) and LATE ELONGATED HYPOCOTYL (LHY) and a protein of the PSEUDO RESPONSE REGULATOR (PRR) family, called TIMING OF CAB EXPRESSION 1 (TOC1) (Alabadi et al., 2001). Since then, many components have been added to the oscillator and the plant circadian clock model has developed into a complex network of interconnected transcriptional feedback loops (Pruenda-Paz and Kay, 2010).

Mutants lacking components of the oscillator have circadian clock periods different from 24 hours or are arrhythmic. To assay the free-running period of the circadian clock in plants, seedlings are usually entrained in a 12 hour light – 12 hour dark cycles and then put into constant light. The free-running period is estimated by measuring various circadian clock outputs (**Section 2.16**). In mutants lacking the components EARLY FLOWERING 3 (ELF3), EARLY FLOWERING 4 (ELF4) and LUX ARRHYTHMO (LUX), circadian rhythms are abolished (arrhythmic) in constant light. Mutants lacking PRR7 and PRR9 have long period phenotypes and mutants affected in CCA1, LHY, PRR5, GIGANTEA (GI), TOC1, JUMONJI DOMAIN CONTAINING 5 (JMJD5), LIGHT-REGULATED WD 1 (LWD1) and NOX (latin word for “night”) have a short period phenotype (Nagel and Kay, 2013).

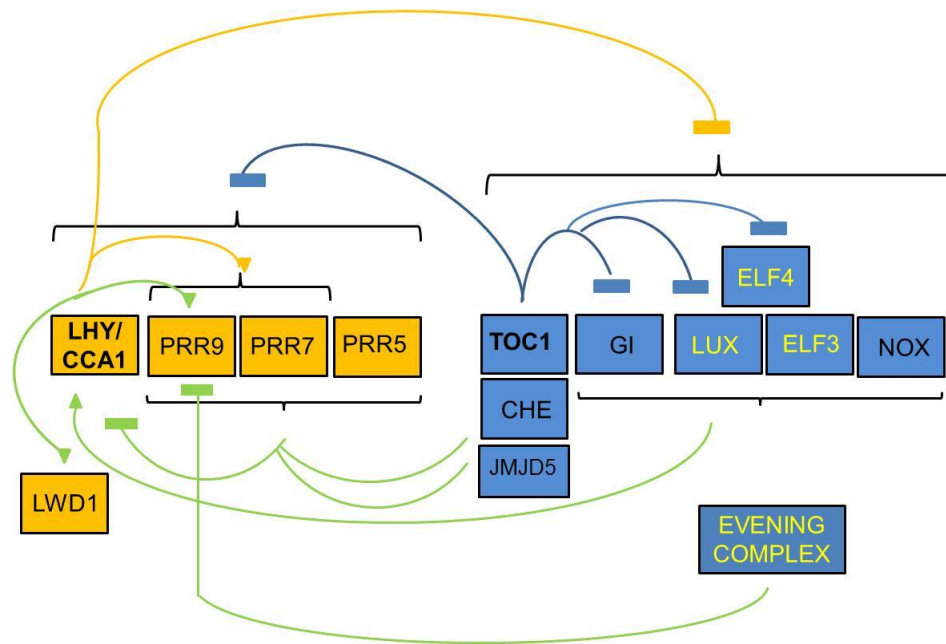


**Figure 1.5: A model of the circadian clock in *Arabidopsis* plants.** The core oscillator of the circadian clock is formed by the Myb transcription factors LATE ELONGATED HYPOCOTYL (LHY) and CIRCADIAN CLOCK ASSOCIATED 1 (CCA1) and a protein called TIMING OF CAB EXPRESSION 1 (TOC1). Other components are expressed throughout the day and night cycle and interconnect with the core oscillator to form multiple feedback loops. CCA1 and LHY repress the expression of TOC1, LUX, GIGANTEA (GI), EARLY FLOWERING 3 (ELF3), ELF4, CCA1, HIKING EXPEDITION (CHE), NOX and JUMONJI DOMAIN CONTAINING 5 (JMJD5) (blue boxes) by binding to their promoters. TOC1 inhibits expression of *CCA1*, *LHY*, *PRR9*, *PRR7*, *PRR5* (orange boxes) but also *LUX*, *ELF4* and *GI*. LUX, GI, NOX and ELF3 positively regulate *CCA1* and *LHY*. CHE and JMJD5 repress *CCA1*. PRR9, PRR7 and PRR5 inhibit the expression of *CCA1* and *LHY*. PRR9 and PRR7 are positively regulated by CCA1 and LHY. PRR9 is positively regulated by LIGHT REGULATED WD 1 (LWD1) and *LWD1* is activated by PRR9. ELF3, ELF4 and LUX were shown to form a protein complex (evening complex) that represses *PRR9* activation. Adapted from Nagel and Kay et al. (2013)

Key processes that are influenced by the circadian clock include the regulation of photosynthesis, hormone levels, nutrient uptake, transition to flowering, defense response and growth (Bell-Pedersen et al., 2005; Nozue et al., 2007; Mizuno et al., 2008; Wang et al., 2011).

One example of a direct mechanistic link between the circadian clock oscillator and one of these downstream pathways is the regulation of hypocotyl growth. The evening expressed clock proteins ELF3 and ELF4 form a complex with the DNA binding protein LUX. This complex, called the evening complex, regulates hypocotyl growth by repressing the expression of two transcription factors PHYTOCHROME INTERACTING FACTOR 4 (PIF4) and PIF5 that activate hypocotyl growth (Nusinow et al., 2011). In consequence, hypocotyl growth is inhibited in the early evening and repression is relieved later at night so that hypocotyl elongation can occur.

### ***1.7.2 Evidence for the regulation of starch degradation by the circadian clock***

The evidence for an involvement of the circadian clock in starch degradation comes from Graf et al. (2010).

Therein it was shown that plants grown from germination in diurnal cycles different from 24 hours cannot adapt their starch degradation rates to the length of the night. Plants grown in 28 hour cycles (14 hour light – 14 hour dark) degraded most of their starch at a near-linear rate during the first ten hours of the night, reaching a low level four hours before dawn. Starvation symptoms were detectable ten hours into the night, which is about 24 hours after the previous dawn. Plants grown in 17 hour cycles (8.5 hours light – 8.5 hours dark) degraded starch too slowly for the length of the night and still retained 40% of the end-of-day starch at the end of the dark period. When the night was extended, these plants exhausted their reserves about six hours later, thus, about 23 hours after the previous dawn. The experiments showed that starch degradation rates are set such that starch runs out about 24 hours after the previous dawn even if plants have been grown in photoperiods different from 24 hours. The maintenance of a 24 hour rhythm is a strong indication for a circadian clock controlled mechanism.

Further evidence supporting a role for the circadian clock came from the analysis of starch degradation rates in circadian clock mutants. The double mutant *cca1 lhy* lacks

core components of the circadian clock. Therefore, it has a circadian clock period different from wild-type. Its free running period is several hours shorter than that of wild-type plants. When grown in 24 h cycles (12 hour light – 12 hour dark), expression of clock and clock-regulated genes showed a phase advance of four hours. The mutant degraded its starch too quickly in comparison to wild-type plants when grown in 24 hour cycles. Starch reserves were exhausted three to four hours earlier than in wild-type, simultaneously with the dawn anticipated by the mutant. This shows that starch degradation rates are set such that starch runs out at the time at which plants anticipate dawn according to their endogenous clock.

It was shown that growth and survival of *Arabidopsis* plants are compromised if the period of the endogenous circadian clock does not match the length of the external light-dark cycle in which the plant is grown (Dodd et al., 2005). The reason for this is very likely to be an inappropriate rate of starch degradation at night. Wild-type plants grown in 28 hour cycles showed reduced growth in comparison to plants grown in 24 hour cycles. When *cca1 lhy* plants were grown in normal 24 hour cycles they grew slower than in 20 hour cycles (10 hour light – 10 hour dark). Thus, plants grew better if the point at which starch reserves were depleted closely matched the actual length of the night (Graf et al., 2010).

Taken together, the presented data established that starch degradation is controlled by the circadian clock. However, the signalling pathway that links outputs from the circadian clock to the control of starch degradation rates have not been identified yet.

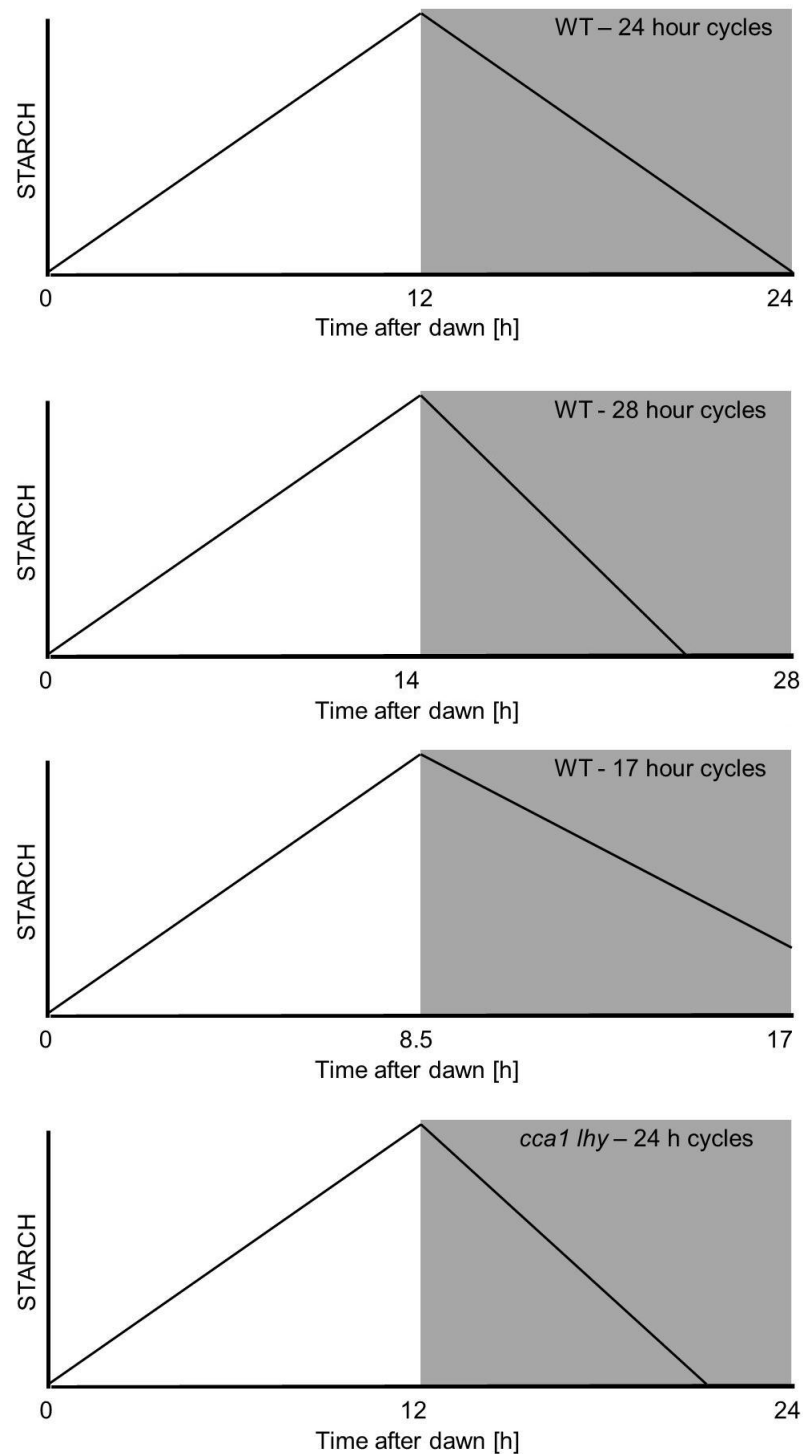


**Figure 1.6: Depletion of starch matches the time of dawn anticipated by the circadian clock.** The graphs illustrate daily turnover of leaf starch during growth in light (white background) and dark (grey background) periods of different length in wild-type plants (WT) and in the circadian clock mutant *cca1 lhy*. Graphs are based on data in Graf et al. (2010).

### 1.8 Measurement of the starch content

To allow starch to last precisely until dawn requires not only a mechanism to measure the length of the night, but also a mechanism to measure the starch content.

Starch degradation rates are adjusted according to the amount of starch available at the end of the day. This was demonstrated by Scialdone et al. (2013). They showed that reduction of the starch content by growing plants in lower light intensities for one day, results in a decrease of the starch degradation rate (**Figure 1.7**). Thus, starch is degraded faster if more starch is available at the end of the day.

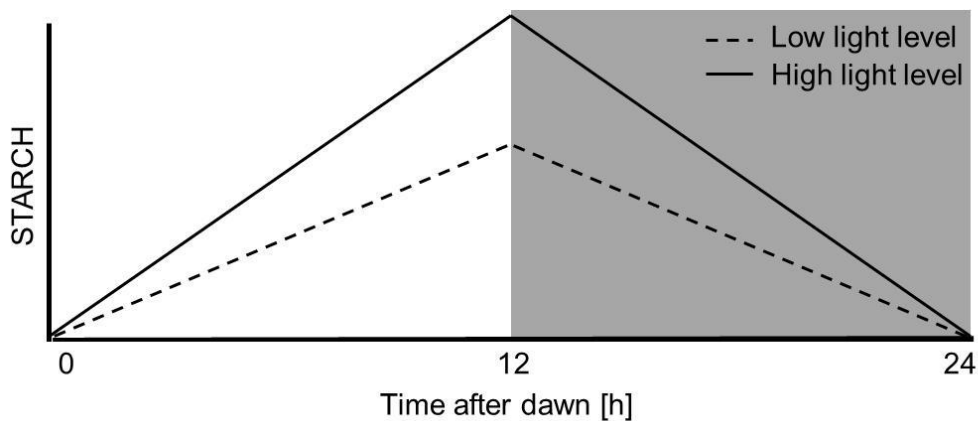


**Figure 1.7: Starch degradation rates in *Arabidopsis* adjust to variations in starch content.** Plants which were grown in 12 hour light – 12 hour dark cycles at  $90 \mu\text{mol m}^{-2} \text{s}^{-1}$  and then exposed to different day time light levels for one day (high light level:  $90 \mu\text{mol m}^{-2} \text{s}^{-1}$ ; low light level:  $50 \mu\text{mol m}^{-2} \text{s}^{-1}$ ) accumulated different amounts of starch. In both conditions, starch degradation rates were adjusted in a way that reserves were almost precisely used up by dawn. Thus, the starch degradation rate was lower if less starch was available. Based on Scialdone et al. (2013).

It is still unknown how plants could measure the amount of starch. In theory, starch contents could be indirectly measured by varying the concentration of a soluble signalling molecule in proportion to the amount of starch. This molecule could allosterically regulate enzymes of the starch degradation pathway. Such a molecule could be sequestered by the growing starch granule, so that its concentration would be inversely related to the amount of starch. Alternatively, the molecule could be produced by an enzyme of the starch synthesis pathway and its concentration would be

proportional to the flux through the pathway. A direct way of measuring the starch content could involve proteins that measure the curvature of the granule as it grows, or by mechanosensitive ion channels that sense membrane distortion caused by starch accumulation.

Alternatively, reversible phosphorylation of the starch granule is a potential point at which information about starch contents could be stored. The amount of granule-bound C6-phosphate shows large increases and decreases over the day-night cycle. Phosphate levels per unit mass of starch increase during the light period and decrease during the night. The amount of phosphate groups could therefore encode information about the starch content. If that was the case, flux through the pathway would be regulated according to the amount of starch by modulating the accessibility for enzymes that hydrolyse the granule (Scialdone et al., 2013).

### **1.9 Arithmetic division for the adjustment of starch degradation rates**

Scialdone et al. (2013) suggested that an arithmetic division computation between starch content and expected time to dawn is required for the adjustment of the appropriate starch degradation rate. They suggest a chemical kinetics model that explains how plants could implement arithmetic division by using analog post-translational chemical kinetics (Scialdone et al., 2013).

In this model, two hypothetical molecules “S” and “T” encode the information about starch content and time, respectively. Both molecules were suggested to be soluble and present in the chloroplast stroma. The concentration of the S molecule was proposed to be in proportion to the amount of starch at all times during the day while the T molecule has a daily pattern of change and “resets” around dawn. The S and T molecule concentrations must be arithmetically divided to set the appropriate starch degradation rate.

Two possible mechanisms were suggested that could achieve this division (**Figure 1.8**). In the first mechanism, the amount of T is proportional to the time remaining until dawn. The S molecule associates with the starch granule to allow starch degradation. This is possibly mediated by interaction of S with enzymes of the starch degradation pathway. The T molecule inhibits starch degradation by binding the S molecule and

thus removing it from the granule. In this way the division is implemented. In the second mechanism, the T molecule concentration is approximately proportional to  $1/(\text{expected time until dawn})$ . In this case the correct rate is set by multiplying S and T concentrations. This could be achieved if S and T form a complex that degrades the granule, e.g. by interacting and thus activating enzymes of the starch degradation pathway. Both models were tested on experimental data and provided equally good fits for starch degradation rates measured in different conditions, e.g. in response to an early or late night, or in response to changes in light intensity. The models also predicted starch degradation rates observed in the circadian clock mutant *cca1 lhy* equally well. Therefore, it could not be concluded which of the two mechanisms is more likely to happen in the plant.

The described model predicts that starch degradation rates are continuously computed during the night, rather than being set at the beginning of the night. This prediction was tested by interrupting the night with a period of light, ending five hours before the expected time of dawn. At the end of this light period, starch contents were comparable to end of day starch levels. The starch degradation rate in the remaining five hours of the night was faster compared to the starch degradation rate at the start of the night. This means that the starch degradation rate had reset due to a change in starch content and was not fixed to a rate that was set at the start of the dark period.

The model proposed by Scialdone et al. (2013) opens up questions concerning the nature of “S” and “T” molecules and about components of the starch degradation pathway that might be regulated by them. In **Chapter 7**, I will describe experiments that I did to find out which known components of the starch degradation pathway could be targets of the proposed mechanism.

In the following section, I will summarise information about mechanisms that regulate components of the starch degradation pathway and could potentially be mechanisms by which “S” and “T” molecules influence flux through the pathway.

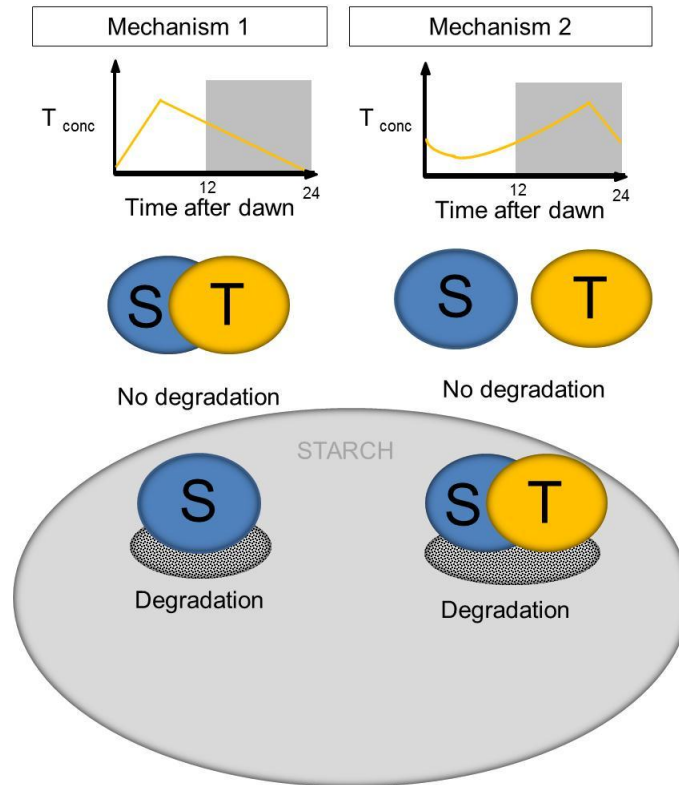


**Figure 1.8: The chemical kinetic model that explains arithmetic division during starch degradation.** Two hypothetical molecules S and T encode information about starch content and time until dawn. S was suggested to accumulate in proportion to starch and T encodes the information about the time until dawn. Two mechanisms were suggested by which plants could implement an arithmetic division of starch content and time until dawn to adjust the appropriate starch degradation rate. In these mechanisms S and T concentrations need to be divided (Mechanism 1), or multiplied (Mechanism 2). In the first mechanism, the concentration of T ( $T_{\text{conc}}$ ) is proportional to the time remaining until dawn. In the second mechanism, the concentration of T is inversely related to time until dawn. Both mechanisms require the T molecule concentration to reset just after dawn (Mechanism 1) or before dawn (Mechanism 2) every day. S, or S in complex with T respectively, allow degradation of the starch granule, possibly by interactions with enzymes of the pathway.

### 1.10 Regulation of the starch degradation pathway

It is not clear which enzymes are target of the mechanisms that regulate flux through the starch degradation pathway. It is possible that the activities of several enzymes are modified to achieve an adjustment of the starch degradation rate. Although most of the

enzymes involved in starch degradation have been identified, information about post-translational modifications that regulate their activity is sparse. The discovery of those mechanisms could help to answer questions about the control of starch degradation rates. In the following, I will summarise some of the information about regulatory mechanisms that have been discovered.

### ***1.10.1 Evidence for post-translational control***

The link between the circadian clock and the regulation of starch degradation rates does not appear to be on the transcriptional level. Transcripts of the key enzymes involved in starch breakdown show co-regulated expression which is subject to strong circadian control (Smith et al., 2004). The transcript levels of *GWD*, *PWD*, *SEX4*, *ISA3*, *AMY3*, *DPE1*, *DPE2*, *PHS1*, *PHS2* peak at dusk, fall throughout the dark period and rise within the light period. This could be interpreted as an increased need for starch degrading proteins at dusk. However, immunoblots showed that the observed changes in transcripts do not result in protein levels changing in the same way. This was shown for *DPE2*, *AMY3* and *GWD* (Smith et al., 2004; Yu et al., 2005; Yu et al., 2001). In fact, levels of these proteins appear not to change over the day-night cycle. This suggests that starch degradation is mainly regulated at the post-transcriptional level.

### ***1.10.2 Reversible glucan phosphorylation could control flux through the pathway***

It seems that the semi-crystalline structure of the granule is important for the control of flux through the pathway. Tight packing of amylopectin chains decreases the accessibility of substrates for hydrolysing enzymes and prevents unregulated starch breakdown. *Arabidopsis* plants lacking either *ISA1* or *ISA2* are unable to build up normal starch granules. The mutants accumulate mainly phytoglycogen rather than starch (**Section 1.4**). Interestingly, degradation of phytoglycogen is not adjusted according to the length of the night and does not follow a linear pattern. Phytoglycogen is degraded faster than starch and runs out after only eight hours of the night when *isa* mutants are grown in 12 hour light – 12 hour dark cycles (Zeeman, et al., 1998a; Delatte et al., 2005).

These results support the hypothesis that opening up the crystalline structure of the granule by reversible glucan phosphorylation is a means of controlling starch

breakdown. The initial step of the pathway and thus all subsequent steps could in theory be controlled primarily through the regulation of GWD, PWD, LSF2 and SEX4. Further evidence for the importance of starch phosphorylation in the regulation of starch degradation rates was given in Scialdone et al. (2013) and is described in **Chapter 7**. However, it is not clear how the activities of GWD, PWD, SEX4 and LSF2 are controlled to adjust starch degradation rates. There are indications that GWD could be regulated on the post-translational level by phosphorylation (Haezlewood et al., 2008), redox-regulation (Mikkelsen et al., 2005) and feedback inhibition (Hejazi et al., 2009). It was suggested that SEX4 is redox-regulated (Sokolov et al., 2006), but also controlled by feedback inhibition (Hejazi et al., 2010). However, none of these proposed regulatory mechanisms has been shown to be of importance *in vivo*, or rigorously established *in vitro*.

### ***1.10.3 Redox-regulation of enzymes of the pathway***

Redox regulation is potentially an important means of control of enzymes involved in starch metabolism. GWD (from potato), SEX4 and BAM1 were shown to be activated under reducing conditions *in vitro* (Mikkelsen et al., 2005; Sokolov et al., 2006; Sparla et al., 2006; Valerio et al., 2011). Also, it was also shown that AMY3 and LDA activity in crude plant extracts is redox sensitive when analysed in gel based assays (Glaring et al., 2012). The same study showed that ISA3 activity in *Arabidopsis* extracts was slightly decreased by treatment with oxidant. Also, a redox-sensitive beta-amylase activity that was attributed to BAM3 was identified after assaying beta-amylase activity in plant extracts of *bam1*, *bam3* and *bam1 bam3* mutants (Glaring et al., 2012).

That so many enzymes of the pathway appear to be redox sensitive seems counter-intuitive, because the chloroplast stroma is a more reducing environment when plants photosynthesise. This implies that enzymes of the starch degradation pathway are more active during the day than at night. Therefore, it was suggested that redox-activation of these enzymes is of relevance in starch degradation in response to abiotic or biotic stress or in heterotrophic tissues (Glaring et al., 2012).

The only enzyme shown to be involved in starch degradation during the day is BAM1 (Sparla et al., 2006). It was shown that wild-type plants express the enzyme in guard

cells where it degrades starch during the day. BAM1 was also shown to play a role in starch degradation in response to osmotic stress (Sparla et al., 2006; **Chapter 6**).

#### ***1.10.4 Protein complex formation between enzymes of the pathway***

A further possibility for post-translational control of the pathway could be protein complex formation. Direct evidence for physical interactions between enzymes of the pathway has so far only been found for LSF1 and BAM1 (Martin Umhang et al., personal communication, ETH Zürich; **Chapter 6**). It was proposed that LSF1 facilitates starch degradation by BAM1, by directing it to the starch granule surface. Thus, LSF1 might have a regulatory role in starch degradation.

The same could be true for BAM4, as the protein seems to have no catalytic activity, despite being required for starch degradation (Fulton et al., 2008). BAM4 was found to bind to starch granules, thus, it might interact with enzymes that degrade starch, but interaction partners have not yet been identified (Li et al., 2009).

Coiled-coil domains which are known to be involved in protein-protein interactions were predicted in GWD and AMY3 (Lohmeier-Vogel et al., 2008), but interaction partners of these enzymes have not been identified yet.

#### ***1.10.5 Feedback inhibition***

*Arabidopsis* plants lacking DPE1, DPE2 or MEX1 have lower rates of starch degradation than wild-type. Interestingly, none of these enzymes is involved in the direct hydrolysis of starch. Instead, they play a role in maltose metabolism and mutants lacking either of the enzymes accumulate abnormally high levels of maltose or maltotriose (Critchley et al., 2001; Chia et al., 2004; Niittylä et al., 2004). Thus, accumulation of intermediates of starch breakdown could feed back on enzymes that directly attack the granule. Beta-amylases could be a target for this feedback-regulation. It was shown that beta-amylase from pea is inhibited by high levels of maltose (Lizotte et al., 1990). Feedback inhibition was also demonstrated *in vitro* for GWD (from potato) and SEX4 (Mikkelsen et al., 2005; Hejazi et al., 2009; Hejazi et al., 2010). Both were inhibited by soluble, linear maltodextrins. Thus, accumulation of products of starch degradation could inhibit the pathway if the demand for carbon is decreased.

### ***1.10.6 Protein phosphorylation of enzymes of the pathway***

It has not yet been shown whether protein phosphorylation contributes to the control of starch breakdown. However, phosphorylation of 12 enzymes involved in starch metabolism was detected in a systems biology approach (Haezlewood et al., 2008; Kötting et al., 2012). Amongst them were GWD, AMY3, BAM1, BAM3, LDA, DPE2, MEX1 and the glucose transporter. The effect of phosphorylation on these proteins has not been shown yet, but it could modulate their activity, conformation, localisation or stability. Chloroplastic protein kinases and phosphatases that are responsible for the reversible phosphorylation of these enzymes are not known yet. Attempts were made to find them using a bioinformatics approach. Based on predictions of chloroplast transit peptides, 45 protein kinases and 21 protein phosphatases were found that could be located in the chloroplast (Schliebner et al., 2008). Mutant studies could help to identify the role of protein phosphorylation and dephosphorylation in the regulation of starch metabolism.

### 1.11 Experimental approach

The components which measure starch contents and link information about starch contents and time until dawn to adjust the appropriate starch degradation rate are still unknown. The aim of my work was to identify some of these components. I applied two different approaches:

Firstly, I used a forward genetic screen to identify mutants which are unable to adjust their starch degradation rates according to the length of the night. Such mutants would be expected to have mutations in genes that encode proteins which are necessary for normal rates of starch degradation. These proteins could be new components of the pathway as well as known proteins involved in starch degradation.

Secondly, I analysed how starch degradation rates in known mutants of the starch degradation pathway respond to an unexpected shortening of the night period. I took this approach to find out which known components of the starch degradation pathway are targets of the mechanism that controls starch degradation rates.

In the following results chapters (**Chapter 3-6**), I will describe the outcomes of the forward genetic screen and focus on the characterisation of two mutants with faster starch degradation. I will describe their phenotypes and the identification of the underlying mutations and hypothesise which functions the affected proteins could have in determining starch degradation rates. In the last results chapter (**Chapter 7**), I will present the results of the analysis of starch degradation rates in known starch degradation mutants.

## 2 Material and Methods

### 2.1 Plant material

The following mutants of the starch degradation and synthesis pathway were originally obtained from The Nottingham Arabidopsis Stock Centre (NASC) and are available from the seed archive kept as resource in the research group of Prof. Alison Smith: *amy3-2* (SAIL\_613 D12); *bam1-1* (SALK\_039895); *bam3-1* (CS92461); *bam4-1* (SALK\_037355); *est1-2* (Gabi\_031C11); *est1-3* (SALK\_040206); *est1-4* (SALK\_070292); *gbss-2* (GABI\_914G01), *gwd3* (SALK\_110814); *isa1* (SALK\_042704); *isa3-2* (Gabi\_280G10); *lsf1-1* (SALK100036); *sex1-3* (Yu et al., 2001); *sex4-3* (SALK\_102567)

Seeds of the mutants *amy3-2*, and *isa3-2* were obtained from the laboratory of Prof. Samuel Zeeman (ETH Zürich, Switzerland).

### 2.2 Plant growth conditions

#### 2.2.1 Growth on plates

Dry seeds were surface-sterilised overnight in a vacuum desiccator using chlorine gas which was generated by addition of 8 ml conc. HCl (12 M) to 200 ml thick bleach (Parazone, Jeyes). Then seeds were left in a laminar flow hood for 30 min. Dry seeds were sown on ½ MS agar plates, sealed with microporus tape and stored at 4°C for two days. Then they were grown in 16 hour light – 8 hour dark conditions, at 20°C and a light intensity of 200  $\mu\text{mol photons m}^{-2} \text{s}^{-1}$ . To select transformed *Arabididopsis* plants (2.9.3), seedlings were grown on agar plates containing the appropriate antibiotics.

#### 2.2.2 Growth on soil

Seeds were sown on soil (Levington's F2, Levington Horticulture, Ipswich, UK) in single pots (9 cm diameter) and stored in the dark at 4°C for two days to break seed dormancy. Then either transferred to growth cabinets (SANYO, Watford, UK) or a controlled environment room (CER) at 20°C and 75% relative humidity with 12 hour night – 12 hour dark cycles. The light intensity was about 160  $\mu\text{mol m}^{-2} \text{s}^{-1}$  in growth cabinets and about 180  $\mu\text{mol m}^{-2} \text{s}^{-1}$  in the CER. Plants were transferred individually to a

40- or 60-cell tray (21x35 cm) after ten days and usually grown for another 11 days before harvest. Plants for seed production were grown in CERs. Inflorescences were bagged as the siliques ripened, then plants were left to dry completely for about two weeks before seeds were collected.

### **2.3 Homogenisation of plant material**

After harvesting, tissue samples were usually immediately frozen in liquid nitrogen and stored at -80°C. Frozen material was ground into a fine powder in 2 ml microcentrifuge tubes containing a 4 mm diameter stainless steel ball (Bearing Supplies) using a mixer mill (Retsch) by shaking for 1 min at 22 strokes s<sup>-1</sup>. Samples were kept frozen by cooling the rack in dry ice.

### **2.4 Bacterial strains**

Generally, *E. coli* strains DH5 $\alpha$  and TOP10 were used for plasmid propagation and construction. Plasmids for site-directed mutagenesis were propagated in high transformation efficiency XL-10 Gold cells (Stratagene, Agilent Technologies). For the maintenance of GATEWAY vectors, *E. coli* DB3.1 was used, as it contains a gyrase mutation (gyrA462) that confers resistance to the lethal effect of CcdB (Bernard et al., 1994) *Agrobacterium tumefaciens* strain GV3101 was used for transformation of *Arabidopsis* plants by floral dipping (2.9.3).

Strain	Antibiotic resistance	Genotype/Properties	Source/Reference
<i>E. coli</i>			
DH5 $\alpha$	-	F $\phi$ 80 <i>lacZ</i> $\Delta$ M15 $\Delta$ ( <i>lacZYA-argF</i> )U169 <i>recA1 endA1 hsdR17</i> (rk $^-$ , mk $^+$ ) <i>phoA supE44 thi-1 gyrA96 relA1</i>	Hanahan, 1983
DB3.1	Streptomycin	F- <i>gyrA462 endA1 D(srI-recA) mcrB mrrhsdS20</i> ( <i>rB<math>^-</math>, mB<math>^-</math></i> ) <i>SupE44 ara14 galK2 lacY1proA2 rpsL20 xyl5 _leu mtl</i>	Hanahan, 1983
TOP10	Streptomycin	F $^-$ <i>mcrA (mrr<math>^-</math>hsdRMS<math>^-</math> mcrBC) 80lacZM15 lacX74 recA1 ara139</i> ( <i>ara-leu</i> )7697 <i>galU galK rpsL (Str<math>^R</math>) endA1 nupG</i>	Invitrogen, <a href="http://www.invitrogen.com">http://www.invitrogen.com</a>
XL-10 Gold	Tetracyclin	$\Delta$ ( <i>mcrA</i> )183 $\Delta$ ( <i>mcrCB<math>^-</math> hsdSMR<math>^-</math>mrr</i> )173 <i>endA1 supE44 thi<math>^-</math>1 recA1 gyrA96 relA1 lac Hte</i> [F $^+$ <i>proAB lacIqZ</i> $\Delta$ M15 <i>Tn10 Amy</i> ]	Agilent Technologies, <a href="http://www.home.agilent.com">http://www.home.agilent.com</a>
<i>Agrobacterium tumefaciens</i>			
GV3101	Rifampicin and Gentamycin	pMP90 (pTiC58 $\Delta$ T-DNA), genes for nopaline biosynthesis	Van Larebeke et al., 1973

**Table 2.1:** Bacterial strains

## 2.5 Media and Antibiotics

In **Table 2.2** the composition of media for plant and bacterial growth is described.

Medium	Composition
<i>Bacterial growth media</i>	
Luria-Bertani Broth (LB)	10 g l <sup>-1</sup> tryptone, 5 g l <sup>-1</sup> yeast extract, 10 g l <sup>-1</sup> NaCl, pH 7.0, agar was added for solid medium (final concentration 1.5% (w/v))
Super Optimal broth with Catabolite repression (SOC)	20 g l <sup>-1</sup> tryptone, 5 g l <sup>-1</sup> yeast extract, 0.5 g l <sup>-1</sup> NaCl, 0.186 g l <sup>-1</sup> KCl, pH 7.0. The medium was autoclaved before addition of glucose at a final concentration of 20 mM and MgCl <sub>2</sub> at a final concentration of 2 mM
<i>Plant growth medium</i>	
Murashige and Skoog (MS)	½ MS plant salt mixture (Duchefa Biochemie, Ipswich, UK), 50 mg l <sup>-1</sup> myo-inositol, 0.5 mg l <sup>-1</sup> thiamine, 0.25 mg l <sup>-1</sup> pyroxidine, 0.25 mg l <sup>-1</sup> nicotinic acid, 0.25 g l <sup>-1</sup> 2-[N-morpholino]-ethanesulphonic acid (MES), 0.8% (w/v) agar, pH 5.7 (with 1 M KOH)

**Table 2.2:** Media used for growth of plants and bacteria

Antibiotic	Final concentration	Solvent	Targets
Ampicillin	100 µg ml <sup>-1</sup>	dH <sub>2</sub> O	Gram-negative bacteria
Gentamycin	50 µg ml <sup>-1</sup>	dH <sub>2</sub> O	Gram-negative bacteria
Kanamycin	50 µg ml <sup>-1</sup>	dH <sub>2</sub> O	Bacteria, fungi, plants
Rifampicin	10 µg ml <sup>-1</sup>	methanol	Bacteria
Spectinomycin	100 µg ml <sup>-1</sup>	dH <sub>2</sub> O	Bacteria
Hygromycin	50 µg ml <sup>-1</sup>	dH <sub>2</sub> O	Bacteria, fungi, plants
Basta (Glufosinate)	100 µg ml <sup>-1</sup>	dH <sub>2</sub> O	Plants

**Table 2.3:** Antibiotic concentrations and usage.

## 2.6 Plasmids

Vector	Resistance	Description	Source
pCR8/GW/TOPO TA	Spectinomycin	Vector for cloning of DNA fragments with terminal 3' A-overhangs	Invitrogen
pGWB2	Kanamycin, Hygromycin	GATEWAY Binary vector for the expression of proteins in plants driven by the 35S promoter	Research Institute of Molecular Genetics, Shimane University, Japan

**Table 2.4:** Cloning vectors

## 2.7 Oligonucleotides

Oligonucleotides were from Sigma-Aldrich Ltd (Haverhill, UK, <http://www.sigmaaldrich.com/united-kingdom.html>) and resuspended in dH<sub>2</sub>O to obtain a 100 µM stock solution. All oligonucleotides used for genotyping, cloning, sequencing and map-based cloning are listed in the following tables.

Oligonucleotide	Purpose	Sequence 5'-3'
BAM1_SDM_Asn_1	SDM BAM1 (S132N)	GAAGAAAGGCGATGAAAGCGA ATTTGCAAGCGTTGAAGAGTGC
BAM1_SDM_Asn_2	SDM BAM1 (S132N)	GCACTCTTCAACGCTTGCAAATT CGCTTTCATCGCCTTCTTC
At1g42430_R8	Cloning cDNA EST1	TCATTGTGGTTGGTCAGGGG
At1g42430_F8	Cloning cDNA EST1	ATGAGCGAAATGGCGGCTAGC
BAM_cloningF	Cloning cDNA BAM1	ATGGCGCTTAATTTATCGCAT
BAM_cloningR	Cloning cDNA BAM1	CTAGTGAGTGAGAGCCACTGC

**Table 2.5:** List of primers used for cloning and site-directed mutagenesis (SDM)

Oligonucleotide	Mutant	Sequence 5'-3'
amy3-2_F	<i>amy3-2</i>	TAACGTCACCCGGTAAATCG
<b>amy3-2_R</b>	<i>amy3-2</i>	ATGAGACCTCCTGGCTCAAT
At1g42430_F6	SALK_040206 SALK_070292	TCTCGTCCGTATTTGTTTTGC
At1g42430_F7	<i>est1-2</i>	AATGTGAATGAAGCTGGCACT
<b>At1g42430_R6</b>	SALK_040206 SALK_070292	GGCACTGCAGAGGAAGAAGT
<b>At1g42430_R7</b>	<i>est1-2</i>	TTGCTTGCTTTTGTGCACTC
At1g42470_F2	<i>est1-1</i>	TCCAAGGTATGCTAATGGTTCA
At1g42470_R2	<i>est1-1</i>	ACCCCTGAAAGGTGACACAA
<b>BAM1_F5</b>	<i>bam1-1</i> and <i>bam1-2</i>	ACAAGGCTCACGGAACAGAT
BAM1_R5	<i>bam1-1</i> and <i>bam1-2</i>	AGACTCTCACGCAACAAAGAAA
BAM3_Tilling	<i>bam3-1</i>	TGAGAGTCTCCTCCCATGAC
BAM3_Tilling	<i>bam3-1</i>	GAACAAGTGGACCTCATGATG
<b>bam4-1_FW</b>	<i>bam4-1</i>	TGGACTACCACCGGTAAAGC
bam4-1_RV	<i>bam4-1</i>	GGCTGCCTTTGCAAGAATAG
GBSS_GABI_F	<i>gbss-2</i>	ACCAGGGAAGATTTGCCTTT
<b>GBSS_GABI_R</b>	<i>gbss-2</i>	TCCAGTCCCCTGTGAAAAAC
LSF1_F	<i>lsf1</i>	AGTAAGAGGAGCTCGCCGAC
<b>LSF1_R</b>	<i>lsf1</i>	TTCGAGAGCTCCTAAACCGG
R1-23-F	<i>sex1-3</i>	AGCAAAAAAGATCACTGGGCTCTGTATG
R1-7-R	<i>sex1-3</i>	CACAACAATGACATATCCGAC
sex4-3_F1	<i>sex4-3</i>	AAGGAAATCCCCAAACATCC
<b>sex4-3_R1</b>	<i>sex4-3</i>	TGTTTCGTCCACCTTTGTCTG
Gabi_LB	Gabi lines	CCCATTGGACGTGAATGTAGACAC
SALK_LB1	SALK lines	GCGTGGACCGCTTGCTGCAACT
SAIL_LB	SAIL lines	TAGCATCTGAATTCATAACCAATCT CGATACAC

**Table 2.6: List of primers used for genotyping.** The table lists gene specific primers used to amplify the wild-type sequence of genes affected in T-DNA insertion mutants. One of the primers of each pair (highlighted in bold) was used in combination with one of the three left border primers (LB) to amplify T-DNA inserts in Gabi-Kat, SALK or SAIL lines, respectively. Mutants containing point mutations were identified by amplification of the sequence flanking the mutation and subsequent restriction digest (Section 2.8.6).

Oligonucleotide	Purpose	Sequence 5'-3'
M13_F	Seq. PCR8 plasmid	CGACGTTGTAAAACGACGGCCAGT
M13_R	Seq. PCR8 plasmid	CACACAGGAAACAGCTATGACCATG
ISA2_F1	Sequencing <i>ISA2</i>	ATGGCGGTGATGATGCTTAT
ISA2_R1	Sequencing <i>ISA2</i>	ACCACGTTTCGTTGAGCTTCT
ISA2_F2	Sequencing <i>ISA2</i>	GTAGAGATCCGGACGGTCAA
ISA2_R2	Sequencing <i>ISA2</i>	ACGCCTCTTCCCCTTAAAAA
ISA2_F3	Sequencing <i>ISA2</i>	TCTGGAGCTCTTCGTGGAAT
ISA2_R3	Sequencing <i>ISA2</i>	CTGCAACGGTCTTCTGCTA
ISA1_F1	Sequencing <i>ISA1</i>	CCAGTTTCCTCCATCACACC
ISA1_R1	Sequencing <i>ISA1</i>	TACGCCATACCACAATGGAA
ISA1_F2	Sequencing <i>ISA1</i>	CACATACCAGGGTGTTGCAG
ISA1_R2	Sequencing <i>ISA1</i>	GGACCGACCAACTACCAGAA
ISA1_F3	Sequencing <i>ISA1</i>	GCTTGCTCAAAGGTAATGC
ISA1_R3	Sequencing <i>ISA1</i>	GGAAAACCGACGCTATCTGA
ISA1_F4	Sequencing <i>ISA1</i>	TGCTTGTTTGGTCCATGTGT
ISA1_R4	Sequencing <i>ISA1</i>	GGTACAGATTTGGGCTTCCA
ISA1_F5	Sequencing <i>ISA1</i>	TGTGTGCACTGTGCTGGATA
ISA1_R5	Sequencing <i>ISA1</i>	CCTGGAAGCAAAGCATAAGG
ISA1_F6	Sequencing <i>ISA1</i>	ATTGTGATGCTCCGGTTTTTC
ISA1_R6	Sequencing <i>ISA1</i>	TATCTGAAGCCGACCAAAGG
ELF3_F1	Sequencing <i>ELF3</i>	ATCTTTTTGGGCTCCACTTTTC
ELF3_R1	Sequencing <i>ELF3</i>	GATTTCAAGGCTTTAAGACAAATTAAC
ELF3_R2	Sequencing <i>ELF3</i>	CTTTATCTGCATCATTACATGAAG
ELF3_F2	Sequencing <i>ELF3</i>	AGATATTGGAACCTATGTTTCCTCG
ELF3_R2	Sequencing <i>ELF3</i>	TTGAAGAGGGTAAAAAAGGATTATTC
ELF3_F3	Sequencing <i>ELF3</i>	ATTCAGACTATTGCAAGGACATGA
ELF3_R3	Sequencing <i>ELF3</i>	ATTTCTAGACTCTTGTCTCAAGGAAGC
ELF3_F4	Sequencing <i>ELF3</i>	AGCATCAAGTCATGATAGAGTAAATGA
ELF3_R4	Sequencing <i>ELF3</i>	TTGGTGATAGTGAAATATGCCCT
ELF3_F5	Sequencing <i>ELF3</i>	TTTTGCTATTTTCATTGAGGACTG
ELF3_R5	Sequencing <i>ELF3</i>	ATGGTAACTAAAATTTAGATCCTGGG
ELF3_F6	Sequencing <i>ELF3</i>	GTAGGGAAATGTTTTTCCGAGG
ELF3_R6	Sequencing <i>ELF3</i>	GCAAATACTCTTTGTTGACTGTAATGA
ELF3_F7	Sequencing <i>ELF3</i>	ATCTTCTTAATGTGACTCTGTTTCTCA
ELF3_R7	Sequencing <i>ELF3</i>	GTCCTCCGAGGGAGACATT
ELF3_F8	Sequencing <i>ELF3</i>	CAGGAAATCATCAGCAATGGT
ELF3_R8	Sequencing <i>ELF3</i>	AACAGTTGTTCTTGTTCGTCGTT

**Table 2.7:** List of primers used for sequencing

Oligonucleotide	Purpose	Sequence 5'-3'
BAM1_F1	Sequencing <i>BAM1</i>	GTCCTGGGGATTCATTTTGG
BAM1_R1	Sequencing <i>BAM1</i>	TTCATGAAAGATCAATGATTCG
BAM1_F2	Sequencing <i>BAM1</i>	TGGATTGCAACAACCTTTTCAT
BAM1_R2	Sequencing <i>BAM1</i>	CGAAATCAAATCAATTTAATAACTCA
BAM1_F3	Sequencing <i>BAM1</i>	TCGAAAACACTACTTGTATTCATCAGAA
BAM1_R3	Sequencing <i>BAM1</i>	TTTTCTTACAAGCAAACGGTGA
BAM1_F4	Sequencing <i>BAM1</i>	GAACACTATCACCGTTTGCTTG
BAM1_R4	Sequencing <i>BAM1</i>	TTCTTCAATGGTCCCGATTC
BAM1_F6	Sequencing <i>BAM1</i>	ACGTGTACGGGAATTGATGA
BAM1_R6	Sequencing <i>BAM1</i>	ATAGCACTGGAAGGCTCCAA
BAM1_F7	Sequencing <i>BAM1</i>	ATTGGAGCCTTCCAGTGCTA
BAM1_R7	Sequencing <i>BAM1</i>	TCTCTCGAGGTTCTCCCTCA
BAM1_F8	Sequencing <i>BAM1</i>	GCACTTTGTGCACCAGAGAA
BAM1_R8	Sequencing <i>BAM1</i>	GAAATGCTATTTATTTGGCTTCA
At1g42430_F1	Sequencing <i>EST1</i>	AACCATGAATTGCGCCTAAC
At1g42430_R1	Sequencing <i>EST1</i>	CACTTTTCTCCCACCACGTT
At1g42430_F2	Sequencing <i>EST1</i>	CTCCGACGAGAAGATTCACC
At1g42430_R2	Sequencing <i>EST1</i>	TTGCTTGCTTTTGTGCACTC
At1g42430_F3	Sequencing <i>EST1</i>	ACCAAATGGGGAGACAAGTG
At1g42430_R3	Sequencing <i>EST1</i>	TCGAGGTTTGGGTAGACACC
At1g42430_F4	Sequencing <i>EST1</i>	TTTCGCACAATTCGAAAACA
At1g42430_R4	Sequencing <i>EST1</i>	CTCCCACCACTGTCAAGGAT
At1g42430_R5.1	Sequencing <i>EST1</i>	CCTGGGGTGATACTTCATGG

**Table 2.7:** List of primers used for sequencing

Oligonucleotide	Purpose	Sequence 5'-3'
Chr1_F_At1g30930	Rough mapping	TCAATGGGATCGAAACTGGT
Chr1_R_At1g30930	Rough mapping	ACTGAAAAGCGAGCCAAAAG
Chr1_F_At1g07810	Rough mapping	GTTACGGACAAAGAGCCTGAAAT
Chr1_R_At1g07810	Rough mapping	AAGCAGTCAATATTGCAGGAAGGG
Chr1_F_At1g49610	Rough mapping	ACATTTTCTCAATCCTTACTC
Chr1_R_At1g49610	Rough mapping	GAGAGCTTCTTTATTTGTGAT
Chr1_F_At1g72650	Rough mapping	TGTTTTTTAGGACAAATGGCG
Chr1_R_At1g72650	Rough mapping	CTCCAGTTGGAAGCTAAAGGG
Chr1_F_At1g09940	Rough mapping	TCATGACGTGAAGAAGAAGAAAA
Chr1_R_At1g09940	Rough mapping	CATATCGCTGCTACTAATTTTAAACAA
Chr2_F_At2g04066	Rough mapping	GGGATAATGGATAGGACTCACG
Chr2_R_At2g04066	Rough mapping	GCTGAGAAGGCAAGGAAGAG
Chr2_R_At2g14890	Rough mapping	GAAACTCAATGAAATCCACTT
Chr2_R_At2g14890	Rough mapping	TGAACTTGTTGTGAGCTTTGA
Chr2_F_At2g39010	Rough mapping	TCGTCTACTGCACTGCCG
Chr2_R_At2g39010	Rough mapping	GAGGACATGTATAGGAGCCTCG
Chr3_F_At3g11220	Rough mapping	GGATTAGATGGGGATTTCTGG
Chr3_R_At3g11220	Rough mapping	TTGCTCGTATCAACACACAGG
Chr3_F_At3g26605	Rough mapping	CCCCGAGTTGAGGTATT
Chr3_R_At3g26605	Rough mapping	GAAGAAATTCCTAAAGCATTC
Chr3_F_At3g50820	Rough mapping	GTTCATTAAACTTGCGTGTGT
Chr3_R_At3g50820	Rough mapping	TACGGTCAGATTGAGTGATTC
Chr4_F_At4g01710	Rough mapping	GGTTAAAAATTAGGGTTACGA
Chr4_R_At4g01710	Rough mapping	AGATTTACGTGGAAGCAAT
Chr4_F_At4g10360	Rough mapping	GCCCAGAGGAAGAAGAGCAAACACTAGC
Chr4_R_At4g10360	Rough mapping	TGGGAATTCATGAGAGAATATGTGGGAC
Chr4_F_At4g29860	Rough mapping	GCCAAACCCAAAATTGTAAAAC
Chr4_R_At4g29860	Rough mapping	TAGAGGGAACAATCGGATGC
Chr5_F_At5g22545	Rough mapping	TAGTGAAACCTTTCTCAGAT
Chr5_R_At5g22545	Rough mapping	TTATGTTTTCTTCAATCAGTT
Chr5_F_At5g42600	Rough mapping	CAGACGTATCAAATGACAAATG
Chr5_R_At5g42600	Rough mapping	GACTACTGCTCAAACCTATTCGG
Chr5_F_At5g63640	Rough mapping	GAGCATTTCACAGAGACG
Chr5_R_At5g63640	Rough mapping	ATCACTGTTGTTTACCATTA

**Table 2.8** List of primers used for rough mapping. Primer names indicate the marker position in the genome (chromosome number and locus of the closest gene).

Oligonucleotide	Purpose	Sequence 5'-3'
1-AC006423-5434F	Fine-mapping 436-1	TGCGGGAGTGTGATAGAATA
1-AC006423-5434R	Fine-mapping 436-1	TCCTCGAAAGATTCATTGAT
1-AC000375-7539F	Fine-mapping 436-1	GAATTCTGTAACATCCCATTGCC
1-AC000375-7539R	Fine-mapping 436-1	GGTCTAATTGCCGTTGTTGC
1-AC010675-8645F	Fine-mapping 436-1	GGACCGACGGTTACGAGAGT
1-AC010675-8645R	Fine-mapping 436-1	TAACGGGCCGTTGCAAGA
1-AC004146-8255F	Fine-mapping 436-1	CAATGAATTGCAAAAAGATGT
1-AC004146-8255R	Fine-mapping 436-1	TTTTCTGCGTAGAAAAAAC
1-AC006193-7914F	Fine-mapping 436-1	CTTCCACGGAGATTGACC
1-AC006193-7914R	Fine-mapping 436-1	TTCTGCAAACCTAACCCACT
1-AC004393-8313F	Fine-mapping 436-1	CTACTGATATCGCTGATAAG
1-AC004393-8313R	Fine-mapping 436-1	ATCGTGGTGCGCCATCAA
1-AC066689-7854F	Fine-mapping 436-1	GTTTGTTTTCTTGTCTATC
1-AC066689-7854R	Fine-mapping 436-1	TGTTTTTGAAAGAAAAGTAG
1-AC010852-7797F	Fine-mapping 436-1	TAGAAGGGGCACATATTAAG
1-AC010852-7797R	Fine-mapping 436-1	TTTGTTAATGTGCGTGTAAG
1-AC006193-7929R	Fine-mapping 436-1	AGTGATTGGATGGTCGGTATG
1-AC006193-7929R	Fine-mapping 436-1	TGGTTTTGGTGAGTTCTGCT
1-AC007230-7957F	Fine-mapping 436-1	GACAATAGATGGGTCAGACA
1-AC007230-7957R	Fine-mapping 436-1	CCAATAACCTGGACAACAAA
1-AC008047-7725F	Fine-mapping 436-1	TATAACCAGTTTTCAATCAAC
1-AC008047-7725R	Fine-mapping 436-1	GCTTCTTGTGGTCGTTTT
1-AC004512-7983F	Fine-mapping 436-1	AACCGAACGAAATGAATAG
1-AC004512-7983R	Fine-mapping 436-1	TCAGTTGAAACCGAGATTG
1-AC001229-7994F	Fine-mapping 436-1	GCCTGCTTTTGTTCCTTTT
1-AC001229-7994R	Fine-mapping 436-1	TCTCCCTCCCTTTTCTTGC
3-AB022217-2402F	Fine-mapping 400-3	ACCTGTTCACTCTATGTTAC
3-AB022217-2402R	Fine-mapping 400-3	GGGAATTATTAACATTATCA
3-AP000731-3394F	Fine-mapping 400-3	GGTAAGCTTCAGGTCGTGCT
3-AP000731-3394R	Fine-mapping 400-3	GTCAACACTTTGACCCGACA
3-AP002461-5399F	Fine-mapping 400-3	GAAGCGGTGTGGCTTGAAC
3-AP002461-5399R	Fine-mapping 400-3	GATGAACGCTTCAGGCCTAT
3-AP000419-2846F	Fine-mapping 400-3	TTTGTTTCGAGTTTAATACAT
3-AP000419-2846R	Fine-mapping 400-3	ATGTGTCACTAGTCGTATTC
3-AB025624-2876F	Fine-mapping 400-3	GCTTCTTCTCGTTGCGATCT
3-AB025624-2876R	Fine-mapping 400-3	TTCAAATGGTGAAGCAGTAA
3-AP001297-3676F	Fine-mapping 400-3	TCAAAAAGCTAAACGATACA
3-AP001297-3676R	Fine-mapping 400-3	GGCGATTATAGAGAAACAGA
3-AB028607-3997F	Fine-mapping 400-3	TTGCGTCTGGCAGATTGTTG

**Table 2.9:** List of oligonucleotides used for fine-mapping.

Oligonucleotide	Purpose	Sequence 5'-3'
3-AB028607-3997R	Fine-mapping 400-3	GGCCATATTTTGCTATGTTT
3-AP001304-3123F	Fine-mapping 400-3	CCAAGGGAATCCAATGAAGC
3-AP001304-3123R	Fine-mapping 400-3	CAATTCTGTATTATCGATGATGTG
3-AB023045-3172F	Fine-mapping 400-3	GTAGCCCAAAGCCGTACAG
3-AB023045-3172R	Fine-mapping 400-3	GAGATGCGTTTCACCTACAA
3-AB026647-03900F	Fine-mapping 400-3	ATGGTAAGCCAAAAGTCATC
3-AB026647-03900R	Fine-mapping 400-3	GTAATTCCAGACCTTGTAGA
3-AB026655-3510F	Fine-mapping 400-3	CAATTCGATCGTCATTACAG
3-AB026655-3510R	Fine-mapping 400-3	ATGTATCTCTTGGCTAAGTT
3-AP002048-3789F	Fine-mapping 400-3	AGAGCTGGAGTCAAGTATC
3-AP002048-3789R	Fine-mapping 400-3	CATCCAACCTCATGACAAG

**Table 2.9:** List of oligonucleotides used for fine-mapping. Primer names contain the name of the marker which was identified using the *Arabidopsis* mapping platform (<http://amp.genomics.org.cn/>).

## 2.8 Molecular Methods

### 2.8.1 Nuclei extraction from *Arabidopsis* leaves

All steps were performed on ice, with pre-cooled buffers and equipment. Buffers used in this protocol were: nuclei isolation buffer (NIB: 10 mM MES, pH 5.3, 0.2 M sucrose, 0.01% (v/v) Triton X-100 and 1 mM fresh DTT), lysis buffer (10% (v/v) Triton X-100 in NIB buffer) and NIBA (1:10 (v/v) protease inhibitor cocktail (Complete<sup>TM</sup>, Roche) in NIB). Frozen leaf tissue was ground with liquid nitrogen using a pre-cooled mortar and pestle. After a fine powder was obtained, the tissue was transferred to a new (room temperature) mortar and the powder was resuspended in NIB (7.5 ml g<sup>-1</sup> tissue). The homogenate was centrifuged for 6 min at 380 g at 4°C to sediment large cellular debris. The supernatant was filtered through a filter mesh into a pre-cooled 500 ml conical flask. Lysis buffer was added to the filtrate (0.25 ml ml<sup>-1</sup> of NIB). The mix was left on ice for 10 min and swirled every 2 min. The lysate was then centrifuged at 100 g for 5 min to precipitate large particles. The resulting supernatant was carefully transferred into a new 50 ml falcon tube, which was spun down in a table top centrifuge with a swinging bucket rotor at 2,600 g for 15 min at 4°C. The supernatant was removed and the pellet resuspended in NIBA (0.1ml g<sup>-1</sup> tissue). The minimal volume of NIBA used was always 0.5 ml. A 1.7 M sucrose solution was aliquoted into 1.5 ml tubes (0.8

ml/tube) and 0.6 ml of the lysate were applied to the top of the sucrose cushions through the side of the tube. To collect nuclei, samples were spun at 12,000 g for 10 min. The upper phase and the sucrose cushion were removed and the pellet washed twice in 1ml NIBA and spun for 5 min at 12,000 g. The pellet was finally resuspended in 100 µl of water as Triton-X in NIBA inhibits RNase activity. The nuclei pellet was then used for DNA extraction. DNA pellets were resuspended in about 7 µl of water and pooled. RNase treatment was carried out in a final volume of 50 µl for three hours at 37°C and DNA quality assessed using agarose gel electrophoresis (2.8.8).

### 2.8.2 DNA isolation from plants

DNA for genotyping and sequencing was isolated using Edwards buffer (200 mM Tris HCl, pH 7.5, 250 mM NaCl, 25 mM ethylenediaminetetraacetic acid EDTA, 0.5% (w/w) SDS). For large numbers of extractions, DNA isolation was carried out in 96-well racks containing strips of 8-well collection tubes (Qiagen, <http://www.qiagen.com/>). The tissue (about 50 mg) was harvested into the tubes which contained a 4 mm diameter stainless steel ball (Bearing Supplies, [www.bearing-supplies.co.uk](http://www.bearing-supplies.co.uk)). The racks were frozen at -80°C. The tissue was then homogenised by shaking the racks in a Genogrinder (SPEX Sample Prep, Metuchen, USA) at 200 strokes per minute for 30 s. Homogenised tissue was resuspended in 300 µl of Edwards buffer. Cell debris was pelleted by centrifugation at 5810 g for 10 min at room temperature. The supernatant (250 µl) was transferred into new tubes containing 250 µl isopropanol. The tubes were inverted several times, incubated at room temperature for 2 min, then centrifuged at 5810 g for 10 min at room temperature. The DNA pellet was washed in 300 µl 70% (v/v) ethanol and re-pelleted using the same centrifugation conditions. The pellet was dried for 20 min and resuspended in 100 µl dH<sub>2</sub>O. For smaller numbers of extractions on a smaller scale, DNA was prepared in 1.5 ml microcentrifuge tubes. The same volume of Edwards buffer was used, but centrifugation was carried out at 20,000 g in a microcentrifuge. DNA for *Arabidopsis* re-sequencing (2.8.15) and long term storage was isolated using the Qiagen Puregene® Kit according to the manufacturer's instructions. Cells were lysed with an anionic detergent in the presence of a DNA stabilizer. RNA was removed by treatment with an RNAase and other contaminants were removed by salt precipitation. In the last step, genomic DNA was recovered by

precipitation with alcohol and dissolved in hydration solution (1 mM EDTA, 10 mM Tris HCl, pH 7.5).

### 2.8.3 DNA extraction from bacteria

To isolate plasmid DNA from *E. coli*, bacterial cultures were grown in LB medium containing the appropriate antibiotics for 16-18 hours at 37°C in a shaking incubator and DNA isolated using the QIAprep Spin Miniprep Kit (Qiagen) according to the manufacturer's instructions.

### 2.8.4 Polymerase chain reaction (PCR)

For map-based cloning (2.8.5), sequencing (2.8.14), colony PCR and genotyping (2.8.6), the GoTaq Flexi Kit (Promega) was used for PCR. For cloning, Platinum™ High-Fidelity DNA polymerase (Invitrogen) was used. PCR reactions contained 50-500 ng of gDNA or 1 pg - 50 ng plasmid DNA as template, 1x polymerase reaction buffer, 0.1 U of GoTaq polymerase (or 0.05 U of Platinum™ High-Fidelity DNA polymerase), 0.4 μM of each primer and 500 μM dNTPs. PCR amplifications were carried out in a DYAD Thermal Cycler (Biorad). The standard PCR amplification protocol for GoTaq started with an initial denaturation step of 95°C for 1 min, followed by 25-35 cycles of: 94°C for 30 s, 50-60°C (Primer  $T_m$ -3°C) for 30 s, 72°C for 1 min  $kb^{-1}$  of target DNA product and a final elongation step at 72°C. For reactions containing Platinum™ High-Fidelity DNA polymerase, the initial denaturation step was carried out for 1 min at 94°C, followed by 25-35 cycles of 94°C for 30 s, 50-60°C (Primer  $T_m$ -3°C) for 20 s, 68°C for 20s  $kb^{-1}$  of target DNA product and 68°C for 2 min. For colony PCR, GoTaq polymerase was used and instead of DNA template, parts of a bacterial colony were added with a pipette tip to the PCR mix. An additional 10 min lysis and denaturation step at 95°C was added at the beginning of the PCR amplification protocol.

### 2.8.5 Map-based cloning

EMS mutants (Col-0 background) were out-crossed to the *Arabidopsis* ecotype Landsberg *erecta* (*Ler*). About 20 F<sub>1</sub> plants were allowed to self-pollinate and set seed. F<sub>2</sub> plants were grown for 10 days in 12h light-12h dark cycles and phenotyped to identify plants homozygous for the gene of interest. In *est1*, the mutation causing the

phenotype was recessive. Therefore, plants in the F<sub>2</sub> were selected if they had the early starvation phenotype. This means, individual plants were kept if they showed detectable luciferase-induced bioluminescence from the *pAt1g10070:LUC* reporter at the end of the normal night. Mutant *bam1-2* had a dominant mutation, therefore plants homozygous wild-type for the gene of interest were selected. This was done by choosing F<sub>2</sub> plants which did not show a bioluminescence signal at the end of an early night. The starvation reporter *pAt1g10070:LUC* is dominant, but segregates in the F<sub>2</sub> mapping population, because it is absent in the *Ler* parent. Luciferase expression in plants without bioluminescence expression was therefore assayed again after five hours into the extended night to confirm that the selected plants contained the reporter. Phenotyping of selected plants was repeated after seven days and in case of *bam1-2*, leaves of individual plants were harvested for an iodine stain, two hours before the end of the night. This was done to confirm that selected plants had no starch degradation phenotype, thus were wild-type for the mutation of interest.

DNA was extracted from individual homozygous F<sub>2</sub> plants. Genetic linkage of the mutant locus to chromosomal *Arabidopsis* regions was determined by using PCR-markers that are polymorphic between *Ler* and Col-0 accessions. To obtain a rough map position for the mutation of interest, each plant was genotyped using 16 genetic markers that were evenly distributed over the five chromosomes (**Table 2.8**). A recombination frequency was calculated for each marker by calculating the percentage of Col-0 (for *bam1-2*) or *Ler* (for *est1-1*) polymorphisms detected at that locus. Markers closely linked to the gene of interest are located in a region with low recombination frequency. The position of three markers which indicated the lowest recombination frequency narrows down the position of the gene of interest to an interval on one of the chromosomes. To obtain a smaller interval, new polymorphic markers upstream and downstream of the marker indicating the lowest recombination frequency in that interval were analysed. New markers were obtained using the *Arabidopsis* mapping platform (Hou et al., 2010; <http://amp.genomics.org.cn/>). The procedure was repeated and additional F<sub>2</sub> plants were phenotyped and genotyped to sufficiently narrow down the interval containing the mutation. Candidate genes in the interval were then sequenced (**2.8.14**) to look for EMS-induced point mutations.

### 2.8.6 Genotyping of mutants

Genotyping of F<sub>2</sub> plants to select homozygous double mutants from the cross of two mutants was carried out on gDNA by PCR-amplification using the primers listed in **Table 2.6**. Genotyping of T-DNA insertion mutants was carried out in two steps. In the first reaction, gene specific primers listed in the table were used to amplify gDNA of the wild-type sequence. This PCR gave a product in heterozygous mutants or wild-type plants, but not in homozygous mutants. In the second step, one gene specific primer was used in combination with either the GABI\_LB1, SALK\_LB1 or SAIL\_LB1 primer respectively. Which gene specific primer was used for the amplification in combination with the T-DNA specific primer was decided considering the orientation of the T-DNA insert in the gene and is indicated in the table. For mutants containing point mutations, gene specific primers were used to amplify the sequence flanking the mutation and a subsequent restriction digest revealed presence or absence of the point mutation after analysis by agarose gel electrophoresis. The mutation in *est1-1* deleted an *AccI* (New England Biolabs, <http://www.neb.uk.com/>) restriction site, which is present in the wild-type sequence. Therefore, only the PCR product of wild-type plants or heterozygous mutants was cut by the enzyme. The point mutation in *bam1-2*, created an *ApoI* (New England Biolabs) restriction site. The point mutation in *bam3-1* deleted a *BsrI* (New England Biolabs) restriction site, therefore only the sequence amplified in wild-type was cut by the enzyme. Mutant *sex1-3* contains a 33 bp deletion (induced by X-ray irradiation) and could therefore be identified by PCR amplification of the flanking sequence and analysis of the product size by agarose gel electrophoresis.

### 2.8.7 Restriction digestion

Restriction enzymes for mutant genotyping and for confirmation of successful cloning were usually obtained from New England Biolabs (NEB) or Invitrogen and reactions carried out according to the manufacturer's instructions. Usually, reactions were carried out in a final volume of 20 µl using 500 ng of DNA, 1 U of enzyme, the appropriate restriction buffer and (bovine serum albumin) BSA as required.

### **2.8.8 Agarose gel electrophoresis**

DNA fragments were mixed with 5 x loading dye (50% (v/v) glycerol, 0.05% (w/v) Orange G) and separated on 1% (w/v) agarose gels, prepared using TAE buffer (40 mM Tris-HCl, 20 mM acetic acid, 1 mM EDTA, pH 8.0) containing 0.01% (v/v) ethidium bromide. Gels containing 2% agarose were routinely used to separate PCR-products during map-based cloning, to allow visualisation of small size differences caused by deletions. The DNA separated on the gel was visualised through fluorescence of the ethidium bromide-DNA complex when exposed to ultraviolet (UV) light from a transilluminator and photographed using a Gel Doc 1000 system (Bio-Rad).

### **2.8.9 RNA extraction**

About 50 mg (equivalent to 1-2 mature leaves) of homogenised frozen leaf tissue were used for RNA extraction, using the RNeasy Plant Mini Kit (Qiagen) following the manufacturer's instructions. RNA was eluted from the RNeasy spin column using 30 µl of RNase-free dH<sub>2</sub>O and its quality assessed by measurements of absorbance at 260 nm and 280 nm using the NanoDrop ND-1000 spectrophotometer (NanoDrop Technologies, <http://www.nanodrop.com/>).

### **2.8.10 DNase treatment and cDNA synthesis**

RNAse samples were treated with RQ1-DNase (Promega, <http://www.promega.co.uk/>) using 1 µg of RNA, 1x RQ1 DNase buffer, 1 U RQ1 DNase, 0.5 µl of RNasin Plus RNase inhibitor (Promega) and DEPC treated water in a final volume of 10 µl. The mix was incubated at 37°C for 15 min. Samples were cooled on ice and 1 µl of 25 mM EDTA was added to stop the reaction. To inactivate DNase, samples were incubated at 65°C for 10 min and subsequently placed on ice. DNA-free RNA samples were used for cDNA synthesis. For the reaction, 2 µl of oligo(dT) 16-18 primer (50 ng µl<sup>-1</sup>) were added and the samples incubated at 70°C for 15 min, then cooled on ice. For reverse transcription, the SuperScriptIII Reverse Transcriptase (RTase) kit (Invitrogen) was used. To each sample, 4 µl of First Strand Buffer, 1 µl of dNTP mix (10 mM each), 1 µl DTT (100 mM) and 1 µl SuperScript III RTase were added. The samples were gently mixed by inversion and incubated at 47°C for 1 h. RTase was inactivated by incubation of the mix at 75°C for 10 min.

### 2.8.11 Cloning of PCR fragments into pCR8/GW/TOPO TA

PCR amplification of cDNA was carried out using Platinum™ High-Fidelity DNA polymerase (Invitrogen), which leaves 3'-A overhangs on the PCR products. Cloning of the PCR fragments was performed using a reaction mix containing: 0.5-3.5 µl PCR product, 1 µl salt solution, 0.5 µl vector (pCR8/GW/TOPO TA) and dH<sub>2</sub>O in a final volume of 5 µl. Samples were incubated 10 min – 1 h at room temperature and transformed into chemically competent *E. coli* TOP10 cells. Successful cloning was confirmed by colony-PCR.

### 2.8.12 LR reaction

The clone in the pCR8 entry plasmid is flanked by attL sites, and the GATEWAY cassette in the destination plasmid is flanked by attR sites. Recombination between sequences within attL and attR sites was catalysed by LR clonase enzyme (Invitrogen). For the reaction, 50-150 ng of the pCR8 plasmid containing the fragment of interest were mixed with the same amount of destination vector and TE buffer (10 mM Tris-HCl, 0.1 mM EDTA, pH 8.0) was added to a final volume of 4.5 µl. LR clonase (0.5 µl) was added and the sample mixed by pipetting. Samples were incubated at room temperature for 4-16 h. The reaction was terminated by addition of 0.5 µl proteinase K solution and incubation at 37°C for 10 min. *E. coli* TOP10 or DH5α cells were transformed (2.9.1) with 2.5 µl of the reaction mix and successful recombination was confirmed by colony PCR.

### 2.8.13 Site-directed mutagenesis

Site-directed mutagenesis of BAM1 was performed using the XL-single site kit (Stratagene, Agilent Technologies) according to the manufacturer's instruction. In this method, primers (Table 2.5) binding to the target sequence contain the mutated sequence and were designed to amplify the target sequence as well as the entry clone. Thus, a mutagenized and non-methylated, single stranded copy of the plasmid was generated. The old strand, consisting of methylated DNA, was digested using *DpnI*. The mutagenized plasmid was transformed into *E. coli* for amplification of the plasmid (2.9.1). The success of the mutagenesis was confirmed by sequencing of DNA extracted from bacterial cultures (2.8.3).

#### 2.8.14 DNA sequencing

PCR-products for sequencing were purified using the QIAquick®PCR-purification kit (Qiagen) or excised from agarose gels and extracted using the Qiagen QIAquick®Gel Extraction kit (Qiagen) according to the manufacturer's instructions. DNA was sequenced by cycle sequencing using the chain termination method in which dideoxynucleotide triphosphates (ddNTPs) serve as DNA chain terminators (Sanger et al., 1977). Reactions were carried out in a final volume of 10 µl containing about 100 ng of template DNA, 1 µl of 2 µM sequencing primer, 2 µl Big Dye sequencing buffer, and 2 µl BigDye version 3.1 sequencing mix (Applied Biosystems). The samples were run in the DYAD Thermal Cycler (Biorad) using following conditions: 25 x (96°C for 10s, 55°C for 5 s, 60°C for 4 min), 10°C for 10 min. Automated sequencing was performed by the Sequencing service at Genome Enterprise Ltd. (Norwich Research Park) on AbiPrism 3730XL and 3730 capillary sequencers (Applied Biosystems). The data were analysed using ContigExpress (Vector NTI Advance Suite 11, Invitrogen).

#### 2.8.15 Arabidopsis re-sequencing and data analysis

Resequencing of EMS mutant 436-1 (mutant A) was performed to identify the underlying point mutation. The mutant was out-crossed to a wild-type Landsberg *erecta* (*Ler*) plant and the phenotype of F<sub>2</sub> plants was analysed to select about 500 homozygous mutant plants. One leaf of each plant was collected and DNA prepared (2.8.2) after nuclei extraction (2.8.1). For re-sequencing, a sample of 5 µg of RNA-free gDNA was required. Library construction, cluster generation and sequencing of the sample on one lane of the Illumina GAIIx with 80 bp paired end reads was carried out as a service by Genome Enterprise Ltd. (Norwich Research Park, UK). The raw data were analysed by Martin Trick (Computational and Systems Biology, JIC, UK). Briefly, Maq v0.71 (Li et al., 2008) was used to align the reads against the TAIR8 Col-0 reference sequence and to generate a list of raw SNPs. The companion Maq.pl Perl script was then employed to filter these SNPs on quality criteria and the survivors used as input to a post-processing script which further filtered using a depth threshold of 5, which eliminated SNPs that corresponded to known Col-0/*Ler* polymorphisms (<http://signal.salk.edu/atg1001/data/>) and which retained only EMS candidates. The output of this script was a GFF2 file that was then loaded into a local instance of the GBrowse genome browser (<http://gmod.org/wiki/GBrowse#Downloads>), together with the TAIR8

pseudochromosome sequences and the TAIR8 gene model annotations, allowing visual inspection through a web browser. By programmatically interrogating the GBrowse MySQL database with a Perl script using `Bio::DB::GFF` methods, a genome-wide set of EMS candidates (G/A -> C/T in annotated coding sequence and inferred to induce either non-synonymous codon or donor/acceptor splice site mutations) could then be further refined based on chromosomal location.

## **2.9 Transformation of organisms**

### ***2.9.1 Transformation of Escherichia coli***

*E. coli* cells were transformed using heat shock. Competent cells (30 µl, stored at -80°C) were thawed on ice and 2 µl of the LR reaction mix (2.8.12) or 0.5 µl of plasmid DNA (2.8.3) were added and cells incubated on ice for 30 min. For the heat shock, the cells were heated to 42°C for 30 s and immediately transferred to ice. After 2 min, 1 ml of SOC medium was added and bacteria grown for one hour at 37°C with gentle shaking. The bacteria were plated on LB agar containing the appropriate antibiotics. Plates were incubated upside down at 37°C overnight. Colony PCR (2.8.4) was used to screen bacterial colonies containing the correct plasmid.

### ***2.9.2 Transformation of Agrobacterium***

Freeze/thaw competent *A. tumefaciens* cells (strain GV3101) were prepared by growth of bacteria in 60 ml LB (plus appropriate antibiotics) at 28°C to an OD<sub>600</sub> of 0.8, collection of cells by centrifugation (4,500 g, 5 min, 4°), two washing steps in 1 ml ice-cold 20 mM CaCl<sub>2</sub>, preparation of 50 µl aliquots and freezing of cells in liquid nitrogen. Cells were stored at -80°C and were thawed on ice. Five µl of plasmid DNA isolated from *E. coli* (2.8.3) were added and mixed with the cells by pipetting. The cells were incubated on ice for 5 min, then in liquid nitrogen for 5 min then thawed at room temperature. One ml of LB medium was added, followed by incubation at 28°C with shaking for 2 h. Cells were pelleted by centrifugation at 5,500 g for 5 min, re-suspended in 100 µl of LB medium and plated on LB agar containing the appropriate antibiotics. Plates were incubated upside down at 28°C for 48 h and success of the transformation assessed by colony-PCR.

### 2.9.3 *Stable transformation of Arabidopsis*

Plants were grown in the CER until flowering and production of secondary inflorescences. *A. tumefaciens* cells transformed with the desired plasmid (2.9.2) were grown at 28°C in 200 ml LB medium containing the appropriate antibiotics until an OD<sub>600</sub> of 1 was reached. Cells were pelleted by centrifugation at room temperature at 2,500 g for 15 min and then re-suspended in 200 ml infiltration medium (5% (w/v) sucrose, 0.05% Silwet® L-77 (GE silicones, <http://www.siliconeforbuilding.com/>), 0.1 mM acetosyringone, 3 mM MES, pH 5.5). Plant inflorescences were dipped into an *Agrobacterium* suspension in a beaker for two min, then placed into clear plastic bags and shaded for 24 hours, then grown in the glasshouse under ambient light conditions with supplemental lightening as required to obtain a 16 hour photoperiod. Transformants were selected by growing seeds on plates containing the appropriate antibiotic (2.2.1).

### 2.10 Cross-pollination of *Arabidopsis* plants

Flowers of the female parent were used for crossing before the anthers began to shed pollen onto the stigma. Therefore flowers were chosen in which the tips of the petals were just visible. From the male parent, flowers were chosen that were open and were visibly shedding pollen. Using scissors and forceps flowers just above and below the selected female flower and all siliques on the stem were removed. From the female flower all sepals, petals and anther were removed, the carpel was left intact. This was done using a magnifying device (jeweler's glass). Exposed carpels were left over night and on the next day, an open flower of the male parent was squeezed near the base with the forceps and then the surface of the anthers was brushed against the stigmatic surface of the exposed carpels of the female parent. For this step, a dissecting microscope was used. Successfully pollinated siliques were left to mature and harvested when they turned yellow. Siliques were dried at room temperature for two weeks before planting to increase germination rates.

## 2.11 Iodine stain of leaf starch

Whole rosettes or individual leaves were heated in 80% (v/v) ethanol at 80°C until decolourised, then washed with water. An I<sub>2</sub> and KI solution (Lugol solution, Sigma-Aldrich) was added for 5 min. Leaves were washed with water to remove excess stain and photographed.

## 2.12 Measurement of luciferase (LUC) activity

The luciferase (LUC) protein of firefly (*Photinus pyralis*) generates light with a spectral maximum of 560 nm by catalysing the oxidative decarboxylation of the substrate D-luciferin in the presence of ATP, O<sub>2</sub> and Mg<sup>2+</sup>. Total light emission of the sample is proportional to the luciferase activity in the sample. The short half-life of LUC protein allows analysis of temporal patterns of reporter gene expression in plants (Millar et al., 1992).

*Arabidopsis* seedlings were grown on soil and first assayed after 10 days of growth in 12 hour light - 12 hour dark cycles. Plants were sprayed with luciferin solution (0.8 mM luciferin (Biosynth, <http://www.biosynth.com/>), 0.01% (v/v) Triton-X-100) 24 hours and additionally one hour before the bioluminescence image was taken. About 10 ml of the luciferin solution were sprayed on each tray (21 cm x 35 cm). The plants were imaged using the NightOwl (LB 983) CCD camera system (Berthold Technologies, <https://www.berthold.com>). Imaging and data analysis were performed using either the Indigo software (Berthold Technologies; imaging settings: 1 min exposure time, 2x2 binning) or the WinLight Software (Berthold Technologies; imaging settings: 1 min exposure time, medium resolution, pixel binning 4x4, single frame accumulation) according to the manufacturer's instructions.

## 2.13 Determination of starch and phytoglycogen contents

### 2.13.1 Starch extraction from *Arabidopsis* leaves

The starch content in *Arabidopsis* leaves was determined using the perchloric acid (HClO<sub>4</sub>) method. One ml of ice-cold 0.7 M perchloric acid was added to frozen and

homogenised leaf tissue (**2.3**) (50 – 150 mg) and the sample re-suspended by vigorous vortexing. Two aliquots of 400 µl were transferred to separate 96 well plates on ice (1.2 ml storage plate, Thermo Scientific, <http://www.thermoscientific.com>) using cut tips. Then 300 µl of 100% ethanol were added to each sample and the plates sealed with a lid (sealing mats, Thermo Scientific). Plates were inverted and centrifuged at 3,000 g for 10 min to pellet the starch. The supernatant was discarded and the pellet washed in 600 µl of 80 % ethanol, and centrifuged as before. The starch pellet was taken up in 150 µl of water and the plates sealed with a thermo stable lid (Thermo Scientific), incubated at 90°C for 15 min and then allowed to cool on ice. Then 600 µl of 100% ethanol were added to each sample and plates were sealed, inverted and centrifuged as before. The supernatant was discarded and samples for 30 min. Pellets were re-suspended in 250 µl of dH<sub>2</sub>O and stored at -20°C until used for enzymatic starch digestion (**2.13.3**).

### ***2.13.2 Phytyglycogen extraction from Arabidopsis leaves***

For phytyglycogen extraction, frozen and homogenised leaf tissue (**2.3**) was re-suspended in 1750 µl of 0.7 M perchloric acid. Tubes were mixed by vortexing and 1500 µl of the sample were transferred into a new 2 ml microcentrifuge tube. The samples were centrifuged to separate starch from soluble phytyglycogen (10 min, 4°C, 3,000 g). A 600 µl aliquot of the supernatant was transferred into a new microcentrifuge tube and the pH adjusted to 5 using ice-cold 2 M KOH, 0.4 M MES, 0.4 M KCl. Precipitated potassium perchlorate was removed by centrifugation (3,000 g, 10 min, 4°C). Phytyglycogen was precipitated overnight at 4°C by addition of 600 µl of 75% methanol (plus 1% KCl) to 200 µl of the sample. Then tubes were centrifuged at 3,000 g for 10 min at 4°C. The pellet was air dried and subsequently re-suspended in 500 µl of dH<sub>2</sub>O. Samples were heated for 20 min in a water bath at 95°C and then stored at -20°C until used for phytyglycogen assay. An aliquot of 250 µl was used for enzymatic digestion (**2.13.3**).

### ***2.13.3 Enzymatic digestion of starch and phytyglycogen digestion***

For measurement of the starch and phytyglycogen content, samples were enzymatically digested to glucose and the amount of glucose released was quantified. To each of the starch samples of one replicate plate (**2.13.1**), 250 µl of a mix of 240 µl of NaOAc (0.2 M, pH 4.8), 9 µl of amyloglucosidase (10 µg µl<sup>-1</sup>, Roche, <http://www.roche.co.uk>)

and 1  $\mu\text{l}$  of alpha-amylase (1 U  $\mu\text{l}^{-1}$ , Megazyme, <http://www.megazyme.com>) were added. To the samples of the second replicate plate, a mix was added that contained water instead of the enzymes. This plate served as control. The plates were mixed and incubated over night at 37°C. Phytoglycogen samples were digested in the same way as starch samples.

#### **2.13.4 Glucose assay**

Prior to the assay, samples were mixed and spun down at 3,000 g for 10 min. Then 20  $\mu\text{l}$  (or 20  $\mu\text{l}$  of samples diluted in 0.2 M NaOAc, pH 4.8) were transferred in triplicates into 96-well microtitre plates. Then, 198  $\mu\text{l}$  of an assay mix (25 mM Hepes (pH 7.9), 1 mM  $\text{MgCl}_2$ , 1 mM ATP (Roche), 1 mM NAD (Roche) and 0.003 U  $\mu\text{l}^{-1}$  Hexokinase (Roche)) was added to each well. In the assay, glucose is converted into glucose-6-phosphate by the action of hexokinase. Glucose-6-phosphate is then further oxidised by glucose-6-phosphate dehydrogenase with reduction of NAD to NADH. NADH release is therefore proportional to the amount of glucose in the sample. To assay NADH concentration, the absorbance at 340 nm was determined using a plate reader (SPECTRAmax 340PC, Molecular Devices, [moleculardevices.com](http://moleculardevices.com)) before and 10 min after addition of 2  $\mu\text{l}$  (1 U) glucose-6-phosphate dehydrogenase (Roche).

### **2.14 Analysis of starch structure and composition**

#### **2.14.1 Purification of starch granules from Arabidopsis**

Leaf tissue (5 g) of 30-day old rosettes was harvested at the end of the day and immediately frozen in liquid nitrogen and stored at -80°C. Leaves were ground using mortar and pestle in four volumes of isolation buffer (100 mM 3-[*N*-morpholino]-propanesulphonic acid (MOPS), pH 7.2, 5 mM EDTA, 2.63 mM Na-metabisulphide, 0.05% (v/v) Triton X-100 and 5 mM DTT). The homogenate was filtered using two layers of Miracloth and the liquid phase centrifuged at 20,000 g for 10 min at 4°C. The pellet was taken up in 5 ml of isolation buffer and applied on top of 20 ml Percoll solution (90% Percoll, 10% isolation buffer) in a 30 ml Corex tube. The sample was centrifuged at 5,000 g for 10 min at 4°C to pellet starch. The pellet was re-suspended in 2 ml isolation buffer and applied to 10 ml of Percoll solution (90% Percoll, 10% isolation buffer) in a 15 ml Corex tube and the centrifugation step repeated as before.

The starch pellet was washed three times with 5 ml of water (centrifugation steps as before), then re-suspended in 1.5 ml 100% acetone and centrifuged at 20,000 g for 5 min at 4°C. Finally, the starch pellet was air-dried and stored at -20°C.

#### 2.14.2 Measurement of the amylose to amylopectin ratio

The amylose content of starch preparations was estimated based on the different absorption spectra of amylose and amylopectin in complex with iodine. Starch was re-suspended in water to a final concentration of 5 mg ml<sup>-1</sup>. The samples were gelatinised in a water bath at 95°C for 15 min. Gelatinised starch (5-20 µl) was added to one of two 1 ml quartz cuvettes, and an equal amount of water to the second cuvette as a reference sample. A 10% (v/v) I<sub>2</sub> and KI solution (Lugol solution, Sigma-Aldrich) was added to give a final volume of 1 ml. The cuvettes were mixed by inversion and the absorbance measured at 525 nm and 700 nm in a spectrophotometer against the reference cuvette. The A<sub>700</sub>/A<sub>525</sub> ratio (R) was determined and the amylose content was calculated according to the following formula (Zeeman et al., 2002):

$$\% \text{ amylose} = \frac{3.039 - (7.154 \times R)}{(3.048 \times R) - 19.192}$$

#### 2.14.3 Determination of starch chain length profile

The analysis of chain length profiles was performed as described by Streb et al. (2008) and is briefly described here. Starch samples (100 µg) prepared by perchloric acid extraction (**Section 2.13.1**) were debranched with *Pseudomonas sp.* isoamylase (Sigma-Aldrich) and *Klebsiella planticola* pullulanase (Megazyme) in 5 mM sodium acetate and then passed through sequential Dowex 50 and Dowex 1 (Sigma-Aldrich) mini-columns to remove the enzyme and charged compounds. The glucan chains were eluted with water, lyophilised and re-dissolved in 120 µL of water. High-performance anion-exchange chromatography coupled with pulsed amperometric detection (HPAEC-PAD) analysis was performed on a Dionex ICS-5000 system (Dionex, <http://www.dionex.com>) with a CarboPac PA-200 column (Thermo Scientific) using the following solutions: eluent A, 100 mM NaOH; eluent B, 150 mM NaOH and 500 mM sodium acetate. Glucans were separated at a flow rate of 0.5 mL min<sup>-1</sup> with the

following gradient programme: 0 -13 min, a linear gradient from 95 % A and 5 % B to 60 % A and 40 % B; 13 to 50 min, a linear gradient to 15 % A and 85 % B; 50 to 70 min, step to 95 % A and 5 % B (for column re-equilibration). Co-elution of known concentrations of glucose and malto-oligosaccharide standards in the range DP 1-7 allowed peak identification. Peak areas were determined using the Chromeleon software (Dionex).

Beta-limit glucans were prepared by incubation of the starch samples with barley beta-amylase (Megazyme) for 2 h at 37°C in 16 mM MES (pH 5.0) and 0.8 mM DTT. The resulting glucans were precipitated with three volumes of methanol and collected by centrifugation. The pellet was dissolved in water and prepared and subjected to HPAEC-PAD analysis as described for starch samples above.

#### ***2.14.4 Transmission electron microscopy (TEM)***

Plants were grown for 23 days in 12 hour light - 12 hour dark cycles and samples harvested six hours into the light period. The middle part of one leaf (omitting the main vein) was cut into small pieces of about 2 mm<sup>2</sup> using a razor blade and immediately fixed in 2.5 % (v/v) glutaraldehyde, 0.05 M Na cacodylate, pH 7.3. The samples were vacuum infiltrated and incubated in fresh fixing solution overnight, then washed in 0.05 M Na cacodylate for one hour at 4°C, dehydrated in an ethanol series and infiltrated with LR White resin by successive changes of resin/ethanol mixes over three days at room temperature. The last infiltration was carried out overnight in 100% in LR White resin. The resin was then polymerised at 60°C for 16h. Ultrathin sections of about 60 nm were prepared using a diamond knife (Leica KMR2, Leica, <http://www.leica-microsystems.com>) on a Leica UC6 ultramicrotome, collected in Formvar-coated 200 µm mesh nickel grids and examined under 200 kV using a FEI Tecnai G2 20 Twin transmission electron microscope (Philips, Eindhoven, The Netherlands). All embedding and ultrathin sectioning was performed by Sue Bunnell (John Innes Centre). Samples were viewed by TEM with the help of Sue Bunnell and Kim Findlay (John Innes Centre).

#### ***2.14.5 Scanning electron microscopy (SEM)***

Purified starch granules (2.14.1), were brushed onto the surface of double-sided, carbonated sticky stils (Leit-tabs, Agar Scientific Ltd., UK) which were attached to

SEM stubs (Agar Scientific Ltd., UK). The samples were sputter coated with gold for 75 s at 10 mA in an argon atmosphere using a high resolution sputter coater (Agar Scientific Ltd., UK). The stubs were then imaged in a FEI XL30 FEG SEM (Philips) at 3kV.

## **2.15 Native PAGE and SDS PAGE for mutant characterisation**

### ***2.15.1 Gels and running conditions***

The separating gel used for native PAGE contained 375 mM Tris-HCl pH 8.8 and 7.5% (w/v) acrylamide. If required, 0.1% (w/v) amylopectin were added to the separating gel to assay the activity of enzymes that act on amylopectin. Gel polymerisation was started by addition of 0.05% (w/v) ammonium persulfate (AMPS, Sigma-Aldrich) and 0.05% (v/v) tetramethylethylenediamine (TEMED, Biorad). The stacking gel contained 3.75% (w/v) acrylamide, 62.5 mM Tris-HCl, pH 6.8; 0.05 % (v/v) of AMPS and 0.05 % (v/v) of TEMED. Electrophoresis of native gels was carried in native running buffer (25mM Tris and 192 mM glycine) at 4°C and 100 V for 3.5 hours.

Gels used for SDS-PAGE were pre-cast NuPAGE® 4 – 12 % Bis-Tris gels (Invitrogen). SDS gels were run at 100 V for 30 min and then at 200 V until the required separation was achieved. For protein size estimation, prestained protein markers (10-230 kDa, New England Biolabs) were used.

### ***2.15.2 Preparation of extracts***

Proteins for native and SDS-PAGE were extracted from frozen homogenised leaf tissue (**Section 2.3**). The samples were weighed and re-suspended in extraction medium (100 mM MOPS pH 7.2, 1 mM ethylenediaminetetraacetic acid (EDTA), 2 mM DTT, 10 % ethanediol) at a tissue:medium ratio of 1:6 (w/v). Samples were centrifuged for 10 min at 20,000 g at 4°C. For native PAGE, sample buffer (60 % glycerol, 0.125 % bromophenol blue) was added to the supernatant at a ratio of 1:5 and 15 µl were loaded on the gel. For SDS-PAGE, the supernatant was diluted 1:1 (v/v) in 2x SDS-PAGE sample buffer (120 mM Tris HCl pH 6.8, 3.4% SDS (w/v), 12% glycerol (v/v), 200 mM DTT, 0.04% (w/v) bromophenol blue), the samples heated at 80°C for 10 min and 18 µl loaded on the SDS gel. If the crude extract was used instead of the supernatant, samples

re-suspended in extraction buffer were not spun down, but directly diluted 1:1 (v/v) in 2 x SDS-PAGE sample buffer, heated at 80°C for 10 min and then loaded on the gel.

### 2.15.3 Assay activity of starch metabolising enzymes after native PAGE

After separation of the samples, amylopectin containing gels were washed twice at 4°C for 15 min in incubation buffer (100 mM Tris, 1 mM MgCl<sub>2</sub>, 1 mM CaCl<sub>2</sub>, 1 mM DTT) and incubated in the same buffer for two hours at 37°C. After the incubation, gels were stained with I<sub>2</sub> and KI solution (Lugol solution, Sigma-Aldrich) to visualise the activity of amylopectin modifying enzymes.

### 2.15.4 MDH activity assay after native PAGE

Malate-dehydrogenase (MDH) activity in soluble protein extracts from rosette leaves was assayed on native gels (2.15.1 and 2.15.2). After protein separation, gels were incubated in a buffer containing 100 mM Tris-HCl, pH 8, 13.3 mM MgCl<sub>2</sub>, 0.008 mg ml<sup>-1</sup> phenazine methosulfate (PMS, Sigma-Aldrich), 0.33 mg ml<sup>-1</sup> nitroblue tetrazolium chloride (NBT, Sigma-Aldrich), 0.17 mg ml<sup>-1</sup> L-malic acid (Sigma-Aldrich) and 0.33 mg ml<sup>-1</sup> NAD (Roche). Incubation was carried out for ten minutes at room temperature and the reaction protected from light. In the assay, MDH activity in the gel converts the substrate L-malate to oxaloacetate resulting in the production of NADH from NAD. NADH production in the gel is visualised by coupling it to the reduction of NBT. PMS is used as an intermediate electron carrier. It is oxidised by NADH and reduces NBT to an insoluble blue-purple formazan (Figure 2.1).

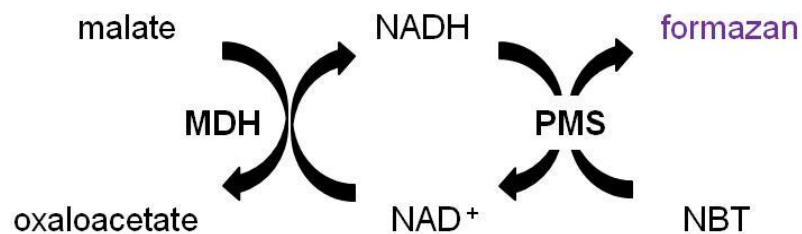


**Figure 2.1: Principle of colorimetric assay for MDH activity.** (after Mayer and Arnold, 2002)

### 2.15.5 Immunoblotting

The transfer of proteins to PVDF membrane (Thermo Scientific) was carried out using the Trans-Blot SD transfer apparatus (Bio-Rad) according to the manufacturer's instructions. Blotting was performed for one hour at 100 V at 4°C. Then the blot was washed in TBST (100 mM Tris, pH 7.5, 150 mM NaCl, 0.1 % (v/v) Tween 20) and incubated for one hour at 4°C in blocking solution (TBST containing 3% (w/v) dried milk powder). Blots were incubated over night at 4°C with primary antibody at a 1:1000 (v/v) dilution in blocking solution. Then the blot was washed six times for five min in TBST. The secondary antibody (anti-rabbit, conjugated to alkaline phosphatase) was used in a 1:10,000 dilution in blocking solution and the blot incubated with it for one hour at room temperature. The membrane was washed in TBST as before. To visualise alkaline phosphatase activity, BCIP®/NBT reagent (Sigma-Aldrich) was used.

For immunoblotting of native gels, gels were incubated twice for five min in warm (75 °C) native running buffer (25mM Tris and 192 mM glycine) containing 1% (w/v) SDS, rinsed in running buffer and then immunoblotted as described for SDS gels.

Antiserum specific for BAM1 protein was generated after immunisation of rabbits with the recombinant protein. It was obtained from Jychian Chen (Academia Sinica, Tapei, Taiwan). Antibodies specific for EST1 were obtained from David Seung (ETH, Zürich). Briefly, rabbits were immunised with purified recombinant AtEST1 protein, expressed in *E. coli*. The protein lacked the first 95 amino acids. Antibodies against EST1 were purified from serum obtained from terminal bleeds using affinity chromatography against NHS-activated sepharose (GE Healthcare), coupled to the recombinant protein used for immunisation. Bound antibodies were eluted by an acidic pH shift (pH 2.3) followed by immediate neutralisation (pH 7). The eluted antibodies were then desalted into PBS using NAP-5 columns (GE Healthcare) and used for immunoblotting at the specified concentrations.

## 2.16 Analysis of the circadian clock period

There are several ways to assay the circadian clock period in plants. Coupling of luciferase to clock-controlled promoters (Millar et al., 1995) is a well-established high-throughput method to assay clock function, but requires plants to be transformed with

the promoter:LUC-construct. Alternative ways to measure the expression of clock-controlled genes is to assay physiological clock-outputs such as hypocotyl elongation (Dowson-Day and Millar, 1999), elongation of the inflorescence stem (Agosti et al., 1997), rhythmic changes in leaf position (Engelmann et al., 1992) or stomatal opening (Somers et al., 1998), because they all display circadian rhythms. However, these methods do not allow high-throughput measurements and recently, measurement of delayed fluorescence was described as a new high-throughput assay for circadian clock function (Gould et al., 2009).

### ***2.16.1 Delayed fluorescence measurements***

Delayed fluorescence (DF) is luminescence that is produced from photosynthetic organisms, shortly after illumination (Strehler and Arnold, 1951). It occurs due to charge recombination in photosystem II leading to excitation of P680 and the subsequent emission of a photon (Rutherford et al., 1984). The amount of DF oscillates with an approximately 24-hour period. DF measurements were carried out as described in Gould et al. (2009). Arabidopsis seedlings were grown in groups of 15-20 in 96-well multiwell plates filled with MS medium containing 3% sucrose. Plants were entrained to 12 hour light – 12 hour dark cycles for nine days at 22°C. To measure DF rhythms in constant light, seedlings were transferred to the imaging system on the dawn of day ten and exposed to constant red-blue light ( $35 \mu\text{l m}^{-2} \text{sec}^{-1}$ ) for four days at 22°C. Delayed fluorescence images were collected every hour, by switching off the lights and collection of photons for one minute. DF was measured using an ORCA-11-BT 1024 16-bit low light charged coupled device (CCD) camera cooled to -80°C (Hamamatsu Photonics; <http://www.hamamatsu.com>). Image acquisition was automated and controlled by the WASABI imaging software (Hamamatsu Photonics; <http://www.hamamatsu.com>). DF in each picture was quantified using the software Metamorph (Molecular Devices Ltd; <http://www.molecular-devices.com>). BRASS software (<http://www.amillar.org>) was used to carry out fast Fourier transformed non-linear least squares (FFT-NLLS) analysis (Plautz et al., 1997) on each DF time course series to generate period estimates and relative amplitude error (RAE). The RAE is obtained by dividing the value of the amplitude error estimate by the value of the most probable amplitude estimated. RAE can range from zero (no error) to one (error equals amplitude value).

### **2.16.2 Leaf movement measurements**

Young leaves and cotyledons of *Arabidopsis* seedlings show a physiological change in position during the diurnal cycle. This circadian rhythm persists in constant light and can therefore be used to estimate the free-running period of the circadian clock in seedlings. Leaf movement analysis was carried out as described in Edwards and Millar (2007). Single seeds were grown on MS agar containing 3% sucrose and entrained to 12 hour light – 12 hour dark cycles at 22°C for 11 days. Then plants were transferred to constant white light in a growth chamber for another seven days at 22°C. A photograph of each plant was taken every 20 min using an automated CCD camera system (Ultrak, Carrollton, TX) and the position of the leaves analysed using the Metamorph software (Molecular Devices Ltd; <http://www.moleculardevices.com>). The position was plotted against time and a rhythm was revealed. An estimate of the circadian clock period was calculated on basis of the oscillation of the leaf using the software system BRASS (<http://www.amillar.org>) which carried out fast-Fourier transform-nonlinear least squares (FFT-NLLS) analysis of the period, phase, and amplitude of the circadian rhythm and the RAE.

### **2.17 Statistical analysis of significance**

The software package GenStat (10 th edition, VSN international) was used for statistical analysis. The unpaired two sample Student's t-test and Analysis of Variance (ANOVA) were used to calculate the significance of differences between data sets. Statistically significant differences were indicated by a p-value of 0.05 or less.

### 3 The Mutant Screen: Mutants with an early starvation phenotype

#### 3.1 Introduction

Starch degradation in *Arabidopsis* leaves is tightly controlled to avoid night-time carbon starvation (Graf et al., 2010). The rate of degradation is nearly linear and set in a way that reserves last almost precisely until dawn under a wide range of day and night lengths (Gibon et al., 2009; Graf et al., 2010; Smith and Stitt, 2007). To compute the appropriate starch degradation rate, it is necessary to integrate information about starch content and the time remaining until dawn (Scialdone et al., 2013). In **Chapter 1** I described how Alexander Graf established that the timing mechanism underlying starch degradation is the circadian clock (Graf et al., 2010). However, it is not known how plants sense the starch content. Also, the pathway that links outputs from the circadian clock and information about starch contents to set an appropriate starch degradation rate remains to be discovered.

To answer some of these questions, Alexander Graf developed a forward genetic screen to identify genes that could play a role in controlling starch degradation rates (PhD thesis Alexander Graf, 2009). With this screen, he expected to identify mutations in genes that encode components of the circadian clock or clock outputs; components of the starch measuring mechanism or enzymes of the starch degradation pathway that are regulated to set the appropriate starch degradation rate.

The screen is based on an *Arabidopsis* “starvation reporter line” that expresses luciferase (LUC) as a symptom of carbon starvation when starch is exhausted (Graf et al., 2010). This approach is a novelty because traditionally, iodine stains of leaf starch were used to identify mutants with defects in starch metabolism (Caspar et al., 1989; Zeeman et al., 1998b; Niittylä et al., 2006). To use iodine staining in a mutant screen is labour-intensive and requires more work, time and growth space than the LUC-based system. Also, it is relatively insensitive and not very robust because of natural leaf-to-leaf variation. The LUC-based system is more efficient, because mutants can already be screened at seedling stage and in a non-invasive way. Thus, the approach that Alexander Graf developed provided us with a tool for high-throughput screening of mutant populations.

In the following sections I will describe how Alexander Graf developed the *Arabidopsis* “starvation reporter line” and how he used it to identify “early starvation mutants”. I will describe the outcomes of the initial screen and the phenotypes of the mutants that were identified.

### 3.1.2 The *Arabidopsis* starvation reporter line

The starvation reporter line used for the screen was established by Alexander Graf (Graf et al., 2010). He stably transformed wild-type Col-0 plants with a construct that consists of a fusion of the starvation responsive promoter *pAt1g10070* and the luciferase (*LUC*) gene (*pAt1g10070:LUC*). The construct was designed by amplification of a 1,100bp long sequence upstream of the start codon of *At1g10070*, which was cloned into pGW-LUC in frame with the coding sequence of *LUC*.

#### 3.1.2.1 “Starvation” genes

The promoter of *At1g10070* was chosen because it is specifically activated in response to low sugar levels as microarray analyses revealed (Usadel et al., 2008). Two other genes that are expressed under similar conditions are *At3g59940* and *At1g76410*. We refer to them as “sugar-repressed” or “starvation genes” and use them as markers for the onset of starvation (Graf et al., 2010). The transcript levels of these genes increase under different carbon-limiting conditions like low atmospheric CO<sub>2</sub> (Bläsing et al., 2005); glucose starvation (Li et al., 2006) and sucrose starvation (Osuna et al., 2007). They are also up-regulated in plants that are subjected to an extended night as a consequence of depleted starch reserves (Usadel et al., 2008). The starvation reporter line carrying the *pAt1g10070:LUC* construct therefore expresses LUC when its starch reserves are exhausted. As a measure of luciferase expression, bioluminescence emitted from the plants following treatment with luciferin substrate can be visualised or quantified using a NightOwl camera system.

#### 3.1.2.2 Expression of starvation gene *At1g10070*

According to TAIR (Release 10), *At1g10070* encodes a chloroplast branched-chain amino acid aminotransferase. The protein is involved in amino acid catabolism, which provides an alternative carbon source in carbon starvation conditions (Usadel et al.,

2008). Basal expression of *Atlg10070* is low during the day and night cycle (Smith et al., 2004). Consistent with that, Alexander Graf could show that the starvation reporter line does not show luciferase-induced bioluminescence in normal day-night cycles (Graf et al., 2010). *Atlg10070* was found to be about 88 times up-regulated in *Arabidopsis* plants subjected to an extended night for six hours (Thimm et al., 2004). Consistent with that, luciferase-induced bioluminescence of the starvation reporter line strongly increases in an extended night. Photon counts were still low after about two hours after the subjective dawn, but increased rapidly after that (Graf, 2009). Starch reserves in *Arabidopsis* are almost precisely used up by dawn. This indicates that the lag-phase between starch exhaustion and the onset of luciferase-induced bioluminescence as starvation symptom is about two hours.

### *3.1.2.3 EMS-mutagenesis*

To introduce mutations into the DNA of the reporter line, T<sub>4</sub> seeds were treated with ethyl methane sulfonate (EMS) and the M<sub>1</sub> population was obtained after growing those plants for seed. M<sub>1</sub> plants were grown on soil and after 10 days, 7,500 seedlings were transferred to 1,500 pots, each of which contained five seedlings. Seeds of these five plants were pooled giving 1,500 pools of M<sub>2</sub> seed. These seeds were used for the screen. Plants of the starvation reporter line that were not treated with EMS were used as controls (Graf, 2009).

### *3.1.3 Rationale and set up of the screen*

Wild-type plants can adjust their starch degradation rate to unexpected changes in the length of the light period. If the night starts up to four hours earlier than normal (referred to as an “early night”), wild-type plants slow down their starch degradation rate so that reserves last until dawn. The reduction of the starch degradation rate compensates for the longer duration of the early night as well as for lower starch contents at the beginning of the early night (**Chapter 1**).

The screening protocol that Alexander Graf developed aimed at the identification of mutants that are not able to adjust their starch degradation rates according to the length of the night, despite being able to synthesise and degrade starch.

The rationale behind the screen was the following: If a mutant is not able to slow down its starch degradation rate in response to an early night, it will degrade its starch with the same speed as in the normal night. Therefore, it will exhaust its reserves before the end of the early night. Exhaustion of starch in the mutant will trigger expression of the starvation reporter and bioluminescence will be detectable earlier than in wild-type plants. Thus, the candidates arising from this screen will be referred to as “early starvation” mutants.

The screen was set up as follows: M<sub>2</sub> plants of the mutagenized reporter line were grown for ten days in 12 hour light – 12 hour dark cycles. Luciferase-induced bioluminescence was assayed at three time points (TP): (**TP1**) at the end of the normal night, (**TP2**) after 12 hours of an early night and (**TP3**) after 18 hours of the early night (**Figure 3.1**). To impose an early night, lights were switched off after only eight hours of light. Therefore, the subsequent night was four hours longer (16 hours long in total). For measurement of bioluminescence at TP3, the night was extended two hours beyond dawn.

Wild-type plants should not show luciferase-induced bioluminescence at any of the three time points, because they adjust their starch degradation rates according to the length of the night. Mutants with the desired phenotype should express luciferase at TP3 (or TP2 and TP3) but not at TP1. Such mutants degrade starch normally in a normal night, but cannot adjust their starch degradation rates in response to the early night. Mutants that expressed luciferase at all three time points were not considered as good candidates. The reason for this is that starvation in these plants might have occurred due to an inability to make or degrade starch. These mutants could also be mutated in the sugar-signalling pathway that activates the reporter, resulting in its constant activation.

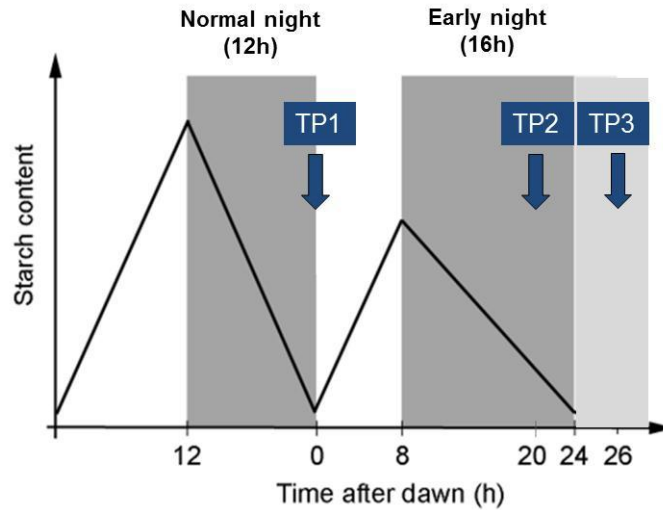


**Figure 3.1: Identification of early starvation mutants in a forward genetic screen.**

Seedlings of the mutagenized *Arabidopsis* starvation reporter line were grown for ten days in 12 hour light-12 hour dark cycles and LUC-induced bioluminescence was measured using a NightOwl camera system at three time points (TP): (TP1) at the end of a normal 12 hour night; (TP2) after 12 hours of an early night; (TP3) after 18 hours of an (extended) early night. Starch turnover during the screen as expected in wild-type plants is represented schematically.

#### **3.1.4 Results of the initial screen**

As part of his PhD project, Alexander Graf initially screened about 150 seedlings of each of 500 M<sub>2</sub> pools (i.e. one third of the EMS-mutant population) in the described way. Candidates with an early starvation phenotype were screened again after another week of growth to confirm the results obtained on seedlings. In total, 120 candidates had a reproducible early starvation phenotype, and were grown to maturity. When the plants were four weeks old, one leaf of each plant was harvested at the end of the day and at the end of the night for iodine stains of leaf starch. This was done to find out if the mutants were able to make and degrade starch. At the end of the day, 87 candidates had starch levels similar to wild-type, 29 had lower levels than wild-type and three had drastically reduced levels of starch and one candidate was starch-less. The end of night starch content was lower in 37 candidates and higher in eight candidates compared to wild-type.

Further interesting mutant phenotypes were observed: late flowering (40 candidates), early flowering (22 candidates), altered chlorophyll content (19 candidates), long petioles and narrow leaves (eight candidates), lost apical dominance (four candidates), sterile flowers (four candidates).

A subset of M<sub>2</sub> plants had a different starvation phenotype from the other candidates. These 12 mutants showed strong levels of *LUC* expression at TP1 and TP3, but not at TP2. This means, the plants displayed starvation symptoms 12 hours into the normal night, but not after 12 hours of the early night. When iodine stain of leaf starch was performed at the end of the day, eleven of these mutants had a slightly reddish stain and only one mutant had a normal blue stain. The reddish stain is characteristic for the isoamylase mutants *isa1* and *isa2* (**Chapter 1**). ISA1 and ISA2 were suggested to assemble as heteromultimeric complex to form the active enzyme (Delatte et al., 2005). In absence of one or both proteins, plants mainly accumulate soluble phytyloglycogen instead of starch. This soluble glucan has a reddish colour when stained with iodine solution (Zeeman et al., 1998; Delatte et al., 2005). In the following I will refer to the 11 candidates which had an *isa*-like starch stain as “*isa*-like” mutants.

All 132 candidates selected in the screen were allowed to set seed for analysis of the phenotype of M<sub>3</sub> plants. Only 114 M<sub>2</sub> plants produced sufficient M<sub>3</sub> seed for further experiments.

### **3.1.6 Aim**

In this chapter I describe how I discovered the genes underlying the phenotypes of several interesting mutants in the screen. At the start of my project I obtained M<sub>3</sub> seeds from 114 lines identified in the initial screen. I measured *LUC*-induced bioluminescence to select candidates with a reproducible and strong early starvation phenotype in the M<sub>3</sub> generation. To confirm that bioluminescence resulting from the expression of the starvation reporter correlated with a de-regulation of starch degradation, I measured starch contents in candidates with a strong early starvation phenotype. On basis of starch contents and other phenotypic characteristics, I decided which mutants I would carry on to map-based cloning to identify the underlying mutations. Some mutant phenotypes allowed predictions about the affected genes. If that was the case, I sequenced the candidate genes to look for EMS-induced mutations.

## 3.2 Results

### 3.2.1 Re-screen of $M_3$ mutant lines

In order to confirm the early starvation phenotype that Alexander Graf reported for  $M_2$  plants, I repeated the bioluminescence imaging for 103 candidates in the  $M_3$  generation. The plants were grown for 10 days in 12 hour light – 12 hour dark cycles and bioluminescence was detected using the NightOwl camera at three time points (TP) (**Figure 3.1**). To focus on mutants with a strong phenotype, I introduced an additional screening time point (TP4), at the end of the early night (16 hours of the early night). This time point lies two hours before TP3. Considering the lag-phase of LUC expression (**3.1.2.2**), mutants showing bioluminescence at this time should have exhausted their starch about two hours before the end of the early night.

All bioluminescence pictures that were taken in this experiment can be found in the Appendix (**Figure A1**). The result of the experiment, listing all mutant lines that were screened, can also be found in the Appendix (**Table A1**). For 71 lines, the early starvation phenotype seen in  $M_2$  plants could not be confirmed in the  $M_3$  generation. These lines either expressed *LUC* at all three time points or had no increase of the signal at TP3. Some of these lines had no uniform signal and only individual plants showed bioluminescence at the desired time points. All 71 lines were excluded from further analysis.

The remaining 31 lines had a strong and uniform bioluminescence signal at TP4 or TP3 (or TP2 and TP3) and no or little bioluminescence at TP1. They are listed in **Table 3.1**. Ten of these lines already gave a signal at the end of the early night (TP4). These were considered as the ones with the strongest phenotype. Unfortunately, there was not much seed available from line 410-2. The plants were very small and did not produce any  $M_4$  seeds. Therefore, this mutant could not be used in further experiments.

Line 436-1 had a slightly different phenotype from the other early starvation mutants. Bioluminescence was observed at TP1, TP3 and TP4 but not at TP2. This pattern is similar to that of the “*isa*-like” mutants, which will be described in section **3.2.2**. However, mutant 436-1 had no reddish end-of-day starch stain (**3.1.4**) and is therefore not an “*isa*-like” mutant.

No.	Line	TP4	TP3	No.	Line	TP4	TP3
1	116a		Yes	17	357-1	Yes	Yes
2	22-1		Yes	18	363-2		Yes
3	172-2		Yes	19	385-2		Yes
4	172-3		Yes	20	393-1		Yes
5	180-1		Yes	21	395-1		Yes
6	208-1		Yes	22	400-3	Yes	Yes
7	252-5		Yes	23	401-8		Yes
8	267-2	Yes	Yes	24	401-9		Yes
9	277-1		Yes	25	410-2	Yes	Yes
10	296-1	Yes	Yes	26	419-2		Yes
11	303-2		Yes	27	431-1	Yes	Yes
12	303-3		Yes	28	436-1	Yes	Yes
13	305-1		Yes	29	459-3	Yes	Yes
14	325-4		Yes	30	494-3	Yes	Yes
15	344-1	Yes	Yes	31	495-3		Yes
16	349-2		Yes				

**Table 3.1 Re-screen of M<sub>3</sub> mutant lines: List of candidates with an early starvation phenotype.** Bioluminescence signals of ten day old seedlings grown in 12 hour light – 12 hour dark cycles were analysed at four time points (TP): at (TP1) the end of the normal 12 hour night, (TP2) after 12 hours of an early night, (TP3) after 18 hours of an (extended) early night and for most mutant lines (TP4) after 16 hours of the early night. Mutant lines with strong bioluminescence signals at TP3 but not at TP1 time point were considered as confirmed early starvation mutants (green). All of these lines which already showed bioluminescence at TP4 were considered as candidates with a very strong early starvation phenotype (yellow). One line (436-1) gave strong bioluminescence signals at TP1, TP3 and TP4, but not at TP2 (highlighted in orange). Pictures taken with the NightOwl camera were used for the analysis of the starvation phenotype. They are shown in **Figure A1**.

### 3.2.2 Characterisation of “isa-like” mutants

The affected genes of some of the M<sub>2</sub> lines isolated in the initial screen could be predicted on basis of the mutant phenotype. A subset of 11 mutants isolated in the initial screen had a distinct starvation pattern but also a distinct colour of the end-of-day iodine stain (3.1.4). The stain indicated that they were affected in *ISA1* or *ISA2*. In the

following I will describe the phenotype of these lines and present the result of candidate gene sequencing.

To confirm the phenotype seen in M<sub>2</sub> plants, I analysed the bioluminescence pattern of the “*isa-like*” mutants in the M<sub>3</sub> generation at three time points (**Figure 3.1**). Consistent with the result on M<sub>2</sub> plants, strong bioluminescence signals were detected at the end of a normal 12 hour night (TP1), and after 18 hours of the early night (TP3), but no or only weak signals after 12 hours of the early night (TP2). The pictures taken with the Nightowl camera are presented in the Appendix **Figure A2**. For all 11 candidates, I could confirm the starvation pattern that was observed in the initial screen. The lines are listed in **Table 3.2**.

No.	Line	TP1&TP3
1	119	Yes
2	171-1	Yes
3	317-1	Yes
4	403-3	Yes
5	430-1	Yes
6	450-1	Yes
7	450-5	Yes
8	451-1	Yes
9	488-1	Yes
10	493-1	Yes
11	495-1	Yes

**Table 3.2: Bioluminescence expression of “*isa-like*” mutants.** The bioluminescence pattern of these M<sub>3</sub> mutant lines was analysed as described in **Table 3.1**. All mutants had strong bioluminescence signals at TP1 and TP3 but weak or no signal at TP2. The bioluminescence pictures from this experiment can be found in the Appendix (**Figure A2**).

Alexander Graf analysed an end-of-day starch stain of these 11 mutants in the initial screen and found that the plants had a reddish end of day starch stain (**3.1.4**). This indicated that they lacked one of the isoamylase proteins ISA1 or ISA2. To find out if isoamylase activity is missing in the mutant lines, I analysed soluble protein extracts from nine lines by native PAGE (**Figure 3.2**).

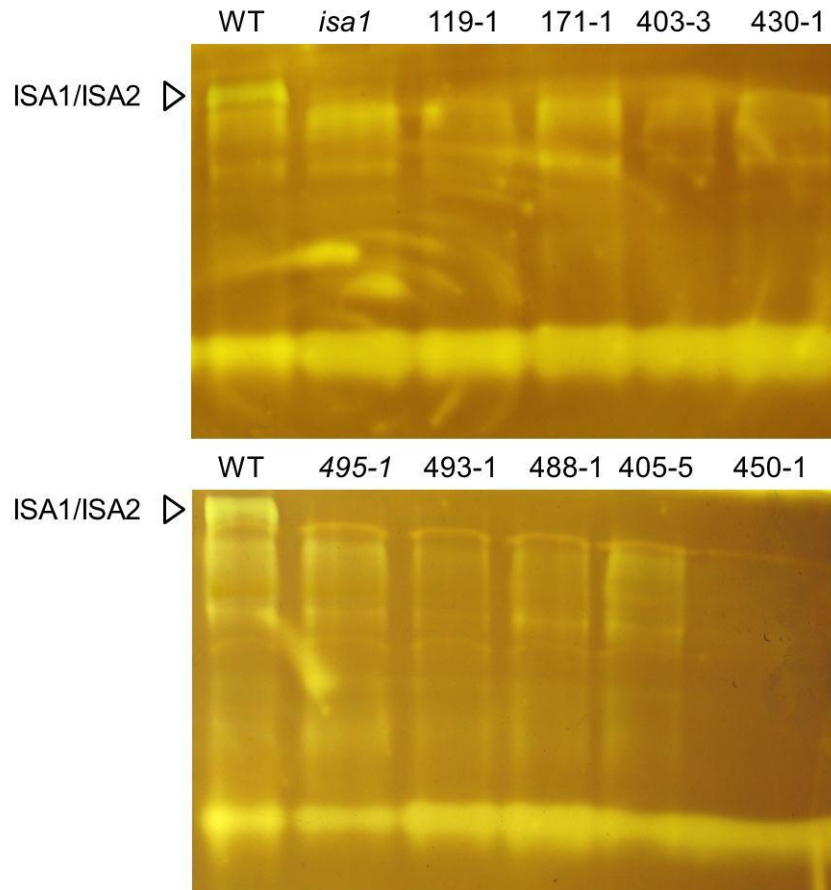


**Figure 3.2: Native activity gel for starch metabolising enzymes: “*isa*-like” mutants isolated from the mutant screen.** Plants of nine M<sub>3</sub> lines were grown for 26 days in 12 hour light -12 hour dark cycles and leaves harvested in the middle of the day. Soluble protein extracts were separated by native PAGE on gels containing amylopectin. The gels were incubated for two hours and then stained with iodine solution to reveal enzyme activities. The position of isoamylase activity (ISA1/ISA2) in the gel is indicated in the wild-type (WT) sample. A mutant lacking isoamylase 1 (*isa1*) was used as control.

In this method, the soluble fraction of plant extracts is separated under native conditions by PAGE. The gels contain amylopectin that serves as substrate for starch metabolising enzymes in the plant extract. To visualise the activities of enzymes that act on starch, the gel is stained with iodine after an incubation time of two hours. Discoloured areas reveal the activity of starch metabolising enzymes. Isoamylase activity is visible as a distinct band on top of the gel. This activity was missing in isoamylase (*isa1*) mutants.

The nine mutant lines I analysed also lacked this activity band, indicating mutations in one of the *ISA* genes.

To confirm that these lines have mutations in *ISA1* or *ISA2*, I sequenced the genes after isolation of gDNA from eight of the “*isa-like*” mutants. All of them carried point mutations (G/A transitions) in either *ISA1* or *ISA2*. These mutations either introduced premature stop codons or 3’ intron splice site mutations (**Table 3.2**). Thus, the phenotype of the mutants was caused by a mutation of *ISA1* or *ISA2*.

No	Line	Mutated gene	Mutation	Position gDNA [bp]	Effect
1	119	n.d.	n.d.	n.d.	n.d.
2	171-1	ISA1	AG to AA	3122	Splicing failure
3	403-3	ISA2	TGG to TGA	1749	Stop codon
4	430-1	ISA1	TGG to TGA	5727	Stop codon
5	450-1	ISA1	TGG to TGA	476	Stop codon
6	450-5	ISA1	TGG to TGA	476	Stop codon
7	488-1	ISA1	AG to AA	416	Splicing failure
8	493-1	ISA2	TGG to TGA	423	Stop codon
9	495-1	ISA1	TGG to TGA	4494	Stop codon

**Table 3.2: EMS-type point mutations found in eight mutants isolated in the screen.**

The table shows G/A transitions found in *ISA1* or *ISA2* genes after sequencing gDNA of eight of the “*isa-like*” mutants that were isolated in the screen. The mutations are given with their position upstream of the ATG start codon in the *ISA1* or *ISA2* gene sequence respectively. The mutations affected either 3’ intron splice sites or introduced premature stop codons as indicated.

Isoamylase mutants mainly accumulate soluble phytyglycogen instead of starch (Delatte et al., 2005). To find out why mutants lacking isoamylase displayed starvation symptoms after 12 hours of the normal, but not after 12 hours of the early night, I quantified phytyglycogen contents in an *isa1* mutant during a normal and an early night (**Figure 3.3**).

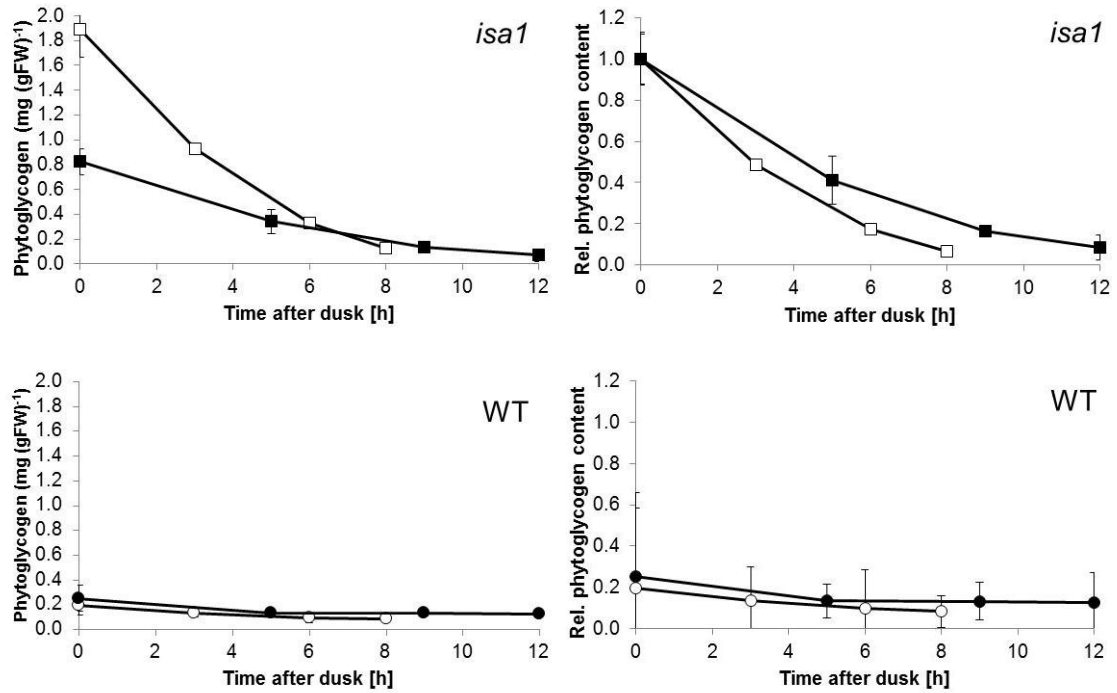


**Figure 3.3: Phytyglycogen contents in *isa1* and wild-type plants (WT) during normal and early nights.** Plants were grown for 22 days in 12 hour light – 12 hour dark cycles and phytyglycogen contents determined for eight hours of the normal night (open symbols) and 12 hours of the early night (closed symbols). On the right, the phytyglycogen contents are shown in relation to end-of-day phytyglycogen. Data are means of measurements on six individual rosettes, error bars are s.e.m, where not visible they are smaller than the symbol.

As expected, phytyglycogen contents in wild-type plants were very low throughout the night in both conditions and did not change significantly. At the end of the 12 hour day, the mutant had about 1.9 mg gFW<sup>-1</sup> of phytyglycogen. Most of it was degraded during the first eight hours of the normal night. At the beginning of the early night, the mutant had accumulated less phytyglycogen, because the light period was four hours shorter. However, phytyglycogen was used up more slowly in the subsequent night. After nine hours of the early night phytyglycogen contents were slightly higher than after eight hours of the normal night. Plotting the relative phytyglycogen contents (in relation to the end of day value) indicated that the rate at which phytyglycogen was degraded in the early night was much slower than in the normal night. This adjustment of the degradation rate could explain the starvation phenotype of the mutant. Starch contents were not measured in this experiment, but should be taken into account as well.

Therefore, this experiment should be seen as preliminary. Previous research on starch contents in *isa* mutants is discussed in **3.3.1.1**.

### **3.2.3 Putative circadian clock mutants**

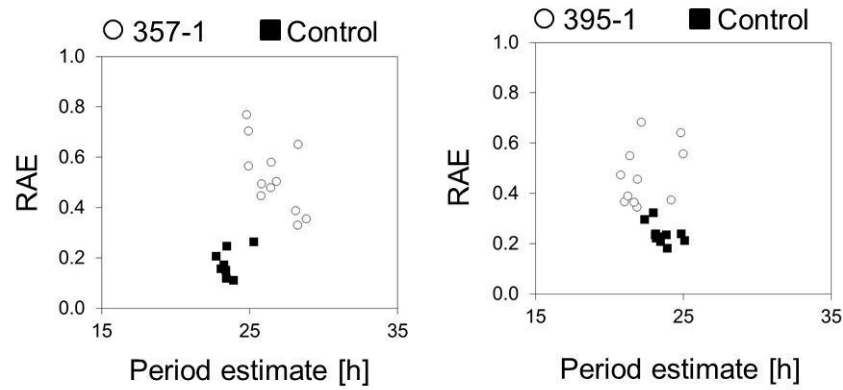
#### *3.2.3.1 Analysis of the circadian clock period in 357-1 and 395-1*

Some of the M<sub>2</sub> plants from the initial screen showed an early flowering phenotype. For two of these mutants (357-1 and 395-1), I could confirm the early starvation phenotype in the M<sub>3</sub> generation (**Table 3.1**).

We expected that the screen would identify mutants that are defective in their circadian clock and thus not able to measure the time until dawn (**3.1**). The circadian clock controls photoperiodic flowering time in *Arabidopsis* (Suarez-Lopez, 2001). Several circadian clock mutants have flowering time phenotypes, e.g. *elf3*, *elf4* or *lhy* (Zagotta et al., 1996; Schaffner et al., 1998; Doyle et al., 2002). Therefore we speculated that some of the early flowering mutants identified in the screen could have defects in the circadian clock.

To find out if candidates 357-1 and 395-1 are circadian clock mutants, I analysed the free-running period of the circadian clock in these two candidates using facilities at the University of Liverpool in the lab of Anthony Hall. I estimated the circadian clock period of both mutants by delayed fluorescence analysis (**Figure 3.4**).

Delayed fluorescence (DF) is weak light-emission from photosystem II that is detectable shortly after illumination of plants or other photosynthetic organisms (Strehler and Arnold, 1951; Rutherford et al., 1984). It is detectable within 50 seconds after illumination, but decays rapidly after 10 seconds. The intensity of light emission varies in the diurnal cycle and is under circadian control. Just like other circadian clock outputs, the rhythmicity of DF levels persists in constant light. Therefore, DF measurement can be used as a tool to estimate the free running period of the circadian clock (Gould et al., 2009).



Genotype	Period [h]	RAE
Control 1	23.5	0.2
Control 2	23.7	0.2
357-1	26.6	0.5
395-1	22.3	0.5

**Figure 3.4: Clock period estimates of two early starvation mutants as determined by delayed fluorescence analysis.** Twelve groups of seedlings of mutant and control plants (starvation reporter line) were grown on MS media containing 3% sucrose and entrained to 12 hour light - 12 hour dark cycles for nine days at 22°C. Then they were transferred to constant red-blue light ( $35 \mu\text{mol m}^{-2} \text{s}^{-1}$ ) to analyse the free-running period of the circadian clock. Pictures for analysis of DF were taken each hour for 96 h, by switching off the lights and analysing the amount of photon emission for one minute. The DF rhythm was estimated from these data using the software BRASS (<http://www.amillar.org>). Each data point represents the analysis of a group of seedlings of about 15-20 plants. Period estimates are plotted against the relative amplitude error (RAE). The RAE indicates rhythm robustness which can vary from 0 (a perfect fit to the cosine wave) to 1 (not statistically significant). The table shows the mean values for all groups of seedlings of each genotype (n=10-12). The data for each mutant were obtained in separate experiments.

For the analysis, the two mutant lines and plants of the starvation reporter line (control) were grown for nine days in 12 hour light – 12 hour dark cycles and then transferred to constant light. DF emission was quantified for four days from 12 groups of seedlings. The data was used to determine the period of each DF rhythm for every group of seedlings and an error (RAE), which indicates the robustness of the rhythm.

Control plants had a period estimate of roughly 24 hours in both experiments. The DF period estimate for mutant 357-1 was about three hours longer, indicating that this mutant has a longer circadian clock period. The period estimate for 395-1 was about one hour shorter, indicating a slower running circadian clock in that mutant line. However, the RAE of the period estimates was higher for both mutants than for wild-type. This means that the DF rhythm in the mutants was not as robust as in the control.

### 3.2.3.2 Sequencing of *ELF3* in 357-1

The growth phenotype of mutant 357-1 was very similar to that of the circadian clock mutant *elf3* (Alexander Graf, personal communication). This mutant is characterised by elongated hypocotyl growth, elongated petioles and early flowering (Zagotta et al., 1996; Reed et al., 2000; Liu et al., 2001). Since mutant 357-1 had an altered circadian clock period, we speculated that it could be affected in *ELF3*. Therefore, Alexander Graf sequenced *ELF3* (At2g25930) in gDNA isolated from 357-1 and found a point mutation in the coding sequence. The G/A transition was located 3042 bp downstream of the start codon. The mutation affected codon “TGG” that encodes Trp-471 in the protein sequence. It was mutated into a premature stop codon “TGA”. Thus, mutant 357-1 turned out to be an *elf3* mutant.

### 3.2.3.3 Analysis of starch degradation in 357-1 and 395-1

Mutant 357-1 and 395-1 had defects in the circadian clock and mutant 357-1 was shown to be mutated in *ELF3*. Both mutants had an early starvation phenotype. Mutant 357-1 had detectable levels of *LUC*-induced bioluminescence at the end of the early night, but not at the end of a normal night. Mutant 395-1 had a weaker early starvation phenotype and showed *LUC*-induced bioluminescence only after an extension of the early night by two hours. To find out if the reason for the expression of the *LUC* reporter is premature exhaustion of starch at the end of the early night, I measured starch contents of both mutants in normal and early night (**Figure 3.5**). Both mutants had end of day starch levels comparable to control plants (starvation reporter line).

The rate of starch degradation was not linear in mutant 357-1. During the first part of early and normal night, starch degradation followed a pattern similar to that of wild-type plants. However, in both conditions the mutant slowed down its starch degradation

rate during the last two to four hours of the night. In the last two hours, starch contents decreased only slightly, especially in the early night. The mutant had about three times more starch left than control plants at the end of the normal night. At the end of the early night, it had about four times more starch than control plants.

The pattern of starch degradation of mutant 395-1 was nearly identical to wild-type in both conditions. In the last two hours of the early night, starch degradation in the mutant slowed down slightly. Therefore, it had about twice as much starch then the control left at the end of the early night.

Thus, the reason for LUC-induced bioluminescence at the end of the early night in both mutants was not premature exhaustion of starch reserves. However, an arrest of starch degradation could be the explanation for expression of the starvation reporter in both mutants.

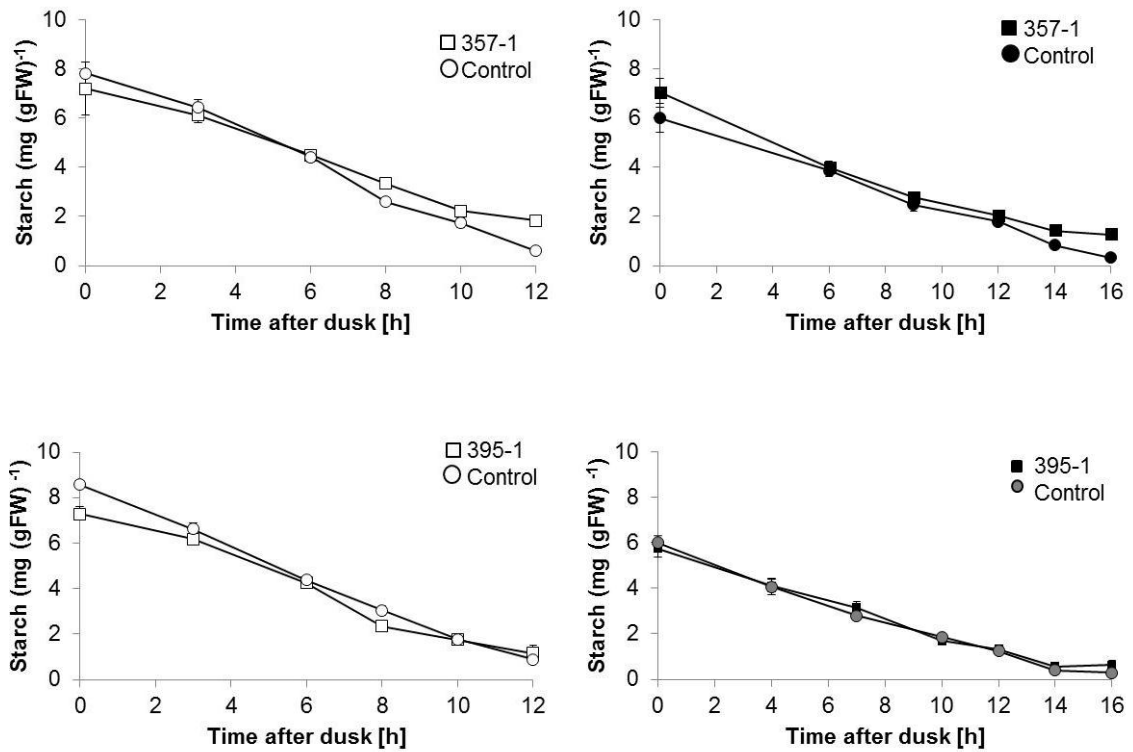


**Figure 3.5: Starch degradation in mutant 357-1 and 395-1 in normal and early night.** Plants were grown in 12 hour light – 12 hour dark cycles for 24 (357-1 and control) or 25 days (395-1 and control). The starch contents were analysed in normal (left) and early night (right). Data are means of measurements on five individual rosettes. Error bars are s.e.m., where not visible they are smaller than the symbol. Control plants are of the starvation reporter line.

### 3.2.4 Analysis of starch degradation in other early starvation mutants

In section 3.2.1 I described the identification of 31 candidates with a strong or weak early starvation phenotype. Two of these with early flowering were shown to have circadian clock defects and one of them was confirmed as an *elf3* mutant. Here, I describe further analysis of the remaining mutants for which there were no obvious clues about the nature of the affected gene.

To find out if the early starvation phenotype of the remaining candidates correlated with an abnormal starch degradation rate, I measured the starch contents of selected M<sub>3</sub> lines throughout a normal night and the early night (**Figure 3.6**). This was done for eight lines with strong early starvation phenotype (yellow and orange in **Table 3.1**) and for

five lines with the weaker early starvation phenotype (green in **Table 3.1**). In the Appendix (**Figure A3**), the data for five mutants with weak early starvation phenotype can be found. There were no indications that any of the five mutants with weak early starvation phenotype were degrading starch significantly faster or slower than wild-type plants.

Of the eight mutants with strong early starvation phenotype, the first four lines (267-2; 344-1; 431-1; 459-3) degraded starch at a similar rate to control plants. The mutants slowed down their starch degradation rates in response to the early night and did not exhaust their starch reserves before dawn. Starch degradation mainly followed a linear pattern in all four mutants. However, in mutants 267-2 and 495-3, a change of the degradation rate was observed in the early night. The rate slowed down towards the end of the night. These differences were subtle and have to be reproduced in further experiments.

The remaining four lines (296-1; 400-3; 436-1; 494-3) had starch degradation patterns clearly different from wild-type. All of them degraded starch faster than the control in normal night as well as early night. The end of day starch content of line 400-3 was about 45% higher than in the control. End of day starch levels in 494-3 were slightly reduced. Mutant 296-1 and 436-1 had end of day starch contents similar to the control. Especially in the normal night, starch degradation rates of all four mutants did not follow a linear pattern. The mutants had faster starch degradation rates in the beginning of the night compared to the end of the night. In the normal night, starch was exhausted prematurely only in mutant 436-1 and 494-3. In the early night, all mutants exhausted their starch quicker than the control. Mutant 296-1 exhausted its starch about two hours before the end of the early night, mutant 400-3 about four hours before end of the early night, mutant 436-1 about four to six hours before the end of the early night, mutant 494-3 about six hours before the end of the early night.

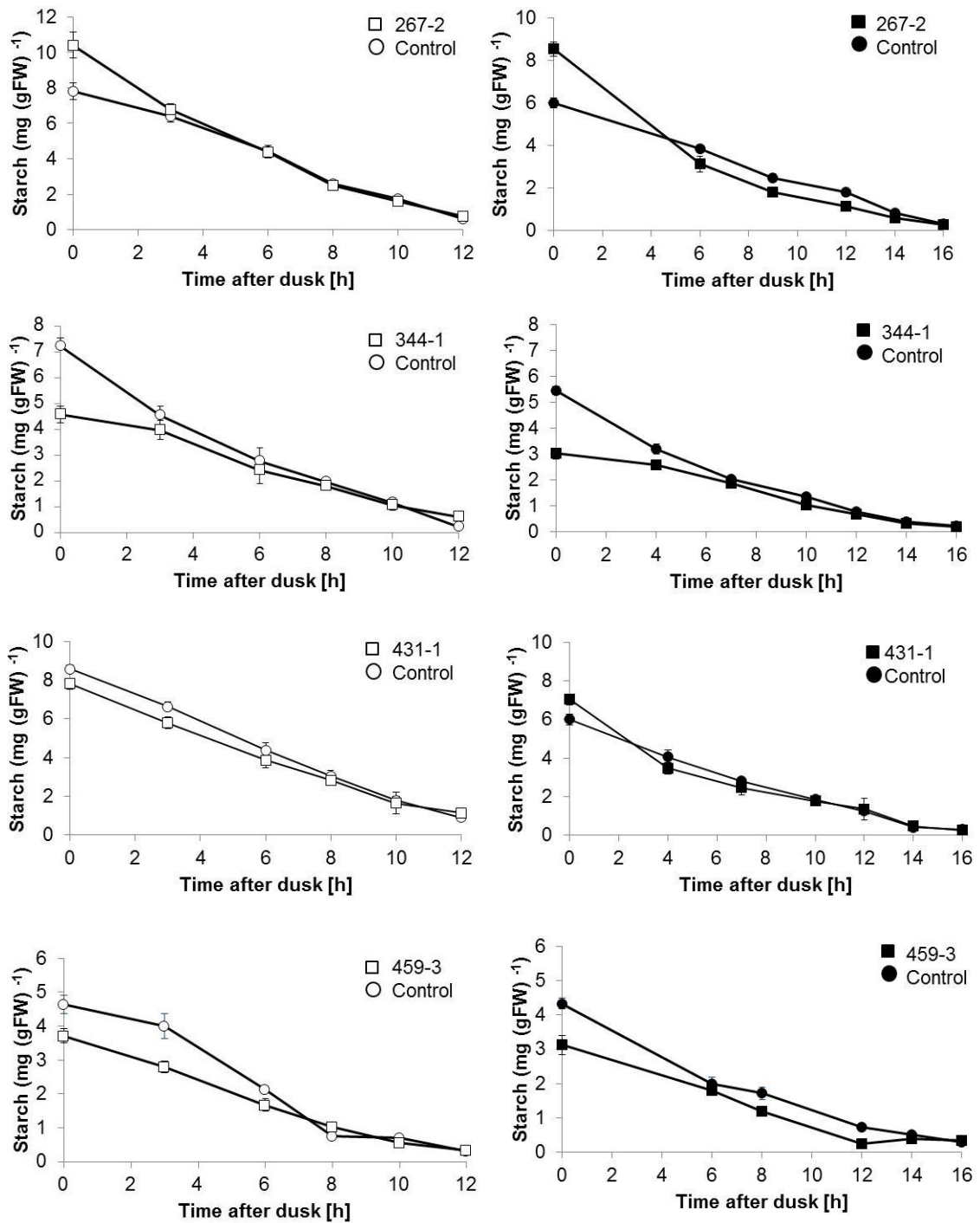


**Figure 3.6: Starch contents in normal and early nights determined in mutants with strong early starvation phenotypes. (Continued on next page)**

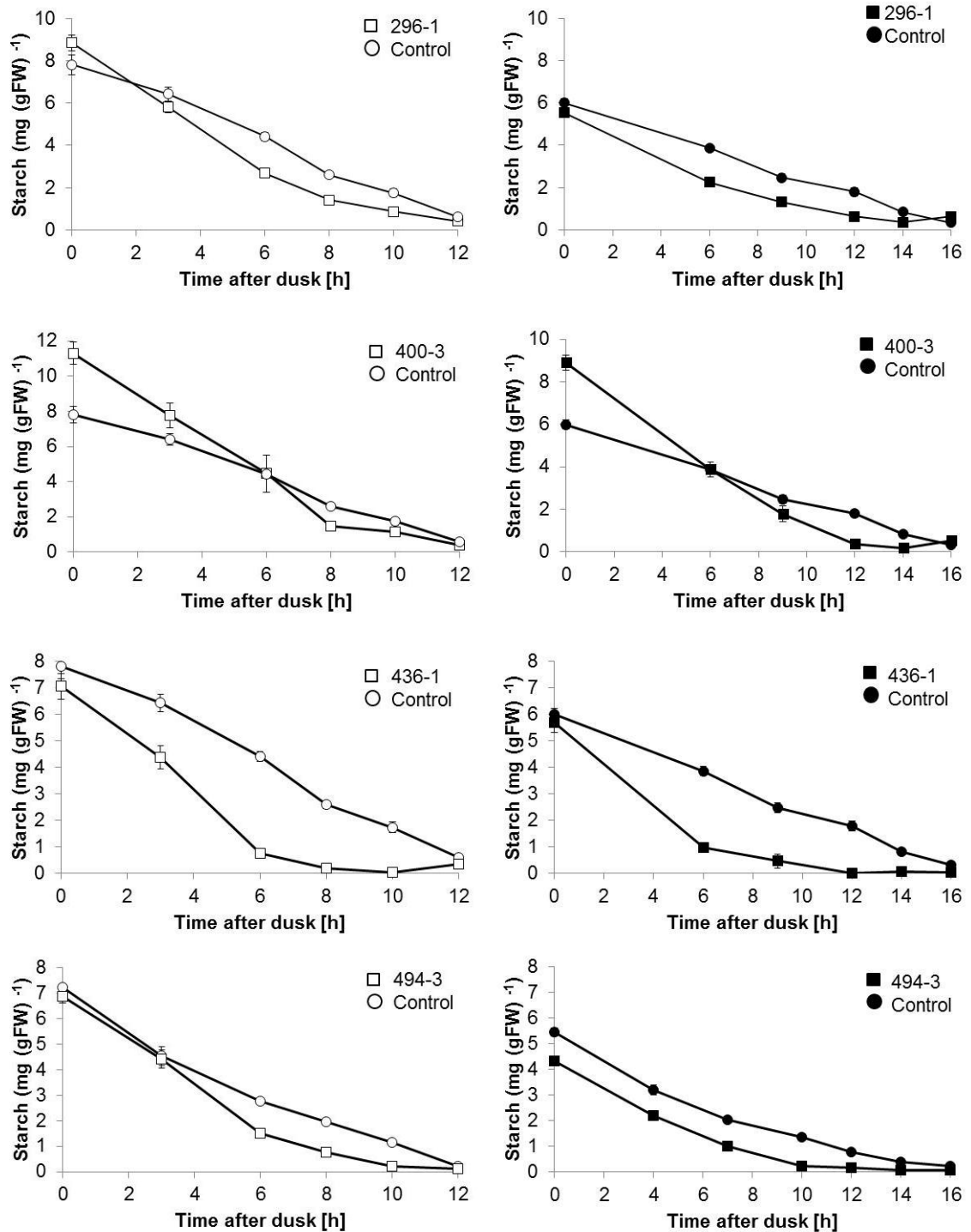


**Figure 3.6: Starch contents in normal and early nights determined in mutants with strong early starvation phenotypes.** The data were collected in four different experiments. Plants of the indicated mutants and the starvation reporter line (control) were grown in 12 hour light – 12 hour dark cycles for 24-28 days and harvested throughout a normal 12 hour night (left) and 16 hours of an early night (right). Starch contents were quantified on five individual rosettes per data point and genotype. The data presented are means  $\pm$  s.e.m. Where not visible, the s.e.m. is smaller than the symbol.

Mutant 296-1 had the mildest starch degradation phenotype. Its starch degradation rate was slower in the early night compared to the normal night, therefore it was still able to adjust its starch degradation rate to a certain extent if the night starts early. Mutant 494-3 exhausted its starch after 10 hours of the normal as well as the early night. Thus, the mutant did not adjust its starch degradation rate according to the length of the night. The mutant with the fastest starch degradation was mutant 436-1. The mutant did not adjust its starch degradation rate according to the length of the night. Mutant 400-3 did not exhaust its starch in the normal night, but after 12 hours of the early night. This mutant was therefore not able to adjust its starch degradation rate in response to an early night.

The early starvation phenotype of these mutants can be explained by premature exhaustion of starch and all four mutants are affected in the control of starch degradation rates at night.

### ***3.2.5 Characterisation of mutants with faster starch turnover***

To identify the genes underlying the phenotype of the four mutants with faster starch degradation rates, I characterised them further to get more information about the affected genes.

One possible explanation for faster starch degradation could be that the underlying mutations affect enzymes that metabolise starch. I analysed the activity of starch metabolising enzymes by native PAGE analysis as described in section 3.2.2. The result can be found in (**Figure 3.7**). Very surprisingly, mutant 494-3 lacked the isoamylase activity band, indicating that the mutated gene is either *ISA1* or *ISA2*, like in mutants identified in section 3.2.2. On the other hand, mutant 436-1 which had a starvation pattern similar to “*isa*-like” mutants, was not affected in isoamylase activity. The other two mutants still contained the *ISA1/ISA2* activity band. I did not sequence the *ISA* genes in any of the four mutants, but I assumed that mutant 494-3 is an *isa* mutant, therefore I did not characterise it further.

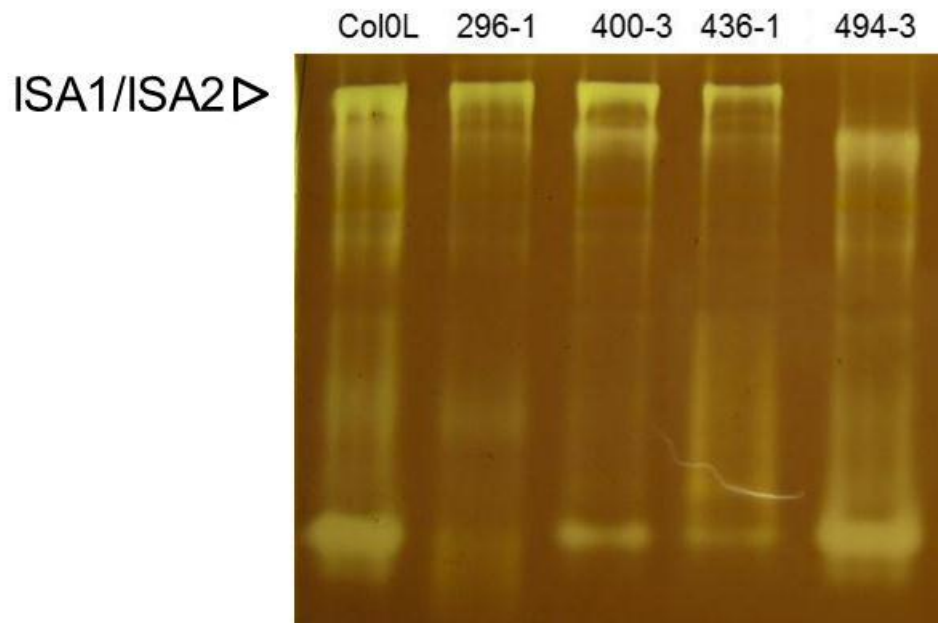


**Figure 3.7: Native activity gel to visualise activities of starch metabolising enzymes: Mutants with faster starch degradation.** For description see **Figure 3.2**.

Another reason for faster starch degradation of the four mutants could be a defect of the circadian clock (**Section 3.1**). I analysed the circadian clock period at the University of Liverpool in the lab of Anthony Hall. The clock period of three mutants with faster starch degradation (296-1, 400-3 and 436-1) was determined by leaf movement analysis or delayed fluorescence analysis (**Figure 3.8**). Delayed fluorescence analysis was carried out as described in section **3.2.3.1**. Leaf movement analysis was used as alternative method to determine the clock period of the mutants. The oscillation of the leaf movement can be used as a marker of the circadian clock in *Arabidopsis*, because leaf position displays a circadian rhythm (Edwards and Millar et al., 2007). These rhythms persist in wild-type *Arabidopsis* seedlings grown in constant light.

For the analysis, individual plants were grown on MS plates and entrained to 12 hour light – 12 hour dark cycles for 11 days. On day 12 they were transferred to constant light and leaf movement was recorded automatically for seven days using a CCD camera. The vertical positions of the primary leaves of each plant were analysed to estimate the period of the rhythm and an RAE. The average period estimate was calculated for all seedlings. None of the three mutants had a clock period significantly different from control plants of the starvation reporter line. It is therefore not likely that any of the three mutants degraded its starch faster due to a defect of the circadian clock.

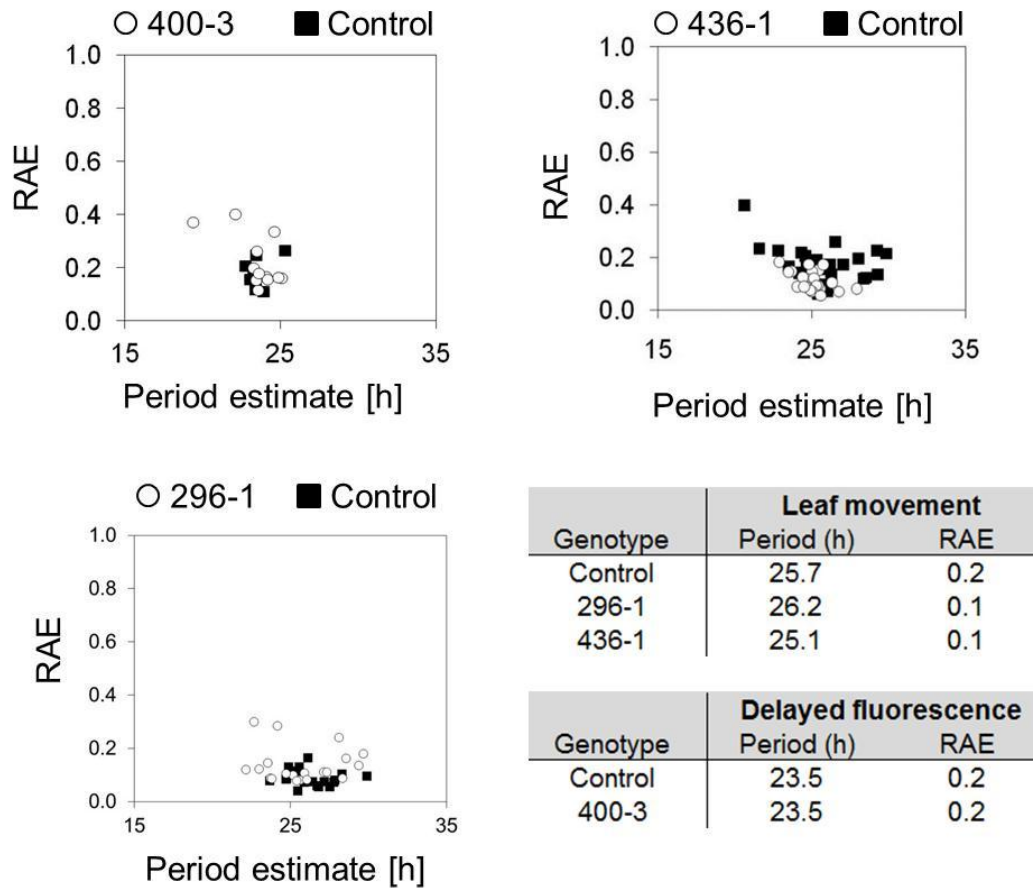


**Figure 3.8: Clock period estimates as determined by leaf movement analysis or delayed fluorescence analysis.** Delayed fluorescence analysis for mutant 400-3 was carried out as described in **Figure 3.4**. For leaf movement analysis of the other two mutants, about 26 single seeds of each line were sown on MS agar plates and grown in 12 light – 12 hour dark cycles for 11 days. Plants were then transferred to constant light for seven days. Leaf movements of the seedling were recorded every 20 min using a CCD camera system. The vertical position of the primary leaf was later analysed using the Metamorph software (Molecular Devices Ltd; <http://www.moleculardevices.com>) and a period was calculated on basis of the oscillation of the leaf. Each data point represents the leaf movement analysis of one plant. Period estimates are plotted against the relative amplitude error (RAE). RAE indicates rhythm robustness which can vary from 0 (a perfect fit to the cosine wave) to 1 (not statistically significant). The table shows the average period estimate for all seedlings of one line.

### 3.2.6 Summary and conclusions

I summarised the outcome of the mutant screen in **Figure 3.9**. The bioluminescence pattern of most of the 114 lines that originated from the initial screen could not be confirmed in the M<sub>3</sub> generation. I could confirm it for 12 mutants that were classified as “*isa-like*” mutants in the initial M<sub>2</sub> screen. These mutants showed bioluminescence expression at TP1 and TP3, but not at TP2. I showed that some of these were mutated in either *ISA1* or *ISA2*.

Thirty plants had a reproducible early starvation phenotype in the M<sub>3</sub> generation, meaning that they showed bioluminescence at either TP4 or TP3, or TP3 and TP4, but not at TP1. Of these, 21 lines had a weak early starvation phenotype. Analysis of starch degradation patterns of five of these lines showed that their starch degradation rates were very similar to those of wild-type plants. Ten lines had a strong early starvation phenotype in the M<sub>3</sub>. One of these lines did not produce enough seeds for further analysis (410-2). Starch degradation was clearly abnormal in four of the ten lines (357-1, 296-1, 400-3, 494-3). Mutant 357-1 turned over starch slower at the end of the early night. It turned out to be mutated in the circadian clock component *ELF3*. The starch degradation rate was clearly faster than in control plants in 296-1, 400-3, 494-3 and in one mutant with an “*isa-like*” starvation pattern (436-1). These mutants exhausted their starch before the end of the early night, which explains premature expression of the starvation reporter. Mutant (494-3) lacked isoamylase activity, despite having no “*isa-like*” starvation pattern and is likely to be mutated in *ISA1* or *ISA2*.

To find out which genes are involved in the control of starch degradation rates, I decided to identify the underlying EMS-induced mutations in the two mutants with the strongest starch turnover phenotype, in 436-1 and 400-3. The two mutants had different starch degradation patterns. Mutant 436-1 degraded its starch inappropriately fast in normal as well as early night. Mutant 400-3 had an appropriate starch degradation rate in the normal night, but did not slow down starch degradation in response to the early night. In the following two chapters I will refer to the two mutants as mutant A (436-1) and mutant B (400-3) respectively.

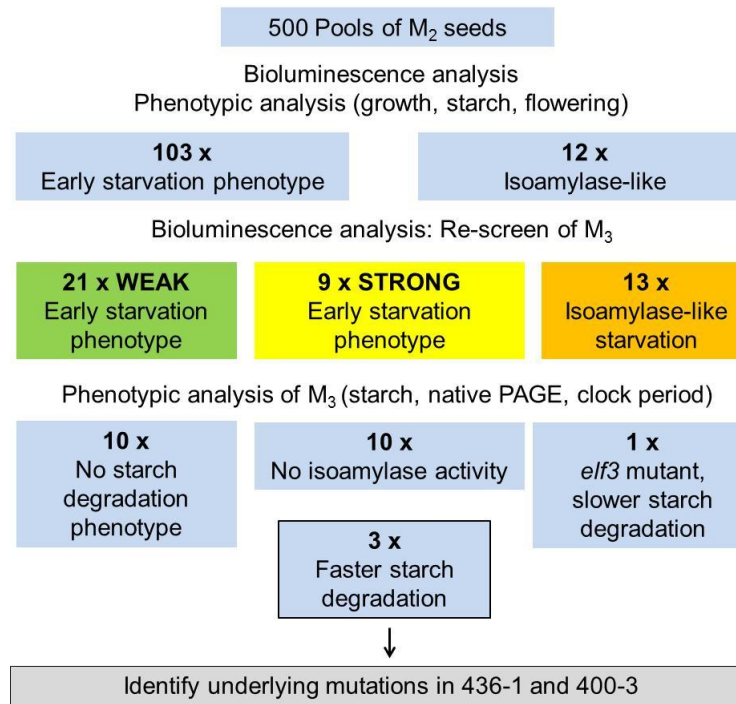


**Figure 3.9: Summary of the results of the forward genetic screen**

### 3.3 Discussion

#### 3.3.1 Aim of the screen and outcomes

The aim of the forward genetic screen was to identify mutants that are not able to adjust their starch degradation rates according to the length of the night. The screening protocol was designed to identify mutants that degrade starch normally in a normal night, but cannot slow down starch degradation if the night comes early. With the screen we hoped to find circadian clock mutants, mutants that are not able to measure the amount of starch, mutants affected in enzymes of the starch degradation pathway and mutants that lack components of the signalling pathway integrating clock outputs and information about starch contents to the post-transcriptional control of starch degradation.

Several mutants identified in the screen had interesting and new phenotypes, but only mutant 400-3 had exactly the desired phenotype. It had an appropriate starch degradation rate in the normal night and reserves were not exhausted before dawn. However, the starch degradation rate in the early night was too fast and reserves were

exhausted after 12 hours of the early night. Thus, this mutant could be affected in the immediate control of starch degradation rates.

It is interesting that I found only one mutant with normal starch degradation rates in the normal night that failed to adjust to an early night. There could be a number of explanations for this. One of them is that several genes could be involved in the immediate adjustment of the starch degradation rate. It is possible that a mutation in one of these genes does not result in a phenotype, because the other genes can complement its function. Also, the phenotype of such a mutation could be very subtle, but the screen aimed at the identification of mutants with a strong phenotype.

I also suggest that the adjustment of the starch degradation rate to an unexpected shortening of the light period may involve the same genes that control starch degradation rates in a normal night. Therefore, it might not be possible to separate these two pathways as intended in the screen. That means that a mutation of a gene controlling starch degradation would result in a phenotype already in the normal night. Mutants with a bioluminescence signal at the end of the normal night were excluded in the screen, therefore such a phenotype would not have been picked up with high probability. The starch degradation phenotype of mutant 357-1, 436-1, 296-1 and the putative isoamylase mutant 494-3 is consistent with my hypothesis. These mutants degraded starch clearly differently from the control in normal night as well as early night.

Another possibility for the low number of candidates with the desired starch degradation phenotype is that mutations of genes involved in the control of starch degradation might not result in faster, but in slower starch degradation rates. Such mutants could be picked up by screening for mutants with a late starvation phenotype. However, it would be hard to distinguish those mutants from known starch-excess mutants that have retardations in starch breakdown (**Chapter 1**).

### ***3.3.2 Why did some mutants not have a reproducible starvation phenotype in the M<sub>3</sub> generation?***

Less than one third of all mutants identified in the initial screen of M<sub>2</sub> plants had a reproducible early starvation phenotype in the M<sub>3</sub> generation. One possible explanation

for this could be that more than one EMS-induced mutation caused the starvation phenotype of M<sub>2</sub> plants. The responsible mutations might have segregated in the M<sub>3</sub> generation and therefore, the bioluminescence signal was not homogenous in the M<sub>3</sub> generation. This is consistent with the finding that several M<sub>3</sub> lines did not give a homogenous bioluminescence signal in all plants, although some individual plants had the desired early starvation phenotype. I excluded these lines from further analysis to select for mutants with a strong early starvation phenotype.

In some M<sub>3</sub> lines, no bioluminescence signal was detected in any of the plants at any of the three time points. The reason for this could be that the mutant phenotype is conditional and dependent on factors that were not controlled for between experiments. The phenotype could vary in different growth conditions and could be responsive to minor changes in light intensities or watering. In the initial screen, the phenotype of a single plant was recorded. It is possible that this plant was stressed and that this affected its phenotype. I also noticed that the bioluminescence phenotype can vary dependent on the age of the plant.

### ***3.3.3 Why did some mutants with an early starvation phenotype not exhaust their starch before dawn?***

I analysed the starch degradation pattern of six mutants with a weak early starvation phenotype and of nine mutants with a strong early starvation phenotype. Only five of these 15 lines had a starch degradation pattern clearly different from wild-type. Four of them exhausted their starch reserves before the end of the early night. The other ten lines did not exhaust their starch before the end of the early night. Thus, it is not clear why the starvation reporter was activated at the end of the early night. There could be different explanations for that. Three of the lines with a strong early starvation phenotype (267-2, 459-3, 357-1) had a non-linear starch degradation rate which slowed down towards the end of the early night. Perhaps these mutants used up most of their starch at the beginning of the night. The slow rate of starch degradation at the end of the night might not have provided enough sugars to suppress the activation of the reporter. However, the observed changes of the starch degradation rate of these mutants were subtle and should be confirmed in further experiments. Mutant 431-1 and 344-1 degraded their starch at a nearly identical rate to the control, especially at the end of the early night. Perhaps the relationship between sugar levels and the activation of the

starvation reporter is altered in these mutants. The reason for this could be a mutation that affects the sugar-signalling pathway that activates the reporter. The same is true for the other five mutants with the weak early starvation phenotype that did not show obvious abnormalities in the starch degradation pattern.

### ***3.3.4 Why were so many isa mutants identified in the screen?***

Isoamylase mutants were found with a high frequency in the mutant screen. Using native PAGE analysis, I confirmed the absence of isoamylase activity in ten mutants. These mutants might have been found so often because they had strong and reproducible starvation phenotypes. Also, a mutation in one of two genes (*ISA1* or *ISA2*) results in an identical phenotype (Delatte et al., 2005). This increases the likelihood of finding a mutant deficient in this isoamylase activity in the mutant screen. However, *isa1* or *isa2* mutants are not so interesting for the questions I am addressing, because they mainly accumulate soluble phytoglycogen and only minor amounts of starch. Thus, they do not directly provide information about the genes that control starch degradation rates. However, the data obtained from the screen open up several questions about the regulation of phytoglycogen and starch degradation in *isa1* mutants.

### ***3.3.5 Why did “isa-like” mutants not display starvation symptoms after 12 hours of the early night?***

All of the “*isa-like*” mutants showed strong bioluminescence resulting from activation of the starvation reporter at TP1 (after 12 hours of the normal night), but not at TP2 (after 12 hours of the early night). This indicated that the mutants can adjust the degradation of their carbohydrate reserves to some extent if the night starts early. This adjustment must be achieved by slowing down phytoglycogen or starch degradation.

Phytoglycogen degradation is not controlled in the same way as starch degradation and is not adjusted according to the length of the night. Previous work has found that phytoglycogen is degraded in an exponential way and reserves are exhausted after about eight hours of a normal 12 hour night (Delatte et al., 2005; Zeeman et al., 1998a). This is consistent with my data, I also found that phytoglycogen in *isa1* was exhausted after eight hours of the normal night (**Figure 3.3**). Premature exhaustion of phytoglycogen

could explain the strong level of bioluminescence seen in “*isa-like*” mutants at the end of the normal night.

To find out if phytoglycogen degradation slows down in the early night, I compared phytoglycogen contents of the *isa1* mutant in normal and early nights (**Figure 3.3**). The data indicated that phytoglycogen was degraded slower in the early night, thus that phytoglycogen degradation can be controlled to some extent. However, after nine hours of the early night, there were only about 0.2 mg gFW<sup>-1</sup> phytoglycogen left. This is about the same amount of starch that a wild-type plant has left at the end of the night. Thus, the phytoglycogen content would probably be too low to avoid symptoms of carbon starvation after 12 hours of the early night. Also, the observation that *isa1* mutants adjust their starch degradation rates in the early night was only made in one experiment. It should be confirmed in further experiments to draw final conclusions.

An alternative explanation for the absence of starvation symptoms in “*isa-like*” mutants after 12 hours of the early night could be the supply of sugars from starch. In addition to phytoglycogen, *ISA1* and *ISA2* mutants still accumulate some starch. Different amounts of residual starch in *isa1* and *isa2* are reported in the literature, but between 10% and 30% of the wild-type amount of starch were observed at the end of the day (Delatte et al., 2005; Zeeman et al., 1998; Wattedled et al., 2008). The data in the literature indicates that starch degradation rates in *isa1* mutants follow a linear pattern and are adjusted so that starch is exhausted by dawn (Delatte et al., 2005, Zeeman et al., 1998a). Therefore, starch degradation might slow down in *isa1* mutants during the early night providing enough sugars to avoid starvation symptoms after 12 hours of the early night. To find out if that is the case, starch degradation of *isa1* mutants should be measured in normal and early nights.

Some information about the control of starch degradation rates in mutants that lack isoamylase activity comes from a mutant isolated in this screen (494-3) and will be discussed in the following section.

### 3.3.6 Is starch degradation adjusted according to the length of the night in mutants lacking isoamylase activity?

Data obtained in the screen opened up questions about the adjustment of starch degradation rates in mutants with lacking isoamylase activity. Mutant 494-3 had a strong early starvation phenotype that differed from that of other “*isa*-like” mutants, because the mutant did not exhibit bioluminescence at the end of a normal 12 hour night (TP1). However, when I analysed soluble protein extracts of that mutant on native gels, I noticed that the ISA1 activity band was missing, just like in “*isa*-like” mutants. This suggests that mutant 494-3 is mutated in *ISA1* or *ISA2*. End of day starch contents 494-3 were similar to wild-type at the beginning of the normal night and slightly reduced at the beginning of the early night. Starch degradation was clearly faster and non-linear in the mutant. It exhausted its starch about ten hours after dusk in the normal night as well as the early night.

The starch data obtained from mutant 494-3 is intriguing, because it contradicts published data about starch contents in *isa1* or *isa2* mutants. As mentioned in the previous section, *isa1* or *isa2* mutants accumulate at most 30% of the wild-type level of starch (e.g. Delatte et al., 2005). Mutant 494-3 clearly accumulated far more starch than *isa1* or *isa2* knock-out mutants. Also starch degradation in the mutant was not linear and not adjusted according to the length of the night. In contrast, residual starch in *isa1* mutants was shown to be degraded in a linear way (e.g. Zeeman et al., 1998a). Only one very recent study (Pyl et al., 2012) showed that residual starch in *isa1* mutants is degraded too fast. It was shown that the mutant exhausts its starch 10 hours after dusk, just as mutant 494-3. My data and the data from Pyl et al. (2012) indicate that degradation of the remaining starch in *isa1* mutants is not adjusted according to the length of the night. The reasons for the differences between studies are not clear.

The data I presented here are preliminary, but they open up many questions about the rate of starch and phytoglycogen degradation in *isa1* mutants. I did not follow these questions further, but they could be potentially interesting for future research.

### 3.3.7 Circadian clock mutants

With the forward genetic screen described here, I expected to identify circadian clock components that are involved in the control of starch degradation in *Arabidopsis* leaves. Two mutants were discovered in the screen that could help us to understand which clock components are essential for setting starch degradation rates.

### 3.3.8 The circadian clock period in 357-1

One of the early starvation mutants was mutated in the gene encoding the circadian clock component ELF3 (3.2.3.2).

ELF3 is a plant specific nuclear protein with no known functional domains (Liu et al., 2001). Together with ELF4 and LUX forms the evening complex (EC) (Nusinow et al., 2011) (**Chapter 1**). LUX is the DNA binding component of the evening complex and negatively regulates the expression of *PRR9* (Helfer et al., 2011; Chow et al., 2012). *PRR9* is a transcription factor that represses the morning expressed circadian clock genes *LHY* and *CCA1* (Nakamichi et al., 2010). The EC also negatively regulates hypocotyl growth by direct binding to the *PIF4* and *PIF5* promoters at dusk (Nusinow et al., 2001). The expression levels of all three proteins of the EC peak around dusk. Protein levels fall during the night and reach a minimum around dawn (Nusinow et al., 2011).

The mutant (357-1) has an early flowering phenotype and a growth phenotype similar to *elf3* mutants. The free-running period of the circadian clock in mutant 357-1 was determined to be about three hours longer than in wild-type plants (**Figure 3.4**).

The free-running period that I estimated for mutant 357-1 is not entirely consistent with data in the literature. Mutants affected in *ELF3* were shown to be arrhythmic in constant light, by using clock-controlled promoter *LUC* reporter fusions (Covington et al., 2001; Hicks et al., 1996), by looking at leaf movement (Reed et al., 2000; Hicks et al., 1996), and by analysis of DF levels (Dixon et al., 2011). However, these studies mentioned that individual *elf3* seedlings still retain rhythmicity of circadian clock outputs in constant light. The amount of seedlings retaining rhythmicity varied between different *elf3* alleles. It was shown that 14% of *elf3-4* mutants (Hicks et al., 1996) and 12% of

*elf3-7* (Reed et al., 2000) mutants show rhythmicity of clock-outputs in constant light, when leaf movements were analysed. The DF analysis I did was carried out on groups of seedlings. I speculate that the rhythmicity of the DF levels observed in mutant 357-1 is due to the presence of individual plants that showed rhythmic DF levels. It could also be that mutant 357-1 has a less severe phenotype than the *elf3-4* or *elf3-7* mutants and therefore retained some rhythmicity of DF in constant light. However, the rhythmicity of DF in mutant 357-1 was not as robust as in wild-type as the RAEs were high, thus the rhythm was damped.

Information about the circadian clock period of *elf3* mutants in 12 hour light – 12 hour dark cycles is not available in the literature. It is possible, that the circadian clock is not arrhythmic in the growth conditions applied in this study. It was shown that *elf3* mutants are still rhythmic in constant darkness (Covington et al., 2001), thus the circadian clock period might vary in different growth conditions. To find out if the circadian clock of the mutant is rhythmic in growth conditions applied in this study, gene expression of circadian clock regulated genes could be analysed in the mutant when grown in 12 hour light – 12 hour dark cycles. Candidate genes include the circadian clock gene *LHY* and the clock-controlled gene *GRANULE BOUND STARCH SYNTHASE 1 (GBS1)* as shown in Graf et al. (2010). In 12 hour light – 12 hour dark cycles, *LHY* and *GBS1* show peak expression around dawn (Mizoguchi et al., 2012; Smith et al., 2004).

### 3.3.9 Starch degradation in 357-1

End of day starch contents in 357-1 were similar to wild-type, but the mutant degraded its starch in a non-linear way and slower than wild-type towards the end of the night. Thus, it had a slight starch excess at the end of the night (**Figure 3.5**).

Similar observations were made by Yazdanbakhsh et al (2011). They found that *elf3* mutants have higher levels of starch throughout the diurnal cycle, when grown in 12 hour light – 12 hour dark cycles. The difference in starch contents was most obvious at the end of the night, when the mutant had more than twice as much starch as wild-type plants. They also found that leaf sugar levels in *elf3* were increased at the end of the night. Further, they investigated root extension growth in the *elf3* mutant and compared it to wild-type plants. They found that root extension growth shows a characteristic diurnal pattern and is circadian clock regulated. In wild-type plants, root extension

growth peaked about two hours after dawn, gradually decreased for about 7-8 hours during the day and gradually increased for the rest of the day and during the following dark period. In *elf3* mutants, the growth pattern showed the opposite trend and root growth gradually decreased during the night to reach a minimum at dawn and a gradual increase during the day. The authors speculated that *ELF3* could have a function to regulate root growth by decreasing growth in the light and promote it in the dark. This is consistent with *ELF3*'s role in controlling hypocotyl growth as part of the evening complex.

The data of Yazdanbakhsh et al. (2011) showed that *elf3* mutants have reduced root growth rates at the end of the night. If starch degradation rates are linked to carbon utilisation for growth, the reduction of starch degradation rates in *elf3* towards the end of the night might be explained by a reduced consumption of carbon from starch in *elf3*. If the mutant stops to grow at the end of the night, it will consume fewer sugars. Sugars might accumulate and this could have a negative feedback effect on starch degradation rates.

My data indicates that *ELF3* is required to obtain normal rates of starch degradation at night. However, how *ELF3* is mechanistically linked to the adjustment of starch degradation rates needs to be investigated in the future.

### ***3.3.10 Clock period and starch degradation in 395-1***

Mutant 395-1 showed bioluminescence two hours after the end of an early night (**Figure A1**). The mutant is early flowering. The DF rhythm in 395-1 was less robust than in wild-type and about one hour advanced, indicating it is a circadian clock mutant. The starch degradation pattern of the mutant was very similar to wild-type, but starch degradation seemed to slow down or even arrest at the end of the normal night. This could explain the bioluminescence that was observed at the end of the early night. I did not investigate which gene is affected in mutant 395-1, because it had only a mild starch degradation phenotype. Possible candidate genes could be clock genes like *TOC1*, *GI*, *LHY* or *CCA1* because the mutants *toc1-2* as well as *gi-11*, *lhy-21* and *cca1-11* were shown to have shorter circadian clock periods than wild-type based on DF measurements (Gould et al., 2009). However, since the RAE of the data was high, it could also be that the mutant has an arrhythmic circadian clock.

### ***3.3.11 Conclusion and outlook***

The mutant screen allowed new insights into the regulation of phytyglycogen and starch degradation in *isa1 (isa2)* mutants and identified a new role for the circadian clock component *ELF3* in the regulation of starch degradation. The data presented here can be basis of future research. I decided to follow up by characterising mutants 400-3 (mutant B) and 436-1 (mutant A), because the mutations in these lines had the strongest impact on starch degradation rates. In the following chapters I will describe how I identified the underlying mutations in both mutants and characterised the mutant phenotypes in more detail.

## 4 Identification of causal mutations in mutants A and B

### 4.1 Introduction

Mutant A and mutant B were identified as early starvation mutants in a forward genetic screen (**Chapter 3**). Measurements of starch contents showed that both mutants degrade starch faster than wild-type. Mutant A exhausted its starch before the end of the normal as well as the early night. Mutant B did not exhaust its starch before the end of the normal, but before the end of the early night.

#### 4.1.1 Aim

In this chapter, I describe how I localised the mutations in mutant A and mutant B by map-based cloning and mapping-by-sequencing. Also, I describe how I confirmed that the identified mutations caused the phenotype of the mutants. I describe the effect of the mutations on the gene products and use *in silico* analysis to speculate about the link between the mutations and the mutant phenotypes.

#### 4.1.2 EMS induced point mutations in mutant A and mutant B

The mutants were obtained by chemical mutagenesis of *Arabidopsis* seeds of the starvation reporter line using ethyl methane sulfonate (EMS). EMS-treatment primarily results in G/A or C/T transitions in the DNA. These are randomly distributed over the genome. The mutation frequency is dependent on the EMS dose, but in comparable studies was reported to be around 1/170 kb or 1/112 kb (Greene et al., 2003; Ashelford et al., 2011). The *Arabidopsis* genome has a size of about 125 Mb (The Arabidopsis Genome Initiative, 2000), therefore an average mutation frequency of 1/141, would result in about 900 EMS-induced mutations per plant. After the identification of mutants in a forward genetic screen, repeated back-crossing of the mutant to the wild-type line is advisable to “clean up” the genetic background by reducing the numbers of EMS-induced mutations that are unlinked to the phenotype of interest. Each back-cross removes half of the unlinked mutations. It is recommended to do five to ten rounds of back-crossing (Weigel and Glazebrook, 2002). That many back-crosses would be expected to remove more than 97% of unrelated mutations.

### ***4.1.3 Characterisation of the mutation***

Segregation analysis is used to determine whether the mutation causing the phenotype is dominant or recessive. Absence or presence of the mutant phenotype in the self-progeny or F<sub>1</sub> plants of the back-cross indicates how the mutation is inherited (Weigel and Glazebrook, 2002). If forward genetic screening leads to the identification of more than one mutant with the phenotype of interest, crosses can be performed to find out if mutations are caused by the same gene, i.e. are allelic (Peters et al., 2003). Allelism test involves crossing two homozygous mutants with the same phenotype to find out if the mutations can complement each other, i.e. if the F<sub>1</sub> plant loses the mutant phenotype.

### ***4.1.4 Identification of the mutation by map-based cloning***

The identification of EMS-induced point mutations is traditionally done by map-based cloning, also called positional cloning, which allows the mapping of the mutation of interest to a small region of the genome (Jander et al., 2002; Lukowitz et al., 2000). For this approach, the mutant plant is out-crossed to another *Arabidopsis* ecotype (**Figure 4.1**). For example, if the EMS mutation is in the Col-0 background, the mutant is crossed to wild-type Landsberg *erecta* (*Ler*) plants. Plants in the F<sub>1</sub> of that cross are allowed to self-pollinate. Meiotic recombination events between Col-0 and *Ler* genomic DNA (gDNA) will occur all over the genome. Thus F<sub>2</sub> plants have gDNA of mixed origin, from the Col-0 and the *Ler* parent. The F<sub>2</sub> population of the cross is called a mapping-population. These plants segregate for the phenotype of interest. Plants homozygous for the mutation are selected by analysing their phenotype. These plants are then genotyped individually at known positions in the genome to analyse the presence of *Ler* and Col-0 polymorphisms. Such polymorphisms are sequences in the gDNA that vary between Col-0 and *Ler*. They can be insertions and deletions (InDels) or single nucleotide polymorphisms (SNPs) that can be detected by PCR-based markers. The position of the mutation of interest is then determined by measuring the recombination frequency between Col-0 and *Ler* gDNA at markers all over the genome.

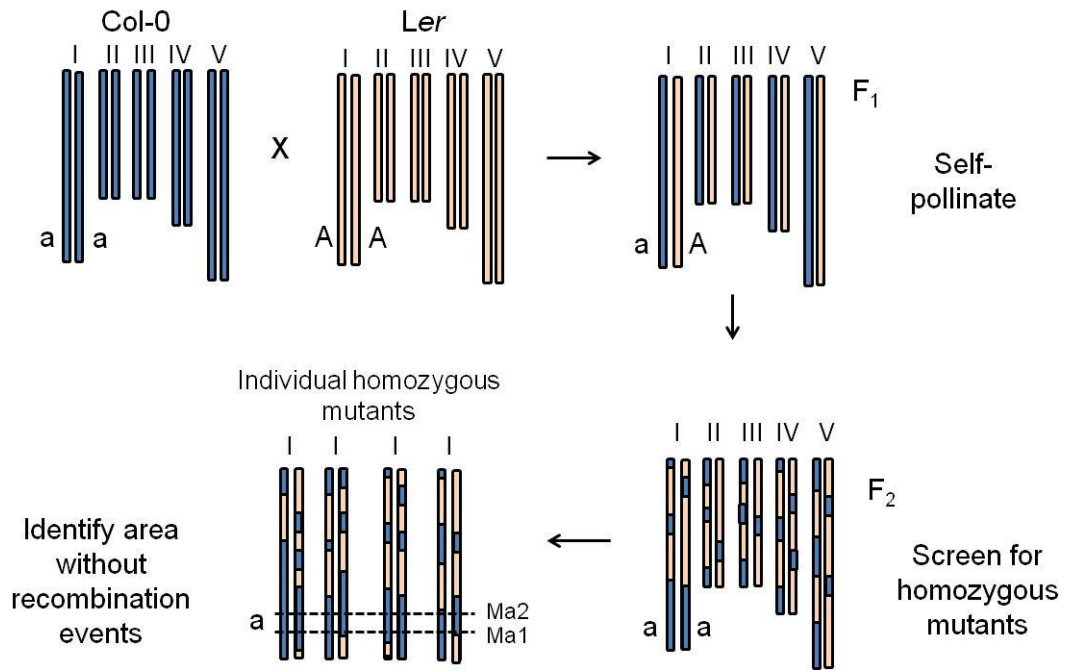


**Figure 4.1: Map-based cloning approach: Schematic representation of recombination events on *Arabidopsis* chromosomes in the out-cross of Col-0 to *Ler*.** Blue bars represent Col-0 chromosomes (I-V), orange bars *Ler* chromosomes. The mutation of interest is in the Col-0 background (aa). *Ler* plants are wild-type for the mutation (AA), and are used as second parent for the out-cross of the mutant. F<sub>1</sub> plants are heterozygous (aA) for the mutation of interest are allowed to self-pollinate. During meiosis, recombination events between Col-0 and *Ler* chromosomes occur. These result in mixed areas of *Ler* and Col-0 gDNA on all chromosomes in the F<sub>2</sub> generation. F<sub>2</sub> plants (mapping-population) are phenotyped to recover individual homozygous mutants (aa). PCR-based markers (Ma) are then used to analyse the chromosomes of those plants for areas with enrichment in Col-0 polymorphisms until a non-recombinant region is found that contains only Col-0 polymorphisms (between Ma1 and Ma2). This region is the target interval which contains the mutation of interest, because the mutation always resides in the Col-0 background. Therefore this is the only region in the genome that cannot contain *Ler* gDNA in homozygous mutants of the out-cross.

The EMS mutation was introduced into the Col-0 background, thus its position can be narrowed down by searching for a chromosomal area that contains only Col-0 gDNA in all F<sub>2</sub> plants that are homozygous for the mutation. The recombination frequency at a certain marker position is directly related to the distance between the marker and the target mutation. The more closely a PCR-marker is physically linked to the mutation, the more Col-0 alleles it will detect. The size of the non-recombinant region with only Col-0 alleles defines the target interval for putative candidate genes. Based on the annotation of genes in the defined target interval, it might be possible to predict candidate genes. These can then be re-sequenced in the homozygous mutant using standard Sanger DNA sequencing to look for EMS-type point mutations.

The progress of map-based cloning can be slowed down or hindered if the mutation maps to a chromosomal area with low recombination frequency, for example in the centromeric region, where meiotic recombination events are very infrequent (Drouaud et al., 2006). This makes it difficult to define the gene of interest by map-based cloning.

#### ***4.1.5 Identification of the mutation by mapping-by-sequencing***

Recent advances in sequencing technologies allow the use of an alternative strategy to map-based cloning, called mapping-by-sequencing (Schneeberger et. al., 2009). With this method, identification of the mutation is much faster. The approach is similar to the mapping approach as it also requires the generation of a mapping population by out-crossing. The difference is, that DNA of F<sub>2</sub> plants homozygous for the mutation of interest is pooled and analysed by whole genome sequencing. Thus, only a single DNA sample needs to be sequenced. Again, the ratio of Col-0 and *Ler* polymorphism is defined all over the genome by analysis of the assembled sequence. SNPs that are polymorphic between Col-0 and *Ler* are analysed to distinguish between Col-0 and *Ler* gDNA. This allows the identification of a chromosomal interval with no recombination. The sequence in that interval is then compared to the Col-0 reference genome to identify homozygous EMS-type point mutations.

#### ***4.1.6 Confirmation of candidate genes***

If a mutation is found in a certain gene, it must be confirmed that it is causing the phenotype of the mutant. This can be achieved by introducing the wild-type candidate gene into mutant plants and demonstrating that the mutant phenotype is rescued. In case

of a dominant mutation it needs to be shown that transformation of wild-type plants with the gene containing the mutation results in a mutant phenotype (Weigel and Glazebrook, 2002). Another way to confirm that a candidate gene is causing the phenotype is to identify T-DNA insertion mutants for the same gene and to show that they have the same phenotype.

## 4.2 Results

### *4.2.1 Characterisation of mutations: Segregation analysis*

Mutant A and mutant B showed an early starvation phenotype at the end of the early night (**Chapter 3**). To find out if the mutations causing the phenotype are recessive or dominant, segregation analysis was performed. The M<sub>3</sub> generation of plants was allowed to self-pollinate and to set seed to analyse segregation rates in the M<sub>4</sub> generation. Also, both mutants were back-crossed to the starvation reporter line (referred to as wild-type in the following) to analyse segregation rates in F<sub>1</sub> and F<sub>2</sub> plants of the cross. After ten days of growth, bioluminescence was measured at the end of an early night, when both mutants should express luciferase from the starvation reporter construct. This analysis showed that the phenotype in mutant A is caused by a recessive mutation (**Figure 4.2**). Plants of the M<sub>3</sub> and M<sub>4</sub> generation showed a uniform and strong starvation signal, indicating that all plants were homozygous mutants. The F<sub>1</sub> from the back-cross to the starvation reporter line had no starvation phenotype. This strongly indicates the presence of a recessive mutation. In the F<sub>2</sub> generation, plants segregated for the starvation phenotype. The observed segregation pattern indicates a 1:3 segregation rate which would be expected for a recessive mutation.

In mutant B, the early starvation phenotype was caused by a dominant mutation (**Figure 4.3**). M<sub>3</sub> plants and their self-progeny segregated for the mutant phenotype, indicating that some of the plants did not have the mutation causing the phenotype.

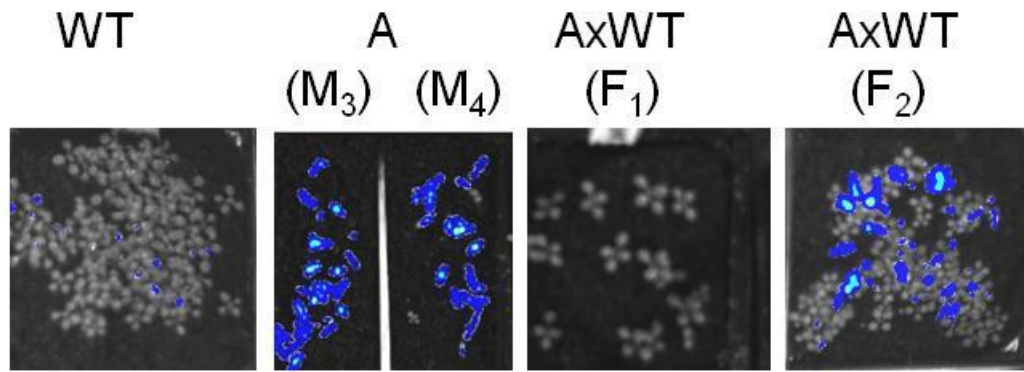


**Figure 4.2: Segregation analysis for mutant A.** Plants of wild-type (WT=starvation reporter line), mutant A (A) and the back-crosses of mutant A to wild-type (AxWT) were analysed for luciferase-induced bioluminescence at the end of the early night after 10 days of growth in 12 hour light-12 hour dark cycles. Plants of the M<sub>3</sub>, M<sub>4</sub>, F<sub>1</sub> and F<sub>2</sub> generation were assayed.

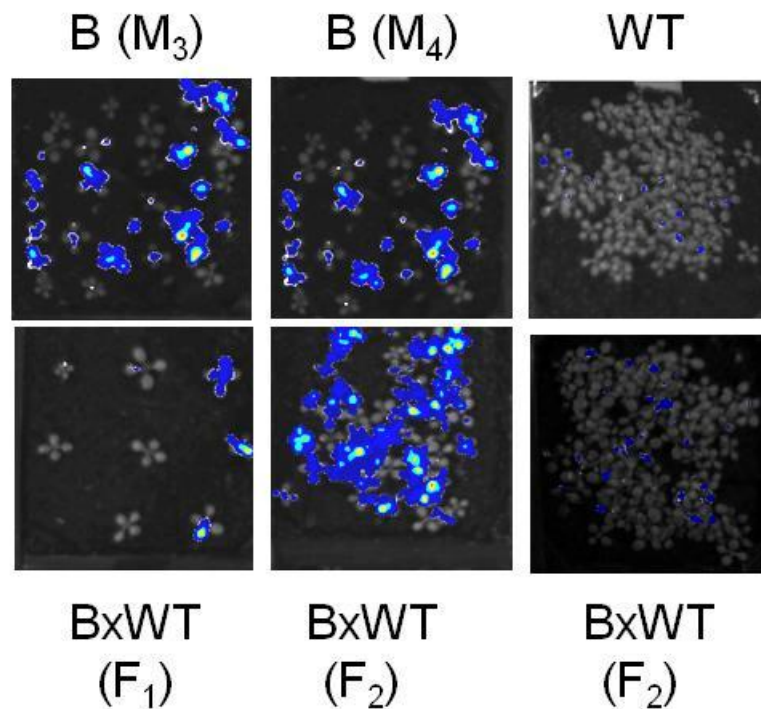


**Figure 4.3: Segregation analysis for mutant B.** Plants of wild-type (WT=starvation reporter line), mutant B (B), and the back-cross of mutant B to wild-type (BxWT) were grown in 12 hour light-12 hour dark cycles and luciferase-induced bioluminescence assayed after ten days at the end of the early night. Plants of the M<sub>3</sub>, M<sub>4</sub> and F<sub>1</sub> and F<sub>2</sub> generation were assayed to analyse segregation in the self-progeny.

About half of the F<sub>1</sub> plants of the back-cross to the starvation reporter line had a detectable bioluminescence signal, indicating segregation of the phenotype in that generation. Since F<sub>1</sub> plants can only contain one copy of the mutant allele, this result strongly indicates that the mutation of interest is dominant. In F<sub>2</sub> lines of the back-cross, different segregation rates were observed. One line segregated for the phenotype, another line had a bioluminescence signal comparable to wild-type. The difference of segregation patterns in different F<sub>2</sub> lines further indicates the presence of an underlying dominant mutation. Based on the result of the segregation analysis, different strategies for map-based cloning were applied to the two mutants.

#### **4.2.2 Identification of EMS-induced point mutations in mutant A**

##### *4.2.2.1 Map-based cloning approach*

Identification of the causative mutation in mutant A was initially attempted by applying a conventional map-based cloning approach. Therefore mutant A (Col-0 background) was out-crossed to a wild-type plant of the Landsberg *erecta* (*Ler*) ecotype. F<sub>1</sub> plants were allowed to self-pollinate and grown for seed. Plants homozygous for the mutation were identified in the F<sub>2</sub> population by selecting individuals that displayed the starvation phenotype at the end of the early night. DNA was extracted from 40 individual homozygous plants and a rough map position was obtained by testing 16 markers that were evenly spread over the genome. These PCR-markers amplify positions in the DNA that are polymorphic between the *Ler* and Col-0 ecotype (**Chapter 2**). Since the mutation was obtained in the Col-0 background, chromosomal areas rich in Col-0 alleles would indicate a close linkage to the mutation. These areas are characterised by a low recombination frequency. As measure of recombination frequency, the percentage of *Ler* alleles was determined at each marker position after genotyping of all 40 plants (**Figure 4.4**). For markers unlinked to the mutation, the representation of *Ler* alleles is expected to be roughly 50%. At marker two, three and four, much lower ratios were found. Thus, the mutation was likely to be located between marker two and four in the centre of chromosome 1. This interval had a size of about 16.3 Mb. Marker three had the closest link to the mutation, only 9% of chromosomes showed the *Ler* genotype at that position.

To narrow down the target interval, further markers upstream and downstream of marker three were analysed and the percentage of *Ler* alleles calculated (**Figure 4.5**).

The marker with the closest linkage was determined and two new markers flanking this marker were identified. This procedure was repeated and DNA of 200 homozygous individual plants genotyped until the target interval was narrowed down to 2.7 Mb. It still included 463 genes and was located between loci At1g36070 and At1g42970, spanning the centromere of chromosome 1.

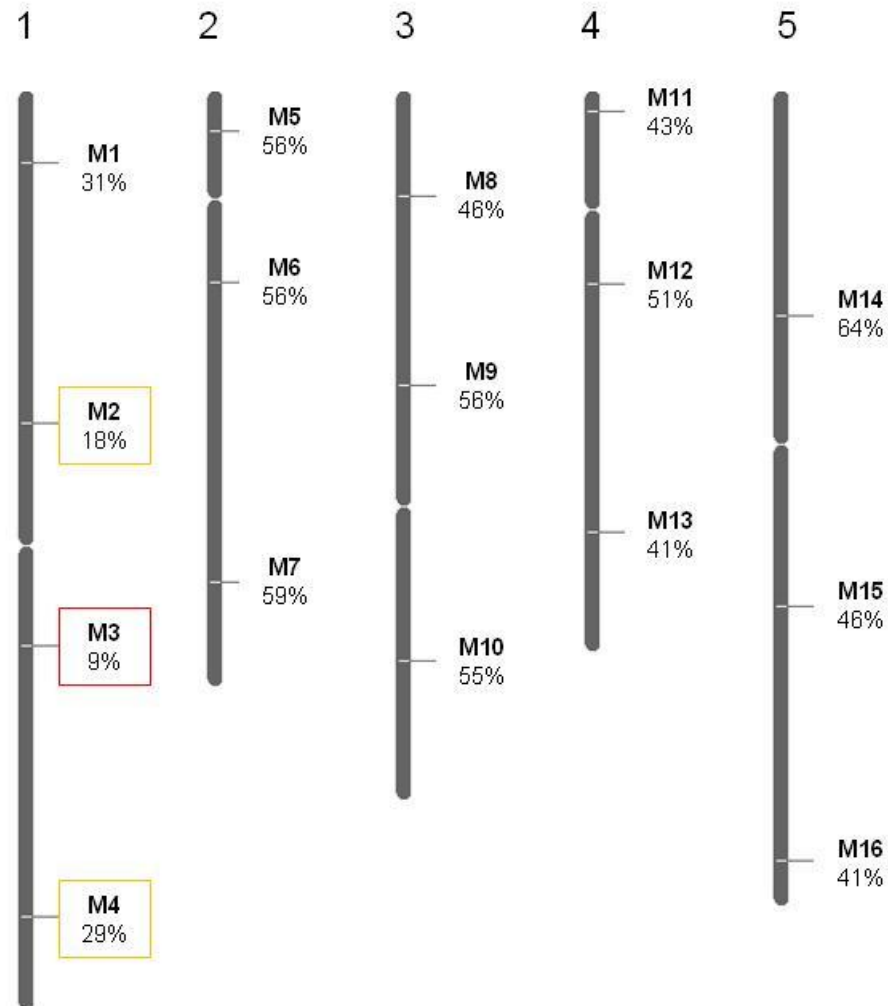


**Figure 4.4: Summary of rough mapping of mutant A.** Linkage analysis was performed on 40 individual  $F_2$  plants of the out-cross to *Ler* after confirmation of the early starvation phenotype. Sixteen markers (M1-16) which were evenly distributed over the five *Arabidopsis* chromosomes were analysed for their linkage to the underlying mutation in mutant A. Linkage of each marker to the mutation was determined by calculating the percentage of detected *Ler* alleles in all individual homozygous mutants of the  $F_2$  generation at the marker position. Orange and red boxes highlight the markers which were closely linked to the target mutation.

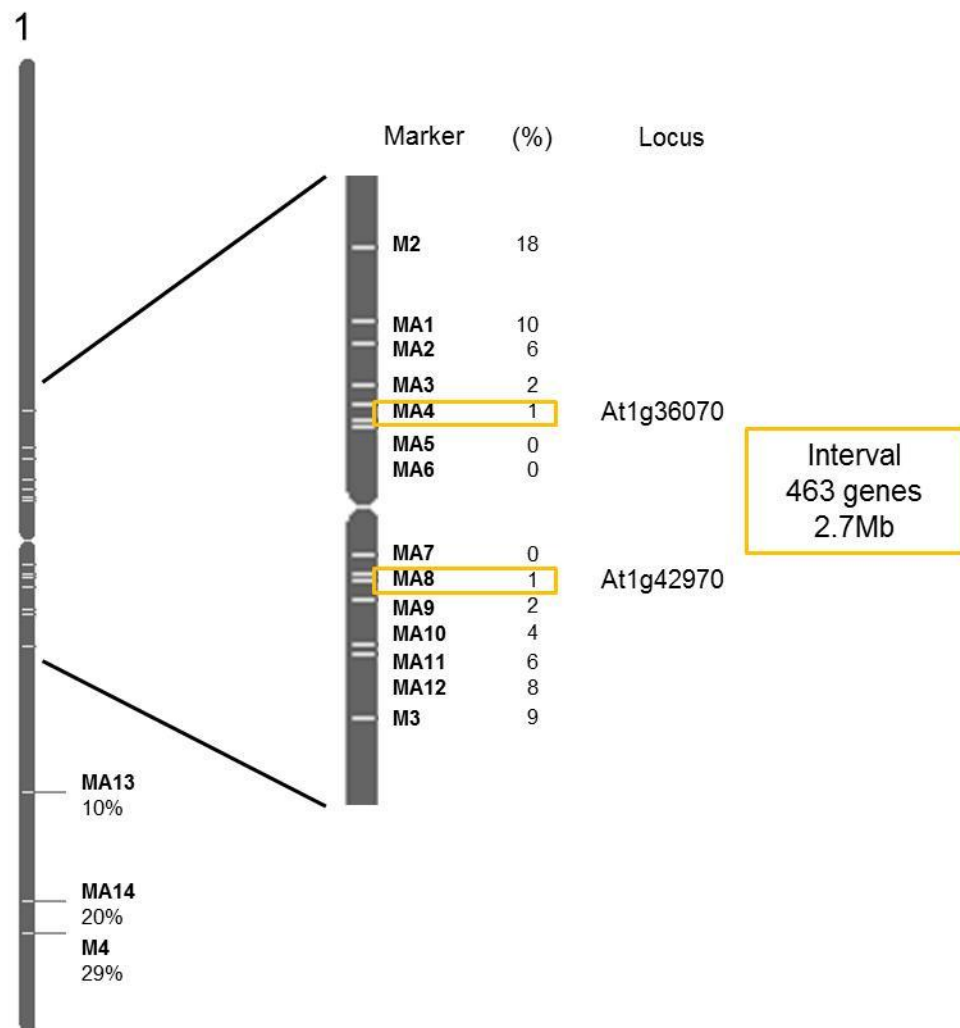


**Figure 4.5: Map-based cloning result of mutant A.** Analysis was performed on 200 individual  $F_2$  plants of the out-cross to *Ler* after confirmation of the early starvation phenotype. 14 additional markers (MA1-MA14) were analysed for their linkage to the underlying mutation in mutant A. Linkage was determined by calculating the percentage (%) of detected *Ler* alleles in all  $F_2$  plants homozygous for the mutation. Orange boxes highlight the markers which frame an area without recombination.

#### 4.2.2.2 Mapping-by-sequencing approach

Since map-based cloning is hindered by the low recombination frequency in the centromeric region, mapping-by-sequencing was chosen as an additional approach to identify the mutation in mutant A. The approach I used was adapted from Scheeberger et al. (2009). F<sub>2</sub> plants of the out-cross to *Ler* were analysed for their phenotype and one leaf of each of 500 homozygous mutant plants harvested. Nuclei from pooled leaf samples were extracted to concentrate the samples for subsequent DNA extraction. A minimum of 5µg of DNA was needed for sequencing. RNA was removed by RNase treatment. Samples were sequenced as a service by TGAC on the Illumina GAIIx platform with paired-end (PE) reads.

The sequencing data were analysed by Martin Trick (Systems and Computational biology, John Innes Centre). In total 35,634,367 PE reads were obtained, with an average read depth of 28. Mapping of the PE reads to the Col-0 reference genome (TAIR, release 8) showed that 83.9% of all reads mapped to Col-0, 95% of them in pairs. The assembled sequence contained about 280,000 SNPs when compared to the reference genome. Most of them (72%) corresponded to known Col-0/*Ler* polymorphisms. These were analysed to calculate the ratio of Col-0 to *Ler* polymorphisms in intervals of 10kb all over the genome. Since the mutation underlying the phenotype was in the Col-0 background, chromosome areas with a high number of Col-0 polymorphisms indicate a close linkage to the mutation of interest. A strong enrichment of Col-0 polymorphisms was detected in the centre of chromosome 1. This indicated the absence of *Ler* gDNA in the region, and hence that it did not undergo recombination. The target interval identified by map-based cloning was in the centre of that region, which validated the result obtained by whole genome sequencing.

The remaining SNPs that were not Col-0/*Ler* polymorphisms were filtered for EMS induced point mutations (G/A or C/T transitions) and 9,000 of these could be detected over the whole genome. All plants were homozygous for 178 of these mutations. Two of these mutations affected genes in the target interval on chromosome 1, which was determined by map-based cloning. Both were G/A transitions, one located in At1g42430 and one in At1g42470. The exact position of the mutations is given in **Table 4.1**. Based on the annotation in TAIR (<http://www.arabidopsis.org>), At1g42430 encodes an unknown protein of about 49 kDa. The mutation disrupts a 3' intron splice site. The

mutation in At1g42470 causes an amino acid substitution (E910K) in a plasma membrane localised hedgehog protein.

To discover the effect of disruption of the 3' intron splice site in At1g42430 on the mRNA, Atg42430 cDNA was amplified from mutant A and wild-type plants using PCR. The product length was then analysed by agarose gel electrophoresis (**Figure 4.6**). This revealed that At1g42430 mRNA was still present in mutant A. However, it was shorter than in wild-type plants. This indicated that disruption of the intron splice site resulted in production of aberrant and shorter mRNA.

	Mutation 1	Mutation 2
<b>Position in gDNA</b>	Chr I: 15,894,697bp	Chr I: 15,934,565bp
<b>Affected gene</b>	At1g42430	At1g42470
<b>Position in gene</b>	+745bp from ATG, intron	+5139 bp from ATG, exon
<b>Gene annotation</b>	unknown protein	hedgehog receptor
<b>Protein location</b>	unknown	plasma membrane
<b>Effect of mutation</b>	disrupted 3'intron splice site	aa substitution (E910K)
<b>Reference sequence</b>	TATAATTG <b>T</b> Ag/a <b>ACACTGGGAT</b>	TTTGACTCC <b>G</b> g/a <b>AACTAAGCTA</b>

**Table 4.1: Description of EMS-induced point mutations found in the mapping interval.** Using a combined map-based cloning and mapping-by-sequencing approach, two point mutations were identified that could be causative of the phenotype in mutant A. Both mutations were G/A substitutions (g/a), one found in an intron (blue capital letters, one in an exon (green capital letters) of genes on chromosome 1 (Chr I).

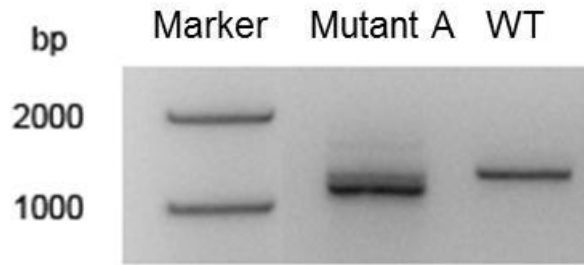


**Figure 4.6: RT-PCR for mutant A and wild-type.** RNA was extracted from mutant A and wild-type (WT) plants and cDNA synthesised by reverse transcription. The cDNA was then amplified by PCR. Primers were designed to amplify the full coding sequence, which in wild-type has a size of 1281bp.

#### ***4.2.3 T-DNA insertion lines of At1g42430 and complementation of mutant A***

To find out if the mutation in At1g42430 causes the phenotype of mutant A, I analysed the phenotype of T-DNA insertion lines and of mutant A expressing At1g42430 cDNA from a wild-type plant.

Four T-DNA insertion mutants disrupted in At1g42430 were obtained. Genotyping of these lines showed that one of the SALK lines (SALK\_080172) did not contain the T-DNA insert at the expected position in the gene, therefore the line was discarded. Two other lines contained a T-DNA insert in the promoter (SALK\_040206 and SALK\_070292). In one line (GABI\_031C11), the T-DNA insert disrupted the fourth exon (**Figure 4.7**). Genotyping of those three lines confirmed the presence of the T-DNA inserts at the expected positions and homozygous lines could be generated for all three of them.

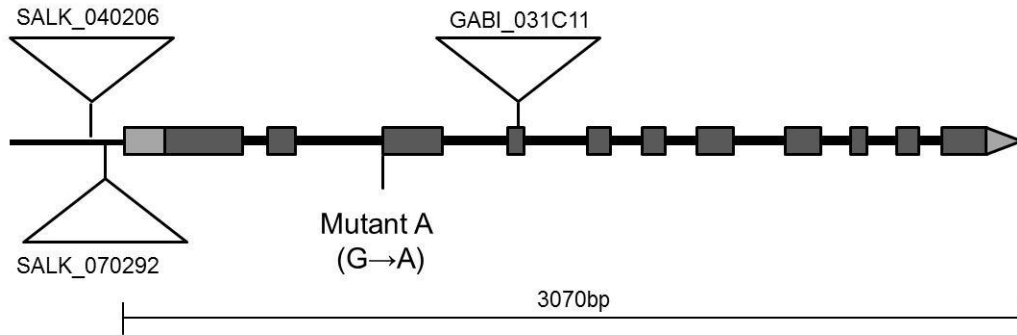


**Figure 4.7: Schematic gene structure of *At1g42430* and position of EMS-induced mutation and T-DNA insertions.** Mutant A carries a G/A substitution in the 3' splice site of the second intron. Mutant GABI\_031C11 has a T-DNA insertion in the fourth exon (+1188 bp from ATG). The two SALK lines contain T-DNA inserts in the promoter region, 376 bp and 392 bp upstream of the ATG start codon respectively. Grey bars represent exons, light grey bars the 5' and 3' UTRs, the black line between the exons represents the introns and the triangles the position of the T-DNA inserts. The scale bar indicates the length of the gene from the beginning of the 5'UTR to the end of the 3'UTR.

To discover whether the mutant phenotype can be rescued by overexpression of the protein encoded by *At1g42430* in mutant A, I transformed mutant A plants with the wild-type cDNA sequence of *At1g42430*. This was done to find out if the mutant phenotype can be rescued. The coding sequence of the gene (from start codon to stop codon) was amplified from cDNA from wild-type plants after RT-PCR. It was then cloned into vector pGWB2, to put it under control of the 35S promoter. Plants were transformed by floral dip and homozygous lines were obtained in the  $T_3$  generation, by selection of plants resistant to kanamycin. Presence of the transgene in the plants was confirmed by PCR amplification of the transgene in the gDNA. I sequenced the PCR product to confirm that it is the wild-type sequence. Unfortunately, I found a point mutation in position 574 bp upstream of the start codon. It is an A/G transition in the middle of this reference sequence: GAAAa/gGTGGA and causes an amino acid substitution (G192S) in the protein. Experiments to transform mutant A with the wild-type sequence are in progress. Results obtained from experiments with the line presented here (*35S:At1g42430*) should be seen as preliminary, as the point mutation in the transgene might affect the function of the protein.

To analyse the starch degradation phenotype of the T-DNA insertion mutants and the transformed mutant line, leaves were stained with iodine. Plants were grown in 12 hour light-12 hour dark cycles for 22 days and rosettes harvested one hour before the end of the night (**Figure 4.8**).

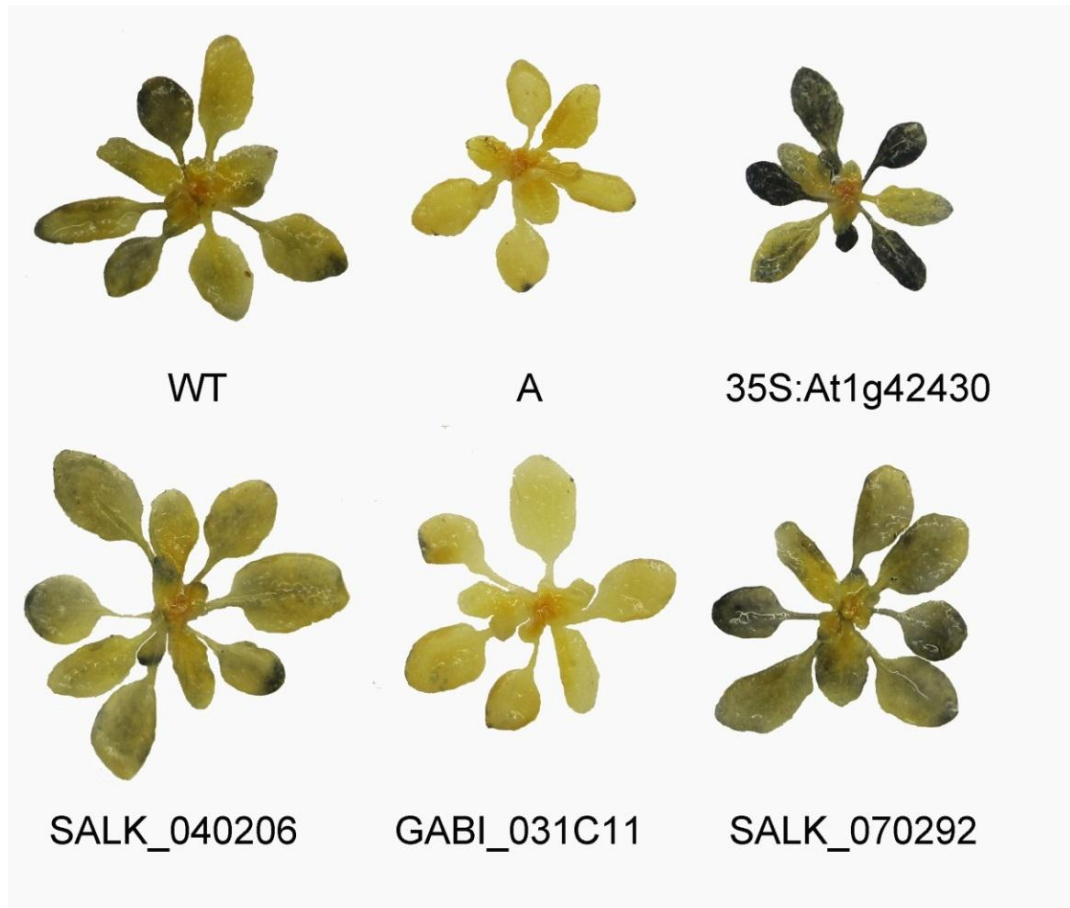


**Figure 4.8: Iodine stain of leaf starch of three T-DNA insertion mutants and mutant A plants transformed with At1g42430 cDNA.** Plants were grown in 12 hour light-12 hour dark cycles for 22 days and rosettes harvested one hour before the end of the night. Rosettes were de-stained in boiling ethanol and stained with iodine solution. Mutant A plants (A) were transformed with a construct containing the cDNA (coding sequence from start to stop codon) of At1g42430 under control of the 35S promoter.

At this time point, wild-type plants still contained small amounts of starch, and parts of rosettes displayed a light blue colour. Mutant A plants did not stain blue, indicating that all starch was exhausted at this time point. Line GABI\_031C11 did not stain blue either. The two SALK lines had a stain comparable to wild-type. Transformation of mutant A with wild-type cDNA of At1g42430 restored the presence of starch in the mutant. However, the stain did not look like the stain of wild-type plants but was darker. This indicated that this line had a different starch content from wild-type plants. To find out if starch contents in the T-DNA lines and transformed mutant A plants differed from wild-type, leaf starch was quantified at the end of the day and end of the night (**Figure 4.9**). Starch contents of GABI\_031C11 were not analysed in this experiment but are described in more detail in **Chapter 5**. For unknown reasons, the two SALK lines accumulated about 45% less starch than wild-type, but at the end of the night their starch contents were similar to wild-type. The line expressing At1g42430 cDNA under control of the 35S promoter, had 55% more starch than wild-type at the end of the day and only 47% of it was broken down at night. This means that the transgenic line had a starch excess phenotype. Thus, the faster starch degradation phenotype of mutant A was rescued. It is possible that an opposite starch degradation phenotype emerged after transformation of mutant A with cDNA of At1g42430. However, this result needs to be verified using a transgenic line, expressing an unmutated version of the wild-type protein.

To find out if levels of the protein encoded at At1g42430 correlated with the starch phenotypes, immunoblot analysis was performed (**Figure 4.10**). Plants were harvested at the end of the day and the crude extract was boiled in SDS and the soluble fraction then separated by SDS-PAGE, blotted on PVDF membrane and probed with an antibody against the protein encoded by At1g42430. This antibody was provided by our collaborator David Seung (ETH Zürich). The immunoblot showed that mutant A and GABI\_031C11 had no detectable protein, thus they were knock-out lines for At1g42430.

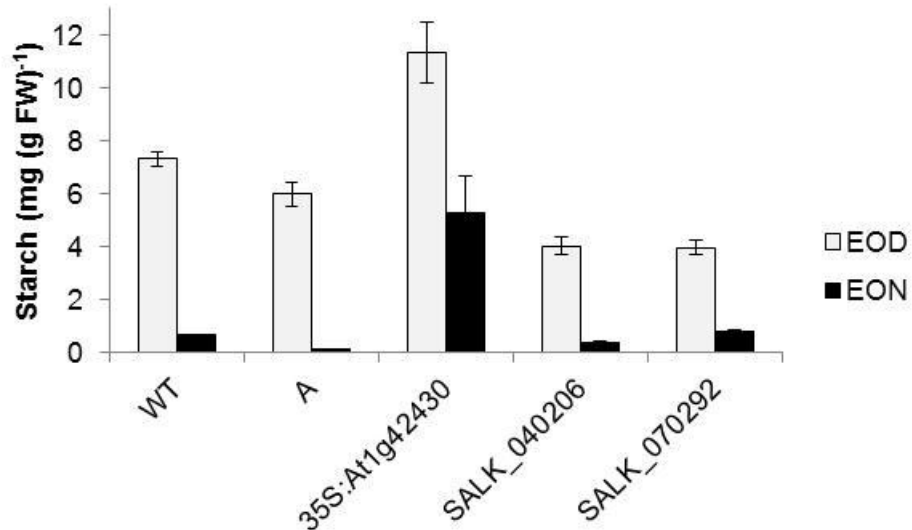


**Figure 4.9: End of day and end of night starch contents of two T-DNA insertion lines of *At1g42430*, mutant A and mutant A transformed with cDNA of *At1g42430*.** Plants were grown in 12 hour light-12 hour dark cycles for 23 days and leaf starch harvested at the end of the day and end of the night. Error bars are s.e.m. of five biological replicates.

The SALK lines and wild-type contained similar amounts of protein derived from *At1g42430*. Thus, the SALK lines were no knock-out lines. This explains the lack of a fast starch degradation phenotype of these lines. Mutant A transformed with *35S:At1g42430* contained more protein than wild-type and a new band with higher molecular weight appeared on the blot.

The results presented so far indicated that knock-out plants for the protein encoded by *At1g42430* had less starch at the end of the night, while plants overexpressing the protein had more starch at the end of the night.

In conclusion, *At1g42430* was shown to be the gene causing the phenotype of mutant A as independent mutation of that gene had a strong effect on starch degradation. Thus, the second gene identified by mapping-by-sequencing (*At1g42470*) was no longer considered to cause the phenotype of mutant A.

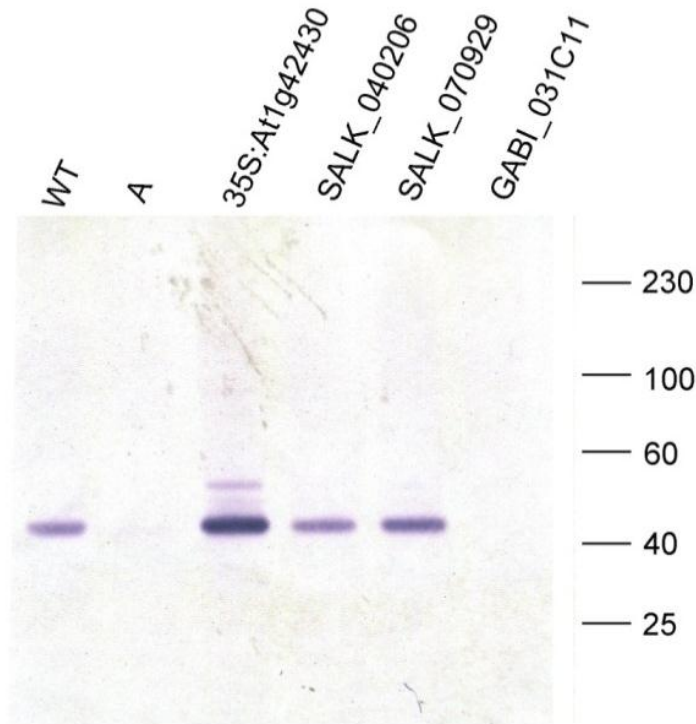


**Figure 4.10: Immunoblot analysis for mutant A, T-DNA lines for At1g42430 and mutant A plants transformed with At1g42430 cDNA.** Plants were grown in 12 hour light-12 hour dark cycles for 23 days. Rosettes from wild-type (WT), mutant A (A), mutant A complemented with At1g42430 cDNA (*35S:At1g42430*) and three T-DNA insertion lines were harvested at the end of day. Crude protein extracts were boiled in SDS and the soluble fraction separated by SDS PAGE (4-12% polyacrylamide), then blotted on PVDF membrane and probed with antiserum against the protein encoded by At1g42430 at a concentration of 1:1000. Protein loads were adjusted on a weight base, i.e. the same amount of fresh weight was loaded in each lane. On the right, molecular weight estimated from protein markers is shown in kDa.

#### 4.2.4 New nomenclature for *At1g42430*: EXCESS STARCH TURNOVER 1

Phenotypic analysis of T-DNA lines, mutant A and mutant A expressing *At1g42430* showed that the mutation in *At1g42430* caused the starch degradation phenotype of mutant A. Further evidence for this will be given in **Chapter 5**, when the phenotype of knockout lines GABI\_031C11 and mutant A is characterised in more detail. Since mutant A and GABI\_031C11 degraded starch faster than wild-type, *At1g42430* will be referred to as EXCESS STARCH TURNOVER 1 (*EST1*). Thus, mutant A and GABI\_031C11 will be called *est1-1* and *est1-2* respectively.

#### 4.2.5 In silico analysis of *EST1*

##### 4.2.5.1 Annotation and subcellular location of *EST1*

Very little information is available about *EST1* in the literature or databases. The present state of knowledge about *EST1* as follows.

*EST1* is annotated as an unknown protein with unknown subcellular location. The protein is composed of 426 amino acids and has a molecular weight of about 49 kDa (TAIR, [www.arabidopsis.org](http://www.arabidopsis.org)). There is no chloroplast transit peptide (cTP) predicted by the programmes TargetP or ChloroP (Emanuelsson et al., 1999 and 2000). Prediction of a cTP in the protein might have failed, because cTPs are very diverse and there is no distinct consensus sequence that defines them (Lee et al., 2008). Evidence for a chloroplastic location of the protein comes from data of a proteomics approach (Bayer et al., 2011). The method applied therein specifically aimed at the enrichment of low-abundant chloroplast proteins purified from pea seedlings by a targeted fractionation approach.

##### 4.2.5.2 Protein structure and motifs

I searched for conserved domains in the *EST* protein using conserved domain (CD) search on NCBI ([www.ncbi.nlm.nih.gov](http://www.ncbi.nlm.nih.gov)), but no conserved domains were detected in the protein (Marchler-Bauer, 2004).

I further used the MotifScan website ([http://myhits.isb-sib.ch/cgi-bin/motif\\_scan](http://myhits.isb-sib.ch/cgi-bin/motif_scan)) to identify motifs in the primary structure. The program identified a proline-rich region at

the C-terminus and a tryptophan-rich region stretching over most of the protein. The high occurrence of tryptophan (7% of the total sequence) might indicate that the protein has starch binding properties as tryptophan is an essential amino acid in starch binding domains (SBDs) of enzymes in starch metabolism (Christiansen et al., 2009). Some enzymes of the starch degradation pathway contain a family of SBDs called carbohydrate-binding modules (CBMs). The ability of CBMs to bind to starch is associated with certain consensus amino acid residues. These include the aromatic amino acids tryptophan, tyrosine and phenylalanine (Christiansen et al., 2009). EST1 does not have a CBM, but residues associated with carbohydrate binding and the amino acid proline are highlighted in the EST1 sequence in **Figure 4.11**.

```

1 MSEMAASSAISLLDIKLRRFVGVGASNHELRLTKWFKGDQA GAPTRRFTCF
51 ADMLAPIRRSEKSEERRFDQKMSAHGAGIKTSSSAVPFASPKSRFLSKQE
101 KFYPRCTPRLTGQSRDTPPKRDTGIANEKDWGIDLLNENVNEAGTNEDG
151 SSWFRESGHDLGDNGYRCRW SRMGGRSHDGSSEWTETWWE KSDWTGYKEL
201 GVEKSGKNSEGDSWWETWQEVLHQDEWSNLARIERSAQKQAKSGTENAGW
251 YEKWWEKYDA KGWTEKGAHKYGR LNEQSWWEKWGEHYDGRG SVLKWTDKW
301 AETELGTKWG DKWEEKFFSGIGSRQGETWHVSPNSDRWSRTWGEEHFGNG
351 KVHKY GKSTTGESWDIVDE ETYEAEPHYGWADVVDSTQLLSIQPRER
401 PPGVYPNLEFGSPPEPDLPPDQPQ

```

**Figure 4.11: Predicted amino acid sequence of EST1.** The protein consists of 426 amino acids and is rich in tryptophan (28 residues; 7%) and proline (23 residues; 5%), which are highlighted in red and orange. Other aromatic amino acids that are important in proteins that have starch binding properties are highlighted green (tyrosine) and blue (phenylalanine).

Analysis of the secondary structure was performed using the protein homology/analogy recognition engine Phyre (<http://www.sbg.bio.ic.ac.uk/phyre2/html/page.cgi?id=index>). This program predicts secondary structures in the protein based on homology to proteins with known structures (Kelley et al., 2009). The analysis showed that large areas of the protein (62%) are not predicted to be folded and are rather structurally disordered. About 22% of all amino acids are predicted to fold into alpha-helices and 13% are part of beta-strands, but these are scattered over the protein in short stretches and interrupted by regions predicted to be disordered.

#### 4.2.5.3 EST2 and EST1 orthologs

BlastP search revealed that the *Arabidopsis* protein with the highest sequence similarity to EST1 on the protein level is encoded by At3g55760. In the following, this protein will be referred to as EST2. There is no information about the function of EST2, but several proteomics studies found the protein in chloroplast samples of *Arabidopsis thaliana* (Zybailov et al., 2008; Peltier et al., 2006; Kleffmann et al., 2004). This is consistent with the presence of a cTP in the N-terminus of the protein as predicted by ChloroP. The protein was identified as a starch binding protein, when it was purified from *Arabidopsis* using affinity chromatography on amylose resin (Edner et al., 2007). EST2 was found in the same fraction that contained these known proteins of starch metabolism: BAM1, SBE3, ISA3 and DPE1. EST2 is 578 amino acids long and has a molecular weight of about 66 kDa (TAIR, <http://www.arabidopsis.org/>). EST1 and EST2 proteins share 146 residues of their amino acid sequence, this corresponds to about 35% identical amino acids of EST2 in EST1 and 25% identity of EST1 in EST2 (**Figure 4.12**). The sequences are more similar towards the C-terminus, but the C-terminal proline-rich region is missing in EST2. In the N-terminus, long stretches of amino acids present in EST2 are missing in EST1. EST2, just as EST1 is rich in tryptophan, which makes up 5% of the sequence.

Searching the Ensembl plants genome browser (<http://plants.ensembl.org/index.html>) for proteins with similar protein sequences revealed that orthologs of EST1 can be found in at least 20 other plant species (**Table 4.2**) including most plant species for which sequence information is available in the Ensembl genome browser. The *Chlamydomonas* ortholog shares 30% of its amino acids with EST1 from *Arabidopsis*. A BLAST search with the EST1 protein sequence against the NCBI protein sequence database (blastp), revealed that proteins with highly similar sequence to EST1 can be found in additional land plant species, in *Sorghum bicolor* (sorghum), *Fragaria vesca* (strawberry), *Cucumis sativus* (cucumber), *Cicer arietinum* (chickpea) and green algae (*Micromonas puscilla*, *Osterococcus tauri*, *Volvox carteri*). Searching the NCBI translated nucleotide databases using EST1 protein as query sequence (tblastn) indicated, that EST1 orthologs are present in several more plant species including *Prunus avium* (cherry), *Lotus japonicus* and *Triticum aestivum* (wheat). Based on the sequence information available, it can be concluded that proteins with similar sequence

to EST1 are widespread in the plant kingdom, but not present in other eukaryotes. None of the EST1 orthologs has an assigned a function.

Proteins with high similarity to EST2 are found in the same plant species as EST1 orthologs when searching the Ensembl Plants genome browser (**Table 4.3**). The NCBI Blast search against protein or nucleotide databases also indicated that proteins with similar sequence to EST2 are found in the same species as EST1, thus are widespread in the plant kingdom. The amino acid conservation between EST1 and EST2 is much lower than the conservation between the orthologs of each protein.

```

EST1      -----MSEMAASSAISLLDIKLRRFVVGAS 25
EST2      MALRLGVSIGAAALGSSHWDDGQRVRQDFASVNFAPVTSRRSLRGSRTGVRILRVSN 60

EST1      NHELRLTKWFKGDQAGAPTRRFTCFADMLAPIRSEK-----SEE 65
EST2      GRESYLDMMKNNAVDREKKEKAEKIAENVVAVDGEKERGGDLEKKSDEFQKILEVSV 120

EST1      RRFQDKMSAHGAGIKTSSSAVPFASPKS----- 93
EST2      DRIQRMQVVDRAAAAIISAARAILASNNSGDGKEGFPNEDNTVTSEVTETPKNAKLGMSR 180

EST1      -----RFLSKQEKFYPRCTPRITGPGSRDT 118
EST2      TVYVPRSETSGTETPGPDFSWTPPGQSEISSVDLQAVEKPAEFPPLPNPVLKDKSADS 240

EST1      PPKRDTGIANEK-----DWGIDLLN----- 138
EST2      LSIPYESMLSSERHSFTIPPFESLIEVRKEAETKPSSETLSTEHDLDLISSANAEVARV 300

EST1      ----ENVNEAGTNEGSSWFRESGHDLDGNGYRCRWSRMGGSRSHDGSSEWTETWNEKSDW 194
EST2      LDSDLDESSTHGVSEDLKWWKQTGVEKRPDGVVCRWIMIRGVTADGVVEWQDKYNEASDD 360

EST1      TGYKELGVEKSGKNSGDSWWEIWEVLHQDEWSNLARIERSAQKQAKSGTENAGWYEKW 254
EST2      FGFKELGSEKSGRDATGNVWREFWRESMSQENG--VVHMEKTADKWKSGQGDE-WQEKW 417

EST1      WEKYDAKQWTEKGAHKYGRRLNEQS-----WWEKNGEHYDGRGSVLKWTDKWAETEL 305
EST2      WEHYDATGKSEKWAHKWCSIDRNTPLDAGHAHVWHERWGEKYDGGGSKYTDKWAERWV 477

EST1      GT---KWGDKWEKFFS-GIGSRQGETWHSVSPNSDRWSRTWGEHFGNGKVHXYGKSTTG 361
EST2      GDGWDKWDKWDENFNPSAQGVKQGETWEGKHGDRWNRWGEHNGSGWVHXYGKSSSG 537

EST1      ESWDIVDEETYYEAEPHYGWADVVDSTOLLSIQPRERPPGVYPNLEFGPSPPPPEPDL 421
EST2      EHWDTHTVPQETWYEKFPHFQFFHCFDNEVQLRAVKK-----P 574

EST1      PDQPQ 426
EST2      SDMS- 578

```

**Figure 4.12: Alignment of EST1 and EST2 protein sequences.** Proteins encoded by At1g42430 and At3g55760 were aligned using ClustalW. Amino acids highlighted in blue are shared by both proteins.

Species	Ensembl identifier	Target %id	Query %id
<i>Arabidopsis lyrata</i>	<a href="#">fgenes2 kg.1 3692 AT1G42430.1</a>	95	94
<i>Brachypodium distachyon</i>	<a href="#">BRADI1G76190</a>	67	68
<i>Brassica rapa</i>	<a href="#">Bra039888</a>	92	88
<i>Chlamydomonas reinhardtii</i>	<a href="#">CHLREDRAFT 167685</a>	30	25
<i>Glycine max</i>	<a href="#">GLYMA06G02120</a>	70	74
<i>Hordeum vulgare</i>	<a href="#">MLOC_57196</a>	83	50
<i>Musa acuminata</i>	<a href="#">GSMUA_Achr1G02740_001</a>	82	64
<i>Oryza sativa</i>	<a href="#">LOC_Os03g04100</a>	68	69
<i>Physcomitrella patens</i>	<a href="#">PP1S130_242V6</a>	49	58
<i>Populus trichocarpa</i>	<a href="#">POPTR_0005s27110</a>	72	74
<i>Selaginella moellendorffii</i>	<a href="#">SELMODRAFT_107335</a>	64	55
<i>Setaria italica</i>	<a href="#">Si035781m.g</a>	67	68
<i>Solanum lycopersicum</i>	<a href="#">Solyc04g082290.2</a>	71	73
<i>Solanum tuberosum</i>	<a href="#">PGSC0003DMG400009975</a>	71	72
<i>Sorghum bicolor</i>	<a href="#">Sb01g048110</a>	80	65
<i>Vitis vinifera</i>	<a href="#">VIT_18s0001g00110</a>	74	75
<i>Zea mays</i>	<a href="#">GRMZM2G110345</a>	64	67

**Table 4.2 List of EST1 orthologs.** Proteins with similar protein sequence to EST1 were found in these plant species according to the Ensembl Plants genome browser (<http://plants.ensembl.org/index.html>; release 18). The table shows the Ensembl gene identifier and the percentage of identical amino acids in the ortholog compared with EST1 (Target %id) and the percentage of identity in EST1 protein compared to the ortholog amino acid sequence (Query %id). **Orthologs** are defined in Ensembl as genes for which the most common ancestor node is a speciation event.

Species	Ensembl identifier	Target %id	Query %id
<i>Arabidopsis lyrata</i>	<a href="#">fgenesh2 kg.5 2004 AT3G55760.2</a>	97	97
<i>Brachypodium distachyon</i>	<a href="#">BRADI4G15010</a>	47	51
<i>Brassica rapa</i>	<a href="#">Bra023783</a>	86	75
<i>Chlamydomonas reinhardtii</i>	<a href="#">CHLREDRAFT 167685</a>	35	21
<i>Glycine max</i>	<a href="#">GLYMA02G00430</a>	52	54
<i>Hordeum vulgare</i>	<a href="#">MLOC 9792</a>	49	52
<i>Musa acuminata</i>	<a href="#">GSMUA Achr8G26900_001</a>	53	52
<i>Oryza sativa</i>	<a href="#">LOC Os11g37560</a>	48	52
<i>Physcomitrella patens</i>	<a href="#">PP1S215_5V6</a>	40	43
<i>Populus trichocarpa</i>	<a href="#">POPTR_0008s15930</a>	57	57
<i>Selaginella moellendorffii</i>	<a href="#">SELMODRAFT_11669</a>	47	43
<i>Setaria italica</i>	<a href="#">Si026146m.g</a>	49	50
<i>Solanum lycopersicum</i>	<a href="#">Solyc06g053920.2</a>	56	54
<i>Solanum tuberosum</i>	<a href="#">PGSC0003DMG400016314</a>	56	54
<i>Sorghum bicolor</i>	<a href="#">Sb05g022830</a>	48	50
<i>Vitis vinifera</i>	<a href="#">VIT_05s0020g04440</a>	56	55
<i>Zea mays</i>	<a href="#">GRMZM2G069092</a>	49	49

**Table 4.3 List of EST2 orthologs.** Proteins with similar protein sequence to EST2 were found in these plant species according to the Ensembl Plants genome browser (<http://plants.ensembl.org/index.html>; release 18). The Ensembl gene identifier and the percentage of identical amino acids are given in the table. “Target %id” indicates amino acid identities in the ortholog compared with EST2 protein and “Query %id” shows the percentage of amino acids of EST2 protein shared with the orthologous protein. **Orthologs** are defined in Ensembl as genes for which the most common ancestor node is a speciation event.

#### 4.2.5.5 Gene expression of At1g42430

There is no information about gene expression of At1g42430, as the gene is not represented on microarrays produced by Affymetrix.

#### ***4.2.6 Preliminary experimental data on EST1 and EST2***

There is little information about EST2 in the literature. However, EST2 protein was found in association with starch granules purified from pea several years ago (Alison Smith and Sam Zeeman, personal communication. The identification was based on N-terminal sequencing.). The *Arabidopsis* knock-out line for EST2 did not show an obvious starch phenotype, therefore it was not characterised further. Recently, our collaborators in Sam Zeeman's lab at the ETH in Zürich sequenced all proteins that were bound to *Arabidopsis* starch. EST2 was found to be the third most abundant protein on granules after GBSS and SSII. EST1 was found as well, but in lower quantities; it was the 8<sup>th</sup> most abundant protein. Both proteins were also found in starch of other plant species, like potato, cassava, rice, wheat and maize. They were present in starches of grains, tubers and leaves. Our collaborators decided to characterise the EST2 knock-out mutant again and found that the mutant has slightly elevated end of day and end of night starch contents compared to wild-type. Mutant *est2* had three times more starch than wild-type at the end of the night (David Seung, ETH Zürich, personal communication). This phenotype seems opposite to the phenotype of the *est1* mutants, which have lower end of day starch contents than wild-type. We are now collaborating with the group in Zürich to characterise EST1 and EST2 function in more detail. Further characterisation of *est1* mutants is presented in **Chapter 5**.

#### ***4.2.7 Identification of an EMS-induced point mutation in mutant B***

To find the underlying mutation in mutant B, a map-based cloning approach was applied. Mutant B (Col-0 background) was crossed to a wild-type *Ler* plant and F<sub>2</sub> plants of the cross were analysed for starvation signals at the end of the early night. For map-based cloning, recombinants used for genotyping have to be homozygous for the gene of interest (**4.1.3**). Since the mutation in mutant B was dominant (**4.2.1**), homozygous mutants are phenotypically not distinguishable from heterozygous mutants. Therefore, DNA was extracted from F<sub>2</sub> plants that had no phenotype, i.e. carried only the wild-type allele of the target gene originating from the *Ler* parent. Like this, it could be ensured that selected recombinants are homozygous for the gene of interest. *Ler* wild-type plants do not contain the starvation reporter construct (*pAt1g10070:LUC*). Therefore, F<sub>2</sub> plants segregated for the transgene. Because the transgene is dominant only one quarter of F<sub>2</sub> plants cannot express luciferase. To

identify plants without the reporter, luciferase expression was also measured three hours after extension of the early night. At this time point, wild-type plants carrying the transgene should express luciferase. F<sub>2</sub> plants that had no starvation signal at the end of the early night, but had a signal after the extended early night, were assumed to be wild-type for the gene of interest. To confirm this, one leaf of each of these plants was used for an iodine stain to confirm that the plants had wild-type amounts of starch at the end of an early night. This strategy required more time and growth space. Therefore, fewer plants were available for map-based cloning.

A rough map position was obtained using 16 markers that were evenly spread over the genome (**Figure 4.13**). The first analysis of 14 plants suggested that the mutation is on chromosome three or four, since low recombination frequencies were observed on these chromosomes. Therefore, markers on chromosome three and four were analysed in another 16 plants. Marker nine showed the closest linkage to the mutation (19% Col-0 alleles). This indicated that the mutation was located on chromosome 3. To narrow down the interval, further markers upstream and downstream of marker nine were analysed. The area with the lowest recombination rate was framed by markers MB4 and MB8, but this interval was not free of recombination events. Some plants were heterozygous for Col-0/*Ler* polymorphisms at markers MB1-MB8. The reason for this could be incorrect phenotyping of recombinants. The interval with the lowest recombination rate had a size of 1.4Mb and contained 453 genes (**Figure 4.14**). Looking at the annotation of the putative candidate genes in that interval, one gene related to starch metabolism was found. It was At3g23920, which encodes beta-amylase 1 (*BAMI*). The gene was sequenced and an EMS-induced point mutation discovered.

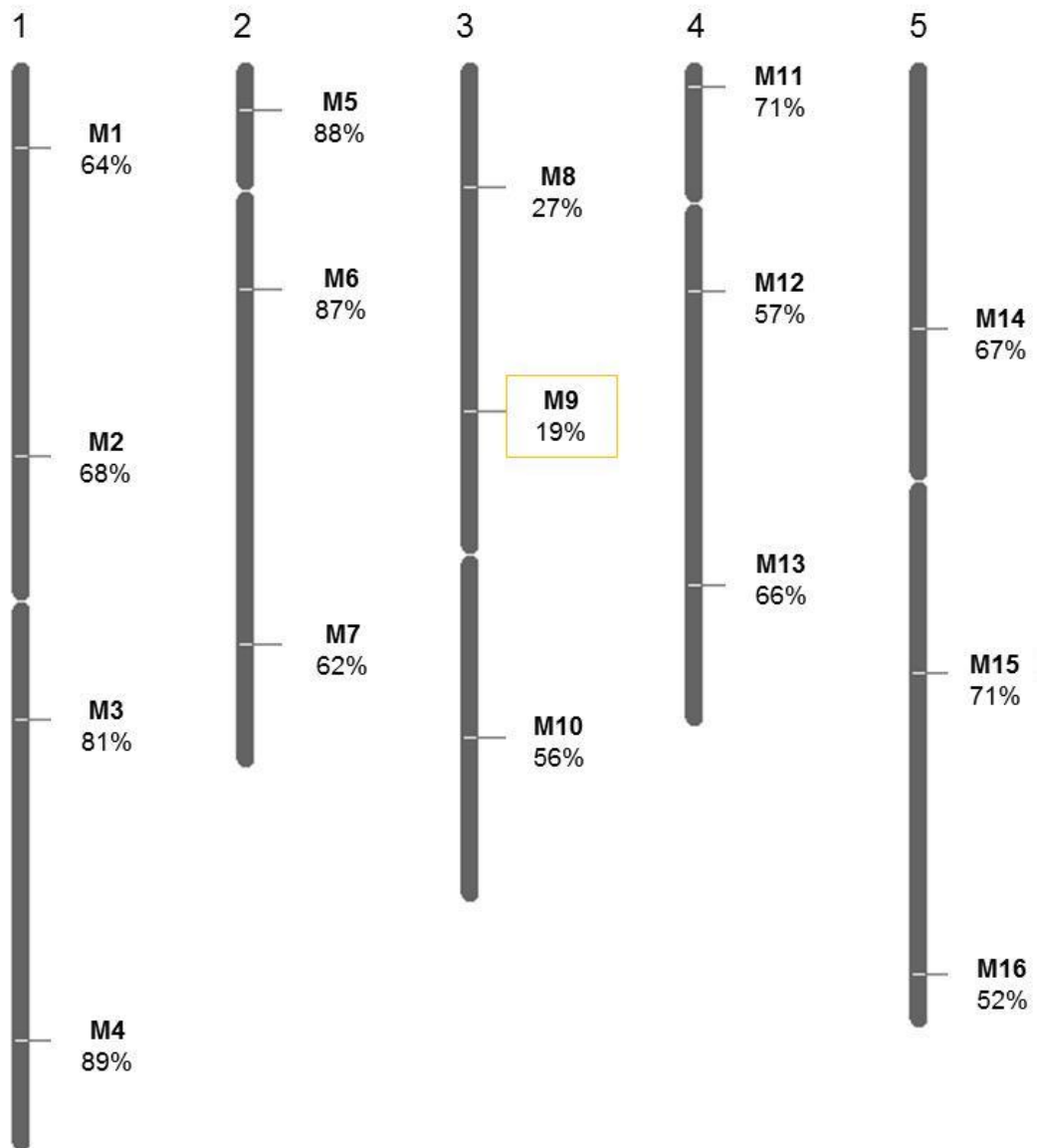


**Figure 4.13: Summary of rough mapping of mutant B.** Sixteen markers (M1-16) which were evenly distributed over the five *Arabidopsis* chromosomes were analysed for their linkage to the mutation causing the phenotype in mutant B. The percentage of detected Col-0 alleles at each marker position was calculated to identify areas with low recombination. The orange box highlights the marker with the closest link to the mutation. Linkage analysis was performed on individual F<sub>2</sub> plants of the out-cross to *Ler* after selection of plants that were homozygous wild-type for the mutation. Thirtyone plants were used for genotyping of markers M8-M13 and 14 plants for all other markers.

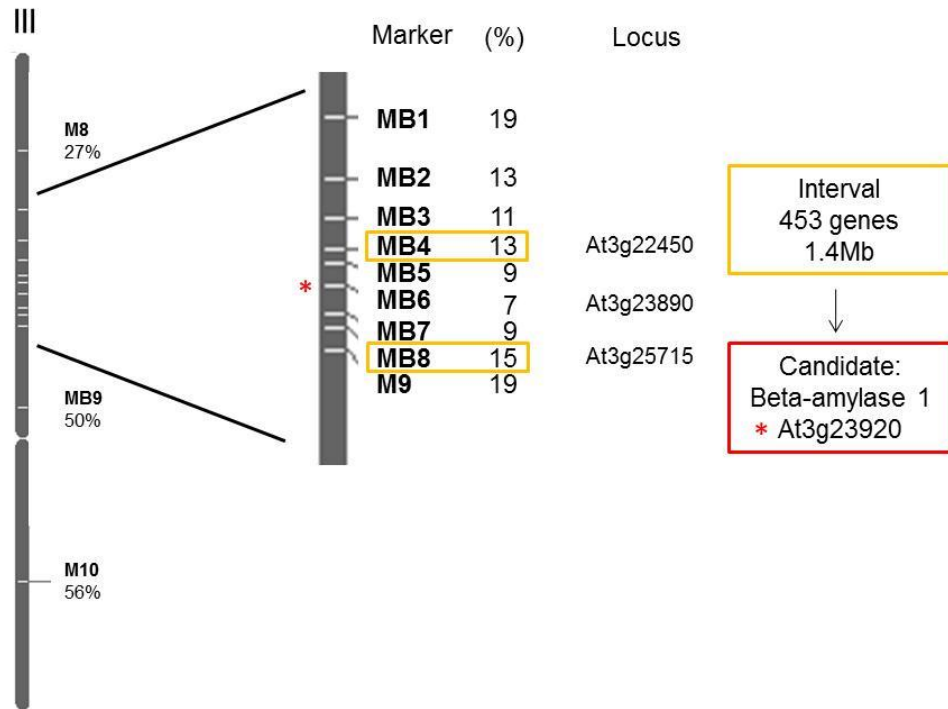


**Figure 4.14: Map-based cloning result of mutant B.** Nine additional markers (MB1-MB9) were analysed for their linkage to the underlying mutation in mutant B. Recombination events at each marker were quantified by calculating the percentage (%) of detected Col-0 alleles in relation to total number of alleles. Orange boxes highlight the markers which had a close link to the target mutation and were defined as borders of the mapping interval. Linkage analysis was performed on 31 individual F<sub>2</sub> plants of the out-cross to *Ler* after selection of recombinants which were wild-type for the mutation. A mapping interval was defined that contained the putative candidate beta-amylase 1 (*BAMI*).

#### 4.2.8 *In silico* analysis of point mutation in *bam1-2*

The mutation in *BAMI* was found in the first exon of the gene, 548 bp downstream of the start codon. This is in position 395 bp of the coding sequence. The mutation is a G/A transition that changes codon AGT to AAT, thus causes a serine to asparagine substitution at position 132 of the protein. In the following, I will refer to mutant B as mutant *bam1-2*, as *bam1-1* is the name of the previously characterised *BAMI* knock-out mutant, SALK\_039895 (Fulton et al., 2008).

To find out how the mutation could affect *BAMI* activity, I investigated the effect of the mutation on the protein by *in silico* analysis. The amino acid substitution is located in the conserved glycosyl hydrolase 14 domain that is present in all beta-amylases

(Figure 4.15). However, Ser-132 is not one of the known active site residues or substrate binding residues (Fulton et al., 2008). There is experimental evidence for BAM1 phosphorylation from plant phosphoproteomic analysis (Reiland et al., 2009; van Bentem et al., 2008). However, the serine in position 132 is not one of the known phosphorylation sites. Two cysteine residues (Cys-32 and Cys-470) were suggested to form an inhibitory disulphide under oxidising conditions (Sparla et al., 2006). The residue Ser-132 is not very close to either of them, but lies between them.

```

1 MALNLSHQLGVLGAGTPIKsGEMtDssLLsI$PPsARMMPKAMNRNYKAHGtDP$PPMSP
61 ILGAtRADLSVACKAFaVENGIgTIEEQRTYREGGIGGKKEGGGGVPVFVMMPLDSVTMG
121 NTVNRRKAMKASLQALKSAGVEGIMIDVWWGLVEKESPGTYNWWGGYNELLELAKKLGLKV
181 QAVMSFHQCcGGNVGDSVTIPLPQWVVEVDKDPDLAYTDQWGRRNHEYISLGADTLPVLK
241 GRTPVQCYADFMRAFRDNFKHLLGETIVEIQVGMGPAGELRYPSYPEQEGTWKFPGIGAF
301 QCYDKYLSLSSLKAAAETYGKPEWGSTGPTDAGHYNNWPEDTQFFKKEGGGWNSEYGDFFL
361 SWYSQMLLDHGERILSSAKSIFENMGVKISVKIAGIHWHYGTRSHAPELTAGYYNTRFRD
421 GYLPIAQMLARHNAIFNFTCIEMRDHEQPQDALCAPEKLVNQVALATLAAEVPLAGE$NAL
481 PRYDDYAHEQILKASALNLDQNNEGEPREMCAFTYL$RMNPELFQADNWWGKFVAFVKKMGE
541 GRDSHRCREEVEREAHFVHVTQPLVQEAVALTH

```

**Figure 4.15: Protein sequence of *Arabidopsis* beta-amylase 1.** The EMS induced point mutation in *bam1-2* causes a serine to asparagine amino acid substitution in position 132 of the protein, which is highlighted in red. The cTP as predicted by ChloroP (<http://www.cbs.dtu.dk/services/ChloroP/>) is shown in italics. The glycosyl-hydrolase 14 domain is underlined. The domain was identified by using the conserved domain search on NCBI (<http://www.ncbi.nlm.nih.gov/Structure/cdd/wrpsb.cgi>). Substrate binding residues are in bold, two catalytic glutamic acid residues are highlighted in blue and bold (Fulton et al., 2008). Cysteines involved in the formation of a disulphide bridge are shown in orange (Sparla et al., 2006). Serine, threonine or tyrosine phosphorylation sites are shown in green. Amino acids were phosphorylation was ambiguous are shown in lower case. (Reiland et al., 2009; Fuente van Bentem et al., 2008; Kötting et al., 2010).

Analysis of the primary protein sequence did not indicate how the amino acid substitution could affect BAM1 activity. Therefore, I analysed the position of the amino acid substitution in the three-dimensional structure of the protein. The structure of soybean beta-amylase (Gm BMY1) has been resolved by X-ray crystallography (Mikami et al., 1994). Alignment of the BAM1 protein sequence with the sequence of the soybean beta-amylase showed that BAM1 Ser-132 is not conserved in Gm BMY1,

but substituted with a glutamine residue (**Figure A4 , Appendix**). This residue is part of an alpha-helix which is located on the surface of the protein, as shown by modelling of this residue in the Gm BMY1 protein structure (Protein Data Bank identifier: PDBID 1BYB) (**Figure 4.17**). The alignment of soybean beta-amylase and *Arabidopsis* BAM1 protein sequences shows that the N-terminal part of BAM1, which contains one of the two cysteine residues (Cys-32) that forms a disulphide bridge (Sparla et al., 2006), does not align with the soybean protein sequence. The second cysteine residue (Cys-470) is substituted with phenylalanine in the soybean enzyme (**Figure A4**). The position of this residue (F-415) in the soybean beta-amylase protein structure is indicated in **Figure 4.17**.

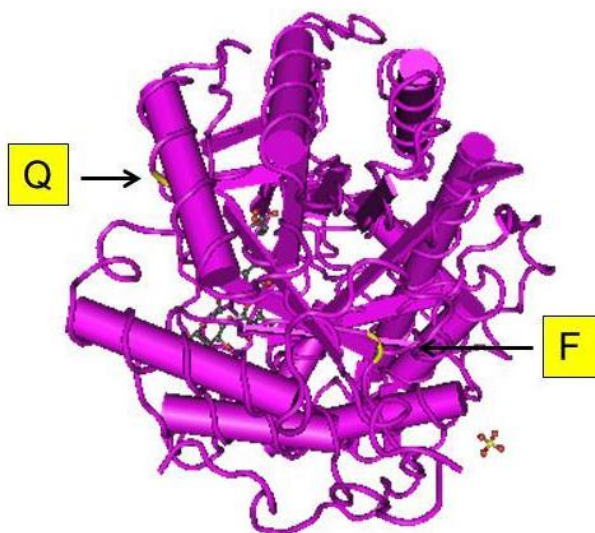


**Figure 4.17: Three dimensional structure of soybean beta-amylase.** The structure was obtained on NCBI Structure using the following identifier: PDB ID 1BYB. The structure was analysed using the Cn3D structure viewer (<http://www.ncbi.nlm.nih.gov/Structure/CN3D/cn3d.shtml>). Glu-38 (Q) and Phe-415 (F) were highlighted in yellow.

To find out if Ser-132 is conserved in all nine beta-amylases found in *Arabidopsis*, the protein sequences of BAM1-9 were aligned using ClustalW (**Figure 4.18**). Only BAM3 and BAM4 contain a serine residue in the equivalent position of Ser-132. Three other beta-amylases have a substitution with glutamine in that position as observed in the soybean enzyme. The alignment also shows that BAM1 Ser-132 is located next to a highly conserved leucine residue.

```

BAM1_At3g23920 KAMKASLQALK
BAM2_At4g00490 EELLDQLRTLK
BAM3_At4g17090 RAMNASLMALK
BAM4_At5g55700 KALTVALKALK
BAM5_At4g15210 ETLETQLKRLK
BAM6_At2g32290 ESLKKQLKKLK
BAM7_At2g45880 DGLLKHLRILK
BAM8_At5g45300 EGVRQELSYMK
BAM9_At5g18670 KAITAGLKALK

```

**Figure 4.18: Alignment of partial protein sequences of nine *Arabidopsis* beta-amylases.** Protein sequences of nine *Arabidopsis* beta-amylases (given with the gene locus identifier) were aligned using ClustalW. Residues conserved between all nine enzymes are shown in blue. BAM1 Ser-132 was conserved in two other beta-amylases as indicated in red.

#### 4.2.9 Confirmation of *BAM1* as gene causing the phenotype of *bam1-2*

To confirm that the mutation I have identified in *BAM1* is responsible for the phenotype of *bam1-2*, I want to show that expression of the *bam1-2* cDNA in the *bam1-1* mutant (which lacks *BAM1* protein and has a wild-type phenotype) results in the starch phenotype seen in *bam1-2*. Transformants are in T<sub>2</sub> and growing at the moment. I will select a homozygous T<sub>3</sub> line to analyse the starch degradation phenotype.

#### 4.2.10 Back-crossing of *est1-1* and *bam1-2*

For further experiments, EMS mutant plants were back-crossed to the starvation reporter line to reduce levels of background mutations. Identification of homozygous *est1-1* mutants was possible in the F<sub>2</sub> generation by analysing bioluminescence signals at the end of the early night. Homozygous *bam1-2* plants were identified by analysis of segregation rates in the F<sub>3</sub> generation, by measurement of luciferase-induced bioluminescence at the end of the early night. For *est1-1*, three back-crosses were performed. Mutant *bam1-2* has only been back-crossed once. In the experiments presented in the following chapters, I used the homozygous mutant progeny from these back-crosses, unless stated otherwise.

### 4.3 Discussion

#### 4.3.1 The mutation in *At1g42430* causes the phenotype of *est1-1*

The underlying mutation in mutant A was identified by a combination of map-based cloning and whole genome sequencing. Mutant *est1-1* is a knock-out for *EST1*, as no more protein was detectable by immunoblotting.

The reason for absence of EST1 protein in *est1-1* could be mis-splicing of the mRNA. Intron splice site consensus sequences are made up of 5'GU and 3'AG dinucleotides. Mutation of these highly conserved nucleotides abolishes mRNA splicing. If the 3'AG splice site is mutated, splicing usually occurs at AG dinucleotides downstream of the mutation. The next AG will usually be in the adjacent exon and thus, parts of the coding sequence will be spliced out. This can result in frame shifts or sometimes the omission of whole exons (reviewed in Brown et al., 1996). In consistence with that, my RT-PCR analysis indicated that a shorter *EST1* mRNA was expressed in *est1-1* (**Figure 4.6**). Absence of EST1 protein in *est1-1* might therefore be the result of synthesis of unstable protein, due to frame shifts or due to misfolding of the protein, caused by translation of aberrant mRNA.

Analysis of the starch phenotype of mutants complemented with *EST1* cDNA and a T-DNA insertion line lacking EST1 protein confirmed that the mutation in *EST1* caused the starch degradation phenotype of *est1-1* mutants. Line GABI\_031C11 (*est1-2*) is a knock-out of *EST1* and the iodine stain of leaf starch looked identical to *est1-1* in that no starch was detectable one hour before the end of the night. This line will therefore be used in further experiments presented in this thesis. Two T-DNA insertion lines (SALK\_070292; SALK\_0402906) still contained wild-type amounts of EST1 protein and starch was detectable one hour before the end of the night, like in wild-type. Therefore, they were not used further. The *est1-1* line overexpressing EST1 (35S:*At1g42430*) had more starch than *est1-1* and wild-type at the end of the night. However, the transgene had a point mutation. This mutation resulted in an amino acid substitution in a serine residue (Ser-192) that is highly conserved in EST1 orthologs in other plant species. Therefore, the mutation could have altered the function of the protein. However, it is undoubted that expression of the cDNA had an effect on leaf starch degradation in *Arabidopsis*. Experiments to express the wild-type cDNA in *est1-1* are in progress.

### 4.3.2 Back-crosses

The EMS mutant *est1-1* was back-crossed three times, which means that about 12.5% of unrelated EMS mutations are still present. More back-crosses could be attempted to reduce the background of unrelated mutations as much as possible. However, in the following chapter, I will show that the knock-out lines *est1-1* and *est1-2* have nearly identical phenotypes. Therefore, the effect of remaining background mutations on the starch degradation phenotype seems to be negligible.

### 4.3.3 Preliminary speculations about EST1 and EST2 function

From the data presented here, EST1 protein is clearly involved in the pathway of starch degradation in *Arabidopsis* leaves. The knock-out mutant *est1-1* degraded starch faster than wild-type (**Chapter 3**) and *est1-2* had no detectable starch one hour before the end of the night. So far, no other mutants with altered starch degradation are known that have a similar phenotype. The line overexpressing EST1 (*35S:Atlg42430*) had a starch excess phenotype. It had about 55% more starch than wild-type at the end of the day and degraded only 47% of it during the night. One mutant of the starch degradation pathway has a comparable mild starch excess. Mutants lacking BAM4 have about 60% more starch than wild-type at the end of the day and degrade about 60% of it during the night (Fulton et al., 2008). Starch contents of *bam4* and other mutants of the pathway can be found in **Chapter 6**. EST1 and EST2 proteins do not have any of the catalytic domains which are found in other enzymes of the pathway. Thus, it is likely that they encode proteins with a previously undiscovered function in the starch degradation pathway.

It seems likely that EST1 plays a role in starch degradation in many plant species. EST1 and EST2 might even be present in all green plants, as they were found in all plant species for which sequence information is available. Green algae also contain proteins orthologous to EST1 and EST2. Experimental evidence from our collaborators showed that EST1 and EST2 proteins are present in storage starch as well as transient starch. This indicates that the function of EST1 and EST2 proteins is not limited to transient starch degradation, but is a more general one.

The structure of the EST1 protein seems to be substantially disordered and no proteins with similar structure are known according to Phyre (<http://www.sbg.bio.ic.ac.uk/phyre2/html/page.cgi?id=index>). Intrinsically disordered proteins have no stable structure without a partner molecule (Ishida and Kinoshita, 2008). Since EST1 was found in association with starch granules, I speculate that it needs to bind starch or other proteins to obtain a stable structure.

In the following chapter, I will characterise the *est1* phenotype in more detail to find out more about its role in starch degradation in *Arabidopsis* leaves. The function of EST2 protein is being investigated by our collaborators at the ETH in Zürich.

#### ***4.3.4 Does the point mutation in BAM1 cause the phenotype of bam1-2?***

The mutation in *bam1-2* was identified by map-based cloning. Unfortunately, only a small number of individual plants was available for mapping. I genotyped about 31 recombinants in the F<sub>2</sub>, but in the literature genotyping of at least 50 plants for rough mapping and at least 200 plants for fine-mapping is recommended (Jander et al., 2002; Weigel and Glazebrook et al., 2002). However, the absolute number of plants required will depend on the position of the mutation in the genome, as recombination frequencies vary. Also, analysis of only 31 plants showed that recombination rates were lower on chromosome three.

Another complication during the mapping process of mutant B was that I did not identify a chromosomal area without recombination. None of the plants analysed between markers MB4 and MB8 was homozygous for Col-0 alleles, but some were heterozygous. Marker MB6 is very close to the *BAM1* locus, so all plants should have contained only gDNA of the *Ler* ecotype at this marker position if the mutation was really caused by *BAM1*. I think that the problem could have been the more complicated phenotyping of plants wild-type for the mutation. It is possible that plants heterozygous for the mutation have a milder phenotype and so can be mistaken for wild-type. Thus, I might have selected some heterozygous plants, assuming they were wild-type. *BAM1* was the most obvious candidate in the mapping-interval. However, I cannot exclude that another mutation has caused the phenotype of mutant *bam1-2* until I have analysed the phenotype of transgenic *bam1-1* plants overexpressing *BAM1* cDNA with the point mutation.

#### 4.3.5 Preliminary speculations about the effect of the mutation in *BAM1*

The position of Ser-132 in the *BAM1* protein sequence did not give an obvious explanation for the mutant phenotype. The amino acid substitution does not affect any of the known substrate binding sites or catalytic site residues of the protein (Fulton et al., 2008). Ser-132 seems to be located on the surface of the protein, as the position of the equivalent residue in soybean beta-amylase indicated. It could therefore be possible that the mutation alters post-translational modification sites and thereby enhances protein activity. However, Ser-132 is very unlikely to be a phosphorylation site, as this position was not found to be phosphorylated in a phosphoproteomics analysis (Reiland et al., 2009, van Bentem et al., 2008). Ser-132 is located between two cysteine residues which form an inhibitory disulphide when the protein is oxidised (Sparla et al., 2006). It is possible that the formation of this inhibitory disulphide is disturbed. For example S132N could cause incorrect protein folding so that the distance between the two cysteine residue changes. Ser-132 is located next to a highly conserved leucine. If this leucine residue is necessary for correct folding of the protein, the serine to asparagine substitution in close proximity to it might interfere with it. This could potentially inhibit formation of the disulphide bridge. Incorrect protein folding could also alter protein-protein interactions in a positive or negative way.

Interestingly, the alignment of *BAM1* with the protein sequence of the eight other *Arabidopsis* beta-amylases showed that Ser-132 is conserved only in *BAM3* and *BAM4*. Beta-amylases 1-4 are located in the chloroplast, while the other five beta-amylases are predicted to be extrachloroplastic (Fulton et al., 2008). *BAM2* is the only chloroplastic beta-amylase that was not shown to be involved in starch degradation in *Arabidopsis*. Knock-out of this protein does not result in a starch excess, even in the absence of other chloroplastic beta-amylases (Fulton et al., 2008). Thus it appears that the *BAM1* residue Ser-132 is only conserved in chloroplastic beta-amylases that are involved in starch degradation in *Arabidopsis* leaves.

To find out how the mutation in *BAM1* affects starch degradation, mutant *bam1-2* will be characterised in **Chapter 6**.

## 5 Characterisation of *est1* mutants

### 5.1 Introduction

In **Chapter 3** I described how I identified *est1-1* in a screen for early starvation mutants. The point mutation underlying the early starvation phenotype was recessive and located in a gene of unknown function, which I named *EST1* (**Chapter 4**). I isolated a T-DNA insertion mutant that is affected in the same gene (*est1-2*). Both mutants lack the EST1 protein and iodine stains showed that the mutants have less starch than wild-type before the end of the night. Mutant *est1-1* degraded starch at a faster rate than wild-type. Further evidence for that will be given in this chapter, when starch degradation rates of both mutants are analysed in more detail.

#### 5.1.1 Aim

With the work presented in this chapter, I aim to gather information about the function of EST1 through analysis of mutant phenotypes. I describe the growth and starvation phenotypes and analyse the rate of starch degradation in *est1-1* and *est1-2*. I compare structure and composition of *est1-1* starch granules to those of wild-type starch granules. Finally, I analyse the starch phenotype of crosses of *est1* to mutants lacking components of the starch degradation pathway. Based on the results, I discuss two hypotheses for faster starch degradation in the mutant.

#### 5.1.2 Hypotheses for faster starch degradation in *est1* mutants

There could be several explanations for a faster starch degradation rate in *est1* mutants. The circadian clock is the timing mechanism that underlies starch degradation (Graf et al., 2009). In theory, a faster running clock could explain the phenotype of *est1*. However, as shown in **Chapter 3**, the circadian clock has a normal free running period in *est1-1* seedlings. Therefore, I hypothesise two other reasons for faster starch degradation in *est1*:

Firstly, it could be the result of a change in granule structure or composition. Such changes could alter the granule in a way that makes it more susceptible to enzymatic attack. In that case, EST1 could have a function in stabilising the starch granule e.g. by increasing its crystallinity.

Secondly, faster starch degradation could be explained if EST1 is a negative regulator of enzymes that degrade starch. In the absence of the protein, starch would be degraded faster. So far, no proteins are known that are negative regulators of enzymes in the pathway.

## 5.2 Results

### 5.2.1 Phenotype of *est1-1*

#### 5.2.1.1 Growth, appearance and flowering of mutant plants

The *est1* mutants showed differences in growth and development compared to wild-type plants. Mutant rosettes that were grown in 12 hour light-12 hour dark cycles for 24 days had a 40% lower fresh weight than wild-type rosettes and a smaller diameter. Otherwise *est1* and wild-type were comparable in leaf colour and shape. Flowering of *est1-1* and *est-2* was delayed in comparison to wild-type plants. When mutant plants flowered, shoot development was slightly different from wild-type, because the axillary shoots of the mutant grew with a wider angle from the primary stem (**Figure 5.1**).

#### 5.2.1.2 Starvation phenotype of *est1-1*

When *est1-1* was identified in the forward genetic screen, symptoms of starvation (i.e. bioluminescence caused by activation of the *pAt1g10070:LUC* reporter) appeared earlier in the mutant than in wild-type. Bioluminescence in mutant seedlings was detected at the end of a normal night and at the end of an early night. Wild-type seedlings did not have detectable levels of bioluminescence at those time points (**Chapter 3**). To analyse the starvation pattern in mature plants, the experiment was repeated on 24-day-old rosettes. Bioluminescence was quantified every hour during the normal and early night. This allowed a comparison between the onsets of starvation in both conditions. (**Figure 5.2**). Wild-type plants did not express luciferase during the night, even if it started early. The mutant had a higher background level of bioluminescence compared to wild-type. After about 11 hours of darkness, bioluminescence increased exponentially and to the same extent in the normal as well as the early night. This suggests that the plants started to experience starvation at about the same time in normal and early nights.

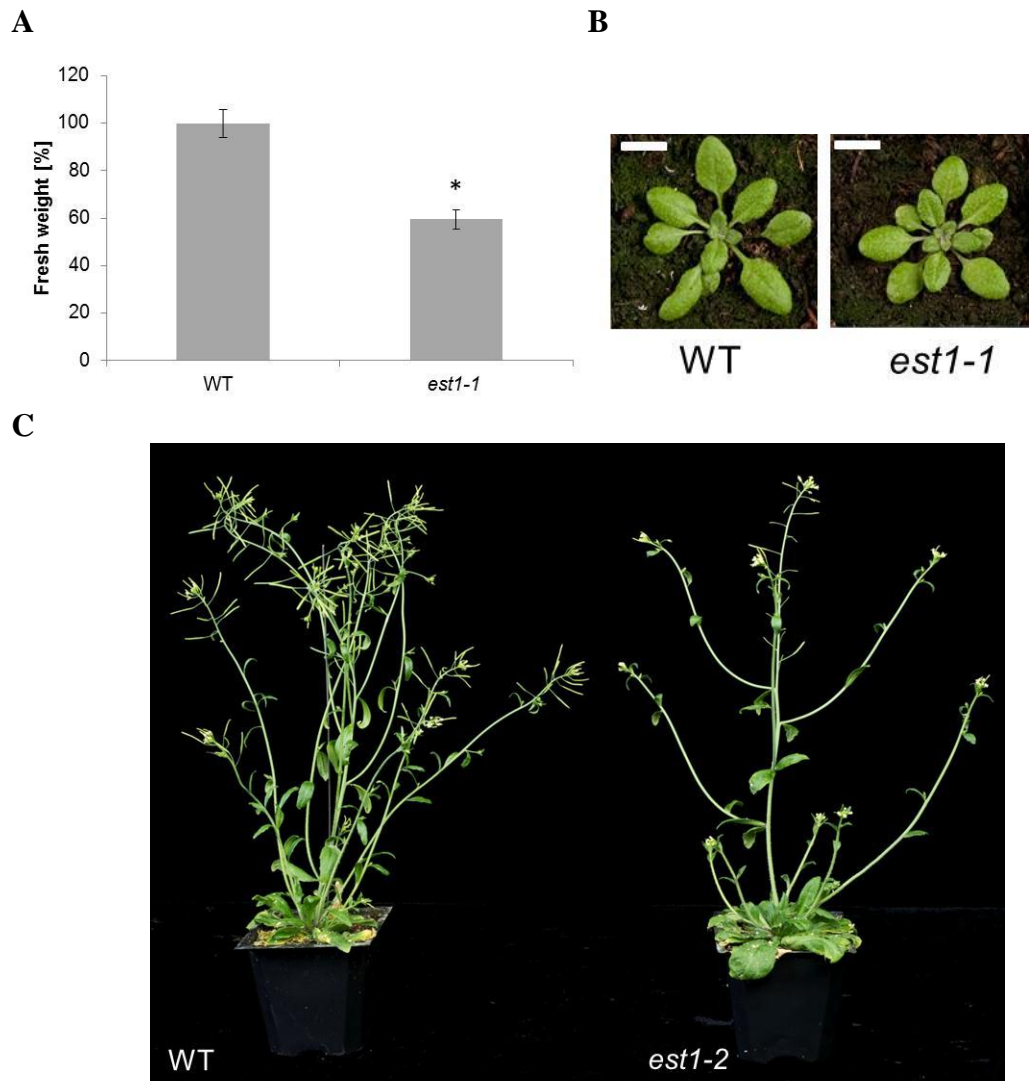


**Figure 5.1: Growth phenotype of *est1*.** (A) Plants were grown in 12 hour light-12 hour dark cycles for 24 days. The fresh weight of whole rosettes was determined and is shown as % of the wild-type fresh weight. Values are means of measurements on 25 rosettes, error bars are s.e.m.. The asterisk indicates a significant difference between the fresh weight of wild-type and mutant plants (t-test,  $p < 0.05$ ). (B) Appearance of *est1-1* and wild-type plants after 30 days, the scale bar indicates a size of 1cm. (C) Appearance of stems of wild-type and *est1-1* plants after about ten weeks of growth. Plants were grown in 12 hour light-12 hour dark cycles.

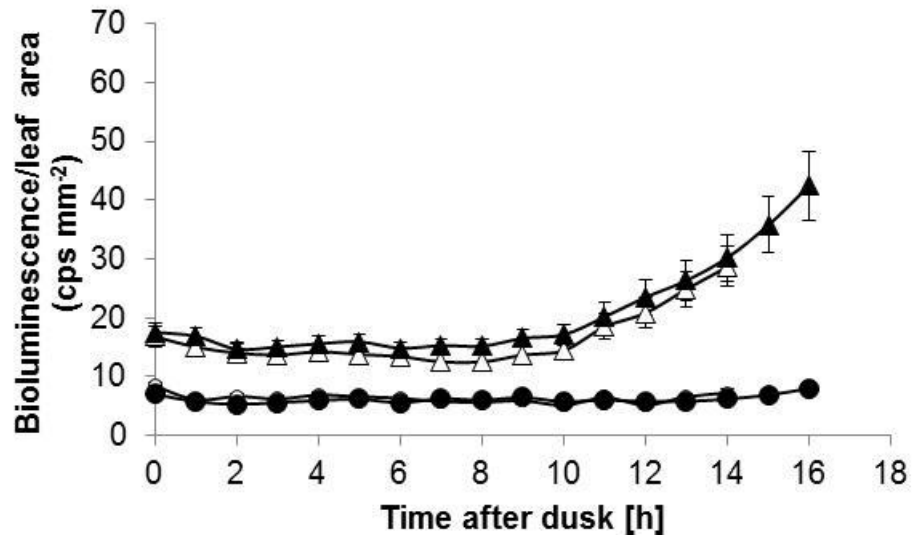


**Figure 5.2: Luciferase induced bioluminescence of *est1-1* and wild-type during normal and early night.** The plants expressed luciferase from the starvation reporter *pAt1g10070:LUC*. Plants were grown for 24 days in 12 hour light-12 hour dark cycles. Bioluminescence of whole rosettes was monitored using the NightOwl camera. It was measured during a normal 12 hour night which was extended by two hours (WT open circles, *est1-1* open triangles) and during an early night (WT closed circles, *est1-1* closed triangles). Total photon emission in counts per second (cps) of each plant is given in relation to leaf area (in mm<sup>2</sup>) which was calculated using the Leaflab program. Values are means of measurements on five rosettes; error bars are s.e.m.; where not visible they are smaller than the symbol.

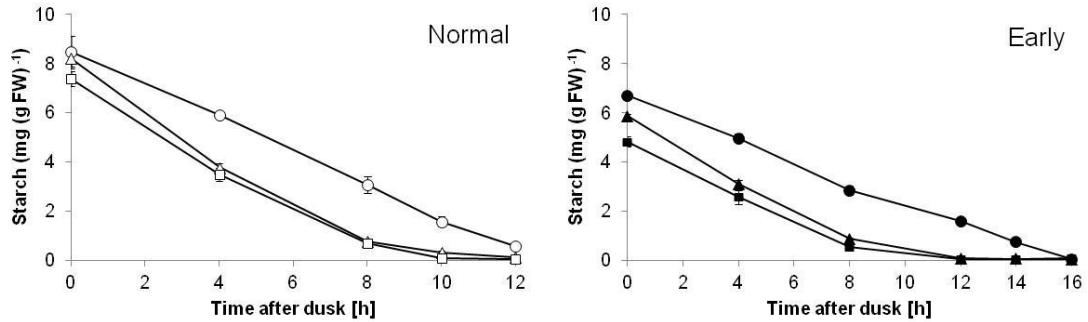
### 5.2.1.3 Starch degradation in *est1-1*

I showed that mutant *est1-1* degrades starch faster than wild-type (**Chapter 3**). To quantify and compare the rates of starch degradation in wild-type, back-crossed *est1-1* plants and *est1-2*, starch contents were measured every two to four hours during the normal and early night (**Figure 5.3.A**). The relative starch contents were calculated to normalise the data for the different end of day starch contents in both conditions and to compare the relative starch degradation rates (**Figure 5.3.B**).

Both mutants had nearly identical starch contents. End of day starch levels of *est1-1* and *est1-2* were comparable to those of wild-type plants. In the normal night starch degradation rates of both mutants were faster than those of wild-type plants. Starch was exhausted earlier than in wild-type plants, between eight and ten hours after dusk. In the early night, starch degradation was also faster than in wild-type and reserves were

exhausted between eight and 12 hours after dusk. Exhaustion of starch roughly coincided with the onset of starvation symptoms in *est1-1* (Figure 5.2).

A



B

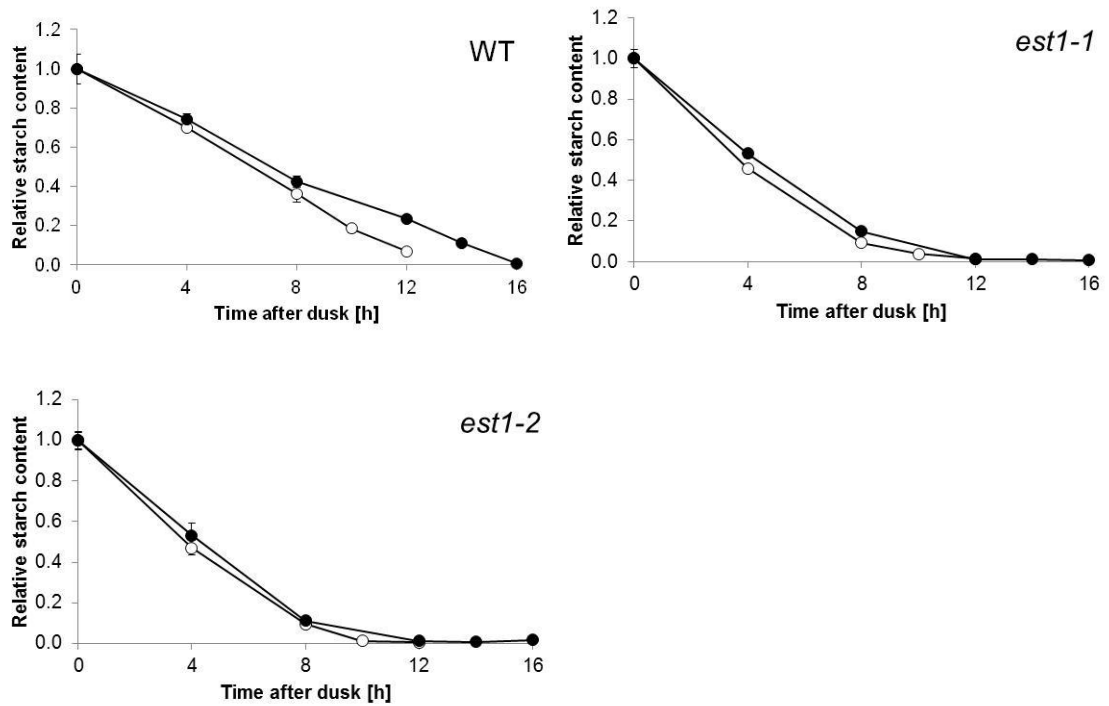


**Figure 5.3: Starch degradation pattern in early and normal night for wild-type and *est1*.** Plants were grown in 12 hour light-12 hour dark cycles for 21 days. (A) Starch contents of three lines (wild-type, circles; *est1-1*, triangles; *est1-2*, squares) were analysed at different time points during a normal night and during an early night. (B) The relative starch contents in both conditions are shown as a fraction of the end of day value for each genotype in both conditions (normal night, open symbols; early night closed symbols). Data are means of measurements on five individual rosettes. Error bars are s.e.m., where not visible, they are smaller than the symbol.

Wild-type plants showed a clear difference between relative starch contents of normal and early night, indicating an adjustment of the starch degradation rate according to the length of the night. In contrast, the relative starch contents of each mutant were nearly identical in normal and early nights (**Figure 5.3 B**).

To quantify starch degradation rates in early and normal night, a linear regression line was fitted through all data points and the slope was determined. This was done for the absolute starch contents (in mg gFW<sup>-1</sup>) and relative starch contents (in % h<sup>-1</sup>) for both conditions and for each genotype (**Figure 5.4**). The mutants exhausted their starch before the end of the night, therefore only values from zero to eight hours after dusk were included in the calculation of the rate.

Mutant *est1-1* and *est1-2* degraded starch with a faster absolute and relative starch degradation rate than wild-type in both conditions. The absolute starch degradation rate of the mutants slowed down in response to the early night. It decreased to a similar extent as in wild-type plants (about 0.3 mg gFW<sup>-1</sup>). However, the relative degradation rate did not change in the early night, i.e. a similar percentage of the initial starch was degraded every hour. In early as well as normal night, the mutants degraded about 11% of the initial starch per hour.

Based on the linear rates, it is possible to extrapolate the time at which starch contents reach zero (**Table 5.1**). According to this estimation, *est1-1* and *est1-2* would both have no starch left after 8.6 hours in the normal night and after 9.3 hours and 8.9 hours respectively in the early night.

I conclude that *est1-1* and *est1-2* have nearly identical starch degradation phenotypes. Both fail to adjust their starch degradation rates according to the length of the night. Their starch degradation rates are faster than those of wild-type plants, but slow down to a similar extent as in wild-type plants when the night starts unexpectedly early. However, the relative starch degradation rate in both mutants was similar in early and normal nights, therefore starch would run out about nine hours after dusk in both conditions.

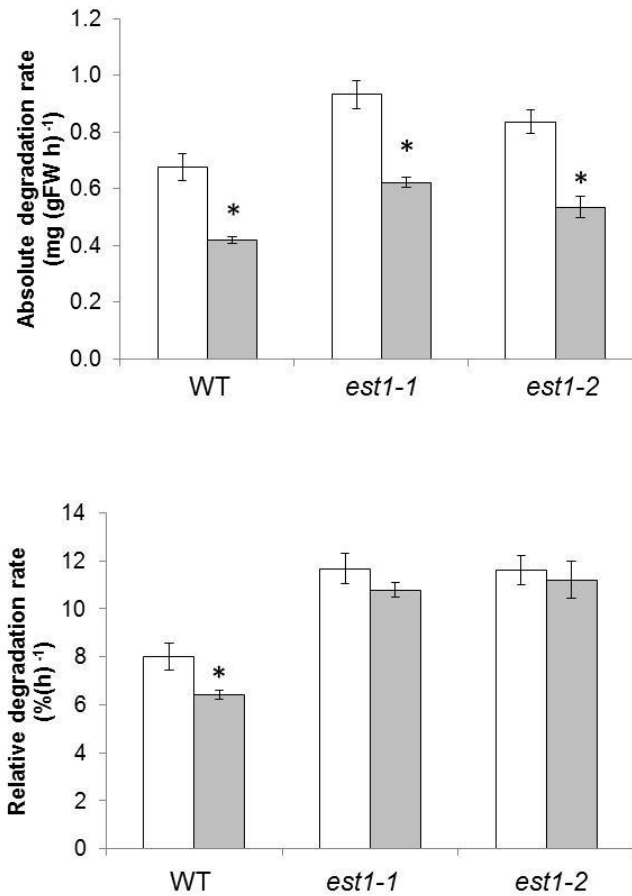


**Figure 5.4: Comparison of starch degradation rates for wild-type, *est1-1* and *est1-2*.** The absolute starch degradation rates and the rates normalised to the end of day value (relative starch degradation rates) were calculated for the linear phase of starch degradation in each genotype based on the data presented in **Figure 5.4**. The rates were determined on basis of the slopes of linear regression lines fitted through all starch contents of the night. For the mutants, only starch contents until eight hours after dusk were taken into account, because starch contents were zero at time points after that. Error bars are s.e.m. on five biological replicates. Rates were analysed for normal night (white bars) and early night (grey bars). Asterisks indicate a significant difference between rates in normal and early nights for each genotype (t-test,  $p < 0.05$ ).

Estimated time of darkness when starch contents would reach zero (h)

	WT	<i>est1-1</i>	<i>est1-2</i>
Normal	12.5	8.6	8.6
Early	15.6	9.3	8.9

**Table 5.1: Estimated time of darkness when starch contents would reach zero for wild-type and *est1-1* and *est1-2*.** Calculations are based extrapolation from starch degradation rates shown in **Figure 5.4** and are given for normal and early night.

#### 5.2.1.4 Iodine stain of leaf starch

An interesting phenotype was revealed by iodine staining of leaves for starch (**Figure 5.5**). Plants were harvested 24 hours into the extended day, to increase starch contents. Iodine staining showed the typical blue colour in mutant and wild-type rosettes. However, wild-type plants displayed the colour throughout, while *est1-1* rosettes did not stain fully. There was no blue colour in the veins of the leaves of *est1-1*, indicating a lack of starch in non-photosynthetic tissue.



**Figure 5.5: Iodine stain of wild-type (WT) and *est1-1*.** Plants were grown in 12 hour light-12 hour dark cycles for 25 days and then transferred to constant light for 24 hours.

Whole rosettes were harvested, decolourised in ethanol and stained with iodine solution. At the bottom, a magnified picture of one leaf is shown.

#### 5.2.1.5 Structure of mutant starch

In theory, faster starch degradation in the mutant could be the result of a change in granule structure. To find out if *est1* produces aberrant granules, leaf sections were viewed by transmission electron microscopy (TEM). This was done with the help of Kim Findlay and Sue Bunnewell (Bioimaging Service, John Innes Centre) (**Figure 5.6**). TEM indicated that granule dimensions and granule numbers per chloroplast in the mutant were in the same range as in wild-type. Leaf starch from mutant and wild-type plants was also purified at the end of the day and viewed by scanning electron microscopy (**Figure 5.7**). This was done with the help of Kim Findlay and Sue Bunnewell (Bioimaging Service, John Innes Centre). The mutant synthesised normal granules with a flat and discoid shape similar to that of wild-type granules. Thus, no obvious changes in the appearance of the granules were observed that could explain the mutant phenotype.

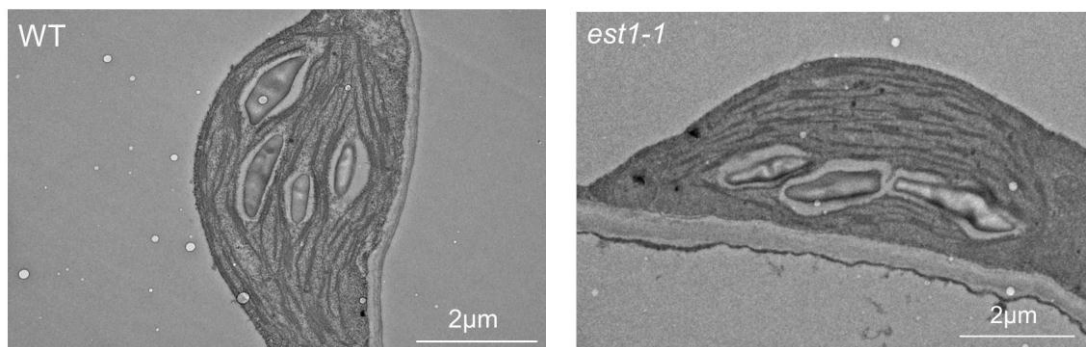


**Figure 5.6: Transmission electron micrographs of leaves.** Mutant and wild-type plants were grown for 23 days in 12 hour light-12 hour dark. Samples from mature leaves were taken in the middle of the day, after six hours of light.

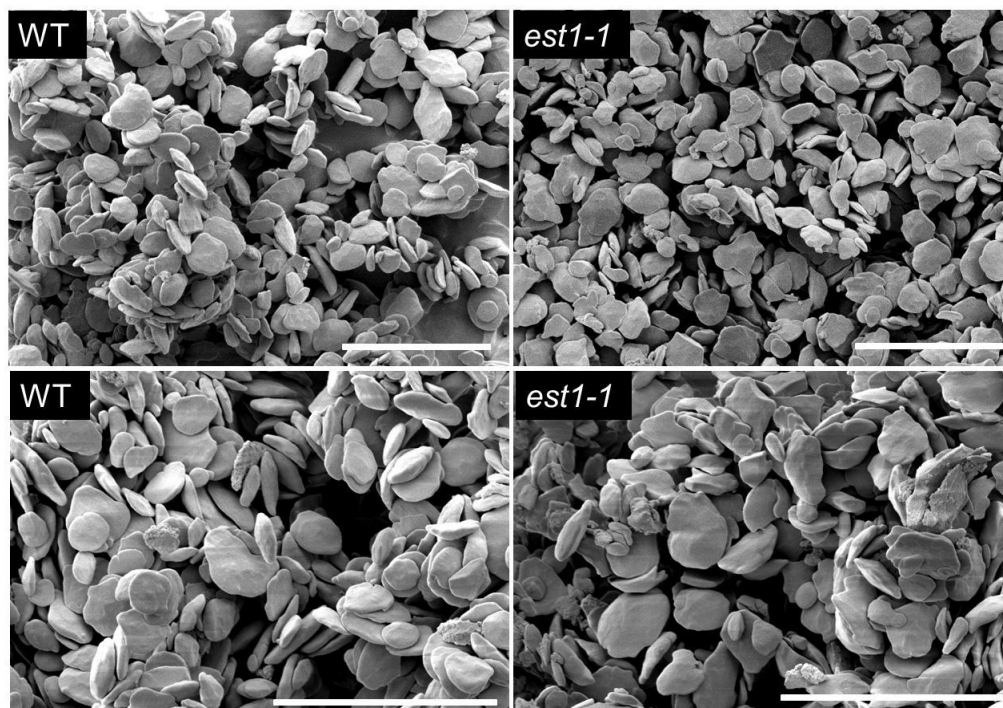


**Figure 5.7: Scanning electron micrographs of starch granules *est1-1* and wild-type.**

Wild-type and *est1-1* plants used for this experiment were 30 days old and grown in 12 hour light-12 hour dark conditions. Plants were harvested at the end of the day and starch was prepared from pooled leaf tissue of whole rosettes. The scale bars indicate a length of 10 $\mu$ m.

#### 5.2.1.6 Composition of mutant starch: Amylose contents

To find out if the mutants have any detectable changes in the composition of their starch granules, the amylose content of *est1-1* and *est1-2* leaf starch was analysed and compared to wild-type (**Figure 5.8**). Starch is composed of amylose and amylopectin (**Chapter 1**). Amylopectin is a highly branched glucose polymer and makes up about 95% of *Arabidopsis* leaf starch. The remainder of the granule consists of amylose, a linear glucose polymer (Zeeman et al., 2002). When complexed with iodine, both polymers can be distinguished on basis of their wavelength of maximal absorbance ( $\lambda_{\text{max}}$ ). The amylose to amylopectin ratio of starch complexed with iodine can be calculated by measuring the absorbance at 700 nm and 525 nm. The  $A_{700}:A_{525}$  ratio is then used to estimate the amylose content, on basis of a pre-established standard curve (Zeeman et. al., 2002). Measurements revealed that mutant starch contained about 60%

more amylose than wild-type starch. Amylose content is not known to play a role in the control of starch degradation. The relevance of amylose for the phenotype of *est1-1* will be analysed later in this chapter, through study of a double mutant lacking EST1 and the enzyme responsible for amylose synthesis (GBSS).

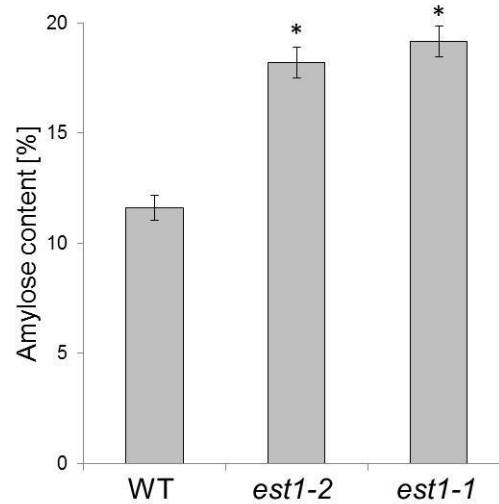


**Figure 5.8: Amylose content of leaf starch in wild-type, *est1-1* and *est1-2*.** Green house grown plants were harvested at the end of the day after 30 days and starch extracted from pooled rosette tissue of about 100 plants. The amylose to amylopectin ratios of starch were determined based on the different wavelengths of maximal absorbance of both polymers after addition of iodine solution. Values are means of 3 technical replicates; error bars are s.e.m. Asterisks indicate a significant difference between amylose contents of wild-type and mutants (t-test,  $p < 0.5$ ).

#### 5.2.1.7 Composition of mutant starch: Chain length profile

To find out whether there are changes in the structure of the amylopectin fraction of mutant starch, the branching pattern of amylopectin was analysed in *est1-2*, and compared to wild-type (**Figure 5.9**). Starch was prepared from leaf tissue at the end of the day and amylopectin branches were cleaved off using a debranching enzyme. This resulted in liberation of linear  $\alpha$ -1,4-glucan chains which were then separated by high performance anion exchange chromatography (HPAEC) and quantified using a pulsed amperometric detector (PAD).

The chain length profile of the mutant was nearly identical to wild-type. It showed a bimodal distribution with glucan chains ranging from a degree of polymerisation (d.p.) 2 to more than d.p. 40 and a peak at about d.p. 12.

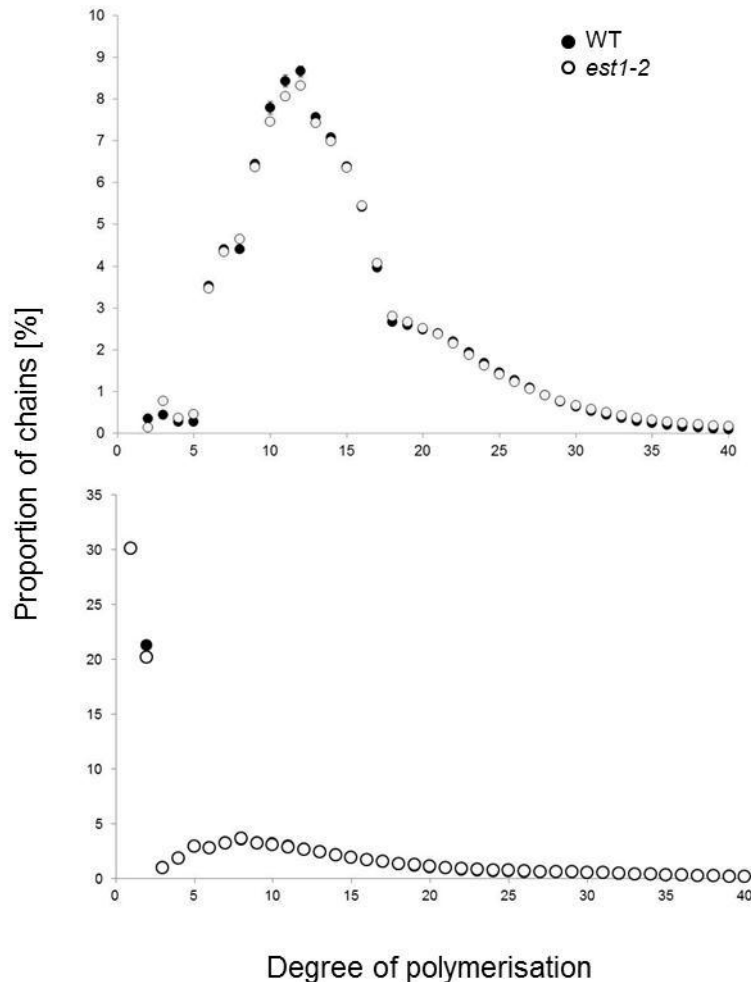


**Figure 5.9: Chain length distribution of amylopectin before and after beta - amylolysis of external chains.** GABI\_031C11 and wild-type plants were grown in 12 hour light-12 hour dark cycles for 25 days and harvested at the end of the day. Starch was extracted from rosettes of four individual plants. Starch was debranched with *Pseudomonas* isoamylase and *Klebsiella* pullulanase. The resulting linear chains were separated and detected using HPAEC-PAD. The resulting peak areas for each degree of polymerisation (d.p.) were added up and the areas of each individual peak were expressed as percentage of the total area. Error bars are s.e.m. of four biological replicates, where not visible, they are smaller than the symbols. The upper graph shows the chain length distribution of all amylopectin chains. The lower graph shows the chain length distribution of samples that were pre-treated with beta-amylase (beta-limit dextrin). Thus, it indicates the distance between branch points of amylopectin. The

chain length distribution of wild-type and mutant were very similar, therefore the data points overlap.

To analyse the branch point distribution of mutant amylopectin, additional starch preparations were treated with beta-amylase to digest the external amylopectin branches. The enzyme hydrolyses external  $\alpha$ -1,4 glucosidic linkages, releasing maltose and stops two to three glucose molecules upstream of the  $\alpha$ -1,6 linked branch points. The resulting polymer is called beta-limit dextrin as it is resistant to further digestion by beta-amylase. Treatment of the beta-limit dextrin with debranching enzyme resulted in liberation of the inner amylopectin chains which were again subjected to HPAEC-PAD. The chain length distribution of mutant beta-limit dextrin was nearly identical to that of wild-type.

Mutant *est1-2* had a normal amylopectin (beta-limit) chain length profile. I conclude that EST1 does not play a role in amylopectin synthesis.

#### 5.2.1.8 Analysis of native activity gels

Apart from the higher amylose content, *est1* had a normal granule composition. Numbers, sizes and shapes of starch granules were comparable to wild-type. Therefore no evidence was found that the fast rate of starch degradation was caused by abnormal starch. An alternative explanation is that EST affects the activity of enzymes that metabolise starch. Native activity gels were used to investigate if *est1-1* shows any alterations in the activities of the enzymes that act on amylopectin and were carried out as described in **Section 3.2.2** using the back-crossed *est1-1* mutant (**Figure 5.10**).

The identity of most of the bands on the activity gel could be assigned by comparison to published results. None of these bands, but one band with unknown activity was missing in *est1-1*. However, the band that is attributed to beta-amylase 5 (BAM5) activity was bigger in the mutant when compared to wild-type. This indicates increased BAM5 activity in *est1-1*.

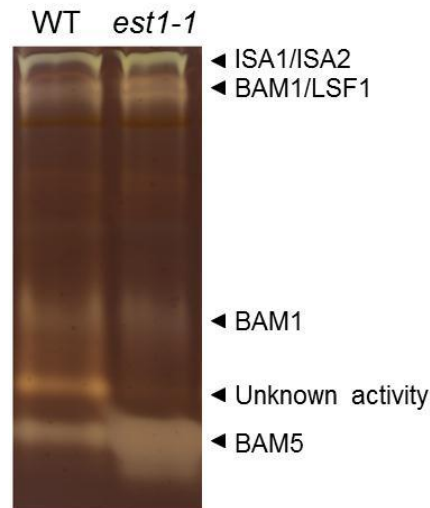


**Figure 5.10: Native activity gel showing the activity of starch modifying enzymes in wild-type and *est1-1*.** Plants were harvested at the end of the day after 23 days. Soluble proteins from leaf extracts of wild-type (WT) and *est1-1* (A) were separated on an amylopectin-containing non-denaturing polyacrylamide gel and stained with iodine after a two hour incubation time. Activities of isoamylase 1 and 2 (ISA1/ISA2), beta-amylase 1 (BAM1) in complex with like sex four 1 (LSF1), beta-amylase 5 (BAM5) and an unknown amylolytic activity are indicated by arrows (BAM5: Wattedled et al., 2005 and Glaring et al., 2012; ISA1/ISA2: Delatte et al., 2005; BAM1 and LSF1: Martin Umhang and colleagues, ETH Zürich, personal communication). Protein loads were adjusted based on tissue weight and the same amount of fresh weight was loaded in both lanes.

## 5.2.2 Characterisation of double mutants

### 5.2.2.1 Rationale

To get an indication where EST1 is positioned in the starch degradation pathway, I analysed the starch phenotype of double mutants that I generated by crossing mutants of the starch degradation pathway with *est1-1* (or *est1-2*). These experiments could show which components of the starch degradation pathway are required for the *est1* phenotype.

Several mutants of the starch degradation pathway have a starch excess phenotype, due to retardation of starch breakdown. These mutants include *sex1*, *bam3* and *bam4*.

I expected that lack of EST1 in these mutants would not result in starch degradation rates comparable to *est1* single mutants, as GWD, BAM3 and BAM4 are required for normal starch degradation. However, if any of the double mutants showed accelerated starch degradation rates, it would be possible to speculate about the function of EST1 and its position in the pathway.

This can be illustrated on the example of GWD. I hypothesised earlier that EST1 might modify the structure of starch to increase its stability, e.g. by facilitating crystallisation of the granule (5.1.2). Analysis of starch contents in the *est1 sex1* double mutant could further test this hypothesis. If absence of EST1 resulted in fast starch degradation in *sex1*, one could speculate that starch phosphorylation is no longer necessary for starch degradation when EST1 is missing. In this case, the function of EST1 could be antagonistic to that of GWD. GWD-catalysed phosphorylation modifies the starch granule surface to facilitate starch degradation, possibly by reducing the crystallinity of the granule; EST1 could then have the opposite function by increasing its crystallinity.

I speculated earlier that EST1 could be a negative regulator of starch degrading enzymes (5.1.2). If lack of EST1 resulted in faster starch degradation in BAM3, one could speculate that EST1 is a negative regulator of a functionally redundant beta-amylase that can compensate for the function of BAM3. Other mutants of the starch degradation pathway have no starch excess phenotype. These include *amy3* and *bam1*. If EST1 was a negative regulator of AMY3 or BAM1, a wild-type starch degradation rate would be expected in the *est1 amy3* or *est1 bam1* double mutants, respectively. The function of BAM4 is not known therefore it would not possible to speculate about the function of EST1 even if absence of EST1 resulted in fast starch degradation rates. However, fast starch degradation rates in *est1 bam4* could indicate that EST1 and BAM4 are functionally related.

#### 5.2.2.2 Starch in the *est1-1 sex1* double mutant

The first step in the pathway of starch degradation is catalysed by the protein glucan water dikinase (GWD). The amylopectin fraction of starch crystallises to tightly-packed structures, which are not easily accessible for starch metabolising enzymes. Starch phosphorylation by GWD reduces the crystallinity and facilitates access for enzymes that attack the granule (**Chapter 1**).

To test if *est1* starch still requires phosphorylation by GWD to be degradable, I crossed *est1-1* with a plant lacking GWD (*sex1*). In *sex1* mutants, lack of phosphorylation results in a starch excess which is caused by strong retardation of starch breakdown. Growth of the mutant is reduced in comparison to wild-type (Yu et al., 2001). I identified four independent double mutants after genotyping about 150 F<sub>2</sub> plants from three independent crosses of *est1-1* and *sex1-3*.

Starch contents of the double mutants were analysed after 28 days at the end of the day and end of the night, at first qualitatively, by iodine staining of rosettes (**Figure 5.11**).

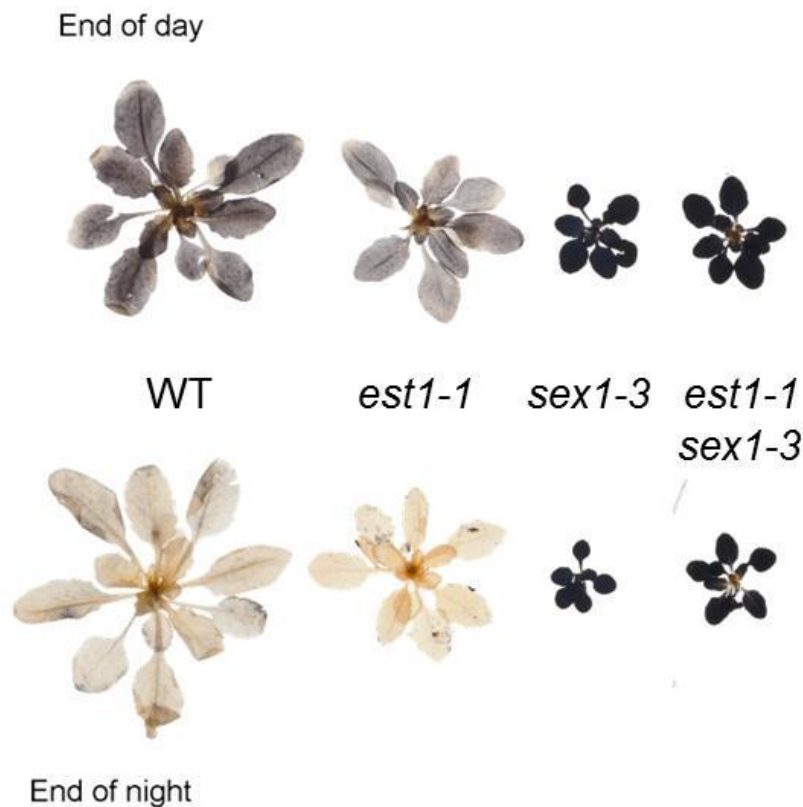


**Figure 5.11: Visualisation of leaf starch in wild-type, *est1-1*, *sex1-3* and *est1-1 sex1-3*.** Plants were grown in 12 hour light-12 hour dark cycles for 28 days. Whole rosettes were harvested, decolourised in ethanol and stained with iodine solution.

At the end of the day, starch in *est1-1* and wild-type plants stained light blue. The *sex1* mutant as well as the double mutant had a much darker colour, indicating elevated starch contents. Hardly any of the stain was remaining in wild-type and *est1-1* at the end of the night. The *sex1* mutant and the double mutant still stained dark, indicating that

starch was not fully degraded during the night. The size of the double mutant was reduced in comparison to wild-type and *est1-1* and was similar to that of *sex1*.

To quantify starch contents, plants of wild-type, *sex1-3*, *est1-1* and three double mutant lines were harvested at the end of the day and at the end of the night, after 23 days of growth (**Figure 5.12**). The *sex1* mutant had about four times more starch than wild-type and *est1-1* at the end of the day. The three double mutant lines had very similar starch contents at the end of the day and end of the night. Therefore, the average starch content of all three lines was calculated. The double mutants had a starch excess comparable to *sex1*. This means that starch degradation in *est1-1* is dependent on starch phosphorylation by GWD.

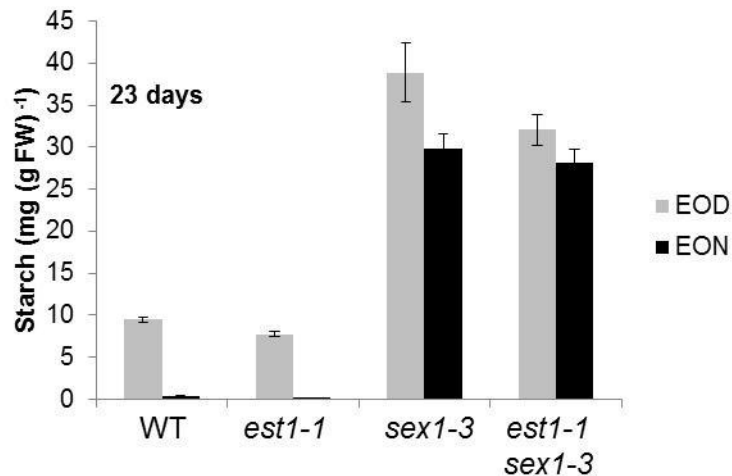


**Figure 5.12 Starch contents in the *sex1 est1* double mutant.** Plants were grown 12 hour light-12 hour dark cycles and harvested after 23 days. End of day (EOD) and end of night (EON) starch was determined for wild-type (WT), *est1-1*, *sex1* and *sex1 est1-1* double mutants. Starch contents of the double mutants are averages of measurements on three double mutant lines. Values are means of measurements on 6-12 individual rosettes, error bars are s.e.m.

### 5.2.2.3 Double mutants from crosses of *est1-2* with *sex4*, *amy3*, *bam1*, *bam3*, *bam4* and *gbss*

I generated more double mutants of *est1* and mutants of the starch degradation pathway by crossing *est1-2* with, *amy3-2*, *bam1-1*, *bam3-1*, *bam4-1* and *gbss-2*. I genotyped about 48-96 F<sub>2</sub> plants of each cross for the *est1-2* mutation to identify homozygous mutants. These were then genotyped for the second mutation until homozygous double mutants were found. For each cross, I identified about one to four double mutant lines. When I analysed the starch phenotype of the mutants, they were still in the F<sub>2</sub> generation. The plants needed to be grown for seed and therefore, only one leaf could be analysed per plant. The plants were 25-30 days old at the day of harvest. Leaves were harvested two hours before the end of the night to assess starch contents by iodine staining. At this time point, *est1-2* has no starch, while wild-type plants still contain detectable amounts of it.

Hydrolytic attack on the granule is primarily catalysed by beta-amylases. In the absence of BAM1, starch can still be degraded normally (**Chapter 1**). The leaf of the *bam1* mutant showed a light blue stain, comparable to wild-type. In the *est1-2 bam1* double mutant, the stain looked comparable to *est1-2* alone. This suggests that BAM1 is not necessary for faster starch degradation in *est1-2*. Loss of BAM3 or BAM4 results in a starch excess phenotype due to retardation in starch breakdown (**Chapter 1**). Leaves of *bam3* and *bam4* had a darker stain than wild-type. In the *est1-2* background, the intensities of the stains were comparable to that of the *bam3* or *bam4* single mutants. That means absence of either BAM3 or BAM4 results in a starch excess, whether EST1 is missing or not. Therefore, BAM3 and BAM4 are still required to degrade starch in *est1-2*.

The enzyme  $\alpha$ -amylase 3 (AMY3) has not been shown to play an essential role in starch degradation (**Chapter 1**). The single mutant (*amy3*) showed a stain comparable to wild-type. In the *est1-2* background, the stain looked like that of *est1-2* alone. Therefore, AMY3 is not necessary for faster starch degradation in *est1-2*.

The *est1-2* mutant had about 60% more amylose than wild-type (**Figure 5.8**). To find out if the higher amylose content is responsible for faster starch degradation in *est1* mutants, the starch content of the *est1-2 gbss* double mutant was analysed. Granule bound starch synthase (GBSS) is the enzyme that synthesises amylose, thus *gbss*

mutants do not contain amylose. However, they have normal levels of starch (Mathilda-Crompton Taylor, personal communication). The leaf stain of *gbss* was less blue than that of wild-type, because a lack of amylose results in a more reddish colour of the starch-iodine complex. The *est1-2 gbss* double mutant showed a stain comparable to *est1-2*. That means there was no starch left two hours before the end of the night. This indicates that faster starch degradation of *est1-2* is independent of the presence of amylose.

In summary, the experiments indicated that enzymes that are necessary for normal starch degradation are still required to degrade starch in the absence of EST1.

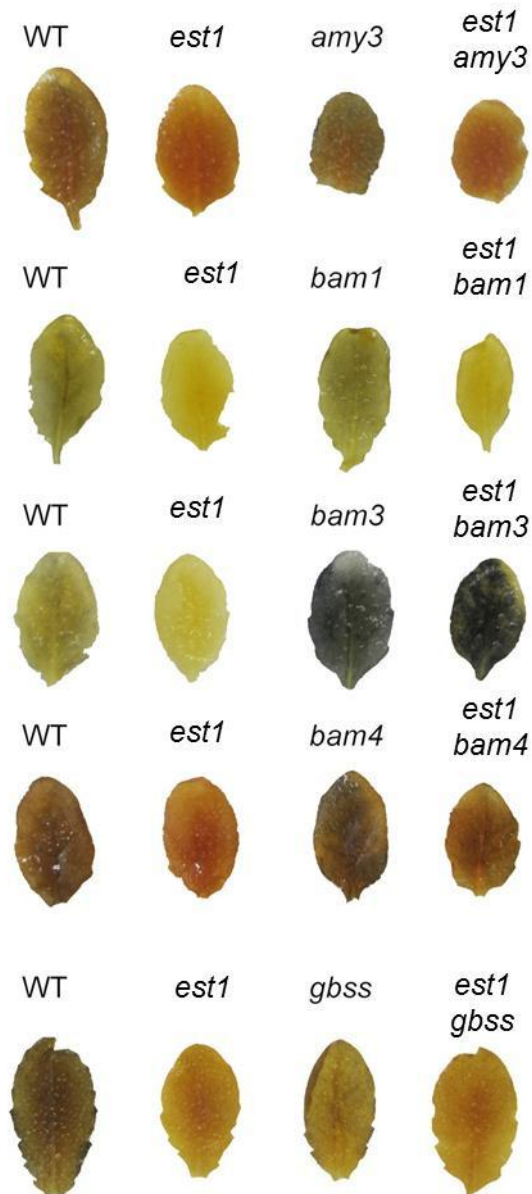


**Figure 5.13: Visualisation of leaf starch in double mutants.** Plants were grown in 12 hour light-12 hour dark cycles for 25-30 days and harvested two hours before the end of the night. One mature leaf of each plant was harvested, decolourised in boiling ethanol and stained with iodine solution. Genotypes analysed were wild-type (WT), *est1-2* (*est1*), *amy3-2* (*amy3*), *bam1-1* (*bam1*), *bam3-1* (*bam3*), *bam4-1* (*bam4*), *gbss-2* (*gbss*) and the respective double mutants.

## 5.3 Discussion

### 5.3.1 Interpretation of the phenotype

#### 5.3.1.1 Starch degradation phenotype

I could demonstrate that *est1* knock-out mutants degrade starch faster than wild-type plants and that EST1 is required for normal starch degradation rates. Mutants lacking EST1 had normal end of day starch contents and degraded about 11% of their end of day starch every hour. This is about 40% more compared to wild-type plants. If the night started unexpectedly early, the relative starch degradation rate in *est1* remained the same as in a normal night. Therefore, mutants ran out of starch nine hours after dusk in normal and early nights. This shows that starch degradation in *est1* mutants is not adjusted according to the length of the night as in wild-type plants.

The adjustment of the starch degradation rate according to the length of the night requires the plant to measure its starch content and the time remaining until dawn. Information about both needs to be integrated to set an appropriate starch degradation rate (Scialdone et al., 2013) (**Chapter 1**). Faster starch degradation in *est1* could therefore be a result of failures in the mechanism that measures starch or in the mechanism that measures the time remaining until dawn. It could, however, also be a defect of the pathway that integrates information about both. Thus, EST1 could be involved in the normal operation of the adjustment mechanism or be a target of it.

The timing mechanism underlying starch degradation is the circadian clock (Graf et al., 2009). In theory, a defect in the circadian clock could explain faster starch degradation in *est1*. This seemed possible as the only mutant with comparable starch degradation rates to *est1* is the circadian clock mutant *cca1 lhy*. Starch degradation in this mutant was analysed by Alexander Graf (Graf et al., 2009 and 2010) and Sam Mugford (Scialdone et al., 2013). The mutant also degraded about 11% of its initial starch every hour and exhausted starch about nine hours after dusk in a normal night (Scialdone et al., 2013). I could show that the circadian clock runs normally in mutant *est1* (**Chapter 3**). Thus, faster starch degradation of *est1* cannot be explained by a faster running circadian clock as in *cca1 lhy*. The *cca1 lhy* mutant anticipated dawn several hours earlier than wild-type and anticipation of dawn still coincided with the time at which

starch was exhausted. In contrast to *est1*, mutant *cca1/lhy* slowed down its relative starch degradation rate in an early night (Scialdone et al., 2013). Thus, *est1* does not seem to be affected in the circadian clock and further work is needed to find out which role EST1 plays in the pathway that adjusts starch degradation rates according to night length.

### 5.3.1.2 Starvation and the effect on growth and flowering

Lack of EST1 resulted in reduced growth rates of the mutant plants, probably due to premature exhaustion of starch during the night. This is consistent with growth retardation observed in other mutants affected in starch metabolism, e.g. *pgm* and *sex1* (Gibon et al., 2004; Smith and Stitt et al., 2007). These mutants cannot produce sugars from starch during the night, due to an inability to make starch or to break it down, respectively. Therefore sugar levels in these plants are very low during the night and they stop growth (Yazdanbakshsh et al., 2011). The lack of sugars also causes symptoms of starvation at the transcriptional level in these mutants and in wild-type plants subjected to an extended night. Genes involved in anabolism are repressed and genes involved in catabolism are up-regulated if plants run out of sugars (Usadel et al., 2008). Premature exhaustion of starch in *est1* mutants might cause depletion of sugars which results in the onset of starvation symptoms and growth cessation at the end of each night.

The delay in flowering time of *est1* mutants could also be a consequence of premature exhaustion of starch and low sugar levels at the end of the night. Carbohydrates were shown to be important in the regulation of flowering time (Srikanth and Schmid, 2011). Mutants like *pgi* and *sex1* that cannot synthesise or break down starch, flower late (Yu et al., 2000; Corbesier et al., 1998). It was suggested that carbohydrates provided from starch degradation are necessary for the transition to flowering (Yu et al., 2000). Recently, it was shown that flowering in *Arabidopsis* is regulated by trehalose-6-Phosphate (T6P) (Wahl et al., 2013). T6P was suggested to function as a signalling metabolite of sugar status in plants (Lunn et al., 2006). Abnormal sugar levels in *est1* might effect T6P signalling and thus alter its flowering time.

### 5.3.1.3 Starch in heterotrophic tissue

I observed that *est1* mutants do not contain starch in the veins of their leaves. This indicates that starch is absent in heterotrophic tissue of the mutant plant, but further work is required to establish whether starch is also absent from other heterotrophic cells in the *est1* mutant. In rosettes of the phosphoglucose isomerase (*pgi*) mutant the opposite phenotype was observed (Yu et al., 2000). The mutant has no starch in photosynthetic leaf tissue, but in heterotrophic tissue of the veins and the roots. The reason for this is that starch in heterotrophic tissue is made from sucrose that is converted to glucose-6-phosphate (G6P) and imported into the plastid. In photosynthetic tissue, fructose-6-phosphate from the Benson-Calvin cycle must be converted to G6P by the action of PGI. Thus in the absence of PGI starch synthesis is blocked in photosynthetic tissue, but not in heterotrophic tissue, because there, PGI is not needed for the interconversion from F6P to G6P.

Another observation that could link in with the absence of starch in non-photosynthetic tissue is the difference in the growth phenotype of *est1* shoots. The lateral shoots grew with a wider angle from the primary shoot than in wild-type plants. Wild-type shoots show a negative gravitropic response, meaning that they bend towards the opposite direction of gravity. This gravitropic response was reduced in *est1* mutants. Starch in amyloplasts of the shoot endodermis was suggested to be important for gravitropic responses of the shoot (Fukaki, 1998; Hashiguchi et al., 2013). Therefore, I suggest that starch is absent in heterotrophic tissue of the shoot endodermis of *est1*, resulting in a reduced gravitropic response. This hypothesis is consistent with the reduction of gravitropic responses in other mutants with reduced starch. A similar shoot growth phenotype to that of *est1* was observed in shoot gravitropism (*sgr*) mutants (Tanimoto et al., 2008; Fukaki et al., 1996). One of them, the *sgr5* mutant had less starch in the amyloplasts of the stem (Tanimoto et al., 2008). The starchless mutant (*pgm*), which has less starch in amyloplasts has also reduced gravitropic responses (Kiss et al., 1997; Weise and Kiss, 1999).

Further work will be required to establish whether the root and shoot of the *est1* mutant have a reduced gravitropic response and whether this correlates with reduced starch contents in cells known to be crucial for this response. If *est1* proves to have no starch in plastids of non-photosynthetic tissue, we could assume that starch is also degraded

faster in these tissues. The absence of starch might be a result of starch degradation competing with starch synthesis and a higher rate of degradation than synthesis.

#### 5.3.1.4 TEM analysis

The structure and size of starch granules in *est1* looked normal when viewed by TEM and SEM. However, TEM analysis was only preliminary and should be repeated and extended.

The absence of starch from veins in the mutant suggested that certain tissue types do not contain starch. Therefore, I would like to use TEM analysis to analyse the appearance and quantity of starch granules in different tissue types. These experiments could give insights into the function of EST1 on starch granule biosynthesis in different tissues. The *isa1* or *isa2* mutants also show variation in the appearance and number of granules in different parts of the leaf. Some tissues do not contain any starch, but others contain granules that appear normal. Also the shape of the granules varies in different tissues of the leaf (Delatte et al., 2005).

#### 5.3.1.5 Relevance of elevated amylose in *est1*

The molecular composition of starch in *est1-1* was comparable to wild-type except that amylose content was 60% higher. The reason for elevated amylose contents in *est1-1* is not obvious. To date it is not known what determines the amylose to amylopectin ratio in *Arabidopsis* leaf starch, although factors are known that influence it. The amylose content was proposed to correlate with the amount of starch because starch excess mutants like *sex1* and *sex4* have more amylose. Wild-type plants grown in continuous light have higher amylose contents, too (Zeeman et al., 2002). This proposal is not consistent with the observation that *est1-1* has higher amylose contents, because the mutant turns over starch faster and high amounts of starch do not build up. However, other mutants that do not have a starch excess were also reported to have elevated amylose contents. Residual starch in *isa1-1* mutants and *isa1 isa3* double mutants contains more amylose (Wattebled, 2008), as well as starch in *ss1 ss2* and *ss1 ss3* double mutants (Szydlowski, 2011). All of these enzymes influence the structure of amylopectin. Thus, higher amylose contents might be a side effect of changes in the structure of amylopectin. However, this can also not explain higher amylose contents in

the mutant as the amylopectin fraction of starch had a normal composition in *est1*. There have been no previous studies on the impact of amylose content on starch degradation rates. I analysed the phenotype of a cross of *est1-2* with the granule-bound starch synthase mutant *gbs* (a mutant lacking amylose) to investigate if amylose is required for faster starch degradation in *est1*. The double mutant had no starch two hours before the end of the night, thus it degraded starch too fast. Therefore amylose is not necessary for faster starch degradation in *est1* mutants and could be a consequence of it.

In conclusion, analysis of granule structure and composition in *est1* could not explain the phenotype of faster starch degradation. However, it is still possible that mutant starch is more susceptible to degradation because of alterations in properties of the granule that were not analysed here. EST1 may alter the physical organisation of the granule matrix, including the degree of crystallinity. Techniques including small-angle x-ray scattering (SAXS) could be used to analyse the organisation of amylopectin in the granule (Fulton et al., 2002; Zeeman et al., 2002).

#### 5.3.1.6 Activity of starch metabolising enzymes

Increased starch degradation rates could be the result of increased activities of the enzymes that act on starch. However, analysis of soluble protein extracts of *est1-1* rosettes on native activity gels did not reveal any difference in the activities of enzymes that act on amylopectin. BAM1 activity and ISA1 activity were clearly present.

BAM5 activity was clearly increased in *est1*. However, it is unlikely that faster starch degradation rates in *est1* are caused by altered BAM5 activity. A *bam5* knock-out mutant was isolated by Laby et al. (2001) and initially called *reduced beta-amylase 1* (*ram1*). It had wild-type levels of starch and sugar, although one study reported slightly elevated starch contents for the same mutant (Kaplan and Guy, 2005). BAM5 is located in the phloem and not found in the chloroplast (Wang et al., 1995), thus it is unlikely to play a role in starch degradation in leaves. The higher BAM5 activity on the native gel might be a consequence of elevated end of day sugar levels in *est1*, because BAM5 activity is sugar-induced (Mita et al, 1995). BAM5 activity is also induced in mutants that do not make starch, like *pgm* (Monroe and Preiss, 1990). The *pgm* mutant

accumulates unusually high levels of soluble sugar at the end of the light period (Caspar et al., 1989; Monroe and Preiss, 1990). Thus, the observed change in BAM5 activity might be a consequence rather than a cause of faster starch degradation in *est1*.

Not all activities of starch modifying enzymes can be visualised on the native activity gel. For example BAM3 activity is not detectable by this method, for unknown reasons. This is a disadvantage, because BAM3 play a major role in starch degradation at night (Fulton et al., 2008). Changes in beta-amylase activity in *est1* extracts could be assessed using beta-amylase assays. However, these assays do not distinguish between the activities of different isoforms and 80% of beta-amylase activity in plant extracts is extra-chloroplastic and likely to be attributable to BAM5 activity (Lin et al., 1988). In the future, levels of BAM3 activity and protein in *est1* could be examined using FPLC fractionation and immunoblot analysis with antiserum specific for BAM3.

### **5.3.2 Interpretation of starch contents in double mutants**

My preliminary analysis of the starch contents of double mutants between *est1* and other mutants of the starch degradation and synthesis pathway suggests that in absence of EST1, the same enzymes are required for the fast rates of starch degradation as for normal rates of starch degradation in wild-type plants.

The double mutant *est1-1 sex1-3* had a starch excess comparable to the *sex1-3* single mutant. Therefore, starch phosphorylation by GWD is still necessary for faster starch degradation in *est1* mutants. Thus, presence of EST1 does not modify the structure of starch in a way that introduces a requirement for GWD-catalysed phosphorylation.

I hypothesised that faster starch degradation in *est1* could be explained if EST1 was a negative regulator of enzymes that degrade starch. In theory, EST1 could repress the activity of enzymes that are not required for starch degradation in wild-type plants, but are present in the chloroplast. Possible candidates were AMY3 and BAM1, as these proteins are not required for starch degradation in wild-type plants. However, analysis of the *est1 amy3* and *est1 bam1* mutants showed that the function of EST1 is not to negatively regulate AMY3 or BAM1. The phenotype of the double mutants did not look different from *est1* alone, in other words, they still seemed to degrade starch faster. Neither AMY3 nor BAM1 are required for faster starch degradation in *est1*.

Loss of EST1 did not rescue the starch excess of *bam3*. This could mean that lack of EST1 does not result in activation of a redundant enzyme that can attack the granule in absence of BAM3. The starch excess of the *bam4* mutant was also not rescued in absence of EST1. Therefore, EST1 and BAM4 are possibly not functionally linked.

### 5.3.3 Conclusion and outlook

At the moment I can only speculate about the function of EST1. I could show that leaf starch is degraded faster in the absence of the protein and that a starch excess builds up in plants overexpressing the protein (**Chapter 4**). Thus, EST1 is required for normal starch metabolism.

EST1 is located on or inside starch granules. Probably it is present in all green plants and in starch granules of source and sink organs (**4.2.5 and 4.2.6**). Thus, the function of the protein is unlikely to be limited to the regulation of transitory starch degradation in *Arabidopsis* leaves. To investigate that, we plan to characterise *est1* mutants of other plant species.

The EST1 protein does not resemble any proteins of known function and could therefore have a new function. A three dimensional structure of the protein could not be predicted and it appears to be intrinsically disordered. Thus, EST1 might bind to the starch granule or other proteins to fold into a stable protein. In theory, it could be part of a protein complex that slows down the activity of starch degrading enzymes. In the future this could be tested by looking for interaction partners of EST1.

At the moment, I can be certain that starch phosphorylation by GWD is still required for starch degradation in *est1* mutants. Thus, in the absence of EST1 the granule is not accessible to hydrolysing enzymes without the addition of C6-phosphate. If EST1 alters the activity of a starch hydrolysing enzyme, this enzyme must act downstream of GWD in the pathway. I can be sure that the function of EST1 is not to negatively regulate AMY3 or BAM1 activity. I have also established that although the EST1 mutant has elevated amylose, this is not the cause of faster starch degradation.

Analysis of the starch phenotype of further double mutants will provide more substantial information about the position of EST1 in the pathway of starch degradation.

Quantification of starch contents in the available double mutants will help to answer that question.

## 6 Characterisation of *bam1-2*

### 6.1 Introduction and rationale

I identified mutant *bam1-2* in a screen for early starvation mutants. The mutant degraded starch faster than wild-type and exhausted its starch prematurely in the early night (**Chapter 3**). Segregation analysis showed that the mutation underlying the phenotype is dominant (**Chapter 4**).

Using map-based cloning, I identified beta-amylase 1 (BAM1) as a candidate gene causing the phenotype of *bam1-2* (**Chapter 4**). The gene (At3g23920) contained an EMS-induced point mutation in an exon which causes a serine to asparagine amino acid substitution in position 132 of the amino acid sequence. To provide further evidence about the importance of this mutation for faster starch degradation phenotype, I expressed BAM1 (S132N) in wild-type plants. These experiments are in progress.

In the following chapter I characterise the phenotype of *bam1-2* in more detail and describe the experiments I did to find out how the mutation in BAM1 (S132N) could accelerate starch degradation. Based on the obtained results, I discuss different hypothesis for faster starch degradation in *bam1-2*.

#### 6.1.1 BAM1 and its role in starch breakdown

The mutant phenotype cannot be explained by our current knowledge about BAM1 function. BAM1 does not seem to play a major role in starch degradation at night as the mutant lacking BAM1 (*bam1-1*) has normal end of day and end of night starch contents (Fulton et al., 2008). It was suggested that at night, BAM1 is important for starch degradation only in the absence of BAM3. This is based on the observation that the *bam1 bam3* double mutant has a more severe starch excess than the *bam3* single mutant.

Valerio et al. (2011) found that in non-flowering *Arabidopsis* plants, BAM1 expression is mainly restricted to guard cells. They also showed that in absence of BAM1, guard cells accumulate more starch than wild-type in the light. Opening of stomata was reduced in *bam1* in comparison to wild-type. Therefore, it was suggested that BAM1 degrades starch in the light in guard cells to provide osmolytes for stomatal opening. It

is difficult to reconcile the claim of Valerio et al. (2011) that BAM1 is only expressed in guard cells with the observation of Fulton et al. (2008), that loss of BAM1 increases the leaf starch content in a *bam3* background. It may be that BAM1 expression in mesophyll cells varies with growth conditions, and/or that loss of BAM3 triggers BAM1 expression in mesophyll cells.

Valerio et al. (2011) also proposed an additional role of BAM1 in the plant's response to osmotic stress. When wild-type plants were treated with mannitol, *BAM1* gene expression increased strongly in mesophyll cells. In mannitol treated plants, the rate of starch synthesis was reduced about 24% compared to plants that were untreated. In the absence of BAM1, starch synthesis rates were not reduced by mannitol treatment. It was proposed that the reduction of starch synthesis was an effect of day time starch degradation by BAM1. Thus, it was proposed, that BAM1 degrades starch in the light, when plants are osmotically stressed. Maltose, the product of beta-amylolysis was suggested to work as an osmoprotectant.

There is more evidence showing that BAM1 might be involved in response to abiotic stress. *BAM1* gene expression was shown to be triggered in response to heat stress (Kaplan and Guy, 2004). When wild-type plants were exposed to 40°C for 1 hour, the *BAM1* transcript level increased about five-fold. Cold stress did not trigger *BAM1* expression. Instead, *BAM3* transcripts increased when plants were cold-stressed at 4°C for 12 hours (Kaplan and Guy 2004; 2005). Expression of beta-amylases under temperature stress correlated with maltose production. It was suggested that maltose accumulation protects the plant from temperature damage by functioning as a compatible-solute in the chloroplast stroma. During stress, compatible solutes stabilise proteins and cell membranes and they contribute to the cell osmotic potential.

There are many indications that BAM1 is part of a pathway that degrades starch in response to stress and in the light. Also, it seems the enzyme is not important for breakdown of transitory starch at night. However, the starch degradation phenotype of *bam1-2* suggests that modulation of BAM1 activity can affect starch degradation rates at night. Although the starch content of *bam1-1* is normal at the end of the night, it has not been tested yet if *bam1-1* degrades starch at a different rate from wild-type.

Therefore, I investigated starch degradation rates over a normal night and in response to an early night in the knock-out mutant *bam1-1*.

### **6.1.2 Putative BAM1 interaction partners**

Recently, BAM1 has been shown to form a complex with the granule bound protein LIKE SEX FOUR 1 (LSF1) and the enzyme plastidial NAD-dependent malate dehydrogenase (pNAD-MDH) (Martin Umhang and colleagues, ETH Zürich, personal communication). The interaction of BAM1 and LSF1 was verified using several techniques including gel permeation chromatography, bi-molecular fluorescence complementation, tandem-affinity purification (TAP) tagging and co-immunoprecipitation. It was proposed that LSF1 targets BAM1 to the starch granule surface to facilitate starch degradation. TAP-tagging experiments also identified pNAD-MDH as an interaction partner of both BAM1 and LSF1. The function of pNAD-MDH in the protein complex remains unclear. The enzyme interconverts malate and NAD with oxaloacetate and NADH. Knock-out of pNAD-MDH in *Arabidopsis* is lethal (Oliver Kötting, ETH Zürich, personal communication). A possible explanation for faster starch degradation in *bam1-2* is that the interaction between BAM1, LSF1 and pNAD-MDH is affected by the amino acid substitution (S132N). To investigate whether the mutation in *BAM1* affects the binding to LSF1 and pNAD-MDH, I used native activity gels.

### **6.1.3 Regulation of BAM1 activity**

In theory, faster starch degradation in *bam1-2* could be the result of an increased activity or stability of the BAM1 protein. To investigate that, I analysed BAM1 activity and protein levels in *bam1-2* plants to find out if they are different from wild-type.

BAM1 was shown to be redox-sensitive and to be inactivated in oxidising conditions, e.g. by incubation with oxidised dithiothreitol (DTT) (Sparla et al., 2006; Valerio et al., 2011; Glaring et al., 2012). It was shown that thioredoxins can restore the activity of the oxidised protein *in vitro* (Sparla et al., 2006; Valerio et al., 2011). Consistent with other lines of evidence, it was hypothesised that BAM1 is activated during the day, when thioredoxins are kept reduced by electrons from photosystem I (Valerio et al., 2011). The amino acid substitution S132N in *bam1-2* is positioned between the two cysteine

residues (Cys-32 and Cys-470) that were proposed to form an inhibitory disulphide (Sparla et al., 2006) (**Chapter 4**). I speculated that the amino acid substitution disrupts formation of the disulphide bridge, resulting in decreased redox-sensitivity of the enzyme. Therefore, I tested the redox-sensitivity of BAM1 (S132N) in *bam1-2* plant extracts using native activity gels.

#### ***6.1.4 BAM1 (S132N) in the pathway of starch degradation***

One hypothesis to explain faster starch degradation in *bam1-2* is that there are protein-protein interactions between BAM1 (S132N) and other proteins of the starch degradation pathway that accelerate their activities. To find out which components of the starch degradation pathway are necessary for faster starch degradation in *bam1-2*, I crossed the mutant to mutants affected in other components of the starch degradation pathway. I analysed the starch contents and starch degradation rates of some of the double mutants.

## **6.2 Results**

### ***6.2.1 Growth and appearance of bam1-2***

Mutant *bam1-2* is different from wild-type in growth and development. The plants had about 20% less fresh weight than wild-type at 24 days after germination and a smaller diameter (**Figure 6.1**). Otherwise the plants appeared normal in colour and shape. Flowering of the mutant was delayed compared to wild-type.

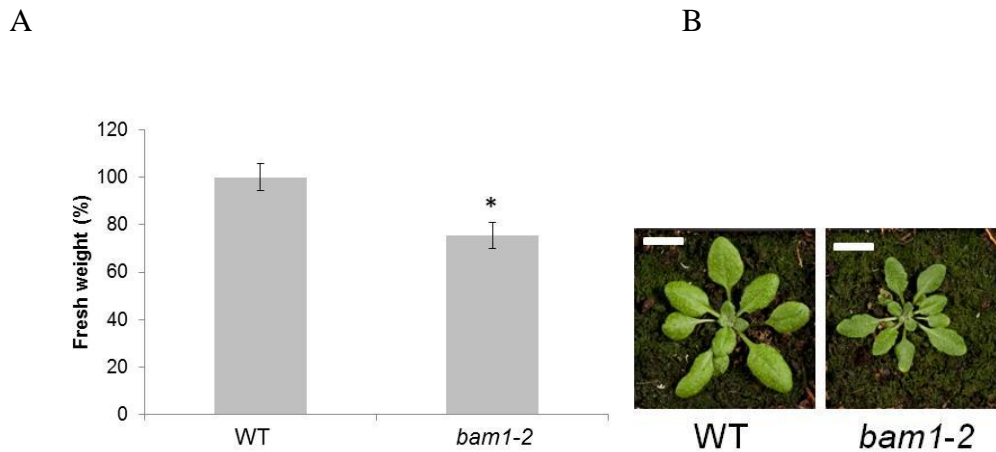


**Figure 6.1: Growth phenotype of *bam1-2*.** The fresh weight of whole rosettes was determined on 24-day-old plants and is shown as % of the wild-type fresh weight. The asterisk indicates a significant difference between the fresh weight of mutant and wild-type plants (t-test,  $p < 0.05$ ) (A). Values are means of measurements on 30 rosettes, error bars are s.e.m. Appearance of *bam1-2* and wild-type plants after 30 days (B). The scale bars indicates 1cm.

### 6.2.2 Starch degradation phenotype of *bam1-2*

In **Chapter 4**, I showed that mutant *bam1-2* (mutant 400-3) degraded starch faster than wild-type. Unlinked EMS mutations could interfere with the mutant phenotype. Therefore, I repeated and extended the analysis of starch degradation rates of the mutant after the first back-cross to the starvation reporter line. Starch contents were measured every two to four hours in normal and early night (**Figure 6.2 A**).

In contrast to the  $M_3$  mutant line, starch contents at the end of the day were nearly identical to wild-type after the first back-cross of the mutant. Apart from that, the starch degradation phenotype of the  $M_3$  mutant resembled that of the mutant after the first back-cross. Starch degradation in the mutant was faster than wild-type in normal night and early night. Starch was not exhausted before the end of the normal night, because degradation slowed down in the end of the night. In the early night, starch was exhausted at least four hours before the end of the night. Thus, the mutant does not adjust its starch degradation rate according to the length of the night.

Relative starch contents were determined to normalise the data for the different end of day starch contents (**Figure 6.2 B**). Wild-type plants slowed down starch degradation rates in response to the early night and had higher relative starch contents in the early night, compared to the normal night. In the mutant, relative starch contents were nearly identical in normal and early night.

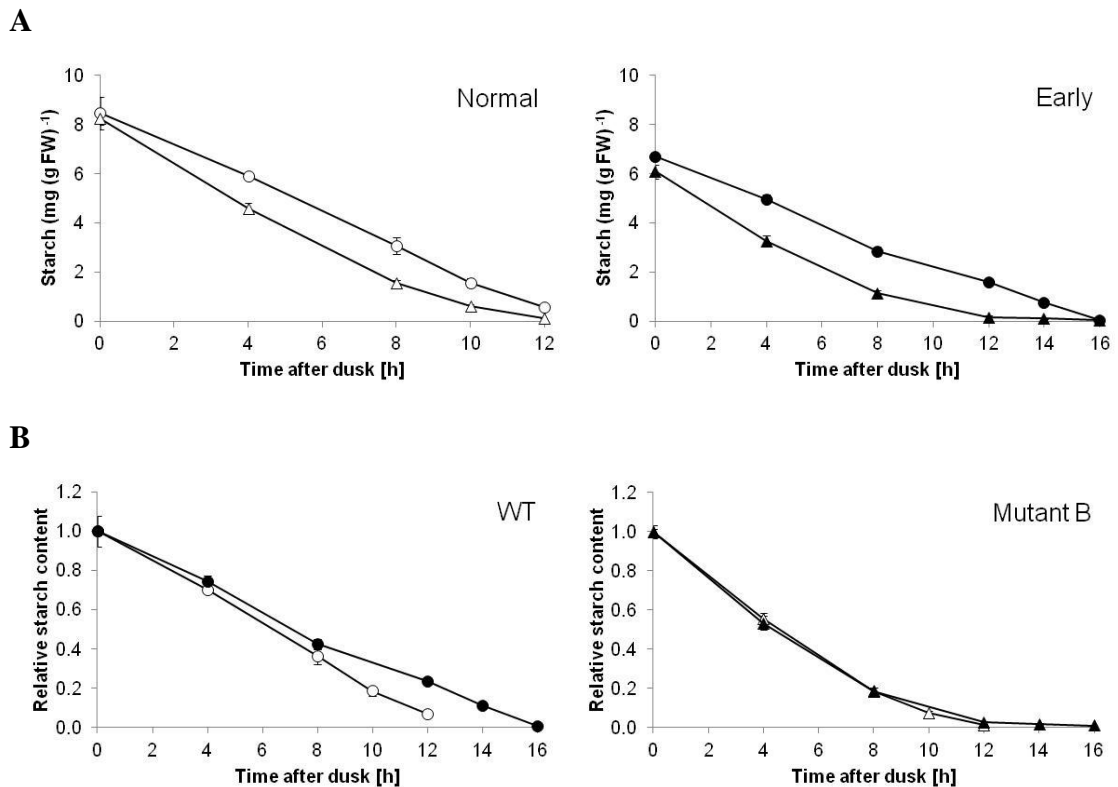
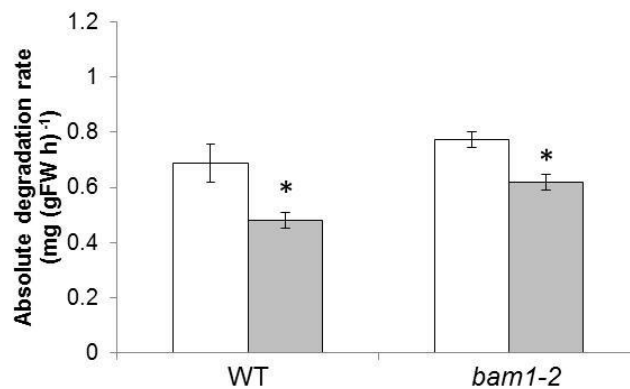


**Figure 6.2: Starch degradation pattern in early and normal night for wild-type (WT) and *bam1-2*.** Plants were grown in 12 hour light-12 hour dark cycles for 21 days. (A) Starch contents of wild-type (circles) and *bam1-2* (triangles) were analysed during a normal night (open symbols) and during an early night (closed symbols). (B) Starch contents of A are shown as a fraction of the end of day value. Mutant *bam1-2* plants of the first back-cross were used. Data are means of measurements on five individual rosettes. Error bars are s.e.m., where not visible, they are smaller than the symbol.

To quantify and compare starch degradation rates in wild-type and mutant, I fitted linear regression lines through all relative starch contents of the early and the normal night for the linear phase of starch degradation. Starch degradation rates were determined by analysing the slopes of the regression lines for absolute and relative starch contents. (Figure 6.3).

A



B

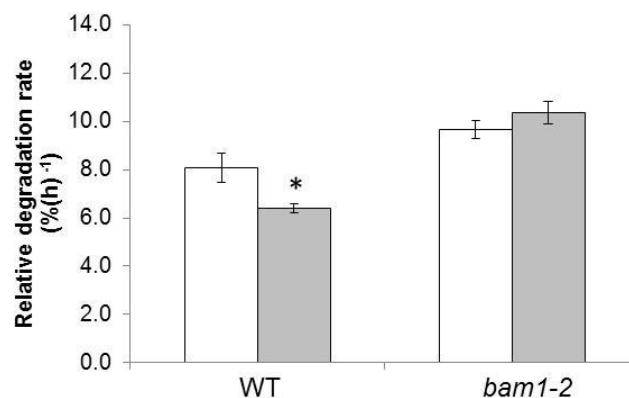


**Figure 6.3: Comparison of starch degradation rates for *bam1-2* and wild-type.** The absolute starch degradation rates (A) and the rates normalised to the end of day value (relative starch degradation rates) (B) were calculated for each genotype based on the data presented in Figure 6.2. The rates were determined for normal night (white bars) and early night (grey bars) by fitting linear regression lines through all starch contents and by analysing their slopes. For *bam1-2* only the starch contents of the first 10 hours (normal night) or the first 8 hours (early night) were included in the calculations as starch was exhausted at some point after that. Asterisks indicate a significant difference between degradation rates in normal and early nights (t-test,  $p < 0.05$ ).

In both, normal and early night, the relative and absolute rates of starch degradation in *bam1-2* were faster than in wild-type plants. The absolute rate of starch degradation of *bam1-2* slowed down to slightly lesser extent than in wild-type, when the night started early (wild-type: 0.26 mg gFW<sup>-1</sup>; *bam1-2*: 0.2 mg gFW<sup>-1</sup>). The relative rates of starch degradation in normal and early nights were similar in *bam1-2* and about 10% of initial starch was degraded every hour. Based on the starch degradation rates it is possible to extrapolate the time at which starch contents reach zero (**Table 6.1**). The extrapolation showed that if a linear rate was maintained, the mutant should exhaust its starch after about 9.7 and 8.9 hours in normal and early night respectively.

	WT	<i>bam1-2</i>
Normal	12.4	9.7
Early	15.6	8.9

**Table 6.1: Estimation of time when starch contents would reach zero in wild-type and *bam1-2*.** Calculations are based on the extrapolation from relative starch degradation rates shown in **Figure 6.3** and are given in hours after dusk for normal and early night.

In conclusion, *bam1-2* does not adjust its starch degradation rate to the length of the night and does not slow down the relative starch degradation rate if the night starts early. Starch degradation rates seem to be set so that starch is exhausted about 9-10 hours after dusk.

### 6.2.3 Composition of starch in *bam1-2*

Above, I hypothesised several reasons for faster starch degradation in the mutant. As the mutation underlying the phenotype was found in *BAMI*, which encodes an enzyme involved in starch degradation, it was unlikely to suspect that changes in the granule composition of the mutant are a primary cause of the phenotype. However, analysis of the molecular composition of starch in *bam1-2* revealed an abnormality in the amylose content. Starch was extracted at the end of the day from 30 day-old plants grown in the green house. The amylose to amylopectin ratio was determined based on the wavelengths of maximal absorbance of both polymers after addition of iodine solution

(**Figure 6.4**). Mutant starch contained about 40% more amylose than wild-type starch. The other mutant with faster starch degradation, *est1*, also had elevated amylose contents (**Chapter 5**). The cross of *est1* with *gbss* showed that amylose was not necessary for faster starch degradation in the mutant. Therefore, I speculate that higher amylose contents are a consequence of faster starch degradation in the mutants, rather than the cause of it. Therefore, I did not follow this up further.

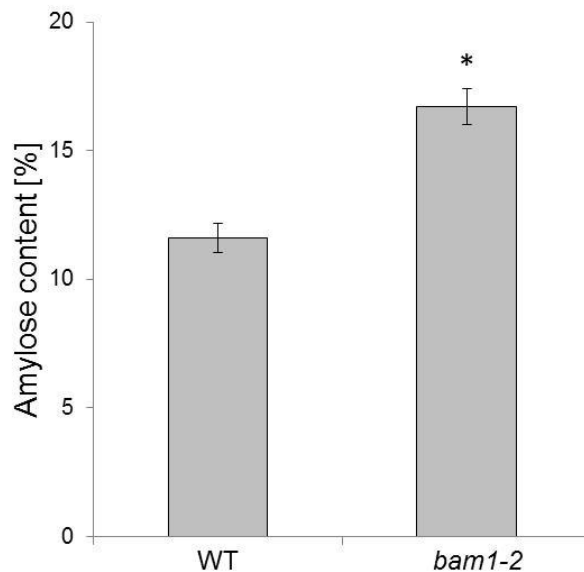


**Figure 6.4: Amylose content of leaf starch in wild-type and *bam1-2*.** Plants were grown in the greenhouse and harvested at the end of the day after 30 days. Starch was extracted from pooled rosette tissue of about 100 plants. The amylose to amylopectin ratios of starch were determined based on the different absorption spectra of both polymers after addition of iodine solution. Values are means of five technical replicates; error bars are s.e.m. The asterisk indicates a significant difference between amylose contents of wild-type and mutant samples (t-test,  $p < 0.05$ ).

#### 6.2.4 BAM1 activity in *bam1-2*

As indicated above, one possible explanation for faster starch degradation in the mutant could be higher activity of BAM1 (S132N). The amino acid substitution could also interfere with the interaction of BAM1 with its putative binding partners, LSF1 and pNAD-MDH. Native activity gels containing amylopectin allow visualisation of BAM1

activity in plant extracts. Also, they allow visualisation of the BAM1-LSF1-complex (Martin Umhang and colleagues, ETH Zürich, personal communication).

To test if *bam1-2* has detectable changes in BAM1 activity or if the BAM-LSF1-interaction is disrupted, I extracted soluble proteins from rosettes of wild-type, *bam1-1*, *lsf1* and *bam1-2* and separated them by native PAGE on gels containing amylopectin. Later in this chapter, I will describe how I created a *bam1-2 lsf1* double mutant. I also separated extracts of this double mutant on the amylopectin containing native gel. After two hour incubation, the gels were stained with iodine. Pale areas indicated the presence of amylolytic activity (**Figure 6.5**).

BAM1 activity was associated with two bands in the gel as they were missing in the *bam1* knock-out mutant. One band with lower electrophoretic mobility was sharp close to the top of the gel. It was suggested that this band represents the LSF1-BAM1 complex (Martin-Umhang and colleagues, ETH Zürich, personal communication). Consistent with this idea, it disappeared in a mutant that lacks LSF1 (*lsf1*). The second band associated with BAM1 activity was suggested to represent BAM1 in its unbound form. It has a higher electrophoretic mobility and is more diffuse. This band was stronger in the *lsf1* mutant, consistent with the possibility that because BAM1 can no longer bind LSF1, more BAM1 protein is in its unbound form. In extracts of *bam1-2*, the lower band associated with BAM1 activity was completely missing. The upper band which represents the BAM1-LSF1 complex was still present but more focused. The data indicate that the BAM1-LSF1 complex in *bam1-2* is still intact. It could even be speculated that mutant BAM1 has a higher affinity for LSF1 than wild-type BAM1 as the band associated with the activity of unbound BAM1 was missing in *bam1-2*.

Interestingly, none of the two bands associated with BAM1 activity could be detected in *bam1-2 lsf1*. This is unexpected, because in the absence of LSF1, mutant BAM1 is expected to be detectable in its unbound form. Thus, the lower band associated with BAM1 activity should be comparable in intensity to the band seen in *lsf1* single mutants.

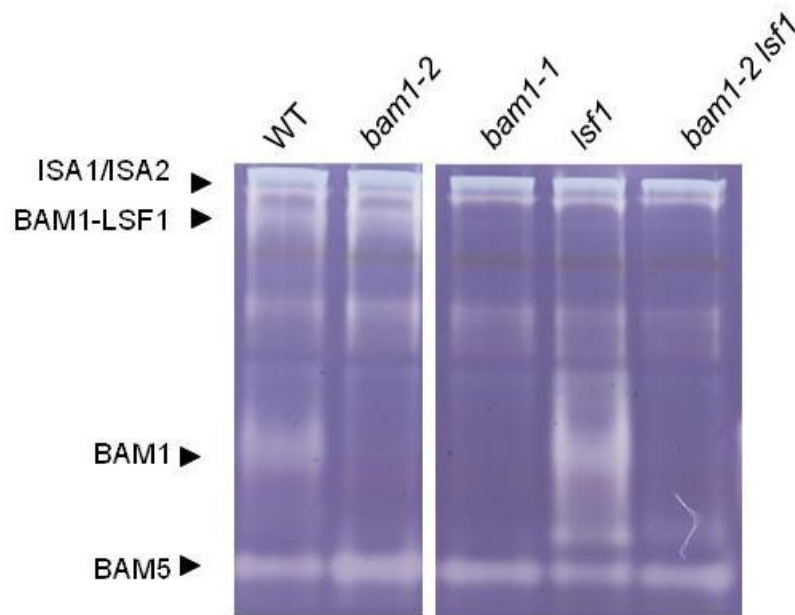


**Figure 6.5: Native gel visualising the activity of starch metabolising enzymes.** The soluble fractions of extracts from wild-type (WT), *lsf1*, *bam1*, *bam1-2* (B) and *bam1-2 lsf1* plants was separated on non-denaturing polyacrylamide gels containing amylopectin. After incubation, the gels were stained with iodine to reveal pale areas where amylopectin was hydrolysed. BAM1 activity can be attributed to two bands. The upper band represents the putative BAM1-LSF1 complex, the lower band free (unbound) BAM1. Plants were 23 days old, and were grown in 12 hour light-12 hour dark cycles and harvested at the end of the day. Protein loadings were adjusted on basis of tissue weight, i.e. the same amount of fresh weight was loaded in each lane. For references see **Figure 5.10**)

### 6.2.5 BAM1 protein levels in *bam1-2*

Analysis of native activity gels containing amylopectin showed that mutant *bam1-2* lacks one of the bands that are attributed to BAM1 activity. In the double mutant *bam1-2 lsf1*, BAM1 activity was undetectable (**Figure 6.5**). To find out if lack of detectable activity in the gel was due to a lack of BAM1 protein, soluble protein extracts from rosettes of wild-type, *bam1*, *lsf1*, *bam1-2* and *bam1-2 lsf1* were analysed by immunoblotting (**Figure 6.6 A**). The extracts were separated on a native gel without amylopectin and transferred to PVDF membrane, before probing with antiserum specific for BAM1. The antiserum was obtained from Jychian Chen (Academia Sinica, Taiwan) and was generated after immunisation of rabbits with the recombinant protein.

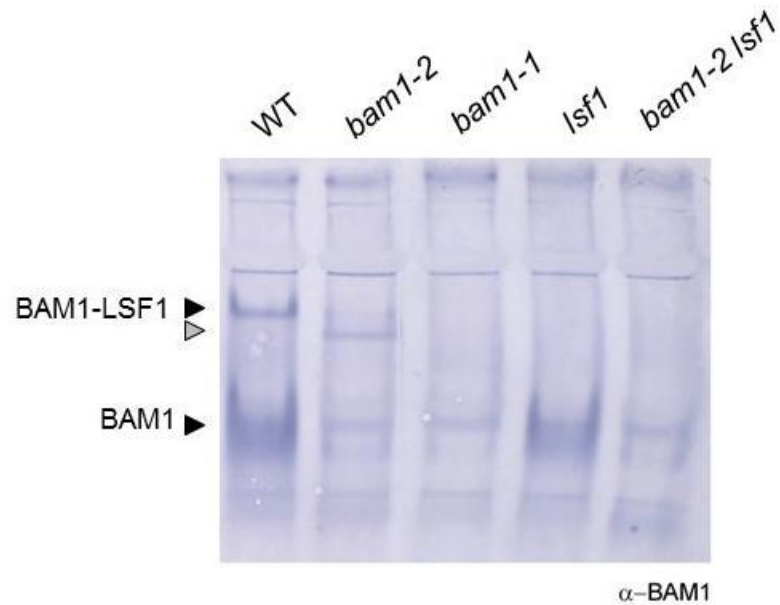
The outcome of the blot roughly confirmed the result obtained by analysis of amylopectin containing activity gels. Two bands that were present in wild-type were missing in *bam1-1* knock-out mutants. The upper band disappeared in *lsf1*. In *bam1-2* the lower band was missing on the immunoblot, consistent with a lack of activity on the amylopectin containing native gel. The top band that represents the putative LSF1-BAM1 complex in wild-type was absent in *bam1-2*. Instead, a weaker band with slightly higher electrophoretic mobility could be detected. It is possible that this band is also attributable to the putative LSF1-BAM1 complex, but shifted in position on the gel relative to the band in wild-type. This is likely, as the band disappeared in the *bam1-2 lsf1* double mutant. Such a band shift was not detectable on the amylopectin activity gel. The reason for this could be that the electrophoretic mobility of the BAM1-LSF1 complex might be affected by the presence of amylopectin in the gel. Consistent with a lack of detectable BAM1 activity on native activity gels, the double mutant *bam1-2 lsf1* had no detectable BAM1 protein on the immunoblot. The immunoblot of this double mutant looked nearly identical to the immunoblot of *bam1-1*.

In conclusion, bands associated with BAM1 activity on native gels containing amylopectin correlated with the presence of BAM1 protein in all genotypes.

To compare the total amount of BAM1 protein in wild-type, *bam1-2*, *bam1-1*, *lsf1* and *bam1-2 lsf1*, immunoblots of SDS gels were used (**Figure 6.6 B**). Proteins in the soluble fraction from 23-day-old plants were separated on SDS gels, transferred to PVDF membrane and probed with antiserum specific for BAM1. The band attributable to BAM1 protein in wild-type and *lsf1* was missing in *bam1-1*. In *bam1-2* and *bam1-2 lsf1*, this band was weaker than in wild-type. This indicates that the soluble fraction contained less BAM1 protein in *bam1-2* and *bam1-2 lsf1*.

To explain lower protein levels in *bam1-2*, I hypothesised that the mutated protein migrates to the insoluble fraction. However, immunoblots of SDS gels using the crude plant extract (soluble plus insoluble fraction) showed similar BAM1 protein levels compared to the soluble fraction for all genotypes. I concluded that *bam1-2* plants contain less BAM1 protein than wild-type plants.

A



B

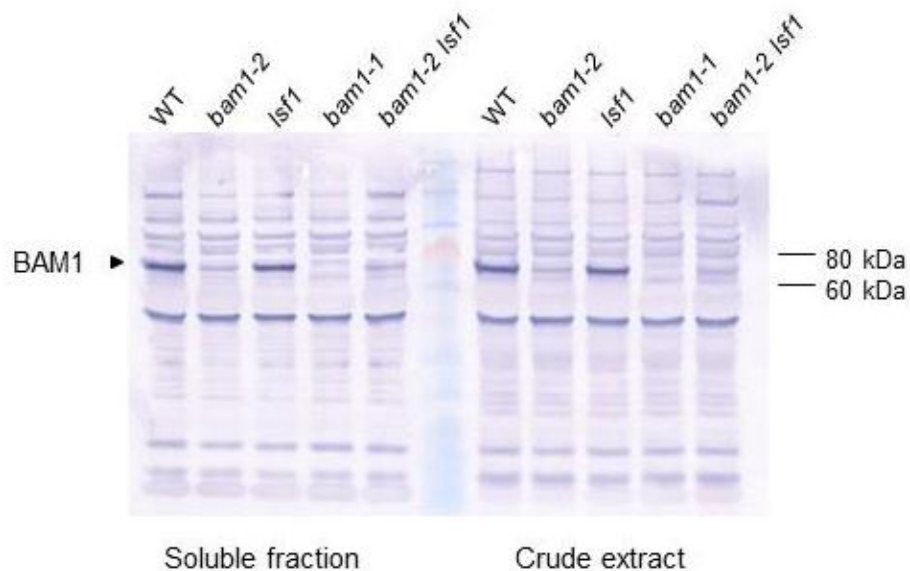


**Figure 6.6: Immunoblot of wild-type and mutant samples on a native gel and a SDS gel probed with antiserum specific for BAM1.** Extracts of soluble protein of rosettes from wild-type (WT), *bam1-2*, *bam1-1*, *lsf1*, and *bam1-2 lsf1* were first separated on a native gel (A) or SDS gel (4-12% polyacrylamide) (B), then blotted on PVDF membrane and probed with antiserum specific for BAM1 at a concentration of 1:1,000. (A) The position of the putative BAM1-LSF1 complex in *bam1-2* (grey arrow) was different from WT (black arrow). Protein loadings were adjusted on a weight base, i.e. the same amount of fresh weight was loaded in each lane.

### 6.2.6 Analysis of native amylopectin and MDH activity gels for *bam1-2*

In theory, the amino acid substitution in BAM1 (S132N) could impair the interaction with pNAD-MDH or alter pNAD-MDH activity in the complex (Section 6.1). To test this possibility, MDH activity gels were analysed (Figure 6.7).

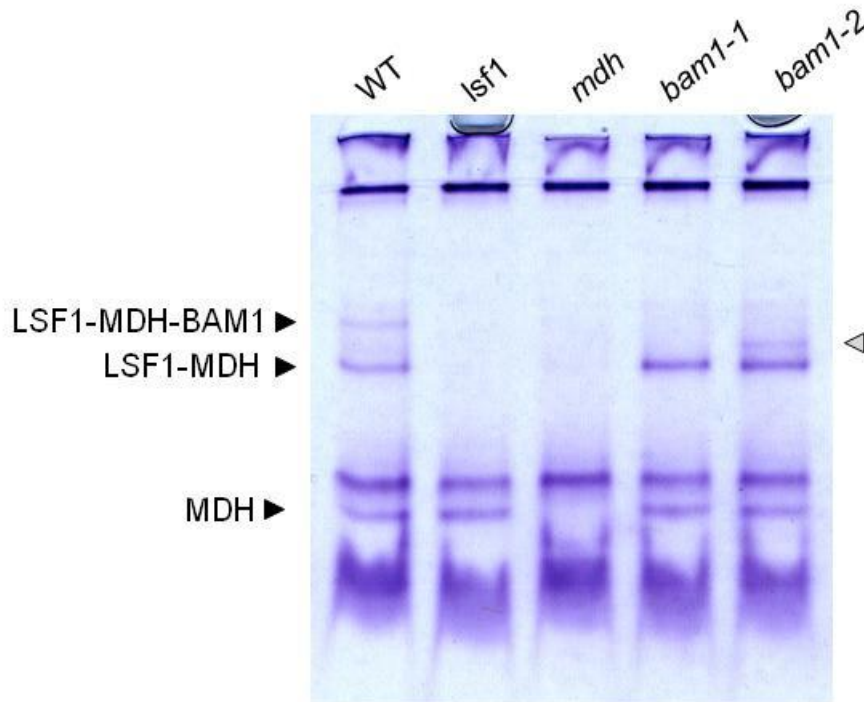


**Figure 6.7: Native activity gel visualising malate dehydrogenase activity.** The soluble fractions of extracts of rosettes from wild-type (WT), *lsf1*, *mdh* (RNAi line), *bam1-1* and *bam1-2* were separated on a native gel (20 µg protein per lane). The gel was then incubated in incubation buffer containing malate and NAD<sup>+</sup>. MDH activity was visualised by coupling the conversion of malate to oxaloacetate and NADH to the reduction of a tetrazolium-dye, resulting in the production of a blue-purple formazan. The grey arrow indicates the position of an additional activity band detected in *bam1-2*, which might represent the LSF1-MDH-BAM1 complex shifted in size.

Soluble proteins were extracted from rosettes of wild-type, *lsf1*, *mdh*, *bam1-1* and *bam1-2* plants and separated on native gels. The *mdh* mutant is a RNAi line with reduced pNAD-MDH expression and was provided by our collaborators in Zürich (Seraina Beeler and Oliver Kötting). The gels were incubated with a buffer containing an excess of the MDH-substrate malate and the cofactor NAD<sup>+</sup>. In the assay, dehydrogenase activity results in the formation of NADH which is coupled to the reduction of a tetrazolium dye, via an intermediate electron carrier. The result is the production of a blue-purple formazan in the gel.

In wild-type samples, pNAD-MDH appeared to be present in three molecular weight forms as three bands were detectable that disappeared in the RNAi line with reduced pNAD-MDH (*mdh*). In the *lsf1* mutant, two of these bands were missing. In the *bam1-1* mutant, only one of these bands was missing. This band, which had the lowest electrophoretic mobility of the three bands, was missing in three mutants, in *mdh*, *bam1-1* and *lsf1*. Therefore, it could represent a BAM1-LSF1-MDH complex, consistent with the idea that the three proteins interact (Martin Umhang and colleagues, ETH Zürich, personal communication). In mutant *bam1-2*, this band was also missing. Instead, another band with slightly higher electrophoretic mobility could be detected. It is possible that this band represents the LSF1-BAM1-MDH complex. The other two bands attributed to pNAD-MDH activity had a similar intensity and position in *bam1-2* and wild-type.

The data indicates that the mutation (S132N) does not disturb the interaction with the putative BAM1 binding partners. However, it remains to be established, why the band representing the putative LSF1-BAM1-MDH complex was shifted in size.

### **6.2.7 Starch degradation in *bam1-1***

In summary, the amino acid substitution in BAM1 (S132N) affects the electrophoretic mobility of the protein on native gels and it reduces the abundance of the protein. It is possible that faster starch degradation and lower BAM1 protein levels in *bam1-2* could be linked. The amino acid substitution could increase instability of the protein by making it more prone to degradation. Low BAM1 protein levels could result in faster starch degradation if the protein was a negative regulator of starch degradation. In that case, starch degradation rates should be faster also in the BAM1 knock-out mutant

*bam1-1*. There is no information in the literature about starch degradation rates in *bam1-1*. Data for end of day and end of night starch contents is available, but these give no indication about starch degradation rates in absence of BAM1 (Fulton et al., 2008).

Therefore, I analysed starch contents in *bam1-1* during the normal and early night and compared them to wild-type (**Figure 6.8**).

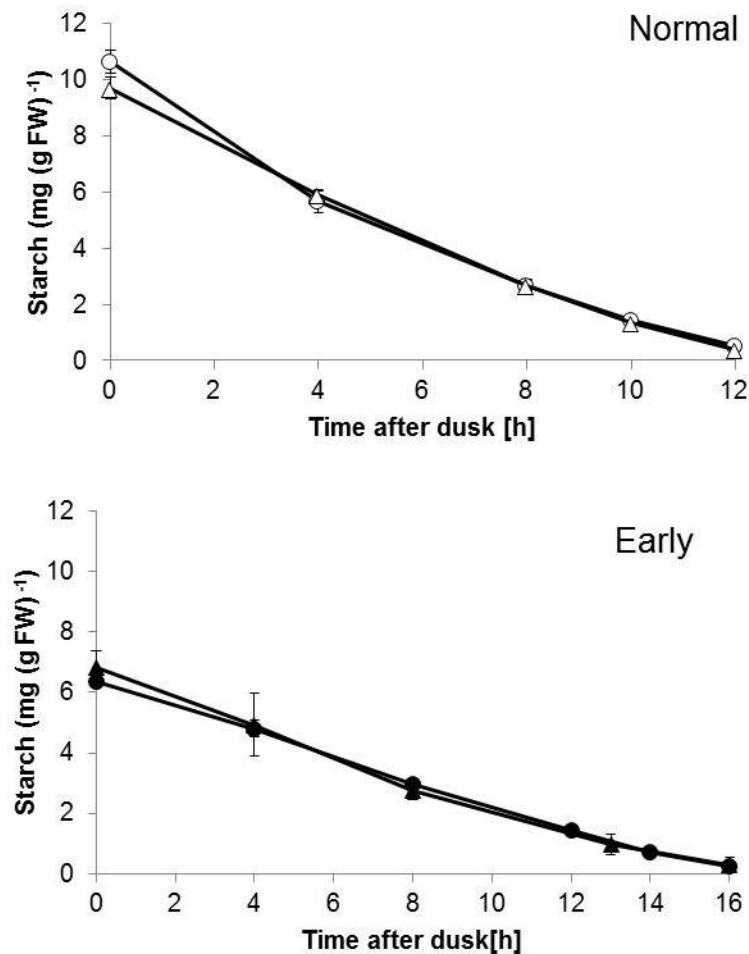


**Figure 6.8 Starch contents of *bam1-1* and wild-type in normal and early night.** Starch contents of wild-type (circles) and *bam1-1* (triangles) were measured during a normal 12 hour night (open circles), as well as during an early night (closed circles). The plants were grown in 12 hour light-12 hour dark cycles for 24 days. Five rosettes were analysed at each time point. Error bars are s.e.m., where not visible they are smaller than the symbol.

Starch contents were determined every 2-4 hours throughout the night in 24-day-old plants. The mutant had nearly identical starch levels to wild-type. Also, it was able to adjust its starch degradation rate in response to the early night. Thus, it did not seem likely that BAM1 is a negative regulator of starch degradation. This indicates that reduced BAM1 protein levels are not the reason for faster starch degradation in *bam1-2*.

### **6.2.8 BAM1 activity and redox-regulation in *bam1-2***

BAM1 was shown to be redox regulated (Sparla et al., 2006; Valerio et al., 2011). The recombinant protein was active in reducing conditions (incubation with 20 mM reduced DTT) and inactive in oxidising conditions (incubation with 20 mM oxidised DTT). It was also shown that redox-mediated changes in BAM1 activity in plant extracts can be visualised on native gels containing amylopectin (Glaring et al., 2012).

In theory, the mutation in BAM1 (S132N) could make the protein less sensitive to oxidation and thereby enhance its activity. To test if BAM1 (S132N) is still redox sensitive, soluble protein extracts of 23-day-old wild-type, *bam1-1*, *lsf1* and *bam1-2* plants were first separated on native polyacrylamide gels containing amylopectin. The gels were then incubated in reducing or oxidising conditions, using incubation buffers containing either 5 mM reduced DTT or 50  $\mu$ M CuCl<sub>2</sub>, respectively. To visualise amylolytic activity, the gels were then stained with iodine solution (**Figure 6.9**).

In presence of 5 mM DTT, BAM1 activity was detectable at two positions in the gel in the wild-type. Under oxidising conditions, the lower band disappeared completely and the top band decreased in intensity. This is the band representing the BAM1-LSF1 complex (compare to **Figure 6.5**). In *bam1-2*, this band was also sensitive to oxidation, as is decreased in intensity under oxidising conditions. Thus, mutant BAM1 (S132N) is not redox-insensitive.

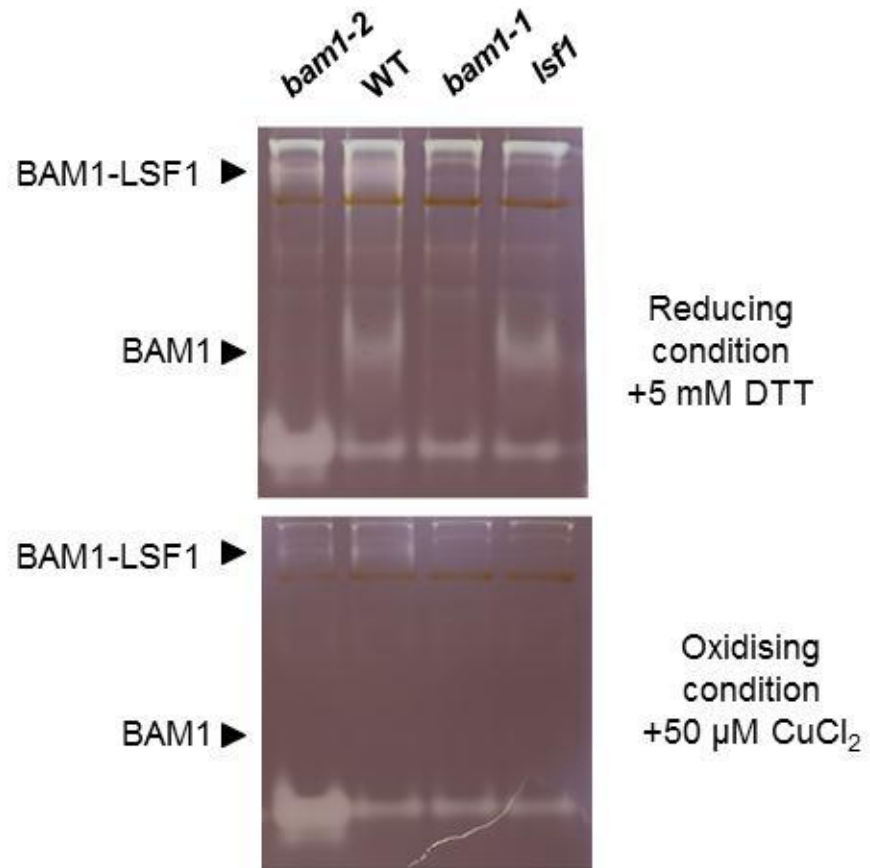


**Figure 6.9: Native activity gels of starch metabolising enzymes under oxidising and reducing conditions.** The soluble fraction of protein extracts from wild-type (WT), *lsf1*, *bam1* and *bam1-2* plants was separated on native polyacrylamide gels containing amylopectin. The gels were incubated in oxidising or reducing conditions by addition of DTT or CuCl<sub>2</sub> to the incubation buffer. Afterwards they were stained with iodine to reveal pale areas that indicate amylopectin degradation. Plants were 23 days old and were grown in 12 hour light-12 hour dark cycles and harvested at the end of the day. Protein loads were adjusted on basis of tissue weight, i.e. the same amount of fresh weight was loaded in each lane.

### 6.2.9 Crosses of *bam1-2* to mutants of the starch degradation pathway

#### 6.2.9.1 Rationale

In this section I describe the creation of double mutants with *bam1-2* to test hypotheses arising from the phenotypic characterisation of *bam1-2*. The native gel analysis presented above suggested that the amino acid substitution in BAM1 (S132N) has a positive effect on the interaction between BAM1 and LSF1. It was hypothesised that LSF1 recruits BAM1 to the starch granule to facilitate starch degradation by BAM1 (**Section 6.1.2**). If mutant BAM1 has a higher affinity for LSF1, the granule might be under permanent attack by BAM1, resulting in faster starch degradation. To test that hypothesis, *lsf1* was crossed with *bam1-2* to analyse the starch degradation pattern in the double mutant. In absence of LSF1, BAM1 (S132N) would not be recruited to the granule and faster starch degradation would no longer be possible. The *lsf1* knockout-mutant has a starch excess phenotype due to retardation of starch breakdown (Comparot-Moss et al., 2010). If the phenotype of *bam1-2* was dependent on LSF1, starch degradation in the double mutant should look like that of *lsf1* single mutants, i.e. the double mutant would also have excess amounts of starch at the end of the night.

An alternative explanation for faster starch degradation in *bam1-2* could be an indirect effect on beta-amylase 3 (BAM3) protein levels or activity. This seems likely, because BAM3 rather than BAM1 is thought to be important for starch degradation at night (Fulton et al., 2008). In the absence of BAM3 starch degradation is slower and there is a starch excess at the end of the night. BAM3 activity is not visible on amylopectin containing native gels, so this type of analysis could not be used to find out if BAM3 activity is increased in *bam1-2*. Therefore, the *bam1-2 bam3* double mutant was analysed for its starch degradation phenotype. If the phenotype in *bam1-2* was dependent on BAM3, then the double mutant should have a starch excess phenotype comparable to that of *bam3* alone.

To find out which other components of the starch degradation pathway are necessary for faster starch degradation in *bam1-2*, I also analysed the phenotype of crosses with *bam1-2* and further mutants of the starch degradation pathway. These included *sex4*, *amy3* and *bam4*.

6.2.9.2 Starch degradation in *bam1-2 lsf1* and *bam1-2 bam3*

Mutant *bam1-2* was crossed to either *bam3-1* or *lsf1* plants. Genotyping of 48 and 96 F<sub>2</sub> plants respectively, led to the identification of two homozygous *bam1-2 bam3-1* and two homozygous *bam1-2 lsf1* double mutants. These plants were grown for seed and the phenotype of F<sub>3</sub> plants was analysed after 24 days. Starch contents of wild-type, *lsf1*, *bam1-1* and *bam1-2 lsf1* double mutants were analysed during a normal night and during an early night (**Figure 6.10**).

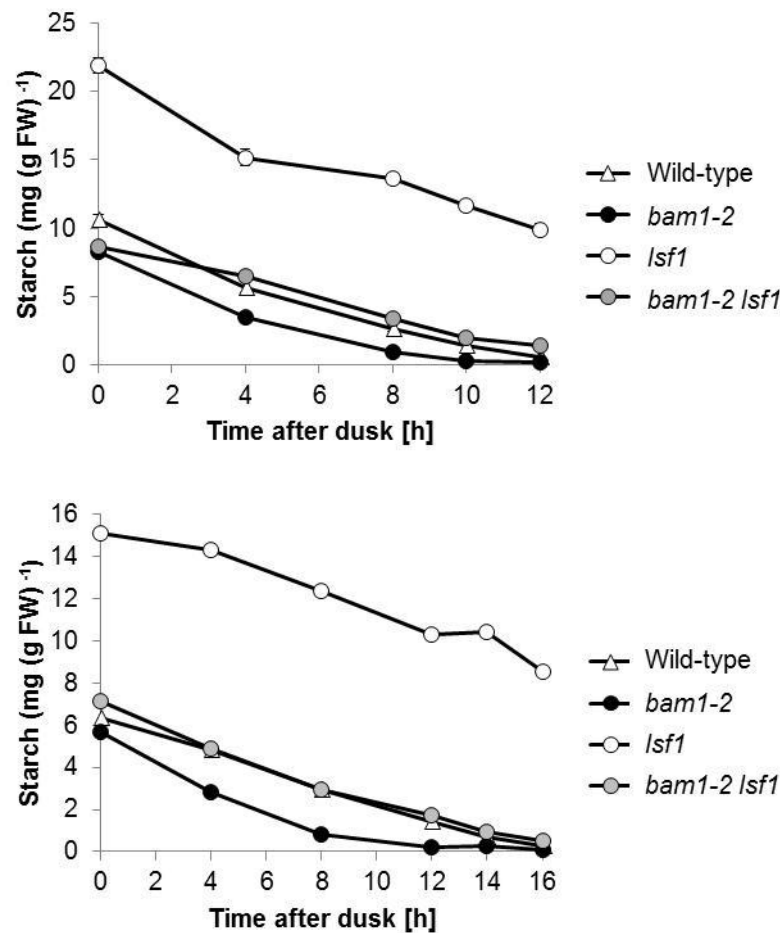


**Figure 6.10: Analysis of starch contents in wild-type, *bam1-2*, *lsf1* and *bam1-2 lsf1* double mutants.** Starch contents for wild-type, *bam1-2*, *lsf1* and *bam1-2 lsf1* double mutants were measured during a normal 12 hour night (top) and during an early night (bottom). The plants were 24 days old at harvest, and five rosettes were analysed at each time point. For this experiment, *bam1-2* plants of the 1st back-cross were used. Error bars are s.e.m., where not visible they are smaller than the symbol.

As expected, the *lsf1* single mutant had about twice as much starch as wild-type plants and did not break it down completely during the normal night (Comparot-Moss et al., 2010). The same was true for the early night. The *bam1-2 lsf1* double mutant had starch contents and degradation rates very similar to wild-type in normal as well as early night. Starch degradation was adjusted according to the length of the night in the double mutant. The phenotype of the double mutant did not resemble the phenotypes of either the *lsf1* or *bam1-2* single mutants. This suggests that the phenotypes are interdependent.

I conclude that faster starch degradation in *bam1-2* requires LSF1. Also, and very unexpectedly, in presence of BAM1 (S132N), LSF1 is no longer required to obtain starch contents and degradation rates comparable to those of wild-type plants.

The starch contents of wild-type, *bam1-2*, *bam3* and *bam1-2 bam3* double mutants were analysed during normal and early nights (**Figure 6.11**). As expected, the *bam3* single mutant had a starch excess at the end of the night (Fulton et al., 2008). The *bam1-2 bam3* double mutant had starch contents very similar to *bam1-2* in both conditions. Thus, the phenotype of *bam1-2* is independent of BAM3. And very unexpectedly, BAM1 (S132N) can compensate for the loss of BAM3.

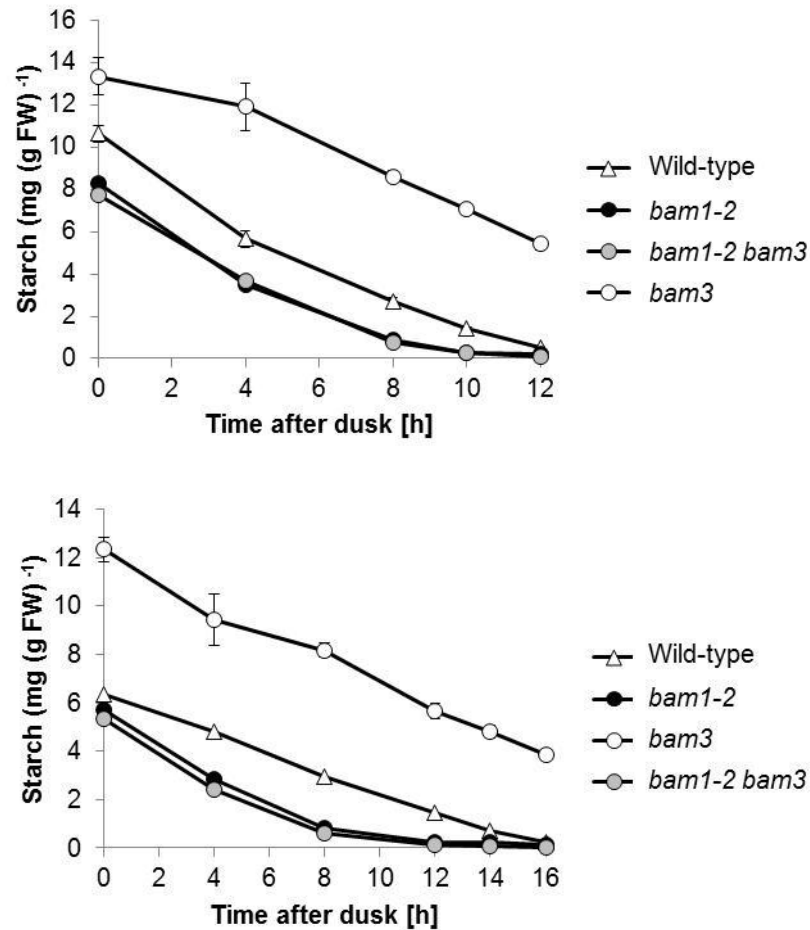


**Figure 6.11: Analysis of starch contents in wild-type, *bam1-2*, *bam3* and *bam1-2 bam3* double mutants.** Starch contents for wild-type, *bam1-2*, *bam3* and *bam1-2 bam3* double mutants were measured during a normal 12 hour night (top) and during an early night (bottom). The plants were 24 days old at the day of harvest, and 5 rosettes were analysed at each time point. For this experiment, *bam1-2* plants of the 1st back-cross were used. Error bars are s.e.m.

6.2.9.3 Starch degradation in crosses of *bam1-2* with *sex4*, *amy3* and *bam4*

To test which other components of the starch degradation pathway are required for faster starch degradation in *bam1-2*, starch contents of further double mutants were analysed by iodine staining of leaves.

Mutant *bam1-2* was crossed to *sex4*, *amy3* and *bam4* single mutants. About 48 F<sub>2</sub> plants of each cross were genotyped and one double mutant for each cross was isolated. Starch contents were analysed in F<sub>3</sub> plants of the cross (**Figure 6.12**).

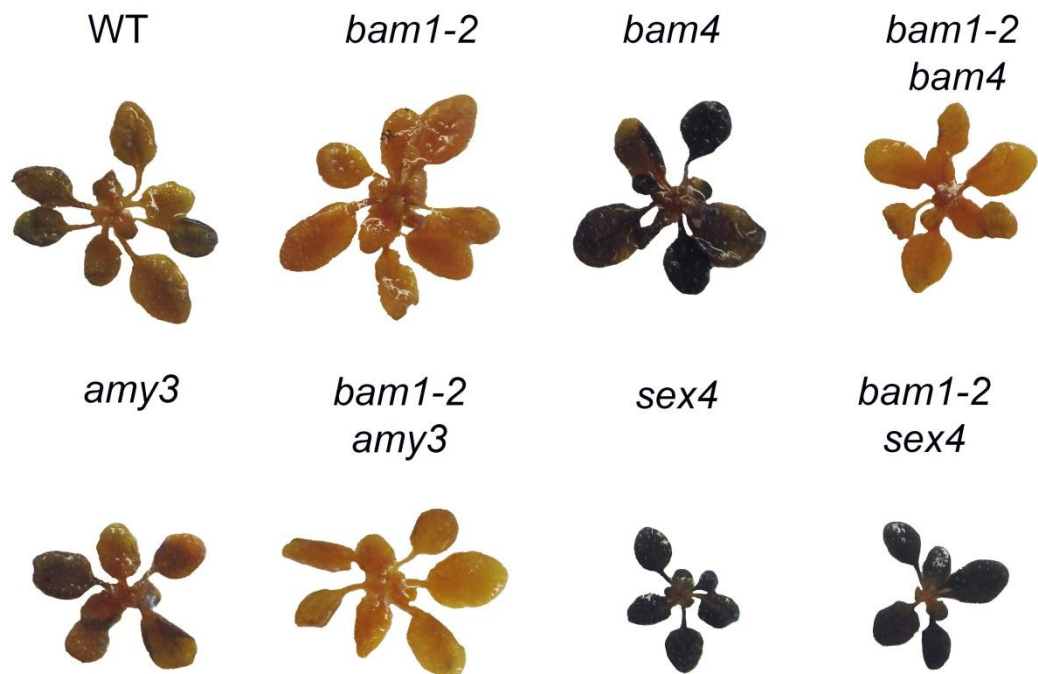


**Figure 6.12: Visualisation of leaf starch in double mutants using iodine staining.**

Plants were grown in 12 hour light-12 hour dark cycles for 24 days and harvested two hours before the end of an early night. Rosettes were harvested, decolourised in boiling ethanol and stained with iodine solution. Genotypes analysed were wild-type (WT), *bam1-2*, *amy3-2* (*amy3*), *bam4-1* (*bam4*), *sex4-3* (*sex4*) and the respective double mutants.

Iodine staining of whole rosettes was performed two hours before the end of the early night, when *bam1-2* should have exhausted its starch reserves. As expected, wild-type plants still contained starch at this time point and showed a blue stain. Mutant *bam1-2* did not stain blue, indicating absence of starch. Mutant *amy3* had a blue stain, comparable in intensity to that of wild-type, thus contained starch. The *bam4* and *sex4* single mutants stained darker than wild-type indicating a starch excess. The *bam1-2 bam4* and the *bam1-2 amy3* double mutants had a stain comparable in colour to *bam1-2*. This indicates that starch contents were exhausted and that neither AMY3 nor BAM4 are required for faster starch degradation in *bam1-2*. The rosette of the *bam1-2 sex4* double mutant had a very dark stain comparable to that of the *sex4* single mutant. This indicates that dephosphorylation of the starch granule by SEX4 is still necessary for faster starch degradation in *bam1-2*.

In summary, the data indicates that *bam1-2* can degrade starch faster than wild-type in absence of BAM3, BAM4 and AMY3. Dephosphorylation of starch catalysed by SEX4 is still necessary to obtain faster starch degradation rates and presence of LSF1 protein is also required to obtain starch degradation rates faster than wild-type.

## 6.3 Discussion

### 6.3.1 Hypotheses for faster starch degradation in *bam1-2*

Starch degradation in *bam1-2* was not adjusted according to the length of the night. I estimated that the initial starch degradation rate in the mutant is set in a way that starch is exhausted about 9-10 hours after dusk. Relative starch degradation rates in the mutant were very similar in normal and early night. On average about 10% of the starch present at the beginning of the night were degraded per hour. Similar starch degradation rates were found in *est1-1*, which degraded about 11% of end of day starch per hour (**Chapter 5**). As discussed in **Chapter 5**, the only other known mutant with faster starch degradation is the circadian clock mutant *cca1lhy*, which degraded 11% of starch per hour (PhD thesis, University of East Anglia, Alexander Graf, 2009). Thus, from the data available, a rate of 11% h<sup>-1</sup> is the maximum rate of starch degradation observed in *Arabidopsis* mutants. So how does the mutation in *bam1-2* cause a faster starch degradation rate? In the following I discuss some hypotheses for faster starch degradation in the mutant.

#### 6.3.1.1 Is BAM1 (S132N) not redox-sensitive?

BAM1 activity was shown to be redox sensitive *in vitro*, both as a recombinant protein and in plant extracts (Sparla et al., 2006; Glaring et al., 2012). I showed that BAM1 (S132N) extracted from mutant plants is still redox-sensitive (**Figure 6.9**). Thus, I did not find any evidence that the disulfide bridge inactivating the enzyme cannot form and that a reduced redox-sensitivity is likely to be responsible for the mutant phenotype.

#### 6.3.1.2 Are lower BAM1 protein levels the reason for faster starch degradation in *bam1-2*?

Immunoblot analysis showed that BAM1 protein levels are reduced in *bam1-2* (**Figure 6.6**). Lower protein levels probably indicate that BAM1 (S132N) is more prone to proteolytic cleavage. Although the possibility that transcript levels are altered through a feedback mechanism cannot be ruled out.

As an alternative way to explain reduced BAM1 protein levels and activity in *bam1-2*, I suggested that the protein has moved into the insoluble fraction of the plant extract. This

could be the case if the amino acid substitution increased the affinity of BAM1 for starch. If that was true, more BAM1 protein should have been present in the insoluble fraction of mutant plant extracts compared to wild-type. However, immunoblots showed that the amount of BAM1 protein in soluble fraction and crude plant extract was equally reduced compared to wild-type. It is therefore unlikely that missing BAM1 protein is bound to starch to a greater extent than wild-type BAM1.

As discussed above, lower protein levels might cause faster starch degradation in *bam1-2* if BAM1 is a negative regulator of starch degradation. However, I showed that mutants lacking BAM1 protein degrade starch normally, thus lower protein levels in *bam1-2* cannot explain the abnormally fast starch degradation rates in the mutant.

#### 6.3.1.3 Does mutant BAM1 still interact with LSF1 and/or pNAD-MDH?

Based on information from Martin Umhang and colleagues (ETH Zürich, personal communication), we know that BAM1 interacts with LSF1 and pNAD-MDH. The physiological relevance of these interactions is not known, although it is reasonable to propose that LSF1 recruits BAM1 to the granule to facilitate starch degradation.

To explain faster starch degradation rates in *bam1-2*, I hypothesised that the amino acid substitution alters the protein-protein interaction between BAM1 and LSF1 and/or pNAD-MDH. Native activity gels to visualise beta-amylolytic activity showed that BAM1 and LSF1 still interact in the *bam1-2* mutant, as the activity band representing the putative complex was visible in wild-type and the mutant (**Figure 6.5**). The activity band representing BAM1-LSF1 was detected in the same position in wild-type and mutant. However, immunoblots with antiserum specific for BAM1 showed that the band representing the putative BAM1-LSF1 complex was shifted to a different position in *bam1-2* on native gels without amylopectin. It is very likely that this band represents the BAM1-LSF1 complex, as it was missing in the *bam1-2 lsf1* mutant.

Martin Umhang and colleagues found that BAM1 and LSF1 can exist in a complex with pNAD-MDH. I found that a MDH activity band in wild-type was missing in *bam1-1*, *lsf1* and *mdh* plant extracts (**Figure 6.7**). Again, this band seemed to be shifted towards a slightly lower molecular weight and to a similar extent as the BAM1-LSF1 complex

on the immunoblot probed with antiserum specific for BAM1 (**Figure 6.6**). I concluded that the BAM1-LSF1-pNAD-MDH complex is still intact in *bam1-2*.

In summary, the data presented here show that neither the interaction between BAM1 (S132N) and pNAD-MDH, nor the interaction of BAM1 (S132N) with LSF1 is disturbed by the amino acid substitution. However, the putative BAM1-LSF1-pNAD-MDH complex has a different electrophoretic mobility in *bam1-2* from that in wild-type plants. The significance of that change remains to be discovered.

#### 6.3.1.4 Can a higher affinity of BAM1 (S132N) to LSF1 explain faster starch degradation in *bam1-2*?

Native activity gel analysis indicated that BAM1 (S132N) can still interact with LSF1. However, unbound BAM1 (S132N) could not be detected in *bam1-2* (**Figure 6.5 and Figure 6.6**). I concluded that BAM1 (S132N) has a higher affinity to LSF1 than wild-type BAM1 and is therefore permanently bound to LSF1.

It was suggested that the granule bound protein LSF1 facilitates starch degradation of BAM1, by recruiting the protein to the granule (**Section 6.1**). A stronger LSF1-BAM1 interaction could therefore explain faster starch degradation in *bam1-2*. To test the relevance of the interaction between LSF1 and BAM1 (S132N) for the *bam1-2* phenotype, I analysed the phenotype of the *bam1-2 lsf1* double mutant. In absence of LSF1, starch degradation in *bam1-2* was no longer faster than in wild-type. This indicates that LSF1 is required for faster starch degradation in the mutant. The reason for this might be the recruitment of the protein to the granule, which requires LSF1 as binding partner.

I also showed that presence of BAM1 (S132N) compensates for the lack of LSF1, as the *bam1-2 lsf1* double mutant degraded starch faster than *lsf1*. This suggests that BAM1 (S132N) can degrade starch in absence of LSF1. The observed starch degradation rates in the double mutant were very similar to those of the wild-type. This could mean that BAM1 (S132N) can to some extent substitute the function of LSF1. It is not obvious how this could be achieved as the function of LSF1 is not fully understood. I will give one possible explanation in the next section.

I conclude that the interaction between LSF1 and BAM1 (S132N) could be the cause of faster starch degradation in *bam1-2*. However, further research is required to support this hypothesis.

#### 6.3.1.5 Could the amino acid substitution affect a BAM1 phosphorylation site?

It is possible that BAM1 is regulated on a posttranslational level by phosphorylation. If BAM1 Ser-132 is the phosphorylation site of a serine protein kinase, deletion of this site in BAM1 (S132N) could result in constant activation of the enzyme.

To discover whether Ser-132 is a phosphorylation site, site-directed mutagenesis of this amino acid could be performed. Substitution of Ser-132 with alanine would reveal whether faster starch degradation is due to lack of serine rather than the presence of asparagine. Substitution of Ser-132 with aspartate could be used to mimic phosphorylation, as it introduces a negative charge (Wang et al., 1992; Huang and Erikson, 1994). These experiments are in progress. However, there is no evidence for that Ser-132 is phosphorylated as two independent proteomics studies did not find that residue to be phosphorylated (Reiland et al., 2009; de la Fuente van Bentem et al., 2008) (**Chapter 4**).

Regulation of BAM1 by phosphorylation could explain the relevance of the interaction between LSF1 and BAM1. Analysis of functional domains in LSF1 indicated that it is a putative phosphatase. Its substrate has not been identified yet (Comparot-Moss et al., 2010). I speculate that BAM1 could be the substrate of LSF1, as both proteins interact. LSF1 could dephosphorylate wild-type BAM1 and thereby activate it. If BAM1 Ser-132 is a phosphorylation site, LSF1 might no longer be necessary to dephosphorylate (and thereby activate) the protein in *bam1-2*. This could explain why starch degradation in *bam1-2 lsf1* was similar to that of wild-type plants. However, it does not explain, why presence of LSF1 is still necessary for faster starch degradation in *bam1-2* unless LSF1 is required to dephosphorylate more than one phosphorylation site in BAM1 for it to achieve its full activity. LSF1 could also be required to dephosphorylate other proteins, e.g. BAM3.

Further research is required to find out if phosphorylation of BAM1 is necessary for its regulation and if it is linked to the starch degradation phenotype of *bam1-2*.

#### 6.3.1.6 Is faster starch degradation in *bam1-2* the result of an indirect effect on BAM3 activity?

*BAM1* and *BAM3* gene expression are inversely regulated under stress conditions (Kaplan and Guy, 2004). It is possible, that lower BAM1 protein levels observed in *bam1-2* result in higher *BAM3* expression compared to wild-type. This could mean that faster starch degradation in *bam1-2* is a result of increased BAM3 activity. This is likely, because in contrast to BAM1, BAM3 plays a major role in starch degradation at night (Fulton et al., 2008). However, analysis of the starch contents in the *bam1-2 bam3* double mutant showed that faster starch degradation in *bam1-2* is independent of BAM3. Starch contents in the double mutant were nearly identical to those of *bam1-2* alone. This suggests that BAM1 (S132N) can fully substitute the function of BAM3, probably because both enzymes catalyse the same reaction.

I conclude that BAM3 activity does not cause faster starch degradation in *bam1-2*.

#### 6.3.1.7 Are other components of the starch degradation pathway no longer necessary for faster starch degradation in *bam1-2*?

I crossed *bam1-2* to *bam4*, *amy3* and *sex4* to find out which other enzymes are required for faster starch degradation in *bam1-2*. The results of this experiment are preliminary and starch contents should be analysed quantitatively. So far, I can conclude that starch phosphorylation by SEX4 is still necessary for faster starch degradation in *bam1-2*. I could also exclude a role for AMY3 for faster starch degradation in *bam1-2*. Interestingly, the *bam1-2 bam4* double mutant had starch contents comparable to *bam1-2*. Thus, the presence of mutant BAM1 can rescue the starch excess of the *bam4* mutant. This shows that mutant BAM1 does not require BAM4 to be fully active. However, the function of BAM4 is not clear, therefore it is hard to speculate how mutant BAM1 (S132N) could compensate for lack of BAM4. Further crosses of *bam1-2* to *pwd* and *lsf2* are in progress to find out if mutant BAM1 is independent of C3 phosphorylation.

### 6.3.3 Conclusion and Outlook

#### 6.3.3.1 Is the mutation in *bam1-2* of physiological relevance?

In absence of BAM1 starch is degraded normally (**Figure 6.8**; and Fulton et al., 2008) BAM1 is also not necessary for adjusting starch degradation rates according to the length of the night, because the *bam1-1* mutant was still able to slow down its starch degradation rate in response to the early night (**Figure 6.8**). Therefore, BAM1 does not play a major role in starch degradation at night in wild-type plants. It is difficult to reconcile this observation with the strong starch degradation phenotype in *bam1-2*.

It was hypothesised that BAM1 is mainly involved in plant responses to osmotic stress (Valerio et al., 2011). Valerio et al. suggested that the protein is part of a redox-regulated stress response pathway that degrades starch in the light. BAM1 was also found to be activated in response to heat stress (Kaplan and Guy, 2004). Maltose resulting from starch breakdown via BAM1 might serve as a compatible solute to protect the cell from damage by high temperatures.

It is conceivable that starch degradation in response to acute stress needs to be activated quickly and that starch needs to be degraded fast. To explain faster and unregulated starch degradation in *bam1-2*, one could hypothesise that the same stress response is activated that would normally be triggered under osmotic stress or heat stress. The cause for this could be the amino acid substitution in BAM1 (S132N) which hinders post-translational modifications that inactivate the wild-type protein in non-stressed conditions.

However, there are several lines of evidence that argue against this suggestion. Firstly, if the mutation prevents normal inactivation of BAM1, the mutant protein should also be active during the day. This is possibly not the case as starch accumulation in the day was normal in *bam1-2*. Secondly, the suggested mechanism of activation of BAM1 in stress is via reduction of a disulphide bond (Sparla et al., 2006). I found no evidence that the redox sensitivity of BAM1 (S132N) differs from that of wild-type protein.

It is also possible that the mutation in BAM1 (S132N) increases the activity of the enzyme in a way that would not happen in wild-type plants. If this is the case, the

phenotype of *bam1-2* may have little direct relevance for starch degradation at night. However, it is still likely that further understanding of the cause of accelerated starch degradation in the mutant will shed light on the mechanisms and control of starch degradation.

### 6.3.3.2 Outlook

The data presented here do not deliver sufficient explanation for the mutant phenotype and opened up many questions. It is difficult to understand that absence of BAM1 has no effect on starch degradation rates, while presence of BAM (S132N) accelerates them strongly. It is also hard to explain the lower BAM1 protein content in *bam1-2* and how it would fit in with faster starch degradation, as one would expect the opposite in a mutant with faster starch mobilisation. The altered electrophoretic mobility of the BAM1-LSF1 complex in *bam1-2* is also intriguing and so far, I have no explanation for it. The starch excess of *bam3* and *bam4* mutants was rescued in the *bam1-2* background, but LSF1 was still required for faster starch degradation in the mutant. Thus, the interaction with LSF1 might be the key to resolving the question about faster starch degradation in *bam1-2*.

Important further experiments to shed light on the *bam1-2* phenotype will include a deeper analysis of the LSF1-BAM1 (S132N) interaction and investigation of the impact of the same amino acid substitution on the *in vivo* function of the major BAM3 isoform. Also, the specific activity of recombinant mutant and wild-type protein should be compared *in vitro* to test if the mutation increases the activity of BAM1.

## 7 Starch degradation rates in *sex* mutants

### 7.1 Aim

In the previous chapters I explained the approach I took to identify new genes involved in controlling starch degradation rates in *Arabidopsis* leaves. With the work presented in this chapter, I want to find out which of the known components of the starch degradation pathway are required to adjust starch degradation rates. In **Chapter 1**, I introduced a chemical kinetic model that proposes how the adjustment of starch degradation rates could be implemented. The model suggests that the interaction of “S” and “T” molecules regulates the flux through the starch degradation pathway, possibly by interaction of the molecules with enzymes of the starch degradation pathway. We hypothesised that it may be possible to identify the components that are the target of the regulation by “S” and “T”, by analysis of starch degradation rates in knock-out mutants lacking individual components of the starch degradation pathway. In this chapter I present the data of my investigation into this suggestion published as part of Scialdone et al. (2013).

#### 7.1.1 Rationale and candidate genes

If one of the enzymes of the starch degradation pathway is necessary for the immediate adjustment of starch degradation rates by the proposed modulation by “S” or an “ST” complex, then lack of this enzyme would result in an inability to adjust the starch degradation rate in response to an early night.

Most mutants of the starch degradation pathway have reduced starch degradation rates and a starch excess (*sex*) phenotype at the end of the night. I analysed starch degradation rates in mutants lacking PWD, BAM4, BAM3, LSF1, ISA3 and SEX4. Mutants lacking GWD (*sex1*) hardly turnover any starch and were excluded from the analysis, because starch degradation rates cannot be calculated for them. Starch degradation data for *bam1-1* was presented in **Chapter 6**. I showed that this mutant responds normally to the early night.

## 7.2 Results

To find out if *sex* mutants are able to slow down their starch degradation rates in response to an early night, I measured starch contents of six mutants (*bam3-1*, *bam4-1*, *pwd*, *isa3-2*, *lsf1-1*, *sex4-3*) in the normal 12 hour night and in the early night. Plants were grown for three weeks in 12 hour light – 12 hour dark cycles and harvested every two to four hours during the dark period. To normalise the data for the different end of day starch contents, I calculated the starch contents in relation to the amount of starch at the beginning of the night (relative starch contents). The data are shown in **Figure 7.1**.

As expected, wild-type plants showed a near-linear pattern of starch degradation. They adjusted their starch degradation rates according to the length of the night and starch was exhausted around dawn in both conditions. The mutants degraded their starch in an almost linear way, but had more starch than wild-type at all time points. For four mutants (*isa3*, *bam4*, *lsf1*, *sex4*) and the wild-type, the amount of starch present after 12 hours of the normal night was lower than after 12 hours of the early night. In other words, these mutants degraded starch faster in the normal than in the early night and slowed down their starch degradation rate in response to the early night. In mutant *pwd* a different pattern was observed, as starch contents in the normal night never fell below starch contents of the early night. In *bam3-1*, starch contents at the end of the normal night were nearly identical to starch contents in the early night. The data indicates that *pwd* and *bam3* slowed down starch degradation rates to a smaller extent than the other mutants and the wild-type.

Relative starch contents during normal and early nights clearly differed for wild-type and four mutants (*isa3*, *bam4*, *lsf1*, *sex4*). These genotypes degraded a bigger fraction of end of day starch during the normal night than during the early night, confirming that they slowed down starch degradation in response to the early night. Mutant *pwd* had nearly identical relative starch contents in normal and early nights. I obtained similar data for *pwd* in two additional experiments (data not shown). Also in *bam3*, the relative starch contents were very similar during normal and early nights. Thus, the relative starch degradation rates of *pwd* and *bam3* did not show an obvious adjustment in response to the early night.

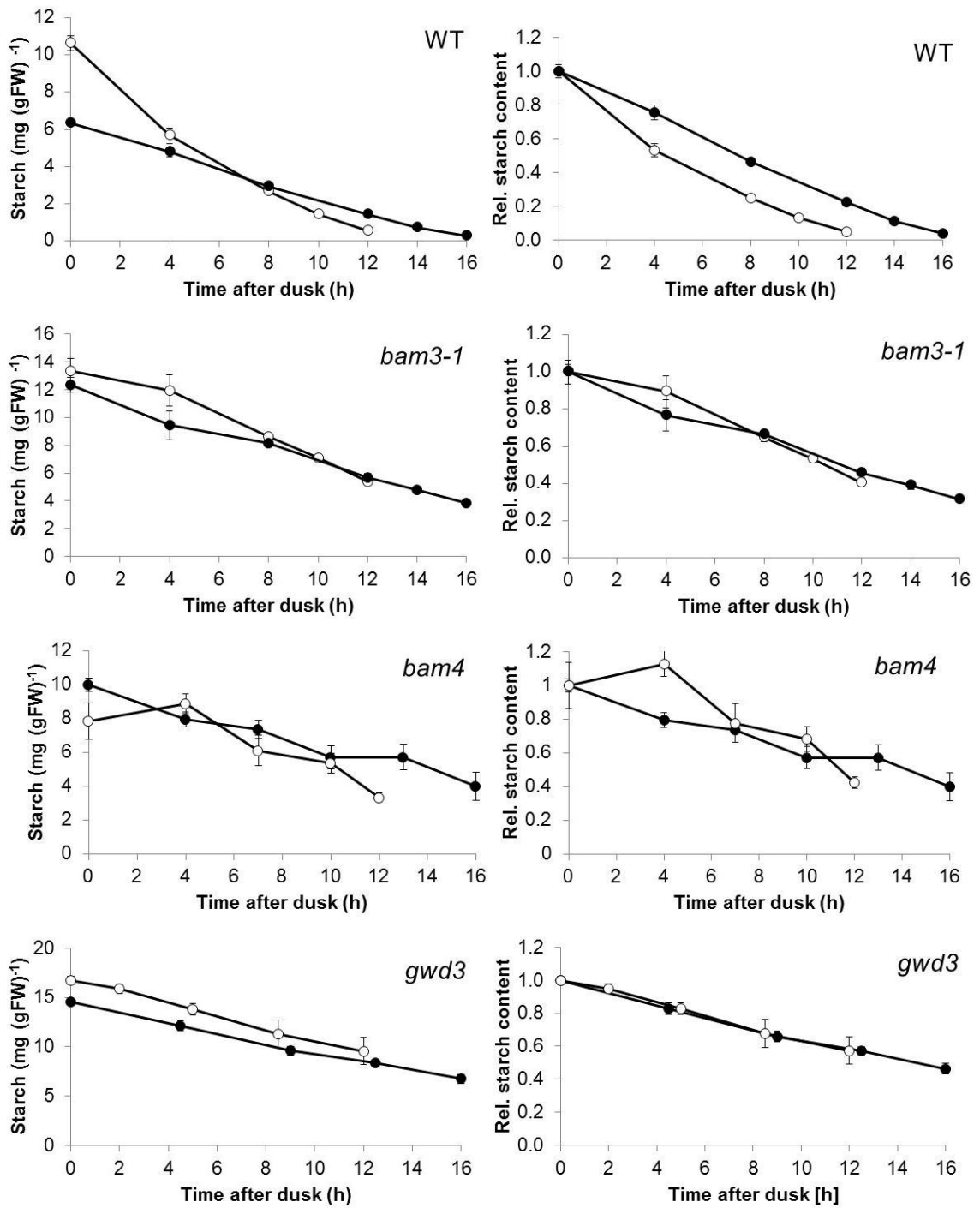


**Figure 7. 1** Starch contents of starch excess mutants during normal and early night. For description see next page.

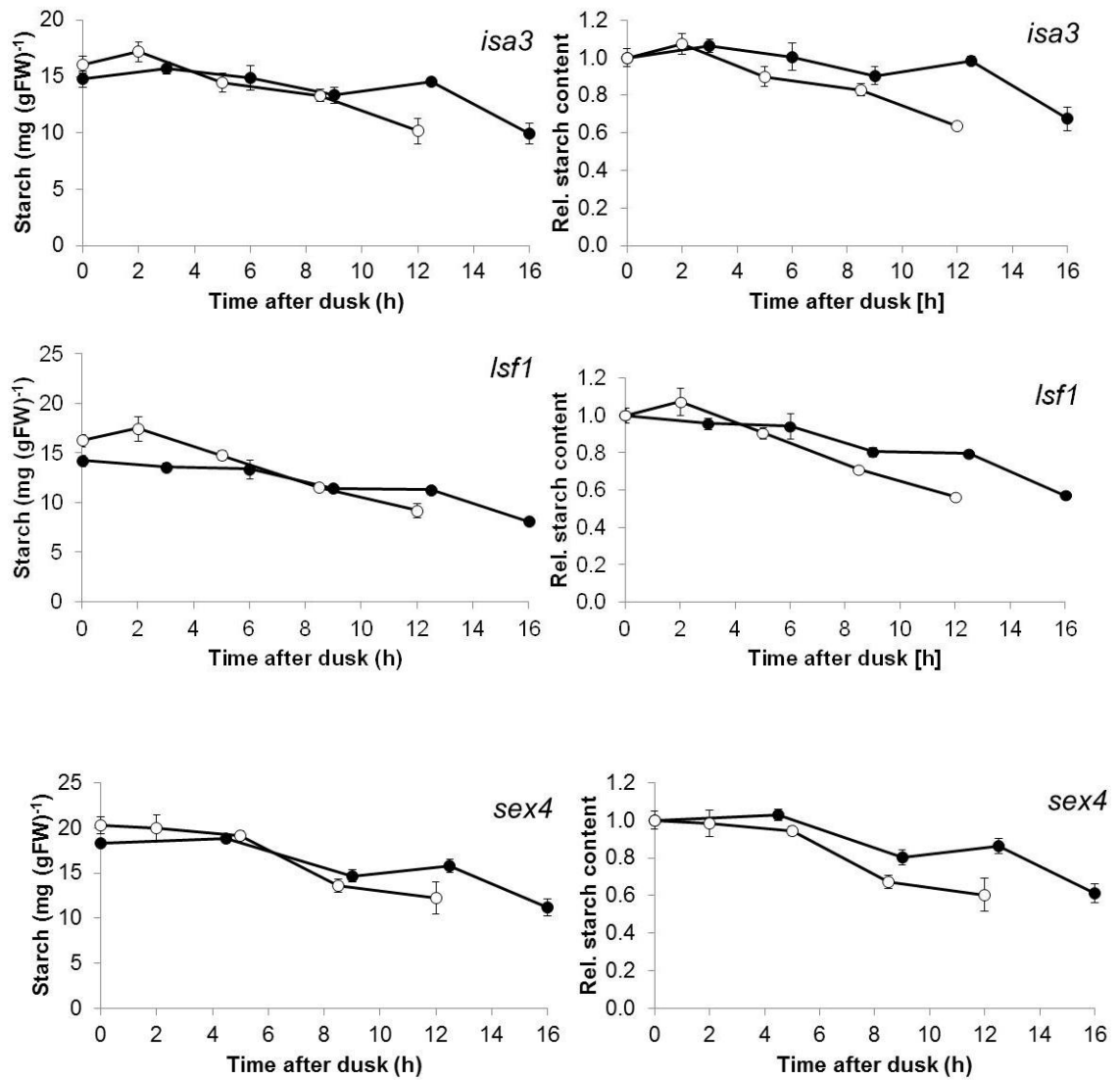


**Figure 7.1 Starch contents of starch excess mutants during normal and early night.** Plants were grown for 24 days in 12 hour light-12 hour dark cycles and harvested during a normal night (open circles) and a night that started four hours early (closed circles). On the right, starch contents are shown in relation to end of day starch contents. (Rel. starch content). Data are means of five biological replicates. Errors are s.e.m., where not visible they are smaller than the symbol.

To quantify starch degradation rates of all mutants and to compare them to wild-type, I calculated the starch degradation rates and relative starch degradation rates based on the slope of linear regression lines fitted through all data points of the time course (**Figure 7.2 A**).

During the normal night, starch degradation rates were lower than wild-type in all mutants. However, the starch degradation rates varied between the different mutants and were very similar to wild-type for most of them, especially for *sex4*. In the early night, starch degradation rates were slower than wild-type in *isa3*, *lsf1* and *bam4*. Mutant *sex4* had a similar starch degradation rate compared to wild-type in the early night. Intriguingly, mutant *pwd* and *bam3* degraded starch at a faster rate than wild-type in the early night. Thus, both mutants could not slow down starch degradation to wild-type level. I analysed starch degradation rates in an additional, independent experiment and confirmed that *pwd* and *bam3* degrade starch at a faster rate than wild-type in the early, but not in the normal night (data not shown).

Comparison of starch degradation rates in early and normal nights shows that all mutants and the wild-type degraded less starch per hour in the early night than in the normal night. Thus, all mutants slowed down starch degradation in the early night. I quantified the rate adjustment by subtracting starch degradation rates of normal and early night (**Figure 7.2.B**). The rate adjustment observed in *pwd* and *bam3* was only about half of the adjustment of wild-type plants. Also *bam4* showed a very small adjustment of the starch degradation rate in the early night. However, the reason for this could be that data for *bam4* were very noisy and end of day starch contents for the early night were higher than those of the normal night. Thus, the calculated starch degradation rate in the normal night might be too low and result in an underestimation of the rate adjustment.

To find out how much starch each of the mutants degraded during normal night and early night, I calculated the amount of starch that was degraded during the whole dark period (**Figure 7.2.C**). The calculation was based on the linear regression lines fitted through the data presented in **Figure 7.1**. As indicated by the higher starch degradation rate, *bam3* and *pwd* degraded more starch in the early night than wild-type plants. This

again shows that the mutants cannot slow down starch degradation rates to wild-type level if the night starts early.

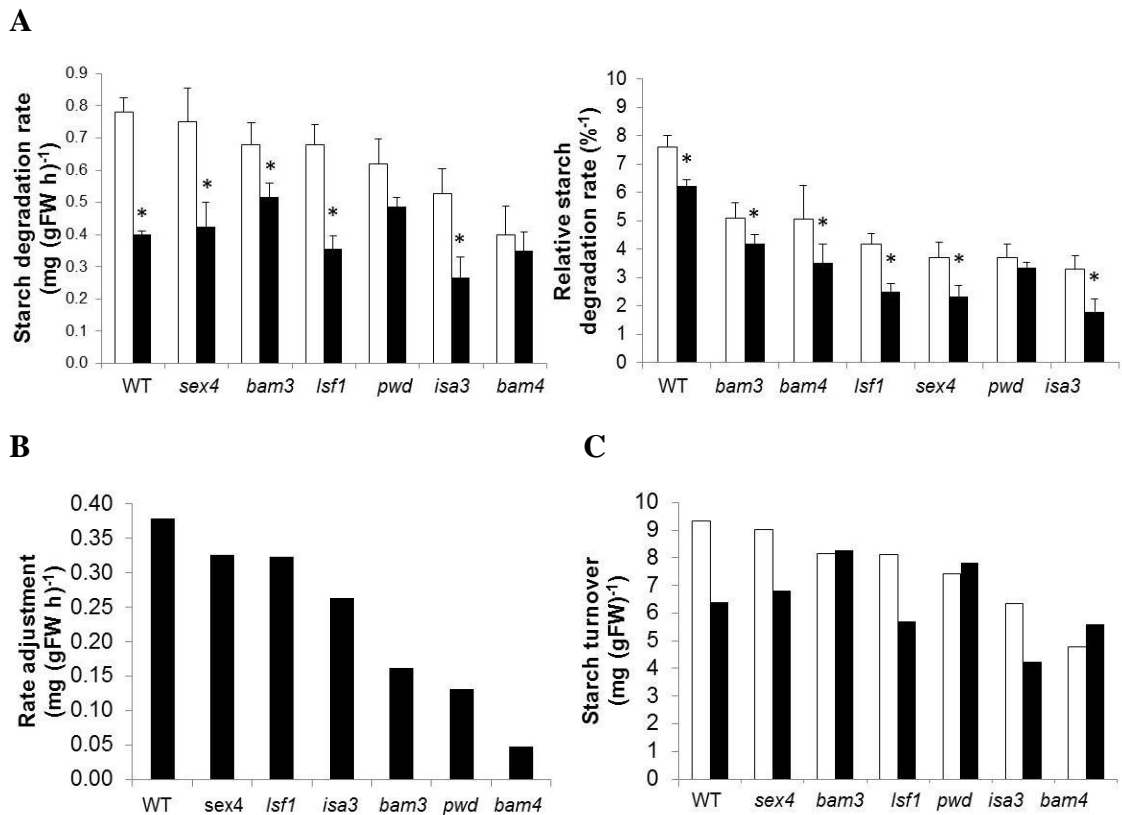


**Figure 7.2: Analysis of starch degradation rates in starch excess mutants using linear fits.** (A) Data presented in **Figure 7.2** were used to calculate starch degradation rates of each mutant in normal night (white bars) and early night (black bars). Therefore, linear regression lines were fitted through all data points during normal and early night and the slopes determined. This was done for absolute and relative starch contents. Asterisks indicate a significant difference in degradation rates of normal and early nights for each genotype (t-test,  $p < 0.05$ ) (B) The rate adjustment was calculated by subtraction of starch degradation rates of the early night from the rates in the normal night. (C) On basis of the regression lines, the total amount of starch degraded during the night (starch turnover) was calculated.

### 7.3 Discussion

#### 7.3.1 Starch contents and degradation rates in sex mutants

The observed starch contents and starch degradation rates in the mutants were comparable to those in the literature. Mutant *lsf1* was shown to have about 80% more starch than wild-type and *sex4* about 150% more starch than wild-type at the end of the day. The mutants degraded about the same amount of starch during the night as a wild-type plant (Comparot-Moss et al., 2010). Mutant *isa3* was shown to have about 80% more starch than wild-type at the end of the day and degraded about 70% of the amount of starch degraded by a wild-type plant during the night, when grown in 12 hour photoperiods (Streb et al., 2008). Mutant *bam4* was shown to have about 60-80% more starch than wild-type at the end of the day and degraded about 60-80% of starch degraded by a wild-type plant during the night, when grown in 12 hour photoperiods (Fulton et al., 2008). Mutant *bam3* was shown to have 80-120% more starch than wild-type and degraded about 80%-150% the amount of starch of a wild-type plant (Fulton et al., 2010). Mutant *pwd* was shown to have 15-20% more starch than wild-type at the end of the day and degraded about 60%-80% of starch degraded by a wild-type plant during the night (Baunsgaard et al., 2005; Kötting et al., 2005).

Starch degradation rates in four of the mutants that were analysed here slowed down to wild-type level or lower in the early night. I conclude that LSF1, BAM4, ISA3 and SEX4 are probably not involved in controlling starch degradation rates in response to an early night. Mutant *bam3* and *gwd3* had lower starch degradation rates in the early night compared to the normal night. However, both mutants showed only a weak adjustment of the starch degradation rate. Also, they degraded starch faster than wild-type in the early night, indicating that they could not slow down starch degradation to wild-type level in the early night. I conclude that PWD and BAM3 might be involved in regulating starch degradation rates in response to an early night.

### ***7.3.2 PWD-catalysed phosphorylation could be important to regulate starch degradation rates***

I showed that a mutant lacking PWD was impaired in slowing down starch degradation in response to an early night. Also, it degraded starch at a faster rate than wild-type in the early night. This is interesting, because the mutant is retarded in starch breakdown in the normal night. The data suggest that PWD might help to adjust starch degradation rates either in response to changes in time until dawn (“T”) or starch content (“S”). Therefore, PWD could be a node in the pathway that integrates information about starch content and time remaining until dawn to set the appropriate starch degradation rate.

PWD is one of the two enzymes that phosphorylate the starch granule, the second enzyme being GWD (**Chapter 1**). PWD phosphorylates starch at the C3 position of glucosyl residues, but only after pre-phosphorylation of C6 by GWD (Baunsgaard et al., 2005; Kötting et al., 2005; Hejazi et al., 2009). C3 phosphates are removed by the glucan phosphatases LSF2 and SEX4 (Santelia et al., 2011). The role of starch phosphorylation is not clear. The addition of phosphate groups to the starch granule is thought to disrupt the ordered packing of the starch granule surface. Therefore it facilitates the access for starch degrading enzymes like BAM3 and ISA3 which attack the granule. However, the phosphate groups have to be removed to allow complete degradation of the granule as the action of beta-amylases is blocked by the phosphates (Edner et al., 2007; Hejazi et al., 2008; Takeda and Hizukuri, 1981; Fulton et al., 2008).

It was hypothesised that addition of phosphate to starch encodes the information about starch contents (Scialdone et al., 2013). The proposed S molecule might affect the activity of enzymes that phosphorylate or dephosphorylate the starch granule (Scialdone et al., 2013; **Chapter 1**). Thus, PWD could adjust starch degradation rates in response to variations in starch contents. For example S might influence PWD activity and thereby regulate the amount of C3 phosphate to control flux through the pathway. To test this, *pwd* mutants could be grown in different light intensities, to vary the starch content (“S”), but to keep the time remaining until dawn (“T”) constant. If PWD is required to integrate information about the starch content for the adjustment of starch degradation rates, then the *pwd* mutant should not be able to slow down or accelerate its starch degradation rate if starch contents vary.

To further investigate the role of C3 phosphorylation on the adjustment of starch degradation rates, starch contents of the *lsf2* mutant could be analysed. The LSF2 protein specifically removes C3 phosphate from starch granules, thus has elevated C3 starch phosphate (Santelia et al., 2011). It would be interesting to investigate if this mutant is able to adjust starch degradation rates in response to an early night. However, so far there are no indications that starch degradation is different from wild-type in *lsf2*, as the mutant has wild-type levels of starch at the end of the day and at the end of the night if grown in 12 hour light – 12 hour dark cycles (Santelia et al., 2011).

### ***7.3.3 Is BAM3 important for controlling starch degradation rates in response to an early night?***

Starch degradation in *bam3-1* did not slow down to wild-type level in the early night, although the mutant is retarded in starch breakdown in the normal night. This indicates that BAM3 might be a target of the pathway that controls starch degradation rates in response to starch content and time to dawn. However, the data should be reproduced to establish the role of BAM3 in the control of starch degradation rates. If the result can be confirmed, I speculate BAM3 is necessary to slow down starch degradation rates in response to variation of starch content or time until dawn. Starch degradation in the absence of BAM3 might be carried out by enzymes that cannot be regulated in the same way. In absence of BAM3, the granule might be attacked by BAM1 as the enzyme was shown to be required for starch degradation only in the absence of BAM3 (Fulton et al., 2008). It is possible that BAM1 cannot be regulated to adjust starch degradation rates in response to changes in day length, as BAM1 normally does not contribute to starch degradation at night.

It is interesting that starch degradation rates in *gwd* and *bam3* showed a similar response to the early night. Lack of PWD and BAM3 resulted in an inability to slow down starch degradation rates to wild-type level. This raises the possibility that both enzymes are part of the same mechanism. It is tempting to speculate that BAM3 is regulated by PWD-catalysed C3-phosphorylation of the starch granule. Beta-amylases cannot degrade past a phosphate group, thus, the presence of C3-phosphates might to some extent slow down the activity of BAM3. This could explain why *pwd* and *bam3* cannot slow down starch degradation rates in the early night. C3-phosphorylation might have a negative effect on BAM3 and slow down starch degradation if the night starts early.

#### ***7.3.4 Conclusions and Outlook***

The work presented here gives a first indication about the components which are involved in regulating starch degradation rates in response to time to dawn and starch content. Also, my work opens up several paths for future research as it remains to be established how starch phosphorylation affects starch degradation rates and which role BAM3 plays in the adjustment of starch degradation rates. Investigation of these questions will shed light on the nature of the mechanisms that link measurement of time to dawn and starch content to flux through starch degradation and could lead to the identification of the proposed S and T molecules.

## 8 General discussion

### 8.1 Summary

The aim of my work was to discover new components of the mechanism that controls starch degradation rates in *Arabidopsis*.

Using a forward genetic screen, I identified two mutants which are not able to adjust their starch degradation rates according to the length of the night. One mutant lacks the novel protein EST1. The second mutant produces aberrant BAM1. In an independent approach, I discovered that BAM3 and PWD could play a role in adjusting starch degradation rates in response to an unexpectedly early night. Also, I found further evidence for an involvement of the circadian clock in controlling starch degradation rates, as an *elf3* mutant degraded starch in a non-linear way and displayed starvation symptoms at the end of the night. Further, I could confirm that ISA1 activity and thus the ability to form semi-crystalline granules is essential for correct adjustment of starch degradation rates according to the length of the night.

In the following, I will summarise the results of my work, describe how these results shape our view about the control of starch degradation rates and suggest directions for future research.

### 8.2 Is EST1 a novel regulator of starch degradation rates?

I showed that EST1 protein is required to obtain normal starch degradation rates in *Arabidopsis* leaves. Plants lacking EST1 degrade starch faster than wild-type. In consequence, *est1* mutants run out of starch before the end of the night, when grown in 12 hour light – 12 hour dark cycles. The rate of starch degradation in *est1* mutants is not adjusted according to the length of the night and is such that about 11% of the EOD starch is degraded every hour of the night. This rate does not decrease if the night starts four hours earlier than normal. Since starch degradation rates are faster than wild-type in absence of EST1, EST1 could be a negative regulator of starch degradation rates. This is consistent with preliminary data showing that overexpression of EST1 results in a starch excess.

The mechanism of action of EST1 remains unclear. To explain faster starch degradation rates in the mutant I hypothesised that (a) EST1 is necessary to form normal starch granules or (b) EST1 is a negative regulator of enzymes that act on starch. To test the first hypothesis, I analysed appearance, structure and composition of starch granules in the mutant. I did not find evidence for alterations in any of the properties tested, apart from elevated amylose contents. These, however, are not the reason for faster starch degradation in the mutant as abolishing amylose biosynthesis in the *est1* background did not prevent faster starch degradation. Therefore, EST1 is likely to be a negative regulator of enzymes that degrade starch, e.g. by inhibiting the function of (an) enzyme(s) that degrades starch. In absence of EST1, the target enzyme(s) would be more active than in a wild-type plant. It is also possible that EST1 inhibits an enzyme that normally does not contribute to degradation of transitory starch like AMY3 or BAM1. Loss of EST1 would result in activation of a normally inactive enzyme, hence faster starch degradation.

To test hypothesis (b) and to place EST1 in the pathway of starch degradation, I generated double mutants that lack EST1 as well as other components of the pathway. Preliminary analysis of starch contents in these lines indicated that neither AMY3 nor BAM1 are required for faster starch degradation in *est1*. Thus, it is not likely that absence of EST1 results in faster starch degradation due to increased BAM1 or AMY3 activity. Crossing *est1* into several *sex* mutants (*sex1*, *bam3*, *bam4*, *sex4*) did not rescue the starch excess phenotype observed in single mutants. This shows that starch phosphorylation and dephosphorylation by GWD and SEX4 are still required for faster starch degradation in *est1*. It also shows that starch degradation in absence of EST1 is still dependent on the activity of BAM3 and presence of BAM4. The generation of further double mutants and the quantification of starch contents in them might give further insights into the function of EST1 and its position in the pathway.

EST1 is necessary for normal rates of starch degradation of transitory starch. It is also likely that EST1 influences degradation of starch in heterotrophic tissue. This is indicated by a lack of starch in veins of *est1* mutant plants. Thus, EST1 could inhibit starch degradation as a part of the pathway which is common in heterotrophic tissue and photosynthetic tissue. Also, EST1 was found to be associated with starch granules of many plant species and was not only found in leaves of *Arabidopsis*, but also in potato

tubers and cereal endosperm. This indicates that EST1 might regulate starch breakdown during sprouting, germination or other developmental processes. Analysis of *est1* mutants of other plant species could help to understand the role of EST1 in metabolism of storage starch

It is also a possibility that EST1 controls starch degradation rates in response to biotic or abiotic stress. Starch degradation in *est1* mutants is very fast, thus, a pathway that triggers starch degradation in response to stress could be activated by down-regulation of EST1 activity or by targeting it for degradation. The pathway that triggers starch degradation in response to stress is not completely understood. BAM1 protein seems to play a role in degrading leaf starch in response to osmotic stress or heat stress in *Arabidopsis* (Valerio et al., 2011; Kaplan and Guy, 2004). BAM3 seems to be involved in starch degradation that produces maltose accumulation in response to cold stress (Kaplan and Guy, 2005), and PHS1 has been suggested to be involved in starch turnover in stress conditions (Zeeman et al., 2004b).

Faster starch degradation rates in EST1 could also mean that the mutant is “overestimating” its starch content. This would happen if, for example, EST1 is a target of the mechanism that estimates the starch content. Scialdone et al. (2013) proposed that information about starch contents may be encoded in the concentration of phosphate residues added to the granule. EST1 could have a role in regulating the number of phosphate groups added to the granule by GWD or PWD. In absence of EST1, the starch granule might be hyper-phosphorylated and therefore more accessible for starch degrading enzymes.

However, so far there is no strong evidence that EST1 exercises a function in controlling starch degradation rates in a wild-type plant. It is required to obtain normal rates of starch degradation, but might not be part of the mechanisms that adjust the starch degradation rate in response to starch content or time remaining until dawn. Nonetheless, the discovery of EST1 shows that our understanding of starch degradation is incomplete, and opens up the possibility that there are further, yet unknown, components of the starch degradation pathway which are involved in controlling starch degradation rates.

### 8.3 Is regulation of BAM1 activity a means of controlling transitory starch degradation?

My work suggests that modulation of BAM1 activity can have an effect on the control of starch degradation rates of transitory starch. The EMS mutant I identified in the screen carries a dominant mutation in *BAM1* which results in a serine to asparagine amino acid substitution in the protein. In the mutant, starch is degraded too fast. The rate of starch degradation is not adjusted according to the length of the night. Starch is degraded at a rate of about 10% of end-of-day starch per hour of darkness, even if the night starts unexpectedly early.

The mechanism by which starch was degraded faster in the mutant is still unknown therefore it is not possible to draw final conclusions about the involvement of BAM1 in controlling starch degradation rates. However, the results presented in my work indicate that BAM1 protein is not required for adjusting starch degradation rates according to the length of the night, as the knock-out mutant degraded starch normally. In the literature, there is mounting evidence that BAM1 is involved in response of plants to abiotic stress (Valerio et al., 2011; Kaplan and Guy, 2004). Therefore, I suggest that faster starch degradation rates in *bam1-2* are the result of an activated stress response pathway. The amino acid substitution might activate BAM1 in a way that would normally happen in response to abiotic stress, e.g. by phosphorylation or dephosphorylation of the protein or by mediating its interaction with other proteins like LSF1.

It is interesting that starch degradation rates in *bam1-2* and *est1* are very similar. This could indicate a mechanistic link between BAM1 and EST1. This link might be a starch degradation pathway that is activated in response to stress. However, it is too early to speculate about a mechanism that links both proteins and further work is needed to understand the reason for faster starch degradation in *bam1-2*.

Analysis of the *in vitro* activity of the protein and of the starch contents in transgenic lines containing mutant BAM1 protein in which Ser-132 is substituted with other amino acids, as well as the analysis of the starch contents in double mutants lacking components of the starch degradation pathway in the *bam1-2* background, could help to understand the mechanism by which presence of BAM1 (S132N) has such a dramatic effect on starch degradation rates. These experiments might help to understand post-

translational mechanisms that regulate BAM1 activity. Knowledge about such mechanisms might allow conclusion to be drawn about the regulation of BAM3 activity and thus advance our knowledge about the control of degradation rates of transitory starch.

#### **8.4 Is C3 phosphorylation the mechanism by which starch degradation rates are adjusted according to night length and starch content?**

I showed that the *pwd* mutant does not slow down its starch degradation rate to the same extent as wild-type plants when the night starts unexpectedly early. Therefore, phosphorylation of glucose residues within amylopectin molecules at the C3 position, which is catalysed by PWD, might be the point at which information about starch content or time until dawn is feeding into the control of starch degradation rates. It is possible that information about starch contents is encoded in phosphorylation of the granule.

Further experiments will be required to test this hypothesis. If the amount of C3 phosphate regulates starch degradation rates, adjustment of starch degradation rates in the *lsf2* mutant should also be abnormal in response to an early night, as the mutant has elevated C3-phosphate (Santelia et al., 2011).

I showed that lack of BAM3 impairs the plant's ability to slow down starch degradation rates in response to an early night, in a similar way to lack of PWD. The data I showed are preliminary; however, they open up the possibility that regulation of BAM3 activity is needed to adjust starch degradation rates according to the length of the night. Since *pwd* and *bam3* had a similar starch degradation phenotype, they might be affected in the same process. It is possible that C3-phosphorylation regulates BAM3 activity to adjust starch degradation rates in relation to the starch content.

Further experiments will be required to test this hypothesis and to discover post-translational mechanisms that might regulate BAM3 activity.

### 8.5 Further evidence for an involvement of the circadian clock in adjusting starch degradation rates

The mechanism that links the circadian clock and the adjustment of starch degradation rates still needs to be discovered. I found further evidence for an involvement of the circadian clock in controlling starch degradation rates, as a mutant lacking the circadian clock component *ELF3* did not adjust its starch degradation rate according to the length of the night and displayed starvation symptoms at the end of the early night (**Chapter 3**). The mutant (357-1) degraded starch at a similar rate to wild-type for the first part of the night, but slowed down starch degradation about four hours before the end of the night.

The only circadian clock mutant which was also shown to have a starch degradation phenotype is *cca1 lhy*. This mutant is unable to adjust its starch degradation rate according to the length of the night (Graf et al., 2010; Scialdone et al., 2013; **Chapter 1**). *CCA1* and *LHY* are morning expressed genes of the circadian clock that repress the expression of evening expressed genes (Nagel and Kay, 2012). The *cca1 lhy* double mutant has a shorter circadian clock period and anticipates dawn four hours too early. Therefore, it exhausts its starch four hours before the end of the night, which corresponds the time of dawn anticipated by the mutant (Graf et al., 2010; Scialdone et al., 2013).

The starch degradation pattern in mutant 357-1 was different from that of *cca1 lhy*, probably because *ELF3* encodes a functionally different component of the circadian clock. *ELF3* is an evening expressed gene, and the *ELF3* protein is part of the evening complex, which regulates the expression of other circadian clock components and suppresses hypocotyl growth at the beginning of the night (Nusinow et al., 2011; **Chapter 1, 3**) The *elf3* mutant has an arrhythmic circadian clock in constant light (Covington et al., 2001). Therefore, it might not be able to anticipate dawn correctly. In consequence it might not estimate the right time until dawn and therefore degrade starch at an inappropriate rate. Thus, the mutant might be affected in the timing mechanism that regulates starch breakdown. It is also possible that the starch degradation phenotype of the mutant could be related to *ELF3*'s role in the regulation of growth (Yazdanbakhsh et al., 2011; **Chapter 3**).

Further circadian clock mutants could be analysed for their ability to adjust starch degradation rates in response to an early night to identify which clock components are necessary for the adjustment of starch degradation rates.

### **8.6 The formation of starch granules is important for the adjustment of starch degradation rates according to night length**

The forward genetic screen identified a high proportion of mutants affected in *ISA1* or *ISA2*. These mutants showed starvation symptoms at the end of the night, probably because they exhausted their leaf carbohydrate reserves before the end of the night. The mutants have a reduced ability to form starch granules and mainly accumulate soluble phytyglycogen. It was already known that phytyglycogen is degraded faster than starch, usually after eight hours of darkness, if plants are grown in 12 hour light – 12 hour dark cycles (Zeeman et al., 1998a; Delatte et al., 2005; Streb et al., 2008). This illustrates that the formation of a starch granule is required to adjust starch degradation rates according to the length of the night. I found indications that phosphorylation of the starch granule may be the point at which the rate of starch degradation can be adjusted according to starch content and time until dawn. If phytyglycogen degradation is independent of phosphorylation, this might explain why formation of starch granules is necessary to adjust starch degradation rates according to the length of the night. To test this, it would be interesting to find out if degradation of phytyglycogen is dependent on phosphorylation by GWD or PWD.

### **8.7 Model of the control of starch degradation rates based on the presented data**

I summarised the results of my work in a model presented in **Figure 8.1**. The model is very preliminary, but shows the interaction of proteins which could be involved in controlling starch degradation rates. I showed that mutants affected in some of these proteins were impaired in the ability to adjust starch degradation rates according to the length of the night. The interaction of these proteins seems to be complex and more work will be required to identify the mechanisms that link them.

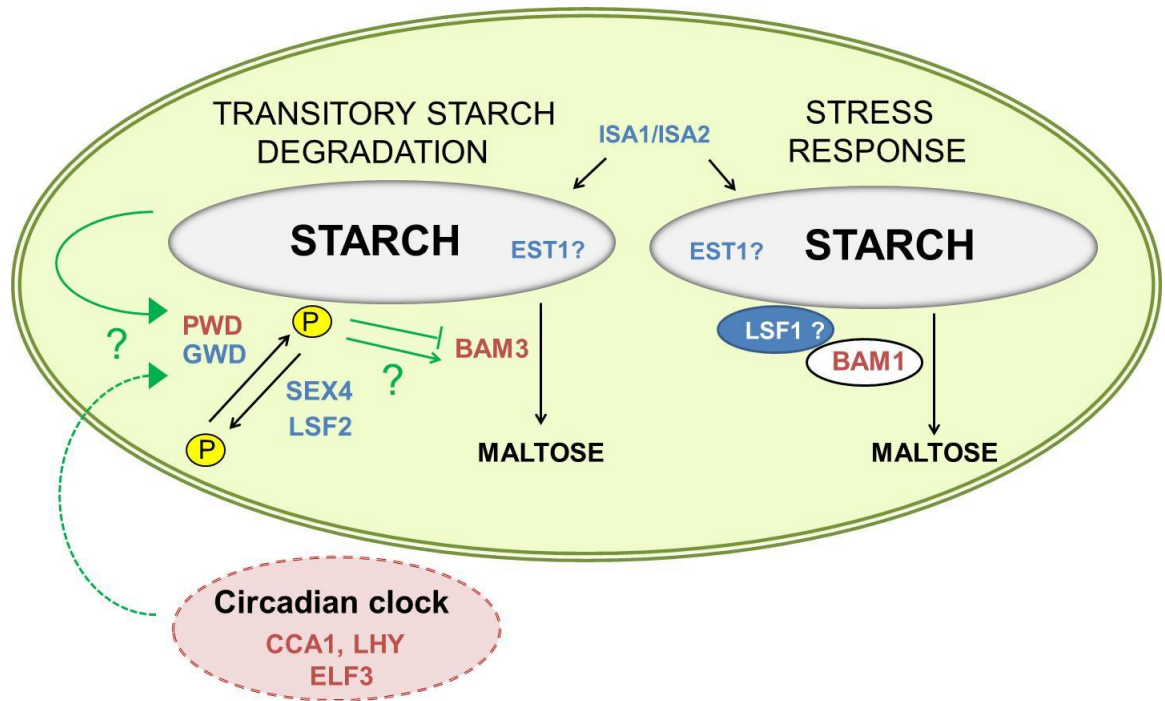


**Figure 8.1: A model illustrating the interplay between proteins shown to be involved in controlling starch degradation rates.** Based on the data presented in this work it is likely that the proteins highlighted in red play a role in the control of starch degradation rates either in transitory starch degradation or in response to abiotic stress. ISA1 and ISA2 are necessary to form normal starch granules, which prevents uncontrolled degradation, possibly by introducing the requirement of starch phosphorylation for breakdown of starch. GWD and PWD phosphorylate the starch granule and LSF2 and SEX4 remove the phosphates. Phosphorylation by PWD might regulate activity of BAM3 to adjust starch degradation rates. The mechanisms that link information about starch content and time remaining until dawn to adjust the appropriate starch degradation rate are still unknown. However, it is possible that starch phosphorylation and dephosphorylation play a role in encoding information about starch content. Fast starch degradation in response to abiotic stress might involve the proteins BAM1 and LSF1. EST1 protein is required for normal starch degradation, but its role is still unknown.

## 8.8 Outlook

My work and the work of our colleagues opened up several directions for future research that could help to understand the control of starch degradation rates. How starch phosphorylation affects starch degradation rates will be an important question to answer. It is possible that information about the starch content is encoded by phosphorylation of the granule. However, it is still not known how the circadian clock is linked to starch degradation and if phosphorylation/dephosphorylation also play a role in that mechanism.

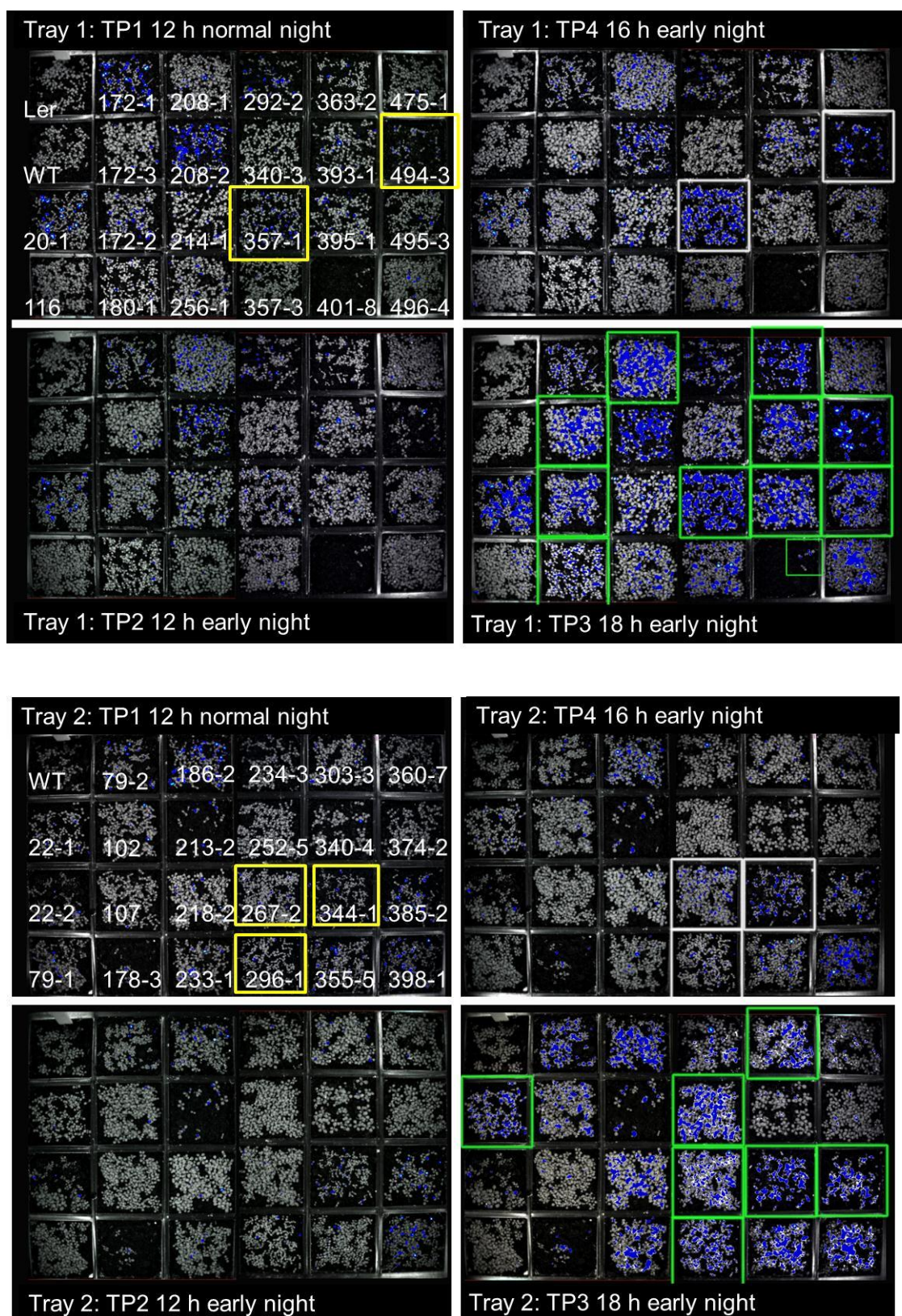
Scialdone et al. (2013) propose that hypothetical molecules S and T convey information about starch content and time to dawn and allow modulation of the starch degradation process. It may be possible to develop new mutant screens or to modify the existing screen to identify the proteins and functions that S and T represent and their targets in the pathway of starch degradation.

The *Arabidopsis* starvation reporter line that I used in the forward genetic screen could be used to identify further mutants affected in control of starch degradation rates. So far, only one third of the total mutant population was screened, thus it might be possible to identify further interesting mutants. It would be profitable to identify mutants with less severe starch degradation phenotypes than *est1* or *bam1-2*, for example mutants that have non-linear starch degradation rates, but do not exhaust their reserves before the end of the night. It is likely that more than one gene is involved in controlling starch degradation rates and that mutations affecting these components do not result in severe starch degradation phenotypes. I identified several mutants with a mild starch degradation phenotype that have non-linear starch degradation rates (**Chapter 3**). Identification of the underlying mutations could be a starting point to find new genes involved in the process underlying the control of starch degradation. Identification of these genes could e.g. help to identify signalling pathways that link the circadian clock and the control of starch degradation rates.

A further important problem is the role of BAM4 and LSF1 in the pathway of starch degradation. It is likely that these proteins have a regulatory function as they showed no catalytic activity (Fulton et al., 2008; Comparot-Moss et al., 2010). The interaction of LSF1 and BAM1 indicates that complex formation between enzymes of the pathway

might be important for the control starch degradation rates. The identification of interaction partners of proteins in the pathway might give new insights into this possibility.

## Appendix

Figure A1: Re-screen of M<sub>3</sub> lines by bioluminescence analysis.

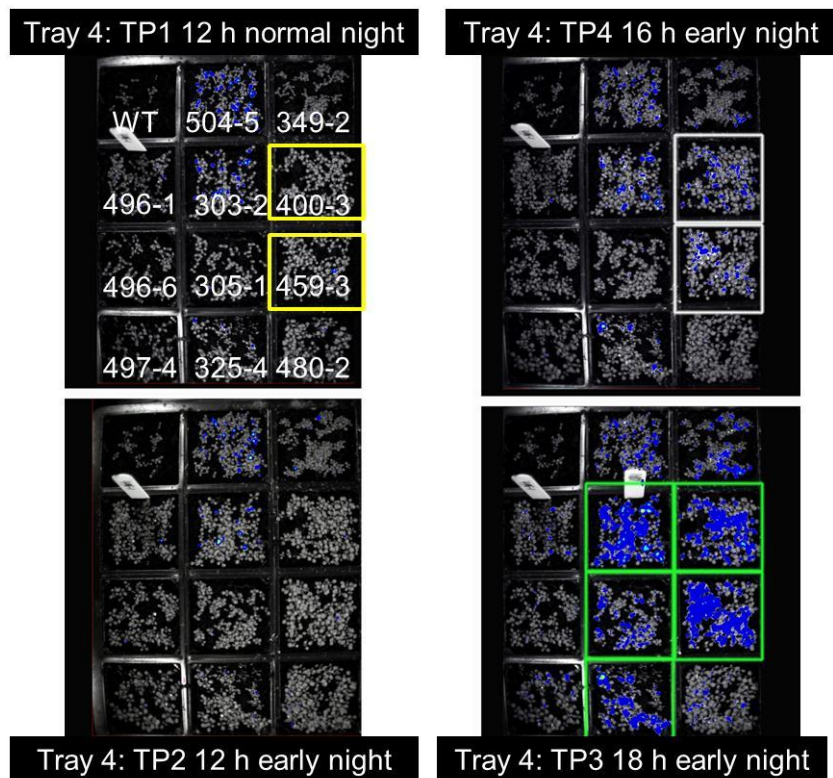
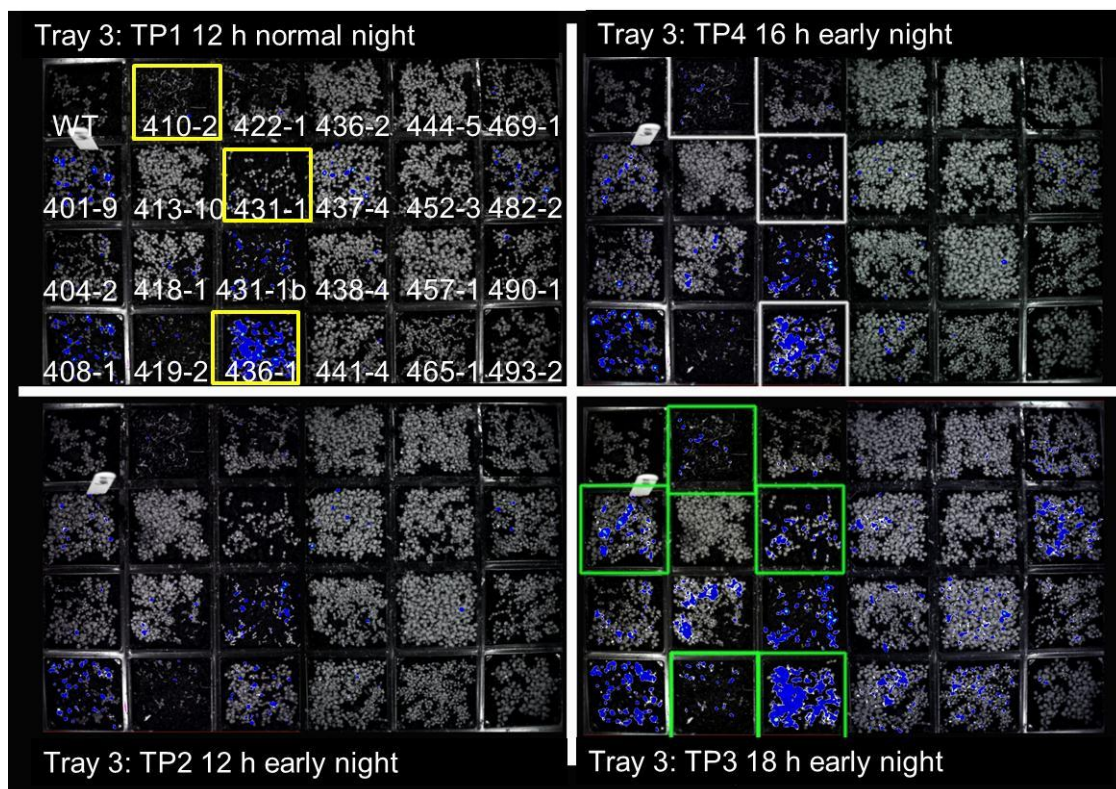


**Figure A1: Re-screen of M<sub>3</sub> lines by bioluminescence analysis.**

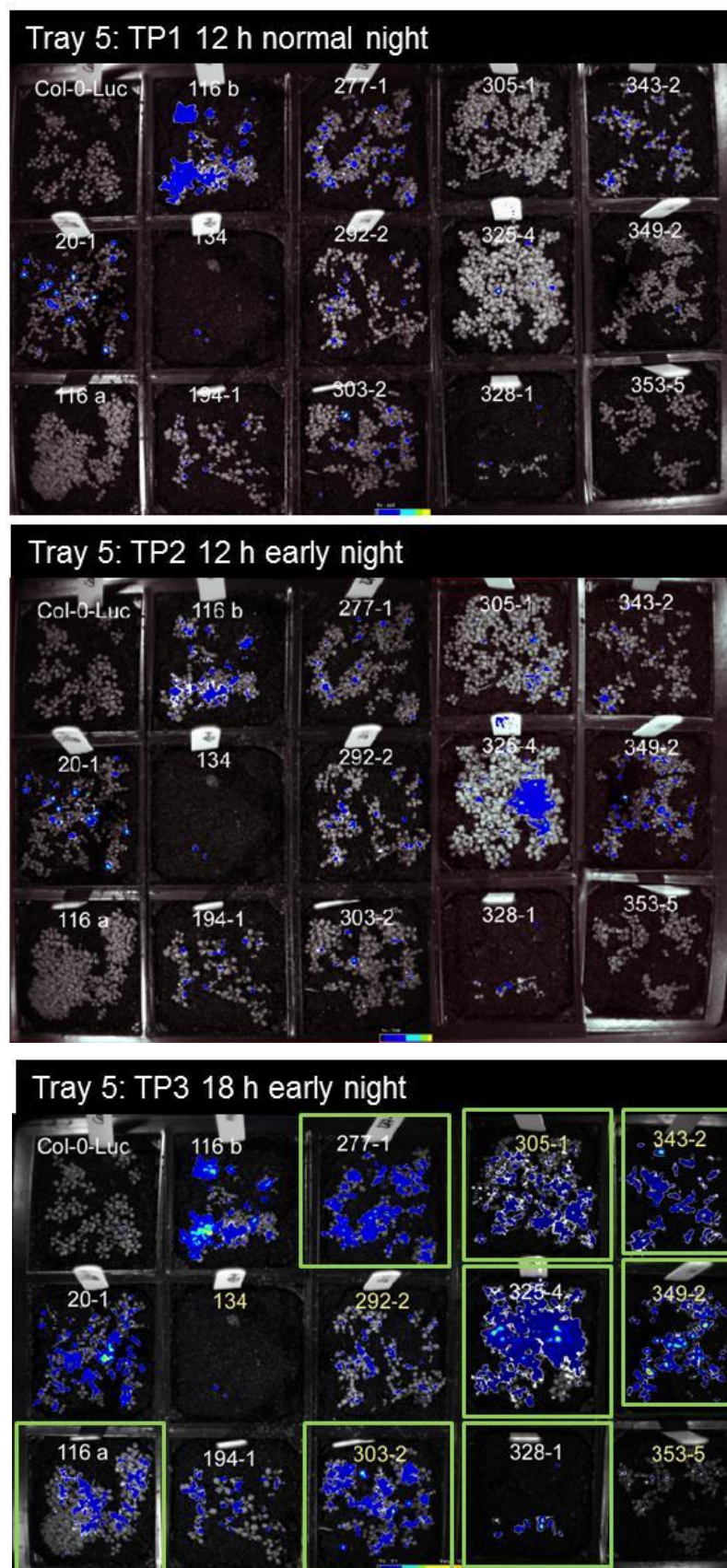
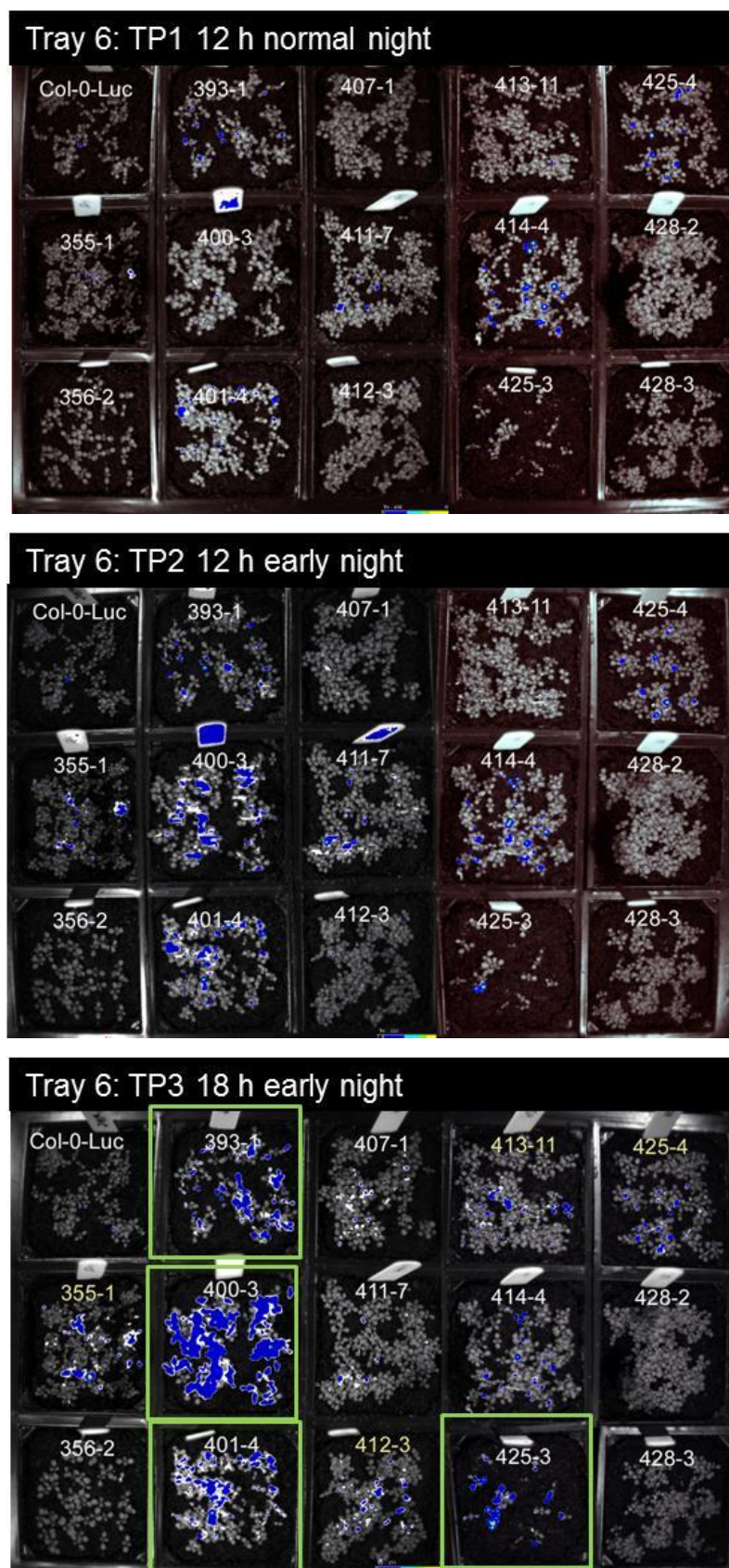


Figure A1: Re-screen of  $M_3$  lines by bioluminescence analysis



**Figure A1: Re-screen of M<sub>3</sub> lines by bioluminescence analysis.**

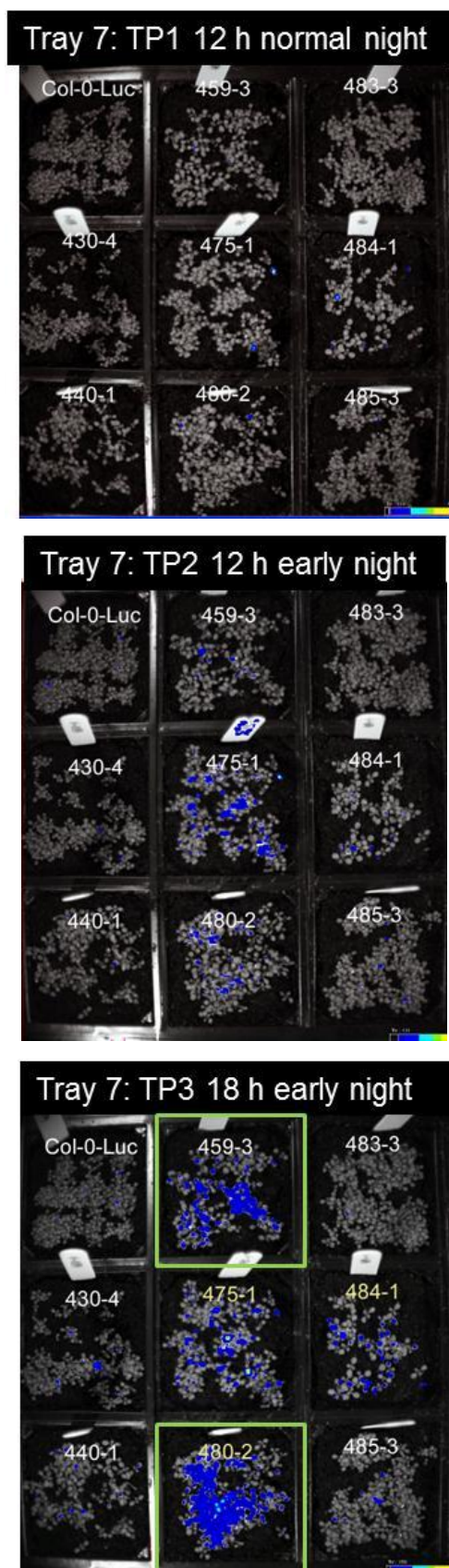
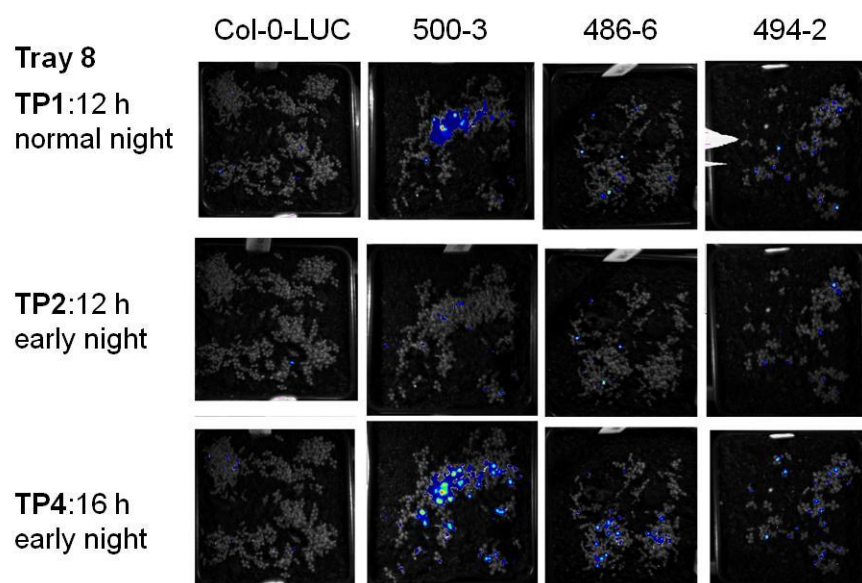


Figure A1: Re-screen of M<sub>3</sub> lines by bioluminescence analysis.



**Figure A1: Re-screen of M<sub>3</sub> lines by bioluminescence analysis.** Bioluminescence of 10 day old seedlings grown in 12 hour light – 12 hour dark cycles was detected and visualised in blue colour using the NightOwl camera system and Winlight software. Pictures were taken at three or four time points (TP): at (TP1) the end of the normal 12 hour night, (TP2) after 12 hours of an early night, (TP3) after 18 hours of an early night and (TP4) after 16 hours of the early night. Tray number and time point are indicated in the picture as well as the number of each mutant line. The starvation reporter line was used as control (Col-0-LUC). The ten mutant lines with the strongest early starvation phenotype (signals at TP4) are highlighted with a yellow box. Mutants with a weaker early starvation phenotype (signal at TP3) are surrounded by a green box.

No.	Line	TP4	TP3	No.	Line	TP4	TP3
1	20-1			53	395-1		Yes
2	102			54	398-1		
3	107			55	400-3	Yes	Yes
4	116a		Yes	56	401-4		
5	116b			57	401-8		Yes
6	22-1		Yes	58	401-9		Yes
7	22-2			59	404-2		
8	79-1			60	407-1		
9	79-2			61	408-1		
10	172-1			62	410-2	Yes	Yes
11	172-2		Yes	63	411-7		
12	172-3		Yes	64	412-3		
13	178-3			65	413-10		
14	180-1		Yes	66	414-4		
15	186-2			67	418-1		
16	194-1			68	419-2		Yes
17	196-6			69	422-1		
18	208-1		Yes	70	425-3		
19	208-2			71	425-4		
20	213-2			72	428-2		
21	214-1			73	428-3		
22	218-2			74	430-4		
23	233-1			75	440-1		
24	234-3			76	431-1	Yes	Yes
25	252-5		Yes	77	436-1	Yes	Yes
26	256-1			78	436-2		
27	267-2	Yes	Yes	79	437-4		
28	277-1			80	438-4		
29	292-2			81	441-4		
30	296-1	Yes	Yes	82	444-5		
31	303-2		Yes	83	452-3		
32	303-3		Yes	84	457-1		
33	305-1		Yes	85	459-3	Yes	Yes
34	325-4		Yes	86	465-1		
35	328-1			87	469-1		
36	340-3			88	475-1		
37	343-2			89	480-2		
38	240-4			90	482-2		
39	277-1		Yes	91	483-3		
40	344-1	Yes	Yes	92	485-3		
41	349-2		Yes	93	486-6		
42	353-5			94	490-1		
43	355-1			95	493-2		
44	355-5			96	494-2		
45	356-2			97	494-3	Yes	Yes
46	357-1	Yes	Yes	98	495-3		Yes
47	357-3			99	496-1		
48	360-7			100	496-4		
49	363-2		Yes	101	497-4		
50	374-2			102	500-3		
51	385-2		Yes	103	504-5		
52	393-1		Yes				

Table A1: Summary of results from re-screen of M<sub>3</sub> mutant lines.

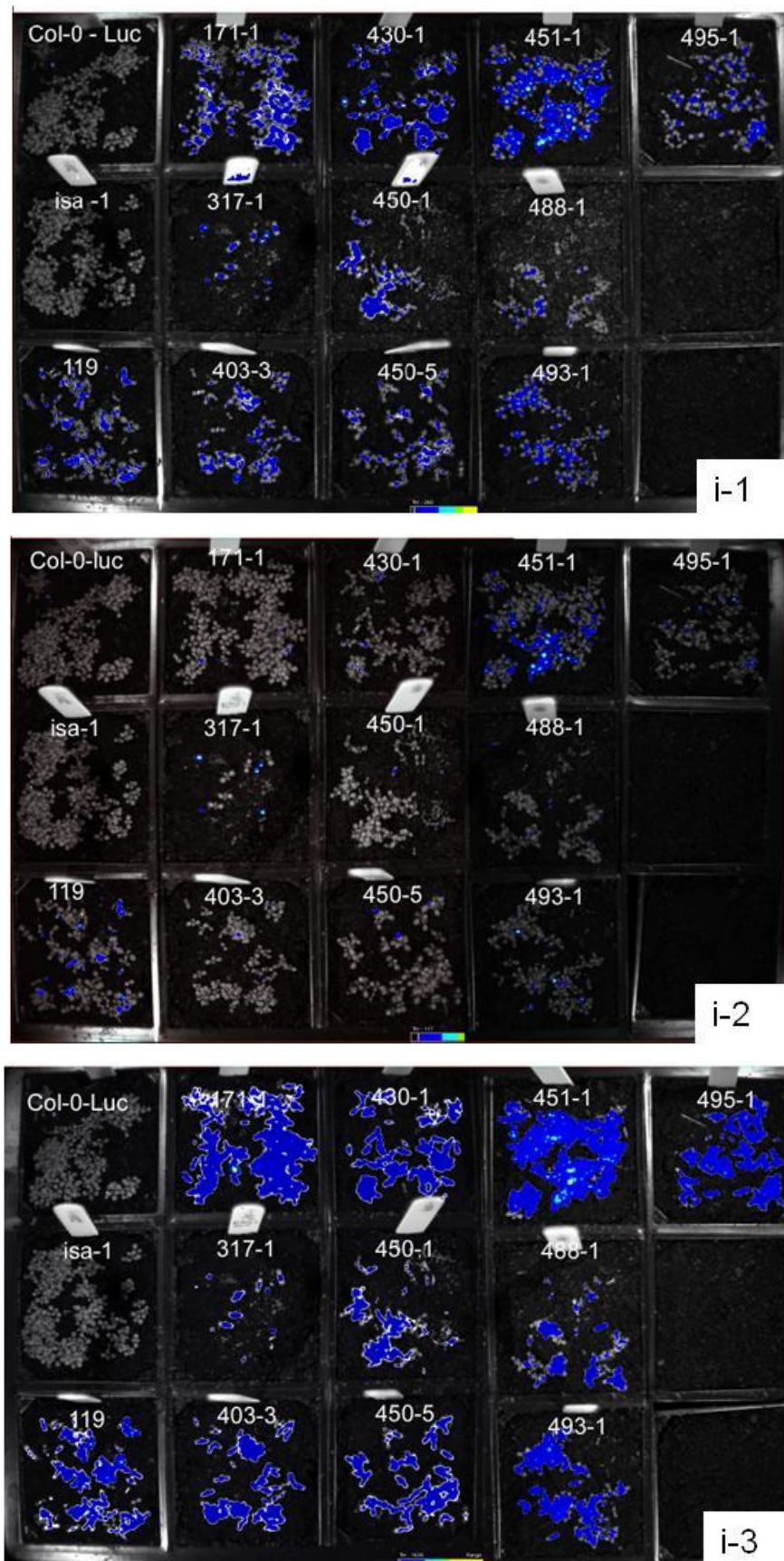


**Figure A2: Re-screen of 11 “*isa*-like mutants”.** Shown are NightOwl pictures from one tray (i) at three time points as explained in **Figure A1**.

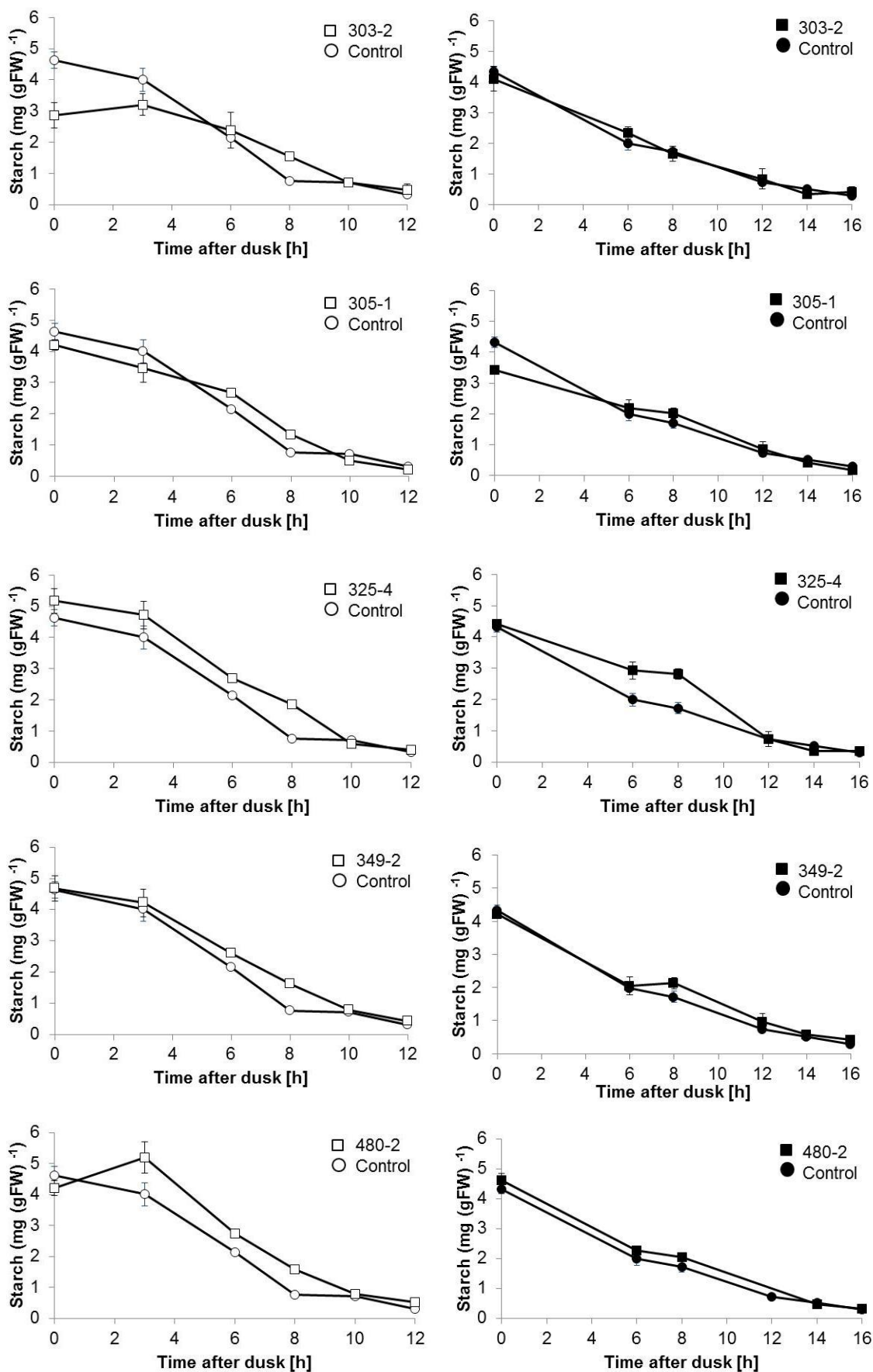


**Figure A3: Starch contents of four mutants with weak early starvation phenotype.**

**Figure A3: Starch contents of four mutants with weak early starvation phenotype.**

The plants were grown for 28 days in 12 hour light – 12 hour dark cycles and harvested during a normal night (left) and an early night (right). The starch contents shown are means of five biological replicates, the standard errors are s.e.m. Where not visible they are smaller than the symbol. Control plants are plants from the starvation reporter line.

```

BAM1AT      MALNLSHQGLVLAGTPIKSGEMTDSSLLSISPPSARMMTPKAMNRRNYKAHGTDPSPPMSP
BMY1GM      -----

BAM1AT      ILGATRADLSVACKAFVENIGIGTIEEQRTYREGGIGGKKEGGGVVVFVMMPLDSVTMG
BMY1GM      -----MATSDSNMLLNYPVYVMLPLGVVNV
                                     *** ** * *

BAM1AT      NTVNRRKAMKASLQALKSAGVEGIMIDVWWGLVEKESPGTYNWGGYNELLELAKKLGLKV
BMY1GM      NVFEDPDGLKEQLLQLRAAGVDGVMVDVWWGI IELKGPQYDWRAYRSLFQLVQECGLTL
*           * * * * * * * * * * * * * * * * * * * * * * * * * *

BAM1AT      QAVMSFHQCGGNVGDVSVTIPLPQWVVEVDKDPDLAYTDQWGRRNHEYISLGADTLPLVK
BMY1GM      QAIMSFHQCGGNVGDIVNIPPIQWVLDIGESNHDI FYTNRSGTRNKEYLTVGVDNEPIFH
** * * * * * * * * * * * * * * * * * * * * * * * * * *

BAM1AT      GRTPVQCYADFMRAFRDNFKHLLG-ETIVEIQVGMGPAGELRYPSPYEQEGTWKFPGIGA
BMY1GM      GRTAIEIYSDYMKSFRENMSDFLESGLIIDIEVGLGPAGELRYPSPYQSQ-GWEFFPGIGE
*** * * * * * * * * * * * * * * * * * * * * * * * * * *

BAM1AT      FQCYDKYSLSSLKAAAETYGKPEWGSTGPTDAGHYNNWPEDTQFFKKEGGWNSEYGDFF
BMY1GM      FQCYDKYLKADFKAARAGHPEWEL--PDDAGKYNDVPESTGFFKSN-GTYVTEKGKFF
***** * * * * * * * * * * * * * * * * * * * * * * * * * *

BAM1AT      LSWYSQMLLDHGERILSSAKSIFENMGVKISVKIAGIHWHYGTRSHAPELTAGYYNTRFR
BMY1GM      LTWYSNKLLNHGDQILDEANKAFLGCKVKLAIKVSGIHWYKVENHAAELTAGYYNLNDR
* * * * * * * * * * * * * * * * * * * * * * * * * * * * * *

BAM1AT      DGYLPQAQMLARHNAIFNFTCIEMRDHEQPQDALCAPEKLVNQVALATLAAEVLPLAGENA
BMY1GM      DGYRPIARMLSRHHAILNFTCLEMRDSEQPSDAKSGPQELVQQLVSGGWREDIRVAGENA
*** * * * * * * * * * * * * * * * * * * * * * * * * * *

BAM1AT      LPRYDDYAHEQILKASALNLDQNNEGEPREMCFTYLRMNPQLFQADNWGKFVAVVKKMG
BMY1GM      LPRYDATAYNQIILNARPQGVNNGPPKLSMFGVTYLRSLDQLQKSNFNIFKKFVLKMH
***** * * * * * * * * * * * * * * * * * * * * * * * * * *

BAM1AT      EGRDSHRCREEVEREAHFVHVVTQPLVQEAVAL-----TH-----
BMY1GM      ADQDYCANPQ-----KYNHAI TPLKPSAPKIP I EVLLEATKPTL PFPWLPETDMKVDG
                                     ** * *

```

**Figure A4: Alignment of soybean beta-amylase and *Arabidopsis* BAM1 protein sequences.** Proteins were aligned using ClustalW. Asterisks indicate amino acids which are conserved in both proteins. The positions of the cysteine residues (Cys-32 and Cys-470) that form a disulphide bridge in *Arabidopsis* BAM1 (BAM1AT) are indicated in green. Cys-470 is substituted with F-415 in the soybean enzyme (BMY1GM, GenBankID: BAD93291.1). The position of Ser-132, which is mutated in *bam1-2* is indicated in yellow.

---

**Bibliography**

**Agosti, R. D., L. Jouve and H. Greppin** (1997). "Computer-assisted measurements of plant growth with linear variable differential transformer (LVDT) sensors." *Archives Des Sciences* 50(3): 233-244.

**Alabadi, D., T. Oyama, M. J. Yanovsky, F. G. Harmon, P. Mas and S. A. Kay** (2001). "Reciprocal regulation between TOC1 and LHY/CCA1 within the *Arabidopsis* circadian clock." *Science* 293(5531): 880-883.

**Andriotis, V. M. E., M. J. Pike, B. Kular, S. Rawsthorne and A. M. Smith** (2010). "Starch turnover in developing oilseed embryos." *New Phytologist* 187(3): 791-804.

**Ashelford, K., M. E. Eriksson, C. M. Allen, R. D'Amore, M. Johansson, P. Gould, S. Kay, A. J. Millar, N. Hall and A. Hall** (2011). "Full genome re-sequencing reveals a novel circadian clock mutation in *Arabidopsis*." *Genome Biology* 12(3).

**Baunsgaard, L., H. Lutken, R. Mikkelsen, M. A. Glaring, T. T. Pham and A. Blennow** (2005). "A novel isoform of glucan, water dikinase phosphorylates pre-phosphorylated alpha-glucans and is involved in starch degradation in *Arabidopsis*." *Plant Journal* 41(4): 595-605.

**Bayer, R. G., S. Stael, E. Csaszar and M. Teige** (2011). "Mining the soluble chloroplast proteome by affinity chromatography." *Proteomics* 11(7): 1287-1299.

**Bell-Pedersen, D., V. M. Cassone, D. J. Earnest, S. S. Golden, P. E. Hardin, T. L. Thomas and M. J. Zoran** (2005). "Circadian rhythms from multiple oscillators: Lessons from diverse organisms." *Nature Reviews Genetics* 6(7): 544-556.

**Bernard, P., P. Gabant, E. M. Bahassi and M. Couturier** (1994). "Positive-selection vectors using the F-plasmid Ccdb killer gene." *Gene* 148(1): 71-74.

**Buléon, A., P. Colonna, V. Planchot and S. Ball** (1998). "Starch granules: structure and biosynthesis." *International Journal of Biological Macromolecules* 23(2): 85-112.

**Blasing, O. E., Y. Gibon, M. Gunther, M. Hohne, R. Morcuende, D. Osuna, O. Thimm, B. Usadel, W. R. Scheible and M. Stitt** (2005). "Sugars and circadian regulation make major contributions to the global regulation of diurnal gene expression in *Arabidopsis*." *Plant Cell* 17(12): 3257-3281.

**Blennow, A. and S. B. Engelsen** (2010). "Helix-breaking news: fighting crystalline starch energy deposits in the cell." *Trends in Plant Science* 15(4): 236-240.

**Brown, J. W., P. Smith and C. G. Simpson** (1996). "*Arabidopsis* consensus intron sequences." *Plant Mol Biol* 32(3): 531-535.

**Caspar, T., S. C. Huber and C. Somerville** (1985). "Alterations in growth, photosynthesis, and respiration in a starchless mutant of *Arabidopsis thaliana* (L) deficient in chloroplast phosphoglucomutase activity." *Plant Physiology* 79(1): 11-17.

**Caspar, T., T. P. Lin, G. Kakefuda, L. Benbow, J. Preiss and C. Somerville** (1991). "Mutants of *Arabidopsis* with altered regulation of starch degradation." *Plant Physiology* 95(4): 1181-1188.

**Caspar, T., T. P. Lin, J. Monroe, W. Bernhard, S. Spilatro, J. Preiss and C. Somerville** (1989). "Altered regulation of beta-amylase activity in mutants of *Arabidopsis* with lesions in starch metabolism." *Proceedings of the National Academy of Sciences of the United States of America* 86(15): 5830-5833.

**Chia, T., D. Thorneycroft, A. Chapple, G. Messerli, J. Chen, S. C. Zeeman, S. M. Smith and A. M. Smith** (2004). "A cytosolic glucosyltransferase is required for conversion of starch to sucrose in *Arabidopsis* leaves at night." *Plant Journal* 37(6): 853-863.

**Cho, M. H., H. Lim, D. H. Shin, J. S. Jeon, S. H. Bhoo, Y. I. Park and T. R. Hahn** (2011). "Role of the plastidic glucose translocator in the export of starch degradation products from the chloroplasts in *Arabidopsis thaliana*." *New Phytologist* 190(1): 101-112.

**Chow, B. Y., A. Helfer, D. A. Nusinow and S. A. Kay** (2012). "ELF3 recruitment to the *PRR9* promoter requires other Evening Complex members in the *Arabidopsis* circadian clock." *Plant Signal Behav* 7(2): 170-173.

**Christiansen, C., M. Abou Hachem, S. Janecek, A. Vikso-Nielsen, A. Blennow and B. Svensson** (2009). "The carbohydrate-binding module family 20-diversity, structure, and function." *Febs Journal* 276(18): 5006-5029.

**Comparot-Moss, S., O. Kotting, M. Stettler, C. Edner, A. Graf, S. E. Weise, S. Streb, W. L. Lue, D. MacLean, S. Mahlow, G. Ritte, M. Steup, J. Chen, S. C. Zeeman and A. M. Smith** (2010). "A putative phosphatase, LSF1, is required for normal starch turnover in *Arabidopsis* leaves." *Plant Physiol* 152(2): 685-697.

**Corbesier, L., P. Lejeune and G. Bernier** (1998). "The role of carbohydrates in the induction of flowering in *Arabidopsis thaliana*: comparison between the wild type and a starchless mutant." *Planta* 206(1): 131-137.

**Cortese, M. S., V. N. Uversky and A. K. Dunker** (2008). "Intrinsic disorder in scaffold proteins: Getting more from less." *Progress in Biophysics and Molecular Biology* 98(1): 85-106.

**Covington, M. F., S. Panda, X. L. Liu, C. A. Strayer, D. R. Wagner and S. A. Kay** (2001). "ELF3 modulates resetting of the circadian clock in *Arabidopsis*." *Plant Cell* 13(6): 1305-1315.

**Critchley, J. H., S. C. Zeeman, T. Takaha, A. M. Smith and S. M. Smith** (2001). "A critical role for disproportionating enzyme in starch breakdown is revealed by a knock-out mutation in *Arabidopsis*." *Plant Journal* 26(1): 89-100.

**Crumpton-Taylor, M., S. Grandison, K. M. Y. Png, A. J. Bushby and A. M. Smith** (2012). "Control of starch granule numbers in *Arabidopsis* chloroplasts." *Plant Physiology* 158(2): 905-916.

**Delatte, T., M. Trevisan, M. L. Parker and S. C. Zeeman** (2005). "*Arabidopsis* mutants *Atisa1* and *Atisa2* have identical phenotypes and lack the same multimeric isoamylase, which influences the branch point distribution of amylopectin during starch synthesis." *Plant Journal* 41(6): 815-830.

**Delatte, T., M. Umhang, M. Trevisan, S. Eicke, D. Thorneycroft, S. M. Smith and S. C. Zeeman** (2006). "Evidence for distinct mechanisms of starch granule breakdown in plants." *Journal of Biological Chemistry* 281(17): 12050-12059.

**Denyer, K., P. Johnson, S. Zeeman and A. M. Smith** (2001). "The control of amylose synthesis." *Journal of Plant Physiology* 158(4): 479-487.

**Denyer, K., D. Waite, S. Motawia, B. L. Moller and A. M. Smith** (1999). "Granule-bound starch synthase I in isolated starch granules elongates malto-oligosaccharides processively." *Biochemical Journal* 340: 183-191.

**Dixon, L. E., K. Knox, L. Kozma-Bognar, M. M. Southern, A. Pokhilko and A. J. Millar** (2011). "Temporal repression of core circadian genes is mediated through EARLY FLOWERING 3 in *Arabidopsis*." *Current Biology* 21(2): 120-125.

**Dodd, A. N., N. Salathia, A. Hall, E. Kevei, R. Toth, F. Nagy, J. M. Hibberd, A. J. Millar and A. A. R. Webb** (2005). "Plant circadian clocks increase photosynthesis, growth, survival, and competitive advantage." *Science* 309(5734): 630-633.

**Dowson-Day, M. J. and A. J. Millar** (1999). "Circadian dysfunction causes aberrant hypocotyl elongation patterns in *Arabidopsis*." *Plant Journal* 17(1): 63-71.

**Doyle, M. R., S. J. Davis, R. M. Bastow, H. G. McWatters, L. Kozma-Bognar, F. Nagy, A. J. Millar and R. M. Amasino** (2002). "The *ELF4* gene controls circadian rhythms and flowering time in *Arabidopsis thaliana*." *Nature* 419(6902): 74-77.

**Drouaud, J., C. Camilleri, P. Y. Bourguignon, A. Canaguier, A. Berard, D. Vezon, S. Giancola, D. Brunel, V. Colot, B. Prum, H. Quesneville and C. Mezard (2006).** "Variation in crossing-over rates across chromosome 4 of *Arabidopsis thaliana* reveals the presence of meiotic recombination "hot spots"." *Genome Research* 16(1): 106-114.

**Dumez, S., F. Wattedled, D. Dauvillee, D. Delvalle, V. Planchot, S. G. Ball and C. D'Hulst (2006).** "Mutants of *Arabidopsis* lacking starch branching enzyme II substitute plastidial starch synthesis by cytoplasmic maltose accumulation." *Plant Cell* 18(10): 2694-2709.

**Edner, C., J. Li, T. Albrecht, S. Mahlow, M. Hejazi, H. Hussain, F. Kaplan, C. Guy, S. M. Smith, M. Steup and G. Ritte (2007).** "Glucan water dikinase activity stimulates breakdown of starch granules by plastidial beta-amylases." *Plant Physiol* 145(1): 17-28.

**Edwards, K. D., A. J. Millar (2007)** "Analysis of circadian leaf movement rhythms in *Arabidopsis thaliana*." *Methods in Molecular Biology* 326: 103-113

**Eimert, K., S. M. Wang, W. L. Lue and J. C. Chen (1995).** "Monogenic recessive mutations causing both late floral initiation and excess starch accumulation in *Arabidopsis*." *Plant Cell* 7(10): 1703-1712.

**Emanuelsson, O., H. Nielsen, S. Brunak and G. von Heijne (2000).** "Predicting subcellular localization of proteins based on their N-terminal amino acid sequence." *Journal of Molecular Biology* 300(4): 1005-1016.

**Emanuelsson, O., H. Nielsen and G. von Heijne (1999).** "ChloroP, a neural network-based method for predicting chloroplast transit peptides and their cleavage sites." *Protein Science* 8(5): 978-984.

**Engelmann, W., K. Simon and C. J. Phen (1992).** "Leaf movement rhythm in *Arabidopsis-thaliana*." *Zeitschrift Fur Naturforschung, Journal of Biosciences* 47(11-12): 925-928.

**Fettke, J., N. Eckermann, S. Poeste, M. Pauly and M. Steup (2004).** "The glycan substrate of the cytosolic (Pho 2) phosphorylase isozyme from *Pisum sativum*.: identification, linkage analysis and subcellular localization." *Plant Journal* 39(6): 933-946.

**Fettke, J., N. Eckermann, A. Tiessen, P. Geigenberger and M. Steup (2005).** "Identification, subcellular localization and biochemical characterization of water-soluble heteroglycans (SHG) in leaves of *Arabidopsis thaliana*: distinct SHG reside in the cytosol and in the apoplast." *Plant Journal* 43(4): 568-585.

**Fettke, J., T. Chia, N. Eckermann, A. Smith and M. Steup (2006).** "A transglucosidase necessary for starch degradation and maltose metabolism in leaves at night acts on cytosolic heteroglycans (SHG)." *Plant Journal* 46(4): 668-684.

**Fettke, J., M. Hejazi, J. Smirnova, E. Hochel, M. Stage and M. Steup** (2009). "Eukaryotic starch degradation: integration of plastidial and cytosolic pathways." *Journal of Experimental Botany* 60(10): 2907-2922.

**Fukaki, H., H. Fujisawa and M. Tasaka** (1996). "SGR-1, SGR2, and SGR3: Novel genetic loci involved in shoot gravitropism in *Arabidopsis thaliana*." *Plant Physiology* 110(3): 945-955.

**Fukushima, A., M. Kusano, N. Nakamichi, M. Kobayashi, N. Hayashi, H. Sakakibara, M. Takeshi and K. Saito** (2009). "Impact of clock-associated *Arabidopsis* pseudo-response regulators in metabolic coordination." *Proceedings of the National Academy of Sciences of the United States of America* 106(21): 8791-8791.

**Fulton, D. C., A. Edwards, E. Pilling, H. L. Robinson, B. Fahy, R. Seale, L. Kato, A. M. Donald, P. Geigenberger, C. Martin and A. M. Smith** (2002). "Role of granule-bound starch synthase in determination of amylopectin structure and starch granule morphology in potato." *Journal of Biological Chemistry* 277(13): 10834-10841.

**Fulton, D. C., M. Stettler, T. Mettler, C. K. Vaughan, J. Li, P. Francisco, D. Gil, H. Reinhold, S. Eicke, G. Messerli, G. Dorken, K. Halliday, A. M. Smith, S. M. Smith and S. C. Zeeman** (2008). "BETA-AMYLASE4, a noncatalytic protein required for starch breakdown, acts upstream of three active beta-amylases in *Arabidopsis* chloroplasts." *Plant Cell* 20(4): 1040-1058.

**Geigenberger, P.** (2011). "Regulation of starch biosynthesis in response to a fluctuating environment." *Plant Physiology* 155(4): 1566-1577.

**Gibon, Y., O. E. Blasing, N. Palacios-Rojas, D. Pankovic, J. H. M. Hendriks, J. Fisahn, M. Hohne, M. Gunther and M. Stitt** (2004). "Adjustment of diurnal starch turnover to short days: depletion of sugar during the night leads to a temporary inhibition of carbohydrate utilization, accumulation of sugars and post-translational activation of ADP-glucose pyrophosphorylase in the following light period (vol 39, pg 847, 2004)." *Plant Journal* 40(2): 332-332.

**Gibon, Y., E. T. Pyl, R. Sulpice, J. E. Lunn, M. Hohne, M. Gunther and M. Stitt** (2009). "Adjustment of growth, starch turnover, protein content and central metabolism to a decrease of the carbon supply when *Arabidopsis* is grown in very short photoperiods." *Plant Cell and Environment* 32(7): 859-874.

**Glaring, M. A., K. Skryhan, O. Kotting, S. C. Zeeman and A. Blennow** (2012). "Comprehensive survey of redox sensitive starch metabolising enzymes in *Arabidopsis thaliana*." *Plant Physiology and Biochemistry* 58: 89-97.

**Gould, P. D., P. Diaz, C. Hogben, J. Kusakina, R. Salem, J. Hartwell and A. Hall** (2009). "Delayed fluorescence as a universal tool for the measurement of circadian rhythms in higher plants." *Plant J* 58(5): 893-901.

**Graf, A.** (2009). "The regulation of starch degradation in *Arabidopsis thaliana* leaves at night." PhD thesis submitted to the University of East Anglia.

**Graf, A., A. Schlereth, M. Stitt and A. M. Smith** (2010). "Circadian control of carbohydrate availability for growth in *Arabidopsis* plants at night." *Proceedings of the National Academy of Sciences of the United States of America* 107(20): 9458-9463

**Greene, E. A., C. A. Codomo, N. E. Taylor, J. G. Henikoff, B. J. Till, S. H. Reynolds, L. C. Enns, C. Burtner, J. E. Johnson, A. R. Odden, L. Comai and S. Henikoff** (2003). "Spectrum of chemically induced mutations from a large scale reverse genetic screen in *Arabidopsis*." *Genetics* 164(2): 731-740.

**Haebel, S., M. Hejazi, C. Frohberg, M. Heydenreich and G. Ritte** (2008). "Mass spectrometric quantification of the relative amounts of C6 and C3 position phosphorylated glucosyl residues in starch." *Analytical Biochemistry* 379(1): 73-79.

**Hanahan, D.** (1983). "Studies on transformation of *Escherichia coli* with plasmids." *Journal of Molecular Biology* 166(4): 557-580.

**Hansen, P. I., F. H. Larsen, S. M. Motawia, A. Blennow, M. Spraul, P. Dvortsak and S. B. Engelsen** (2008). "Structure and hydration of the amylopectin trisaccharide building blocks-synthesis, NMR, and Molecular Dynamics." *Biopolymers* 89(12): 1179-1193.

**Hargreaves, J. A. and T. Aprees** (1988). "Turnover of starch and sucrose in roots of *Pisum sativum*." *Phytochemistry* 27(6): 1627-1629.

**Harrison, C. J., C. L. Hedley and T. L. Wang** (1998). "Evidence that the *rug3* locus of pea (*Pisum sativum* L.) encodes plastidial phosphoglucomutase confirms that the imported substrate for starch synthesis in pea amyloplasts is glucose-6-phosphate." *Plant Journal* 13(6): 753-762.

**Hashiguchi, Y., M. Tasaka and M. T. Morita** (2013). "Mechanism of higher plant gravity sensing." *American Journal of Botany* 100(1): 91-100.

**Heazlewood, J. L., P. Durek, J. Hummel, J. Selbig, W. Weckwerth, D. Walther and W. X. Schulze** (2008). "PhosPhAt: a database of phosphorylation sites in *Arabidopsis thaliana* and a plant-specific phosphorylation site predictor." *Nucleic Acids Research* 36: D1015-1021.

**Hejazi, M., J. Fettke, S. Haebel, C. Edner, O. Paris, C. Froberg, M. Steup and G. Ritte** (2008). "Glucan, water dikinase phosphorylates crystalline maltodextrins and thereby initiates solubilization." *Plant Journal* 55(2): 323-334.

**Hejazi, M., J. Fettke, O. Paris and M. Steup** (2009). "The two plastidial starch-related dikinases sequentially phosphorylate glucosyl residues at the surface of both the A- and B-type allomorphs of crystallized maltodextrins but the mode of action differs." *Plant Physiology* 150(2): 962-976.

**Hejazi, M., J. Fettke, O. Kotting, S. C. Zeeman and M. Steup** (2010). "The laforin-like dual specificity phosphatase *SEX4* from *Arabidopsis* hydrolyzes both C6- and C3-phosphate esters introduced by starch-related dikinases and thereby affects phase transition of alpha-glucans." *Plant Physiology* 152(2): 711-722.

**Helfer, A., D. A. Nusinow, B. Y. Chow, A. R. Gehrke, M. L. Bulyk and S. A. Kay** (2011). "LUX ARRHYTHMO encodes a nighttime repressor of circadian gene expression in the *Arabidopsis* core clock." *Current Biology* 21(2): 126-133.

**Hicks, K. A., A. J. Millar, I. A. Carre, D. E. Somers, M. Straume, D. R. MeeksWagner and S. A. Kay** (1996). "Conditional circadian dysfunction of the *Arabidopsis* *EARLY FLOWERING 3* mutant." *Science* 274(5288): 790-792.

**Hostettler, C., K. Kolling, D. Santelia, S. Streb, O. Kotting and S. C. Zeeman** (2011). "Analysis of starch metabolism in chloroplasts." *Chloroplast Research in Arabidopsis: Methods and Protocols*, Vol II 775: 387-410.

**Huang, W. D. and R. L. Erikson** (1994). "Constitutive activation of Mek1 by mutation of serine phosphorylation sites." *Proceedings of the National Academy of Sciences of the United States of America* 91(19): 8960-8963.

**Ishida, T. and K. Kinoshita** (2008). "Prediction of disordered regions in proteins based on the meta approach." *Bioinformatics* 24(11): 1344-1348.

**Jander, G., S. R. Norris, S. D. Rounsley, D. F. Bush, I. M. Levin and R. L. Last** (2002). "*Arabidopsis* map-based cloning in the post-genome era." *Plant Physiology* 129(2): 440-450.

**Kaplan, F. and C. L. Guy** (2004). "Beta-amylase induction and the protective role of maltose during temperature shock." *Plant Physiology* 135(3): 1674-1684.

**Kaplan, F. and C. L. Guy** (2005). "RNA interference of *Arabidopsis* beta-amylase 8 prevents maltose accumulation upon cold shock and increases sensitivity of PSII photochemical efficiency to freezing stress." *Plant Journal* 44(5): 730-743.

**Kaplan, F., D. Y. Sung and C. L. Guy** (2006). "Roles of beta-amylase and starch breakdown during temperatures stress." *Physiologia Plantarum* 126(1): 120-128.

**Kelley, L. A. and M. J. E. Sternberg** (2009). "Protein structure prediction on the Web: a case study using the Phyre server." *Nature Protocols* 4(3): 363-371.

**Kiss, J. Z., R. Hertel and F. D. Sack** (1989). "Amyloplasts are necessary for full gravitropic sensitivity in roots of *Arabidopsis thaliana*." *Planta* 177(2): 198-206.

**Kleffmann, T., D. Russenberger, A. von Zychlinski, W. Christopher, K. Sjolander, W. Gruissem and S. Baginsky** (2004). "The *Arabidopsis thaliana* chloroplast proteome reveals pathway abundance and novel protein functions." *Current Biology* 14(5): 354-362.

**Kötting, O., K. Pusch, A. Tiessen, P. Geigenberger, M. Steup and G. Ritte** (2005). "Identification of a novel enzyme required for starch metabolism in *Arabidopsis* leaves. The phosphoglucan water dikinase." *Plant Physiology* 137(1): 242-252.

**Kötting, O., D. Santelia, C. Edner, S. Eicke, T. Marthaler, M. S. Gentry, S. Comparot-Moss, J. Chen, A. M. Smith, M. Steup, G. Ritte and S. C. Zeeman** (2009). "STARCH-EXCESS4 is a laforin-like phosphoglucan phosphatase required for starch degradation in *Arabidopsis thaliana*." *Plant Cell* 21(1): 334-346.

**Kötting, O., J. Kossmann, S. C. Zeeman and J. R. Lloyd** (2010). "Regulation of starch metabolism: the age of enlightenment?" *Current Opinion in Plant Biology*.

**Laby, R. J., D. Kim and S. I. Gibson** (2001). "The *ram1* mutant of *Arabidopsis* exhibits severely decreased beta-amylase activity." *Plant Physiology* 127(4): 1798-1807.

**Lao, N. T., O. Schoneveld, R. M. Mould, J. M. Hibberd, J. C. Gray and T. A. Kavanagh** (1999). "An *Arabidopsis* gene encoding a chloroplast-targeted beta-amylase." *Plant Journal* 20(5): 519-527.

**Lee, D. W., J. K. Kim, S. Lee, S. Choi, S. Kim and I. Hwang** (2008). "*Arabidopsis* nuclear-encoded plastid transit peptides contain multiple sequence subgroups with distinctive chloroplast-targeting sequence motifs." *Plant Cell* 20(6): 1603-1622.

**Li, Y. H., K. K. Lee, S. Walsh, C. Smith, S. Hadingham, K. Sorefan, G. Cawley and M. W. Bevan** (2006). "Establishing glucose- and ABA-regulated transcription networks in *Arabidopsis* by microarray analysis and promoter classification using a Relevance Vector Machine." *Genome Research* 16(3): 414-427.

**Li, H., J. Ruan and R. Durbin** (2008). "Mapping short DNA sequencing reads and calling variants using mapping quality scores." *Genome Research* 18(11): 1851-1858.

**Li, J., P. Francisco, W. Zhou, C. Edner, M. Steup, G. Ritte, C. S. Bond and S. M. Smith** (2009). "Catalytically-inactive beta-amylase BAM4 required for starch breakdown in *Arabidopsis* leaves is a starch-binding-protein." *Arch Biochem Biophys* 489(1-2): 92-98

**Lin, T. P., S. R. Spilatro and J. Preiss** (1988). "Subcellular-localization and characterization of amylases in *Arabidopsis* leaf." *Plant Physiology* 86(1): 251-259.

**Liu, X. L., M. F. Covington, C. Fankhauser, J. Chory and D. R. Wagner** (2001). "*ELF3* encodes a circadian clock-regulated nuclear protein that functions in an *Arabidopsis* PHYB signal transduction pathway." *Plant Cell* 13(6): 1293-1304.

**Lu, Y. and T. D. Sharkey** (2004). "The role of amylomaltase in maltose metabolism in the cytosol of photosynthetic cells." *Planta* 218(3): 466-473.

**Lu, Y., J. P. Gehan and T. D. Sharkey** (2005). "Daylength and circadian effects on starch degradation and maltose metabolism." *Plant Physiol* 138(4): 2280-2291.

**Lu, Y., J. M. Steichen, J. Yao and T. D. Sharkey** (2006). "The role of cytosolic alpha-glucan phosphorylase in maltose metabolism and the comparison of amylomaltase in *Arabidopsis* and *Escherichia coli*." *Plant Physiology* 142(3): 878-889.

**Lukowitz, W., C. S. Gillmor and W. R. Scheible** (2000). "Positional cloning in *Arabidopsis*. Why it feels good to have a genome initiative working for you." *Plant Physiology* 123(3): 795-805.

**Lunn, J. E., R. Feil, J. H. M. Hendriks, Y. Gibon, R. Morcuende, D. Osuna, W. R. Scheible, P. Carillo, M. R. Hajirezaei and M. Stitt** (2006). "Sugar-induced increases in trehalose 6-phosphate are correlated with redox activation of ADPglucose pyrophosphorylase and higher rates of starch synthesis in *Arabidopsis thaliana*." *Biochemical Journal* 397: 139-148.

**Marchler-Bauer, A. and S. H. Bryant** (2004). "CD-Search: protein domain annotations on the fly." *Nucleic Acids Research* 32: W327-W331.

**Mayer, K. M. and F. H. Arnold** (2002). "A colorimetric assay to quantify dehydrogenase activity in crude cell lysates." *Journal of Biomolecular Screening* 7(2): 135-140.

**Mikami, B., M. Degano, E. J. Hehre and J. C. Sacchettini** (1994). "Crystal-structures of soybean beta-amylase reacted with beta-maltose and maltal - active-site components and their apparent roles in catalysts." *Biochemistry* 33(25): 7779-7787.

**Mikami, B., E. J. Hehre, M. Degano and J. C. Sacchettini** (1994). "crystallographic elucidation of the active-site structure of beta-amylase." Abstracts of Papers of the American Chemical Society 207: 95-Carb.

**Mikkelsen, R., K. E. Mutenda, A. Mant, P. Schurmann and A. Blennow** (2005). "Alpha-glucan, water dikinase (GWD): A plastidic enzyme with redox-regulated and coordinated catalytic activity and binding affinity." Proceedings of the National Academy of Sciences of the United States of America 102(5): 1785-1790.

**Millar, A. J., I. A. Carre, C. A. Strayer, N. H. Chua and S. A. Kay** (1995). "Circadian clock mutants in *Arabidopsis* identified by luciferase imaging." Science 267(5201): 1161-1163.

**Millar, A. J., S. R. Short, N. H. Chua and S. A. Kay** (1992). "A novel circadian phenotype based on firefly luciferase expression in transgenic plants." Plant Cell 4(9): 1075-1087.

**Mita, S., K. Suzukifujii and K. Nakamura** (1995). "Sugar-inducible expression of a gene for beta-amylase in *Arabidopsis thaliana*." Plant Physiology 107(3): 895-904.

**Mizuno, T. and T. Yamashino** (2008). "Comparative transcriptome of diurnally oscillating genes and hormone-responsive genes in *Arabidopsis thaliana*: Insight into circadian clock-controlled daily responses to common ambient stresses in plants." Plant and Cell Physiology 49(3): 481-487.

**Mizoguchi, T., K. Wheatley, Y. Hanzawa, L. Wright, M. Mizoguchi, H. R. Song, I. A. Carre and G. Coupland** (2002). "*LHY* and *CCA1* are partially redundant genes required to maintain circadian rhythms in *Arabidopsis*." Developmental Cell 2(5): 629-641.

**Monroe, J. D. and J. Preiss** (1990). "Purification of a beta-amylase that accumulates in *Arabidopsis thaliana* mutants defective in starch metabolism." Plant Physiology 94(3): 1033-1039.

**Nagel, D. H. and S. A. Kay** (2013). "Complexity in the wiring and regulation of plant circadian networks." Current Biology 23(1): 95-96.

**Nakamichi, N., T. Kiba, R. Henriques, T. Mizuno, N. H. Chua and H. Sakakibara** (2010). "PSEUDO-RESPONSE REGULATORS 9, 7, and 5 are transcriptional repressors in the *Arabidopsis* circadian clock." Plant Cell 22(3): 594-605.

**Nakamura, T., M. Yamamori, H. Hirano, S. Hidaka and T. Nagamine** (1995). "Production of waxy (amylose-free) Wheats." Molecular and General Genetics 248(3): 253-259.

**Niittylä, T., S. Comparot-Moss, W. L. Lue, G. Messerli, M. Trevisan, M. D. J. Seymour, J. A. Gatehouse, D. Villadsen, S. M. Smith, J. C. Chen, S. C. Zeeman and**

**M. S. Alison** (2006). "Similar protein phosphatases control starch metabolism in plants and glycogen metabolism in mammals." *Journal of Biological Chemistry* 281(17): 11815-11818.

**Niittylä, T., G. Messerli, M. Trevisan, J. Chen, A. M. Smith and S. C. Zeeman** (2004). "A previously unknown maltose transporter essential for starch degradation in leaves." *Science* 303(5654): 87-89.

**Nozue, K., M. F. Covington, P. D. Duek, S. Lorrain, C. Fankhauser, S. L. Harmer and J. N. Maloof** (2007). "Rhythmic growth explained by coincidence between internal and external cues." *Nature* 448(7151): 358-U311.

**Nusinow, D. A., A. Helfer, E. E. Hamilton, J. J. King, T. Imaizumi, T. F. Schultz, E. M. Farre and S. A. Kay** (2011). "The ELF4-ELF3-LUX complex links the circadian clock to diurnal control of hypocotyl growth." *Nature* 475(7356): 398-U161.

**Osuna, D., B. Usadel, R. Morcuende, Y. Gibon, O. E. Blasing, M. Hohne, M. Gunter, B. Kamlage, R. Trethewey, W. R. Scheible and M. Stitt** (2007). "Temporal responses of transcripts, enzyme activities and metabolites after adding sucrose to carbon-deprived *Arabidopsis* seedlings." *Plant Journal* 49(3): 463-491.

**Peltier, J. B., Y. Cai, Q. Sun, V. Zabrouskov, L. Giacomelli, A. Rudella, A. J. Ytterberg, H. Rutschow and K. J. van Wijk** (2006). "The oligomeric stromal proteome of *Arabidopsis thaliana* chloroplasts." *Molecular Cell Proteomics* 5(1): 114-133.

**Peters, J. L., F. Cnudde and T. Gerats** (2003). "Forward genetics and map-based cloning approaches." *Trends in Plant Science* 8(10): 484-491.

**Pilling, E. and A. M. Smith** (2003). "Growth ring formation in the starch granules of potato tubers." *Plant Physiology* 132(1): 365-371.

**Pittendrigh, C. S. and D. H. Minis** (1964). "The entrainment of circadian oscillations by light and their role as photoperiodic clocks." *American Naturalist* 98(902): 261-294.

**Plautz, J. D., M. Straume, R. Stanewsky, C. F. Jamison, C. Brandes, H. B. Dowse, J. C. Hall and S. A. Kay** (1997). "Quantitative analysis of *Drosophila* period gene transcription in living animals." *Journal of Biological Rhythms* 12(3): 204-217.

**Pokhilko, A., A. P. Fernandez, K. D. Edwards, M. M. Southern, K. J. Halliday and A. J. Millar** (2012). "The clock gene circuit in *Arabidopsis* includes a repressilator with additional feedback loops." *Molecular Systems Biology* 8.

**Pruneda-Paz, J. L. and S. A. Kay** (2010). "An expanding universe of circadian networks in higher plants." *Trends in Plant Science* 15(5): 259-265.

**Pyl, E. T., M. Piques, A. Ivakov, W. Schulze, H. Ishihara, M. Stitt and R. Sulpice** (2012). "Metabolism and growth in *Arabidopsis* depend on the daytime temperature but are temperature-compensated against cool nights." *Plant Cell* 24(6): 2443-2469.

**Reed, J. W., P. Nagpal, R. M. Bastow, K. S. Solomon, M. J. Dowson-Day, R. P. Elumalai and A. J. Millar** (2000). "Independent action of ELF3 and phyB to control hypocotyl elongation and flowering time." *Plant Physiology* 122(4): 1149-1160.

**Reiland, S., G. Messerli, K. Baerenfaller, B. Gerrits, A. Endler, J. Grossmann, W. Gruissem and S. Baginsky** (2009). "Large-scale *Arabidopsis* phosphoproteome profiling reveals novel chloroplast kinase substrates and phosphorylation networks." *Plant Physiology* 150(2): 889-903.

**Ritte, G., M. Heydenreich, S. Mahlow, S. Haebel, O. Kotting and M. Steup** (2006). "Phosphorylation of C6- and C3-positions of glucosyl residues in starch is catalysed by distinct dikinases." *Febs Letters* 580(20): 4872-4876.

**Ritte, G., L. Jr, N. Eckermann, A. Rottmann, J. Kossmann and M. Steup** (2002). "The starch-related R1 protein is an alpha-glucan, water dikinase." *Proceedings of the National Academy of Sciences of the United States of America* 99(10): 7166-7171.

**Roldán, I., F. Wattedled, M. M. Lucas, D. Delvalle, V. Planchot, S. Jimenez, R. Perez, S. Ball, C. D'Hulst and A. Merida** (2007). "The phenotype of soluble starch synthase IV defective mutants of *Arabidopsis thaliana* suggests a novel function of elongation enzymes in the control of starch granule formation." *Plant Journal* 49(3): 492-504.

**Rutherford, A. W., Govindjee and Y. Inoue** (1984). "Charge accumulation and photochemistry in leaves studied by thermo-luminescence and delayed light-emission." *Proceedings of the National Academy of Sciences of the United States of America-Biological Sciences* 81(4): 1107-1111.

**Sanger, F., S. Nicklen and A. R. Coulson** (1977). "DNA sequencing with chain-terminating inhibitors." *Proceedings of the National Academy of Sciences of the United States of America* 74(12): 5463-5467.

**Santelia, D., O. Kotting, D. Seung, M. Schubert, M. Thalmann, S. Bischof, D. A. Meekins, A. Lutz, N. Patron, M. S. Gentry, F. H. T. Allain and S. C. Zeeman** (2011). "The phosphoglucan phosphatase Like Sex Four2 dephosphorylates starch at the C3-position in *Arabidopsis*." *Plant Cell* 23(11): 4096-4111.

**Schaffer, R., N. Ramsay, A. Samach, S. Corden, J. Putterill, I. A. Carre and G. Coupland** (1998). "The late elongated hypocotyl mutation of *Arabidopsis* disrupts circadian rhythms and the photoperiodic control of flowering." *Cell* 93(7): 1219-1229.

**Schliebner, I., M. Pribil, J. Zuhlke, A. Dietzmann and D. Leister** (2008). "A survey of chloroplast protein kinases and phosphatases in *Arabidopsis thaliana*." *Current Genomics* 9(3): 184-190.

**Schneeberger, K., J. Hagmann, S. Ossowski, N. Warthmann, S. Gesing, O. Kohlbacher and D. Weigel** (2009). "Simultaneous alignment of short reads against multiple genomes." *Genome Biology* 10(9).

**Scialdone, A., S. T. Mugford, D. Feike, A. Skeffington, P. Borrill, A. Graf, A. M. Smith and M. Howard** (2013). "*Arabidopsis* plants perform arithmetic division to prevent starvation at night." *eLife* 2: e00669.

**Shure, M., S. Wessler and N. Fedoroff** (1983). "Molecular-Identification and Isolation of the Waxy Locus in Maize." *Cell* 35(1): 225-233.

**Smith, S. M., D. C. Fulton, T. Chia, D. Thorneycroft, A. Chapple, H. Dunstan, C. Hylton, S. C. Zeeman and A. M. Smith** (2004). "Diurnal changes in the transcriptome encoding enzymes of starch metabolism provide evidence for both transcriptional and posttranscriptional regulation of starch metabolism in *Arabidopsis* leaves." *Plant Physiology* 136(1): 2687-2699.

**Smith, A. M. and M. Stitt** (2007). "Coordination of carbon supply and plant growth." *Plant Cell Environment* 30(9): 1126-1149.

**Smith, A. M.** (2012). "Starch in the *Arabidopsis* plant." *Starch-Stärke* 64(6): 421-434

**Sokolov, L. N., J. R. Dominguez-Solis, A. L. Allary, B. B. Buchanan and S. Luan** (2006). "A redox-regulated chloroplast protein phosphatase binds to starch diurnally and functions in its accumulation." *Proceedings of the National Academy of Sciences of the United States of America* 103(25): 9732-9737.

**Somers, D. E., A. A. R. Webb, M. Pearson and S. A. Kay** (1998). "The short-period mutant, *toc1-1*, alters circadian clock regulation of multiple outputs throughout development in *Arabidopsis thaliana*." *Development* 125(3): 485-494.

**Sparla, F., A. Costa, F. Lo Schiavo, P. Pupillo and P. Trost** (2006). "Redox regulation of a novel plastid-targeted beta-amylase of *Arabidopsis*." *Plant Physiology* 141(3): 840-850.

**Srikanth, A. and M. Schmid** (2011). "Regulation of flowering time: all roads lead to Rome." *Cellular and Molecular Life Sciences* 68(12): 2013-2037.

**Streb, S., T. Delatte, M. Umhang, S. Eicke, M. Schorderet, D. Reinhardt and S. C. Zeeman** (2008). "Starch granule biosynthesis in *Arabidopsis* is abolished by removal of all debranching enzymes but restored by the subsequent removal of an endoamylase." *Plant Cell* 20(12): 3448-3466.

**Streb, S., S. Eicke and S. C. Zeeman** (2012). "The simultaneous abolition of three starch hydrolases blocks transient starch breakdown in *Arabidopsis*." *Journal of Biological Chemistry* 287(50): 41745-41756.

**Strehler, B. and W. Arnold** (1951). "Light production by green plants." *Federation Proceedings* 10(1): 255-255.

**Suarez-Lopez, P., K. Wheatley, F. Robson, H. Onouchi, F. Valverde and G. Coupland** (2001). "CONSTANS mediates between the circadian clock and the control of flowering in *Arabidopsis*." *Nature* 410(6832): 1116-1120.

**Sulpice, R., E. T. Pyl, H. Ishihara, S. Trenkamp, M. Steinfath, H. Witucka-Wall, Y. Gibon, B. Usadel, F. Poree, M. C. Piques, M. Von Korff, M. C. Steinhauser, J. J. B. Keurentjes, M. Guenther, M. Hoehne, J. Selbig, A. R. Fernie, T. Altmann and M. Stitt** (2009). "Starch as a major integrator in the regulation of plant growth." *Proceedings of the National Academy of Sciences of the United States of America* 106(25): 10348-10353.

**Szydlowski, N., P. Ragel, T. A. Hennen-Bierwagen, V. Planchot, A. M. Myers, A. Merida, C. d'Hulst and F. Wattedled** (2011). "Integrated functions among multiple starch synthases determine both amylopectin chain length and branch linkage location in *Arabidopsis* leaf starch." *Journal of Experimental Botany* 62(13): 4547-4559.

**Takeda, Y. and S. Hizukuri** (1981). "Studies on starch phosphate .5. Reexamination of the action of sweet-potato beta-amylase on phosphorylated (1-]4)-alpha-D-glucan." *Carbohydrate Research* 89(1): 174-178.

**Tanimoto, M., R. Tremblay and J. Colasanti** (2008). "Altered gravitropic response, amyloplast sedimentation and circumnutation in the *Arabidopsis* shoot gravitropism 5 mutant are associated with reduced starch levels." *Plant Molecular Biology* 67(1-2): 57-69.

**Tauberger, E., A. R. Fernie, M. Emmermann, A. Renz, J. Kossmann, L. Willmitzer and R. N. Trethewey** (2000). "Antisense inhibition of plastidial phosphoglucomutase provides compelling evidence that potato tuber amyloplasts import carbon from the cytosol in the form of glucose-6-phosphate." *Plant Journal* 23(1): 43-53.

**Thimm, O., O. Blasing, Y. Gibon, A. Nagel, S. Meyer, P. Kruger, J. Selbig, L. A. Muller, S. Y. Rhee and M. Stitt** (2004). "MAPMAN: a user-driven tool to display

genomics data sets onto diagrams of metabolic pathways and other biological processes." *Plant Journal* 37(6): 914-939.

**Tsai, H. L., W. L. Lue, K. J. Lu, M. H. Hsieh, S. M. Wang and J. Chen** (2009). "Starch synthesis in *Arabidopsis* is achieved by spatial cotranscription of core starch metabolism genes." *Plant Physiology* 151(3): 1582-1595.

**Usadel, B., O. E. Blasing, Y. Gibon, K. Retzlaff, M. Hoehne, M. Gunther and M. Stitt** (2008). "Global transcript levels respond to small changes of the carbon status during progressive exhaustion of carbohydrates in *Arabidopsis* rosettes." *Plant Physiology* 146(4): 1834-1861.

**Valerio, C., A. Costa, L. Marri, E. Issakidis-Bourguet, P. Pupillo, P. Trost and F. Sparla** (2011). "Thioredoxin-regulated beta-amylase (BAM1) triggers diurnal starch degradation in guard cells, and in mesophyll cells under osmotic stress." *Journal of Experimental Botany* 62(2): 545-555.

**van Bentem, S. D. F., D. Anrather, E. Roitinger, A. Djamei, T. Hufnagl, A. Barta, E. Csaszar, I. Dohnal, D. Lecourieux and H. Hirt** (2006). "Phosphoproteomics reveals extensive in vivo phosphorylation of *Arabidopsis* proteins involved in RNA metabolism." *Nucleic Acids Research* 34(11): 3267-3278.

**Van Larebeke, N., I. Zaenen, H. Teuchy and J. Schell** (1973). "Circular DNA plasmids in *Agrobacterium* strains. Investigation of their role in the induction of crown-gall tumors." *Arch Int Physiol Biochim* 81(5): 986.

**Vanderleij, F. R., R. G. F. Visser, A. S. Ponstein, E. Jacobsen and W. J. Feenstra** (1991). "Sequence of the structural gene for granule-bound starch synthase of potato (*Solanum tuberosum*) and evidence for a single point deletion in the *amf* allele." *Molecular and General Genetics* 228(1-2): 240-248.

**Wahl, V., J. Ponnu, A. Schlereth, S. Arrivault, T. Langenecker, A. Franke, R. Feil, J. E. Lunn, M. Stitt and M. Schmid** (2013). "Regulation of flowering by trehalose-6-phosphate signaling in *Arabidopsis thaliana*." *Science* 339(6120): 704-707.

**Wang, Q., J. Monroe and D. Sjolund** (1995). "Identification and characterization of a phloem-specific beta-amylase." *Plant Physiology* 109(3): 743-750.

**Wang, W., J. Y. Barnaby, Y. Tada, H. Li, M. Tor, D. Caldelari, D. U. Lee, X. D. Fu and X. N. Dong** (2011). "Timing of plant immune responses by a central circadian regulator." *Nature* 470(7332): 110-U126.

**Wang, Y. H., S. M. G. Duff, L. Lepiniec, C. Cretin, G. Sarath, S. A. Condon, J. Vidal, P. Gadal and R. Chollet** (1992). "Site-directed mutagenesis of the phosphorylatable serine (Ser(8)) in C4-phosphoenolpyruvate carboxylase from sorghum

- the effect of negative charge at position-8." *Journal of Biological Chemistry* 267(24): 16759-16762.

**Wattebled, F., Y. Dong, S. Dumez, D. Delvalle, V. Planchot, P. Berbezy, D. Vyas, P. Colonna, M. Chatterjee, S. Ball and C. D'Hulst** (2005). "Mutants of *Arabidopsis* lacking a chloroplastic isoamylase accumulate phyto glycogen and an abnormal form of amylopectin." *Plant Physiology* 138(1): 184-195.

**Wattebled, F., V. Planchot, Y. Dong, N. Szydlowski, B. Pontoire, A. Devin, S. Ball and C. D'Hulst** (2008). "Further evidence for the mandatory nature of polysaccharide debranching for the aggregation of semicrystalline starch and for overlapping functions of debranching enzymes in *Arabidopsis* leaves." *Plant Physiology* 148(3): 1309-1323.

**Weigel, D. and J. Glazebrook** (2002): *Arabidopsis: A Laboratory Manual*. Cold Spring Harbour Laboratory Press, Cold Spring Harbour, New York, ISBN 0-87969-572-2

**Weise, S. E. and J. Z. Kiss** (1999). "Gravitropism of inflorescence stems in starch-deficient mutants of *Arabidopsis*." *International Journal of Plant Sciences* 160(3): 521-527.

**Yazdanbakhsh, N., R. Sulpice, A. Graf, M. Stitt and J. Fisahn** (2011). "Circadian control of root elongation and C partitioning in *Arabidopsis thaliana*." *Plant Cell Environment* 34(6): 877-894

**Yu, T. S., H. Kofler, R. E. Hausler, D. Hille, U. I. Flugge, S. C. Zeeman, A. M. Smith, J. Kossmann, J. Lloyd, G. Ritte, M. Steup, W. L. Lue, J. C. Chen and A. Weber** (2001). "The *Arabidopsis* *sex1* mutant is defective in the R1 protein, a general regulator of starch degradation in plants, and not in the chloroplast hexose transporter." *Plant Cell* 13(8): 1907-1918.

**Yu, T. S., W. L. Lue, S. M. Wang and J. C. Chen** (2000). "Mutation of *Arabidopsis* plastid phosphoglucose isomerase affects leaf starch synthesis and floral initiation." *Plant Physiology* 123(1): 319-325.

**Yu, T. S., S. C. Zeeman, D. Thorneycroft, D. C. Fulton, H. Dunstan, W. L. Lue, B. Hegemann, S. Y. Tung, T. Umemoto, A. Chapple, D. L. Tsai, S. M. Wang, A. M. Smith, J. Chen and S. M. Smith** (2005). "Alpha-amylase is not required for breakdown of transitory starch in *Arabidopsis* leaves." *Journal of Biological Chemistry* 280(11): 9773-9779.

**Zagotta, M. T., K. A. Hicks, C. I. Jacobs, J. C. Young, R. P. Hangarter and D. R. MeeksWagner** (1996). "The *Arabidopsis* *ELF3* gene regulates vegetative photomorphogenesis and the photoperiodic induction of flowering." *Plant Journal* 10(4): 691-702.

**Zeeman, S. C., T. Umemoto, W. L. Lue, P. Au-Yeung, C. Martin, A. M. Smith and J. Chen** (1998a). "A mutant of *Arabidopsis* lacking a chloroplastic isoamylase accumulates both starch and phytylglycogen." *Plant Cell* 10(10): 1699-1712.

**Zeeman, S. C., F. Northrop, A. M. Smith and T. ap Rees** (1998b). "A starch-accumulating mutant of *Arabidopsis thaliana* deficient in a chloroplastic starch-hydrolysing enzyme." *Plant Journal* 15(3): 357-365.

**Zeeman, S. C. and T. ap Rees** (1999). "Changes in carbohydrate metabolism and assimilate export in starch-excess mutants of *Arabidopsis*." *Plant Cell and Environment* 22(11): 1445-1453.

**Zeeman, S. C., A. Tiessen, E. Pilling, K. L. Kato, A. M. Donald and A. M. Smith** (2002). "Starch synthesis in *Arabidopsis*: granule synthesis, composition, and structure." *Plant Physiol* 129(2): 516-529.

**Zeeman, S. C., S. M. Smith and A. M. Smith** (2004a). "The breakdown of starch in leaves." *New Phytologist* 163(2): 247-261.

**Zeeman, S. C., D. Thorneycroft, N. Schupp, A. Chapple, M. Weck, H. Dunstan, P. Haldimann, N. Bechtold, A. M. Smith and S. M. Smith** (2004b). "Plastidial alpha-glucan phosphorylase is not required for starch degradation in *Arabidopsis* leaves but has a role in the tolerance of abiotic stress." *Plant Physiology* 135(2): 849-858.

**Zeeman, S. C., J. Kossmann and A. M. Smith** (2010). "Starch: its metabolism, evolution, and biotechnological modification in plants." *Annual Review of Plant Biology*, Vol 61 61: 209-234.

**Zybilov, B., H. Rutschow, G. Friso, A. Rudella, O. Emanuelsson, Q. Sun and K. J. van Wijk** (2008). "Sorting signals, N-terminal modifications and abundance of the chloroplast proteome." *PLoS One* 3(4): e1994.